Publishing House ASV

begell house, inc. publishers

PAACH

Scientific coordination is carried out by the Russian Academy of Architecture and Construction Sciences (RAACS)

*Volume 21 • Issue 3 • 2025*

**ISSN 2588-0195** (Online)
**ISSN 2587-9618** (Print) Continues ISSN 1524-5845

*International Journal for*

# Computational Civil and Structural Engineering

## Международный журнал по расчету гражданских и строительных конструкций

**https://ijccse.iasv.ru/**

**DOI: 10.22337/2587-9618**
**GICID: 71.0000.1500.2830**

## PUBLISHER

ASV Publishing House
(ООО «Издательство АСВ»)
19/1,12, Yaroslavskoe Shosse, 120338, Moscow, Russia
Tel. +7(925)084-74-24; E-mail: iasv@iasv.ru; Интернет-сайт: http://iasv.ru/

# ADVISORY EDITORIAL BOARD

## TECHNICAL EDITOR

# EDITORIAL TEAM

## INVITED REVIEWERS



## AIMS AND SCOPE

**The aim of the Journal** is to advance the research and practice in structural engineering through the application of computational methods. The Journal will publish original papers and educational articles of general value to the field that will bridge the gap between high-performance construction materials, large-scale engineering systems and advanced methods of analysis.

**The scope of the Journal** includes papers on computer methods in the areas of structural engineering, civil engineering materials and problems concerned with multiple physical processes interacting at multiple spatial and temporal scales. The Journal is intended to be of interest and use to researches and practitioners in academic, governmental and industrial communities.

# ОБЩАЯ ИНФОРМАЦИЯ О ЖУРНАЛЕ

## *International Journal for Computational Civil and Structural Engineering*

**(Международный журнал по расчету гражданских и строительных конструкций)**

**Международный научный журнал "International Journal for Computational Civil and Structural Engineering (Международный журнал по расчету гражданских и строительных конструкций)" (IJCCSE)** является ведущим научным периодическим изданием по направлению «Инженерные и технические науки», издаваемым, начиная с 1999 года (ISSN 2588-0195 (Online); ISSN 2587-9618 (Print) Continues ISSN 1524-5845). В журнале на высоком научно-техническом уровне рассматриваются проблемы численного и компьютерного моделирования в строительстве, актуальные вопросы разработки, исследования, развития, верификации, апробации и приложений численных, численно-аналитических методов, программно-алгоритмического обеспечения и выполнения автоматизированного проектирования, мониторинга и комплексного наукоемкого расчетно-теоретического и экспериментального обоснования напряженно-деформированного (и иного) состояния, прочности, устойчивости, надежности и безопасности ответственных объектов гражданского и промышленного строительства, энергетики, машиностроения, транспорта, биотехнологий и других высокотехнологичных отраслей.

В редакционный совет журнала входят известные российские и зарубежные деятели науки и техники (в том числе академики, члены-корреспонденты, иностранные члены, почетные члены и советники Российской академии архитектуры и строительных наук). Основной критерий отбора статей для публикации в журнале − их высокий научный уровень, соответствие которому определяется в ходе высококвалифицированного рецензирования и объективной экспертизы, поступающих в редакцию материалов.

*Журнал входит в Перечень ВАК РФ ведущих рецензируемых научных изданий, в которых должны быть опубликованы основные научные результаты диссертаций на соискание ученой степени кандидата наук, на соискание ученой степени доктора наук* по научным специальностям и соответствующим им отраслям науки:

- 1.1.8 – Механика деформируемого твердого тела (технические науки),
- 1.2.2 – Математическое моделирование численные методы и комплексы программ (технические науки),
- 2.1.1 – Строительные конструкции, здания и сооружения (технические науки),
- 2.1.2 – Основания и фундаменты, подземные сооружения (технические науки),
- 2.1.5 – Строительные материалы и изделия (технические науки),
- 05.23.07 – Гидротехническое строительство (технические науки),
- 2.1.9 – Строительная механика (технические науки)

В Российской Федерации журнал индексируется Российским индексом научного цитирования (РИНЦ).

*Журнал входит в базу данных Russian Science Citation Index (RSCI), полностью интегрированную с платформой Web of Science*. Журнал имеет международный статус и высылается в ведущие библиотеки и научные организации мира.

**Издатели журнала** – *Издательство Ассоциации строительных высших учебных заведений /АСВ/* (Россия, г. Москва) и до 2017 года *Издательский дом Begell House Inc*. (США, г. Нью-Йорк). Официальными партнерами издания является *Российская академия архитектуры и строительных наук* (РААСН), осуществляющая научное курирование издания, и *Научно-исследовательский центр СтаДиО* (ЗАО НИЦ СтаДиО).

**Цели журнала** – демонстрировать в публикациях российскому и международному профессиональному сообществу новейшие достижения науки в области вычислительных методов решения фундаментальных и прикладных технических задач, прежде всего в области строительства.

**Задачи журнала**:

• предоставление российским и зарубежным ученым и специалистам возможности публиковать результаты своих исследований;

• привлечение внимания к наиболее актуальным, перспективным, прорывным и интересным направлениям развития и приложений численных и численно-аналитических методов решения фундаментальных и прикладных технических задач, совершенствования технологий математического, компьютерного моделирования, разработки и верификации реализующего программно-алгоритмического обеспечения;

• обеспечение обмена мнениями между исследователями из разных регионов и государств.

**Тематика журнала**. К рассмотрению и публикации в журнале принимаются аналитические материалы, научные статьи, обзоры, рецензии и отзывы на научные публикации по фундаментальным и прикладным вопросам технических наук, прежде всего в области строительства. В журнале также публикуются информационные материалы, освещающие научные мероприятия и передовые достижения Российской академии архитектуры и строительных наук, научно-образовательных и проектно-конструкторских организаций.

Тематика статей, принимаемых к публикации в журнале, соответствует его названию и охватывает направления научных исследований в области разработки, исследования и приложений численных и численно-аналитических методов, программного обеспечения, технологий компьютерного моделирования в решении прикладных задач в области строительства, а также соответствующие профильные специальности, представленные в диссертационных советах профильных образовательных организациях высшего образования.

**Редакционная политика**. Политика редакционной коллегии журнала базируется на современных юридических требованиях в отношении авторского права, законности, плагиата и клеветы, изложенных в законодательстве Российской Федерации, и этических принципах, поддерживаемых сообществом ведущих издателей научной периодики.

*За публикацию статей плата с авторов не взымается. Публикация статей в журнале бесплатная.* На платной основе в журнале могут быть опубликованы материалы рекламного характера, имеющие прямое отношение к тематике журнала.

Журнал предоставляет непосредственный открытый доступ к своему контенту, исходя из следующего принципа: свободный открытый доступ к результатам исследований способствует увеличению глобального обмена знаниями.

**Индексирование**. Публикации в журнале входят в системы расчетов индексов цитирования авторов и журналов. «Индекс цитирования» – числовой показатель, характеризующий значимость данной статьи и вычисляющийся на основе последующих публикаций, ссылающихся на данную работу.

**Авторам**. Прежде чем направить статью в редакцию журнала, авторам следует ознакомиться со всеми материалами, размещенными в разделах сайта журнала (интернет-сайт Российской академии архитектуры и строительных наук (http://raasn.ru); подраздел «Издания РААСН» или интернет-сайт Издательства АСВ (http://iasv.ru); подраздел «Журнал IJCCSE»): с основной информацией о журнале, его целями и задачами, составом редакционной коллегии и редакционного совета, редакционной политикой, порядком рецензирования направляемых в журнал статей, сведениями о соблюдении редакционной этики, о политике авторского права и лицензирования, о представлении журнала в информационных системах (индексировании), информацией о подписке на журнал, контактными данными и пр. Журнал работает по лицензии Creative Commons типа cc by-nc-sa (Attribution Non-Commercial Share Alike) – Лицензия «С указанием авторства – Некоммерческая – Копилефт».

**Рецензирование**. Все научные статьи, поступившие в редакцию журнала, проходят обязательное двойное слепое рецензирование (рецензент не знает авторов рукописи, авторы рукописи не знают рецензентов).

**Заимствования и плагиат**. Редакционная коллегия журнала при рассмотрении статьи проводит проверку материала с помощью системы «Антиплагиат». В случае обнаружения многочисленных заимствований редакция действует в соответствии с правилами COPE.

**Подписка**. Журнал зарегистрирован в Федеральном агентстве по средствам массовой информации и охраны культурного наследия Российской Федерации. Индекс в общероссийском каталоге РОСПЕЧАТЬ − 18076.

По вопросам подписки на международный научный журнал “International Journal for Computational Civil and Structural Engineering (Международный журнал по расчету гражданских и строительных конструкций)” обращайтесь в Агентство «Роспечать» (Официальный сайт в сети Интернет: http://www.rosp.ru/) или в издательство Ассоциации строительных вузов (АСВ) в соответствии со следующими контактными данными:

*ООО «Издательство АСВ»*

Юридический адрес: 129337, Россия, г. Москва, Ярославское ш., д. 26, офис 705;

Фактический адрес: 129337, Россия, г. Москва, Ярославское ш., д. 19, корп. 1, 5 этаж, офис 12 (ТЦ Соле Молл);

Телефоны: +7 (925) 084-74-24;

Интернет-сайт: www.iasv.ru. Адрес электронной почты: iasv@iasv.ru.

**Контактная информация**. По всем вопросам работы редакции, рецензирования, согласования правки текстов и публикации статей следует обращаться к главному редактору журнала академику РААСН *Сидорову Владимиру Николаевичу* (адреса электронной почты: sidorov.vladimir@gmail.com, sidorov@iasv.ru, iasv@iasv.ru, sidorov@raasn.ru) или к техническому редактору журнала советнику РААСН *Кайтукову Таймуразу Батразовичу* (адреса электронной почты: tkaytukov@gmail.com; kaytukov@raasn.ru). Кроме того, по указанным вопросам, а также по вопросам размещения в журнале рекламных материалов можно обращаться к генеральному директору ООО «Издательство АСВ» *Никитиной Надежде Сергеевне* (адреса электронной почты: iasv@iasv.ru, nsnikitina@mail.ru, ijccse@iasv.ru).

**Журнал становится технологичнее**. Издательство АСВ с сентября 2016 года является членом Международной ассоциации издателей научной литературы (Publishers International Linking Association (PILA)), осуществляющей свою деятельность на платформе CrossRef. Оригинальным статьям, публикуемым в журнале, будут присваиваться уникальные номера (индексы DOI – Digital Object Identifier), что значительно облегчит поиск метаданных и местонахождение полнотекстового произведения. DOI – это система определения научного контента в сети Интернет.

С октября 2016 года стал возможен прием статей на рассмотрение и рецензирование через онлайн систему приема статей Open Journal Systems на сайте журнала (электронная редакция): https://ijccse.iasv.ru.

Автор имеет возможность следить за продвижением статьи в редакции журнала в личном кабинете Open Journal Systems и получать соответствующие уведомления по электронной почте.

В феврале 2018 года журнал был зарегистрирован в Directory of open access journals (DOAJ) (это один из самых известных поисковых сервисов в мире, который предоставляет открытый доступ к материалам и индексирует не только заголовки журналов, но и научные статьи), в сентябре 2018 года включен в продукты EBSCO Publishing.

В ноябре 2020 года журнал начал индексироваться в международной базе Scopus.

Журнал International Journal for Computational Civil and Structural Engineering входит в первый уровень Единого государственного перечня научных изданий – «Белого списка» – Министерства Науки и высшего образования Российской Федерации (ЕГПНИ)

*International Journal for*
# Computational Civil and Structural Engineering
**(Международный журнал по расчету гражданских и строительных конструкций)**
***Volume 21, Issue 3*** ***2025***

Scientific coordination is carried out by the Russian Academy of Architecture and Construction Sciences (RAACS)

## CONTENTS

**Stress Fields Near Earthquake Epicenters**
*Hydyr M. Saparliev, Sergey V. Kuznetsov* **14**

**Optimal Design of Timber-Frame Buildings**
*Tatiana L. Dmitrieva, Kristina A. Podshivalova, Alexander E. Botkhoev* **22**

**Bio-Resistant Cement Composites with Active Mineral Additive**
*Vladimir T. Yerofeev, Margarita A. Goncharova, Vasily.F. Smirnov, Alexander. I. Rodin, Alexander P. Volkov* **33**

**Solution to Filtration Problem with Linear Porosity Function**
*Galina L. Safina* **41**

**Warping Effect in a Steel Box Girder Bridge Structure**
*Trong Chuc Nguyen, Ba Thang Phung* **54**

**Automated Analysis of Electricity Consumption During Water Transportation Through a Pipeline After Its Renovation by Alternative Technologies with Consideration of Temperature Factor**
*Vladimir A. Orlov, Sergey P. Zotkin, Maria A. Bolshakova* **67**

**Deformation of Composite Shells Dilating Materials Beyond Elastic Limits**
*Alexander A. Treshchev* **80**

**Comprehensive Intellectual and Statistical Analysis of Water Consumption**
*Elena V. Ignatova, Elena Kh. Kitaytseva* **93**

**Analytical Evaluation of Base Control System Effectiveness for Regulation Seismic Response of Suspended Equipment Braced with Metal Frames by Hysteresis Dampers**
*Aleksandr M. Anushchenko* **105**

**Estimation of Resistance of Steel Frames with Rigid and Hinged Joints to Progressive Failure**
*Anatoly V. Alekseytsev, Valentina M. Tusnina* **121**

**Particle Transport with Finite Filtration Time** 135
*Liudmila I. Kuzmina, Yuri V. Osipov*

**Axisimmetric Fluid Motion in a Porous Medium in the Presence of a Non-Stationary External Source or Absorption** 148
*Yuri A. Chirkunov, Yuri L. Skolubovich, Mihail Yu. Chirkunov, Sergey V. Fedosov, Vladimir N. Sidorov, Evgeniy V. Alekseev*

**Hydrodynamic Loads on The Walls of a Turbine Block with a Counter Vortex Damper** 158
*Genrih V. Orehov, Andrey L. Zuykov, Mihail K. Sklyadnev*

**Choosing the Type of Shore Protection Structures in Reservoirs (Using the Example of the Novosibirsk Reservoir)** 172
*Tatiana V. Pilipenko, Dmitry V. Kozlov, Alexander Yu. Kudryashov, Vladimir V. Degtyarev, Anton S. Antonov, Alexander N. Yurchenko, Alexander S. Anshakov, Elena N. Guselnikova*

**Comparative Study of Earthquake-Resistant Building Design Standards** 188
*Dwi Yanto, Tavio*

**The modified method of sequential loads for the analysis of slender shallow shells** 201
*Vladilen V. Petrov, Olga A. Gorbacheva*

*International Journal for*
# Computational Civil and Structural Engineering
**(Международный журнал по расчету гражданских и строительных конструкций)**
***Volume 21, Issue 3*** ***2025***

Scientific coordination is carried out by the Russian Academy of Architecture and Construction Sciences (RAACS)

## СОДЕРЖАНИЕ

**Поля напряжений вблизи эпицентров землетрясений** **14**
*Х.М. Сапарлиев, С.В. Кузнецов*

**Оптимальное проектирование деревянных каркасных зданий** **22**
*Т.Л. Дмитриева, К.А. Подшивалова, А.Е. Ботхоев*

**Биостойкие цементные композиты с активной минеральной добавкой** **33**
*В.Т. Ерофеев, М.А. Гончарова, В.Ф. Смирнов, А.И. Родин, А.П. Волков*

**Решение задачи фильтрации с линейной функцией пористости** **41**
*Г.Л. Сафина*

**Эффект коробления в конструкции моста с коробчатой стальной балкой** **54**
*Нгуен Чонг Чык, Пхунг Ба Тханг*

**Автоматизированный анализ потребления электроэнергии с учетом температурного фактора при транспортировке воды по трубопроводу после его ремонта альтернативными технологиями** **67**
*В.А. Орлов, С.П. Зоткин, М.А. Большакова*

**Деформирование оболочек из композитных дилатирующих материалов за пределами упругости** **80**
*А.А. Трещев*

**Комплексный интеллектуально-статистический анализ водопотребления** **93**
*Е.В. Игнатова, Е.Х. Китайцева*

**Аналитическая оценка эффективности применения системы контроля перемещений (BCS) для регулирования сейсмического отклика подвешенного оборудования, раскрепленного упругопластическими демпферами с металлическими каркасами** **105**
*А.М. Анущенко*

**Оценка сопротивления прогрессирующему разрушению стальных рам с шарнирными и жесткими соединениями элементов** **121**
*А.В. Алексейцев, В.М. Туснина*

**Перенос частиц с конечным временем фильтрации** **135**
*Л.И. Кузьмина, Ю.В. Осипов*

**Осесимметричное движение жидкости в пористой среде при наличии нестационарного внешнего источника или поглощения** **148**
*Ю.А. Чиркунов, Ю.Л. Сколубович, М.Ю. Чиркунов, С.В. Федосов, В.Н. Сидоров, Е.В. Алексеев*

**Гидродинамические нагрузки на стенки турбинного блока с контрвихревым гасителем** **158**
*Г.В. Орехов, А.Л. Зуйков, М.К. Скляднев*

**Выбор типа берегоукрепительных сооружений на водохранилищах (на примере новосибирского водохранилища)** **1172**
*Т.В. Пилипенко, Д.В. Козлов, А.Ю. ,Кудряшов , В.В. Дегтярев, А.С. Антонов, А.Н. Юрченко, А.С. Аншаков, Е.Н. Гусельникова*

**Сравнительное исследование стандартов проектирования сейсмостойких зданий** **288**
*Дви Янто, Тавио*

**Особенности применения модифицированного метода последовательных нагружений при расчете гибких пологих оболочек** **201**
*В.В. Петров, О.А. Горбачева*

International Journal for Computational Civil and Structural Engineering, 21(3) 14–21 (2025)

DOI:10.22337/2587-9618-2025-21-3-14-21

# STRESS FIELDS NEAR EARTHQUAKE EPICENTERS

***Hydyr M. Saparliev*** [1]***, Sergey V. Kuznetsov*** [2]

[1] Turkmen State Architecture and Construction Institute, Ashgabat, TURKMENISTAN
[2] Moscow State University of Civil Engineering, Moscow, RUSSIA

**Annotation:** The closed form expressions for stress fields are derived. The analysis of stress fields reveals several phenomena, which may be essential for the design of seismic protection of underground structures, namely (i) infinite peaks in both pressure and second stress invariant at the arrival of Rayleigh wave at any points on the free surface; (ii) finite values of stress invariant fields at any of the undersurface points; and (iii) the presence of an infinite peak in the displacement magnitude

**Keywords:** Bulk wave, v. Mises equivalent stress, plastic dissipation energy; seismic source

# ПОЛЯ НАПРЯЖЕНИЙ ВБЛИЗИ ЭПИЦЕНТРОВ ЗЕМЛЕТРЯСЕНИЙ

***Х.М. Сапарлиев*** [1]***, С.В. Кузнецов*** [2]

[1]Туркменский государственный архитектурно-строительный институт, Ашхабад, Туркменистан
[2] Московский государственный строительный университет, Москва, Россия

**Аннотация:** Выведены выражения в замкнутой форме для полей напряжений. Анализ полей напряжений выявляет несколько явлений, которые могут быть существенными для проектирования сейсмозащиты подземных сооружений, а именно: (i) бесконечные пики как давления, так и второго напряжения, инвариантного при приходе волны Рэлея в любые точки на свободной поверхности; (ii) конечные значения полей инвариантов напряжений в любой из точек под поверхностью; и (iii) наличие бесконечного пика в величине смещения

**Ключевые слова:** объемная волна, эквивалентное напряжение Мизеса, диссипация энергии; сейсмический источник

## 1. INTRODUCTION

Both analytical and numerical solutions for stress and displacement fields in an isotropic linearly elastic halfspace loaded with a surface delta-like force normal to the plane boundary are constructed and analyzed. Analytical solutions for stress fields are derived apparently for the first time using the Cagniar – de Hoop method, developed for the construction of a displacement field in a halfspace.

Instead of analyzing individual stress components, stress invariants are analyzed, revealing several interesting phenomena, (i) both first and second stress invariants, together with the associated pressure and v.Mises equivalent stress are finite at the internal points of the halfspace; (ii) both pressure and the equivalent v.Mises stress tend to infinity when approaching the free surface at the moment of arrival of the Rayleigh wave; (iii) near the free surface the pressure field suddenly changes sign at the moment of arrival of the Rayleigh wave; (iv) at any time both pressure and equivalent v.Mises stress decrease exponentially with depth; and (v) everywhere in the halfspace both stress invariants remain finite at the moments of arrival of bulk waves. These observations and, in particular, the observed abrupt change in the sign of the pressure field at the arrival of

Rayleigh wave, are important for the development of seismic protection systems for undersurface structures, since at the appearance of negative pressure, the soil loses its bearing capacity, even if the equivalent v.Mises or Tresca criteria are small [1-18].

The outer plane Lamb problem of displacement field in a halfspace or halfplane loaded with a concentrated dynamic force applied to the plane boundary is most often solved by applying different analytical and numerical methods.

(A) The Cagniar – de Hoop method, used to invert Fourier and Laplace integral transforms and allowing to obtain the closed form solutions for displacement fields. Most of the works in this group are confined to deriving displacement fields on a free surface only, however, several works relate to the displacement fields in the whole halfspace, e.g.. It should also be noted that quite a large number of works in this group is concerned with the inner Lamb problem for a delta-like force acting inside the halfspace).

(B) Self-similar solutions, known also as the functionally-invariant solutions. This method is based on an analogy between plane or axisymmetric problems of the linear elasticity and the complex potential method. The method of self-similar solutions is mainly used for constructing solutions of the inner Lamb problem, however, some plane problems, including ones related to the moving cracks, can also be considered; see. Another remark concerns the application of the self-similar method to solving both inner and outer Lamb problems for an anisotropic halfspace.

(C) The construction of a 1D hyperbolic equation for the Rayleigh wave in a plane outer Lamb problem is suggested in, enabling to exclude vertical coordinate from the governing equation, but retaining it in the pseudo-differential operator acting on the applied surface load. In this regard see also.

(D) Finite element (FE) approaches are usually combined with either Lax – Wendroff energy preserving explicit numerical scheme or Godunov energy preserving explicit scheme for time integration, where Lamb problems were studied by FE coupled with Lax – Wendroff scheme. Other FE formulations include spectral finite element methods, allowing to considerably decreasing dispersion errors associated with the Runge phenomenon at solving Lamb problems.

(E) Finite difference (FD) schemes are used much less frequently compared to FE approaches. In [1-3] the outer and inner Lamb problems were studied by the FD approaches combined with Godunov type schemes for time-integration.

In summary, most of the reviewed publications are concerned with the analysis of the displacement fields at the free surface of a halfspace or half-plane. Meanwhile, the displacement and stress fields in the interior of the halfspace or half-plane, appears to be at least as important as the displacement field on the free surface, especially taking into account various undersurface structures affected by the arrival of technogenic seismic waves.

## 2. PRINCIPAL EQUATIONS

Equation of motion for a linearly-elastic medium can be written in the form

$$\left(c_1^2\nabla_{\mathbf{x}}\mathrm{div}_{\mathbf{x}} - c_2^2\mathrm{rot}_{\mathbf{x}}\,\mathrm{rot}_{\mathbf{x}} - \mathbf{I}\partial_{tt}^2\right)\cdot\mathbf{u}(\mathbf{x},t) = 0$$
$$x_2 \equiv \mathbf{x}\cdot\boldsymbol{\nu} < 0, \qquad t \geq 0 \tag{2.1}$$

where $\mathbf{u}$ is the displacement field; $\mathbf{x}$ is the spatial coordinate; $t$ is the time; $\mathbf{I}$ is the unit $3\times 3$-matrix; $\boldsymbol{\nu}$ is the unit outward normal to the plane boundary; and $c_1$, $c_2$ are respectively longitudinal and shear bulk wave velocities

$$c_1 = \sqrt{\frac{\lambda+2\mu}{\rho}}; \qquad c_2 = \sqrt{\frac{\mu}{\rho}} \tag{2/2}$$

Herein, $\lambda$, $\mu$ are Lame's constants

$$\lambda = \frac{E\nu}{(1-2\nu)(1+\nu)}; \qquad \mu = \frac{E}{2(1+\nu)} \tag{2.3}$$

where $E$ is Young's modulus; and, $\nu$ is Poisson's ratio.
The boundary plane is assumed to be traction-free, except one point, where a delta-like force is applied

$$\mathbf{t}_{\boldsymbol{\nu}}(\mathbf{x},t)\big|_{\mathbf{x}\in\Pi_{\nu}} = -P_0\delta\big(\mathbf{x}\cdot(\mathbf{k}\times\boldsymbol{\nu})\big)\delta(t)\boldsymbol{\nu} \quad (2.4)$$

where $\Pi_{\boldsymbol{\nu}}$ is the boundary plane; $\mathbf{k}\in\Pi_{\boldsymbol{\nu}}$ is a unit vector, specifying the direction of the applied line-load; and, $P_0$ is an amplitude multiplier. The initial conditions correspond to the state of rest:

$$\mathbf{u}(\mathbf{x},t)\big|_{t=0} = 0; \qquad \partial_t\mathbf{u}(\mathbf{x},t)\big|_{t=0} = 0\,. \quad (2.5)$$

Conditions (2.4) and (2.5) should be supplemented by the Sommerfeld radiation condition

$$\begin{aligned}
&\mathbf{u}(\mathbf{x},t)\big|_{\mathbf{x}\cdot\boldsymbol{\nu}\to-\infty} = 0;\\
&\nabla_{\mathbf{x}}\mathbf{u}(\mathbf{x},t)\big|_{\mathbf{x}\cdot\boldsymbol{\nu}\to-\infty} = 0\\
&\mathbf{u}(\mathbf{x},t)\big|_{|\mathbf{x}\cdot(\mathbf{k}\times\boldsymbol{\nu})|\to\infty} = 0;\\
&\nabla_{\mathbf{x}}\mathbf{u}(\mathbf{x},t)\big|_{|\mathbf{x}\cdot(\mathbf{k}\times\boldsymbol{\nu})|\to\infty} = 0
\end{aligned} \quad (2.6)$$

Following Cagniar – de Hoop method, the desired equations for the displacement field in a halfspace can be represented in the form

$$\mathbf{u}(\mathbf{x},t) = \frac{P_0}{\pi c_1\mu R(\xi)}\times\mathrm{Im}\big(\mathbf{p}(\mathbf{x},t)\big) \quad (0.1)$$

where functions the Rayleigh function)

$$R(\xi) = \left(\gamma^2 - 2\xi^2\right)^2 + 4\xi^2\sqrt{\left(\gamma^2-\xi^2\right)\left(1-\xi^2\right)} \quad (2.8)$$

Herein,

$$\begin{aligned}
&\gamma = \frac{c_1}{c_2} > 1; \qquad r = \sqrt{x_1^2 + x_2^2}\\
&x_1 = \mathbf{x}\cdot\big(\mathbf{k}\times\boldsymbol{\nu}\big); \qquad x_2 = \mathbf{x}\cdot\boldsymbol{\nu}
\end{aligned} \quad (2.9)$$

Equation (0.1) defines the displacement field everywhere in the considered halfspace.
Performing differentiation with respect to spatial variables in the infinitesimal Cauchy relations

$$\varepsilon(\mathbf{x},t) = \frac{1}{2}\Big(\nabla_{\mathbf{x}}\mathbf{u}(\mathbf{x},t) + \big(\nabla_{\mathbf{x}}\mathbf{u}(\mathbf{x},t)\big)^T\Big) \quad (0.2)$$

where $T$ means transposition, yields strain tensor. Now, Hooke's law with account of plane strain condition

$$\boldsymbol{\varepsilon}\cdot\cdot\,\mathbf{k}\otimes\mathbf{k} = 0 \quad (0.3)$$

where double dots mean convolution with respect to two indices, gives

$$\boldsymbol{\sigma}(\mathbf{x},t) = \lambda\mathrm{Tr}\big(\boldsymbol{\varepsilon}(\mathbf{x},t)\big)\mathbf{I} + 2\mu\boldsymbol{\varepsilon}(\mathbf{x},t) \quad (0.4)$$

The behavior of individual stress components is less interesting than the behavior of the corresponding stress invariants

$$\begin{aligned}
&I_\sigma = \mathrm{Tr}(\boldsymbol{\sigma}); \qquad II_\sigma = \frac{1}{2}\Big(\mathrm{Tr}(\boldsymbol{\sigma})^2 - \mathrm{Tr}(\boldsymbol{\sigma}\cdot\boldsymbol{\sigma})\Big)\\
&J_\sigma = \frac{I_\sigma^2}{3} - II_\sigma; \qquad III_\sigma = \det(\boldsymbol{\sigma})
\end{aligned} \quad (0.5)$$

where $J$ is second deviatoric invariant, from which the following two associated functions are of great importance in various applications

$$p = -\frac{I_\sigma}{3}; \qquad \sigma_i = \sqrt{3J_\sigma} \quad (0.6)$$

where $p$ is the pressure; and, $\sigma_i$ is the v.Mises equivalent stress.
Performing differentiation with respect to spatial variables in the infinitesimal Cauchy relations

$$\varepsilon(\mathbf{x},t) = \frac{1}{2}\Big(\nabla_{\mathbf{x}}\mathbf{u}(\mathbf{x},t) + \big(\nabla_{\mathbf{x}}\mathbf{u}(\mathbf{x},t)\big)^T\Big) \quad (0.7)$$

where $T$ means transposition, yields strain tensor. Now, Hooke's law with account of plane strain condition

$$\boldsymbol{\varepsilon} \cdot\cdot \mathbf{k} \otimes \mathbf{k} = 0 \tag{0.8}$$

where double dots mean convolution with respect to two indices, gives

$$\boldsymbol{\sigma}(\mathbf{x},t) = \lambda \mathrm{Tr}\left(\boldsymbol{\varepsilon}(\mathbf{x},t)\right)\mathbf{I} + 2\mu\boldsymbol{\varepsilon}(\mathbf{x},t) \tag{0.9}$$

The behavior of individual stress components is less interesting than the behavior of the corresponding stress invariants

$$\begin{aligned} I_\sigma &= \mathrm{Tr}(\boldsymbol{\sigma}); \qquad II_\sigma = \frac{1}{2}\left(\mathrm{Tr}(\boldsymbol{\sigma})^2 - \mathrm{Tr}(\boldsymbol{\sigma}\cdot\boldsymbol{\sigma})\right) \\ J_\sigma &= \frac{I_\sigma^2}{3} - II_\sigma; \qquad III_\sigma = \det(\boldsymbol{\sigma}) \end{aligned} \tag{0.10}$$

where $J$ is second deviatoric invariant, from which the following two associated functions are of great importance in various applications

$$p = -\frac{I_\sigma}{3}; \qquad \sigma_i = \sqrt{3J_\sigma} \tag{0.11}$$

where $p$ is the pressure; and, $\sigma_i$ is the v.Mises equivalent stress.

The invariant stress fields are shown in Fig. 1, 2 and 3.

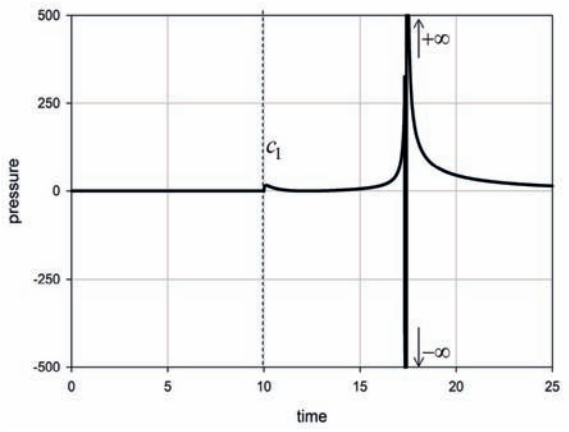


*a)*

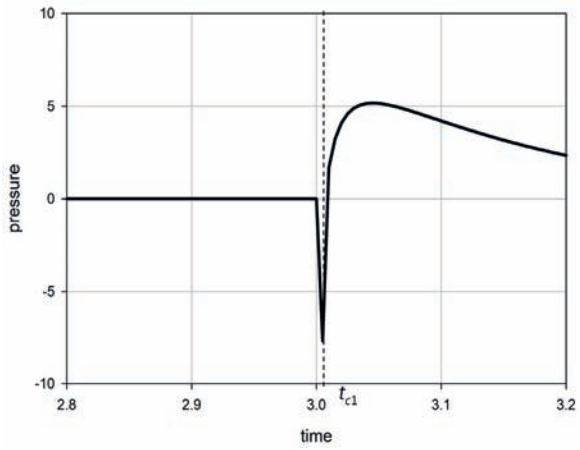


*b)*

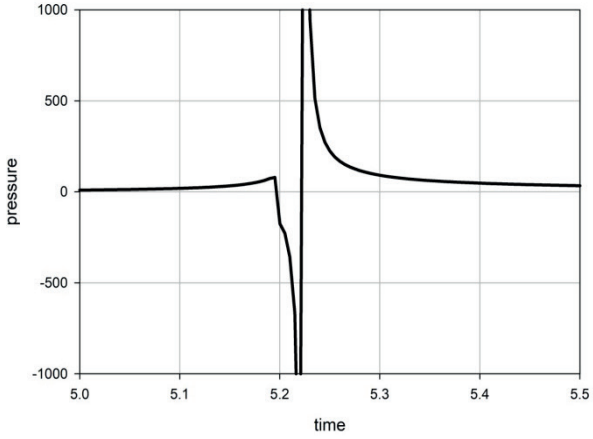


*c)*

*Figure 1. Pressure variation over time; a) overview; b) near P-wave arrival; c) near arrival of Rayleigh wave*

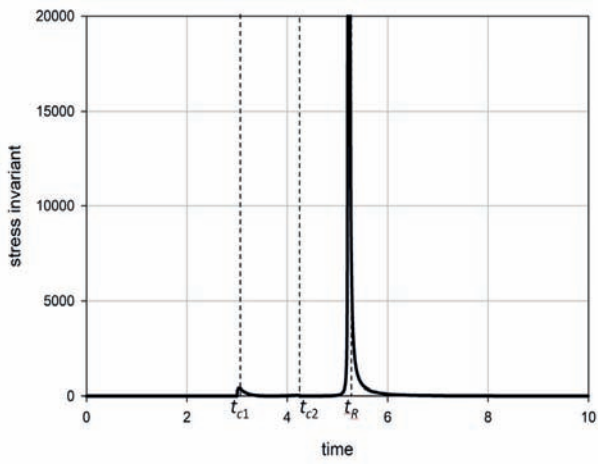


a)

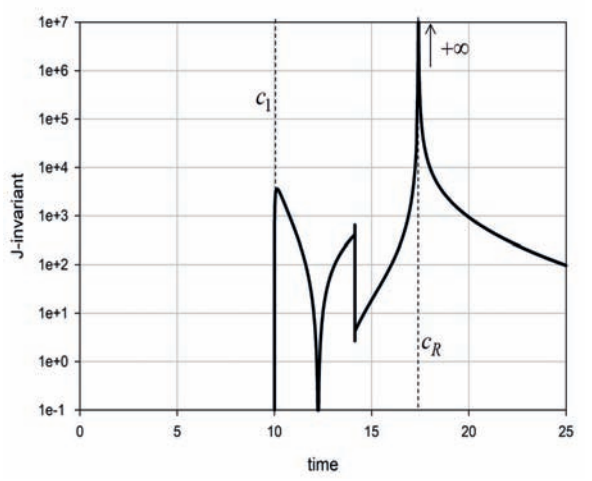


*b)*

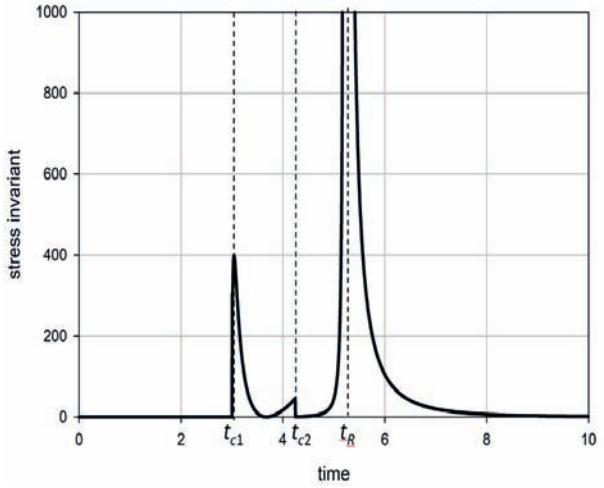


*c)*

*Figure 2. J-invariant stress field over time; a) overview; b) near P-wave arrival; c) near arrival of Rayleigh wave*

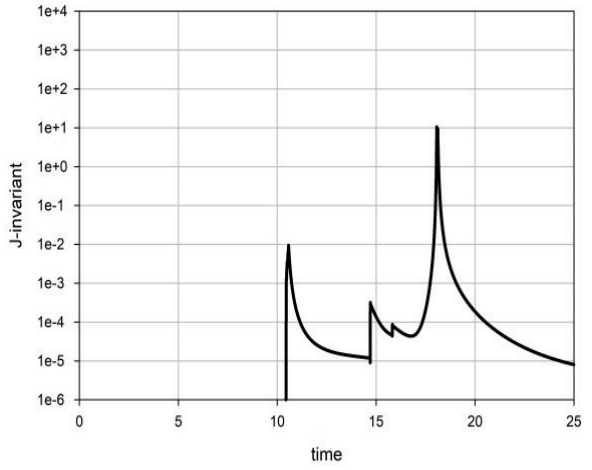


*Figure 3. The modified second invariant stress field over time: an overview*

These plots reveal,
(I) small peaks corresponding to the arrival of $P$-waves in both pressure and v.Mises equivalent stress, which is a square root of the second deviatoric invariant;
(II) infinite peaks related to the arrival Rayleigh waves at a point $\mathbf{x}_0$ located on the free surface; moreover,
(III) the pressure field exhibits a double discontinuity upon arrival of a Rayleigh wave;
(IV) the peaks associated with the arrival of Rayleigh waves, being finite at the inner points of the considered halfspace, still dominate over peaks associated with bulk waves, at least on depths not exceeding $\frac{1}{3}l$;
(V) the $J_\sigma$-invariant field and hence, the v.Mises equivalent stress, becomes infinite at the arrival of Rayleigh wave; and
(VI) at the inner points of the halfspace, the peak of the $J_\sigma$-invariant at the arrival of Rayleigh wave dominates over the peaks associated with bulk wave arrivals

## 3. CONCLUDING REMARKS

According to the obtained results, the outer Lamb problem for displacement and stress invariant fields caused by a vertical delta-like force, applied at the free surface, reveals several phenomena, some of which are observed apparently for the first time:
The displacement magnitude on the free surface exhibits an infinite discontinuity at the arrival of Rayleigh wave, while the arrival of the longitudinal $P$-wave produces a finite peak.
The displacement magnitudes in the inner points of the halfspace are finite, even at a close distance to the free surface; the peak associated with the arrival of Rayleigh wave dominates over bulk wave arrivals up to a depth $\frac{1}{3}l$.
The pressure field in the close vicinity of the free surface exhibits a double discontinuity upon arrival of a Rayleigh wave at $t \to t_R \pm 0$, where $t_R$ is the time of the Rayleigh wave arrival. Moreover, at

$t \to t_R - 0$, $p \to -\infty$, while at $t \to t_R + 0$, $p \to +\infty$. In the interior points of the halfspace the double peaks corresponding to the arrival of Rayleigh waves dominate over peaks related to bulk wave arrivals, at depths $\leq \frac{1}{3} l$. The appearance of infinite or large negative pressure values eventually means deterioration of soil properties.

The $J$-invariant field and the associated v.Mises equivalent stress defined by Eq. (0.6), reveal the infinite peak at the Rayleigh wave arrival and a finite peak associated with the arrival of bulk $P$-wave. Similarly to the preceding fields, at the inner points of the halfspace the peak associated with Rayleigh wave dominates over peaks related to the bulk waves, at least for the studied depths $\leq \frac{1}{3} l$.

The observed negative pressure values associated with the Rayleigh wave arrival, being extremely dangerous for soil and the undersurface structures, stipulates the necessity in developing specific methods of seismic protection, primarily against short-duration Rayleigh waves, which create large negative pressure. In this regard, widely used seismic barriers, which are mainly designed against relatively long-period harmonic Rayleigh waves producing no (or small) negative pressure, could hardly be used in the considered case of short-duration waves [18-24].

The observed infinite peaks of the pressure and deviatoric stress invariant, associated with the arrival of Rayleigh wave, stipulate the development of seismic barriers against Rayleigh waves, which should be filled with elastoplastic materials, obeying (i) low cohesion to achieve dissipation of the deviatoric strain energy, which is proportional to the -stress invariant; (ii) either a small or preferably vanishing angle of internal friction to ensure energy dissipation at high pressure values; and, (iii) equal acoustic impedances (or similar ) of the barrier material and the ambient soil for trapping wave energy within the barrier material, to prevent diffraction of Rayleigh wave into protected region; see [22-24] for heuristic suggestions on the construction of seismic barriers.

And the concluding remark concerns the assumed infinitesimality of strain fields, implying linear relations between displacement and strain fields. A natural extrapolation of these results could lead to applying both geometrically and physically nonlinear equations for finding displacement, strain and stress fields in the near epicenter regions.

**Acknowledgments**. The research of S.V.K. was funded by the Ministry of Science and Higher Education of RF, grant FSWG-2023-0004.

## REFERENCES

1. **Goodman, M.A. & Cowin, S.C.** A continuum theory for granular materials, Arch. Rational Mech. Anal., 1977, vol. 44, pp. 250-267.
2. **Li, S. et al.** Benchmark for three-dimensional explicit asynchronous absorbing layers for ground wave propagation and wave barriers, Comp. Geotech., 2021, Paper 103808.
3. **Li, S. et al.** Explicit/implicit multi-time step co-simulation in unbounded medium with Rayleigh damping and application for wave barrier, Eur. J. Environ. Civ. Eng., 2020, vol. 24, pp. 2400–2421.
4. **Terentjeva, E.O. et al.** Planar internal Lamb problem: Waves in the epicentral zone of a vertical power source, Acoust. Phys., 2015, vol. 61(3), pp. 356–367.
5. **Willis, J.R., & Bedding, R.J.** Arrivals associated with a class of self-similar problems in elastodynamics, Math. Proc. Cambridge Philos. Soc., 1975, vol. 77(3), pp. 591–607.
6. **Petrashen, G.I.** Propagation of seismic wave fields in layered media. Part I. General notions of the theory, *J. Math. Sci*., 2003, vol. 116(2), pp. 3077–3229.
7. **Ilyashenko, A.V. et al.** Theoretical aspects of applying Lamb waves in nondestructive testing of anisotropic media, Russ. J. Nondestruct. Test., 2017, vol. 53(4), pp. 243–259.

8. **Dudchenko, A.V. et al.** Vertical wave barriers for vibration reduction, Arch. Appl. Mech., 2021, vol. 91, pp. 257–276.
9. **Bedding, R.J., & Willis, J.R.** (1973) The dynamic indentation of an elastic half-space, J. Elast., 1973, vol. 3, pp. 289–309.
10. **Bedding, R.J., & Willis, J.R.** High speed indentation of an elastic half-space by conical or wedge-shaped indentors, J. Elast., 1976, vol. 6(2), pp. 195–207.
11. **Kostrov, B.V. & Das, S.** Principles of Earthquake Source Mechanics. Cambridge: Cambridge Univ. Press. 1975.
12. **Kuznetsov, S.V.** "Forbidden" planes for Rayleigh waves. Quart. Appl. Math., 2002, vol. 60, pp. 87–97.
13. **Hafeez, M.B. & Krawczuk, M.** A Review: Applications of the spectral finite element method, *Arch.* Computat. Meth. Eng., 2023, vol. 30, pp. 3453–3465.
14. **Kaplunov, J.D., Prikazchikov, D.A. & Sabirova, R.F.** On a hyperbolic equation for the Rayleigh wave, Dokl. Phys., 2022, vol. 67, pp. 424–427.
15. **Kuznetsov, S.** Smooth hyperelastic potentials for 1D problems of bimodular materials, Acta Mech., 2023, vol. 235, pp. 1–12.
16. **Clayton, J.D.** Universal phase-field mixture representation of thermodynamics and shock-wave mechanics in porous soft biologic continua, Phys. Rev. E, 2024, vol. 110, Paper 035001.
17. **Maslov, V.P. & Mosolov, P.P.** General theory of the solutions of the equations of motion of an elastic medium of different moduli, J. Appl. Math. Mech., 1985, vol. 49(3), pp. 322–336.
18. **Kuznetsov, S.** Love waves in nondestructive diagnostics of layered composites. Survey, Acoust. Phys., 2010, vol. 56, pp. 877–892.
19. **Pu, X., Palermo, A., & Marzani, A.** Lamb's problem for a half-space coupled to a generic distribution of oscillators at the surface, Int. J. Eng. Sci., 2021, vol. 168, Paper 103547.
20. **Rasulova, N.B.** A method of solving self-similar problems in membrane dynamics, J. Appl. Math. Mech., 2013, vol. 77, pp. 659–663.
21. **Kuznetsov, S.V.** Love waves in stratified monoclinic media, Quart. Appl. Math., 2004, vol. 62(4), pp. 749–766.
22. **Morozov, N. et al.** Seismic barriers for protection against surface and head waves: Multiple scatters and metamaterials, Mech. Solids, 2021, vol. 56, pp. 911–921.
23. **Sánchez-Sesma, F.J. et al.** A new closed analytical solution for the elastodynamic half-space Green's function, Earth Planets Space, 2023, vol. 75, Paper 29.
24. **Madsen, P.A. et al.** Uniform asymptotic approximations for transient waves due to an initial disturbance, J. Geophys. Res.: Oceans, 2015, vol. 121, pp. 60–84.

## СПИСОК ЛИТЕРАТУРЫ

1. **Goodman, M.A. & Cowin, S.C.** A continuum theory for granular materials, Arch. Rational Mech. Anal., 1977, vol. 44, pp. 250-267.
2. **Li, S. et al.** Benchmark for three-dimensional explicit asynchronous absorbing layers for ground wave propagation and wave barriers, Comp. Geotech., 2021, Paper 103808.
3. **Li, S. et al.** Explicit/implicit multi-time step co-simulation in unbounded medium with Rayleigh damping and application for wave barrier, Eur. J. Environ. Civ. Eng., 2020, vol. 24, pp. 2400–2421.
4. **Terentjeva, E.O. et al.** Planar internal Lamb problem: Waves in the epicentral zone of a vertical power source, Acoust. Phys., 2015, vol. 61(3), pp. 356–367.
5. **Willis, J.R., & Bedding, R.J.** Arrivals associated with a class of self-similar problems in elastodynamics, Math. Proc. Cambridge Philos. Soc., 1975, vol. 77(3), pp. 591–607.
6. **Petrashen, G.I.** Propagation of seismic wave fields in layered media. Part I. General notions of the theory, *J. Math. Sci*., 2003, vol. 116(2), pp. 3077–3229.

7. **Ilyashenko, A.V. et al.** Theoretical aspects of applying Lamb waves in nondestructive testing of anisotropic media, Russ. J. Nondestruct. Test., 2017, vol. 53(4), pp. 243–259.
8. **Dudchenko, A.V. et al.** Vertical wave barriers for vibration reduction, Arch. Appl. Mech., 2021, vol. 91, pp. 257–276.
9. **Bedding, R.J., & Willis, J.R.** (1973) The dynamic indentation of an elastic half-space, J. Elast., 1973, vol. 3, pp. 289–309.
10. **Bedding, R.J., & Willis, J.R.** High speed indentation of an elastic half-space by conical or wedge-shaped indentors, J. Elast., 1976, vol. 6(2), pp. 195–207.
11. **Kostrov, B.V. & Das, S.** Principles of Earthquake Source Mechanics. Cambridge: Cambridge Univ. Press. 1975.
12. **Kuznetsov, S.V.** "Forbidden" planes for Rayleigh waves. Quart. Appl. Math., 2002, vol. 60, pp. 87–97.
13. **Hafeez, M.B. & Krawczuk, M.** A Review: Applications of the spectral finite element method, *Arch.* Computat. Meth. Eng., 2023, vol. 30, pp. 3453–3465.
14. **Kaplunov, J.D., Prikazchikov, D.A. & Sabirova, R.F.** On a hyperbolic equation for the Rayleigh wave, Dokl. Phys., 2022, vol. 67, pp. 424–427.
15. **Kuznetsov, S.** Smooth hyperelastic potentials for 1D problems of bimodular materials, Acta Mech., 2023, vol. 235, pp. 1–12.
16. **Clayton, J.D.** Universal phase-field mixture representation of thermodynamics and shock-wave mechanics in porous soft biologic continua, Phys. Rev. E, 2024, vol. 110, Paper 035001.
17. **Maslov, V.P. & Mosolov, P.P.** General theory of the solutions of the equations of motion of an elastic medium of different moduli, J. Appl. Math. Mech., 1985, vol. 49(3), pp. 322–336.
18. **Kuznetsov, S.** Love waves in nondestructive diagnostics of layered composites. Survey, Acoust. Phys., 2010, vol. 56, pp. 877–892.
19. **Pu, X., Palermo, A., & Marzani, A.** Lamb's problem for a half-space coupled to a generic distribution of oscillators at the surface, Int. J. Eng. Sci., 2021, vol. 168, Paper 103547.
20. **Rasulova, N.B.** A method of solving self-similar problems in membrane dynamics, J. Appl. Math. Mech., 2013, vol. 77, pp. 659–663.
21. **Kuznetsov, S.V.** Love waves in stratified monoclinic media, Quart. Appl. Math., 2004, vol. 62(4), pp. 749–766.
22. **Morozov, N. et al.** Seismic barriers for protection against surface and head waves: Multiple scatters and metamaterials, Mech. Solids, 2021, vol. 56, pp. 911–921.
23. **Sánchez-Sesma, F.J. et al.** A new closed analytical solution for the elastodynamic half-space Green's function, Earth Planets Space, 2023, vol. 75, Paper 29.
24. **Madsen, P.A. et al.** Uniform asymptotic approximations for transient waves due to an initial disturbance, J. Geophys. Res.: Oceans, 2015, vol. 121, pp. 60–84.

---

*Hydyr M. Saparliev,* Candidate of Science, Docent, Turkmen State Architecture and Construction Institute, Baba Annanow köçesiniň, Ashgabat, 744025, Turkmenistan.

*Sergey V. Kuznetsov*, DSc, Professor, Department of Structural and Theoretical Mechanics, Moscow State unversity of Civil Enginnering, 26, Yaroslavskoye Shosse, Moscow, 129337, kuzn-sergey@yandex.ru, tel+7(495)583-79-04

*Хыдыр М. Сапарлиев*, кандидат технических наук, доцент, Туркменский государственный архитектурно-строительный институт, Ашгабат, 744025, Туркменистан

*Сергей В. Кузнецов*, доктор физико-математических наук, профессор кафедры Строительной и теоретической механики, Московский Государственный Строительный Университет, Ярославское ш., 26, Москва, 129337, Россия, kuzn-sergey@yandex.ru, тел+7(495)583-79-04

DOI:10.22337/2587-9618-2025-21-3-22-32

# OPTIMAL DESIGN OF TIMBER-FRAME BUILDINGS

***Tatiana L. Dmitrieva, Kristina A. Podshivalova, Alexander E. Botkhoev***

Irkutsk National Research Technical University, Irkutsk, RUSSIA

**Abstract.** The problem of optimal design of timber frame structures is addressed. A computational algorithm has been developed and tested for selecting the cross-sectional areas of structural elements to minimize material volume while satisfying code requirements for strength and stiffness. The mathematical model is formalized as a nonlinear programming problem and solved using a method based on a modified Lagrange function, which ensures a wide convergence region. The algorithm was implemented in the MathCAD software environment, ensuring clarity and making it accessible to design engineers. To verify the optimization results, validation calculations were performed using the Lira-Soft software (CAD system). The research results demonstrated the robust convergence of the developed algorithm and the high accuracy of the obtained solutions. A demonstration of its practical applicability is provided using an example of an actual frame structure.

**Keywords**: timber frame buildings; optimal design; Lagrangian function; nonlinear programming; finite-element analysis

# ОПТИМАЛЬНОЕ ПРОЕКТИРОВАНИЕ ДЕРЕВЯННЫХ КАРКАСНЫХ ЗДАНИЙ

***Т.Л. Дмитриева, К.А. Подшивалова, А.Е. Ботхоев***

Иркутский национальный исследовательский технический университет, Иркутск, РОССИЯ

**Аннотация:** Рассмотрена проблема оптимального проектирования деревянных каркасных сооружений. Разработан и апробирован вычислительный алгоритм, позволяющего подбирать площади поперечных сечений конструкций из условия минимума объем материала при соблюдении нормативных ограничений по прочности и жесткости. Математическая модель формализована в виде задачи нелинейного программирования, где использован метод на основе модификации функции Лагранжа, имеющий широкую область сходимости. Реализация алгоритма выполнена в среде пакета MathCAD, что обеспечивает его наглядность, делает его доступным и понятным для инженеров-проектировщиков. Для верификации результатов оптимизации проведен их поверочный расчет в ПК LIRA SOFT. Результаты исследования продемонстрировали устойчивую сходимость разработанного алгоритма и высокую точность полученных решений. Дана демонстрация его практической применимости на примере реальной каркасной конструкции.

**Ключевые слова:** деревянные каркасные здания, оптимальное проектирование, функция Лагранжа, нелинейное программирование, конечно-элементный анализ

## INTRODUCTION

In recent years, there has been a significant increase in interest in optimization methods for the design of timber structures. Research is focused on finding optimal shapes, cross-sectional dimensions, and element layout schemes that enable the minimization of material consumption and construction costs while ensuring the required strength and stiffness. For instance, studies [1-3] address the application of genetic algorithms for optimizing beams and trusses. In [4], methods for optimizing the geometry of timber frame structures using nonlinear finite-element analysis are considered. References [5-11] investigate the optimization of connections in timber structures, taking into account their flexibility and influence on overall load-bearing capacity.

Despite the progress achieved, existing optimization methods often face several limitations. Many require significant computational resources and are complex to implement in practice. Conse-

quently, there is a need to develop an efficient, transparent, and accessible tool for the optimal design of timber frame structures. Such a tool should account for the specific behavior of timber and allow design engineers to control each stage of the optimization process. This would enhance the competitiveness of timber construction and broaden its scope of application.

The objective of this research is the development and testing of a computational algorithm for the optimal design of timber frame structures, based on the application of the Lagrange function and its modification, and implemented within the MathCAD mathematical software environment. Unlike existing approaches, this algorithm aims to strike a balance between computational efficiency, transparency, and adaptability to specific design conditions.

The main stages of the research are as follows:

1. Development of a mathematical model for the optimal design of timber frame structures, incorporating code requirements for strength, stiffness, and stability.
2. Implementation of the computational design optimization algorithm within the MathCAD environment.
3. Testing of the developed algorithm using an example of an actual frame structure.
4. Assessment of the reliability of the optimal design through verification analysis using the LIRA-SOFT software.
5. Evaluation of the efficiency and practical applicability of the developed algorithm.

## 1. MATERIALS AND METHODS

The design calculation for timber frame structures is carried out under the criterion of minimum weight (or volume). In this formulation, the design problem can be posed as an optimization task, where the feasible domain of the structures is constrained by regulatory requirements for strength and stiffness. One of the most versatile and robust methods for optimal design employs a modified Lagrangian function, which serves to enlarge the convergence domain of the underlying algorithm [12]. The problem is thus cast as a nonlinear programming task, in which the design variables – here, the cross sectional areas of the members – are sought within prescribed bounds.

### Mathematical Model Used in the Optimization Problem

We present the mathematical model, formulated as a nonlinear programming problem

$$\text{Find} \quad \min f(x), \quad x \in E^{nx}, \tag{1}$$

subject to the following constraints:

$$g_j\left(x, P(x)\right) \le 0, \quad j = 1,2,...m, \tag{2}$$

$$x_i^L \le x_i \le x_i^U, \quad i = 1,2,...nx. \tag{3}$$

Here $f(x)$ – is the objective function (the volume or weight of the structure under consideration);

$\{X\}$ – is the vector of unknown (or design) variables over the interval $\{X^L\}$-$\{X^U\}$ (the cross-sectional parameters of the elements);

$nx$ – is the number of these variables;

$g_j(x)$ – are the constraint functions for strength, stiffness, and stability, $j=1,..., m$;

$P(x)$ – denotes the state parameters of the system (displacements and internal forces developing in the structure), which depend on the design variables $x$,

$\{P(x)\} = \psi(\{\delta(x)\}, (S(x)\})$, here,

$\{\delta_i(x)\}^T = \{u_i(x)\ v_i(x)\ w_i(x)\ \varphi_{xi}(x)\ \varphi_{yi}(x)\ \varphi_{zi}(x)\}$ – displacement vector at node $i$ of the FE model in 3D space $(x,y,z)$;

$\{S_k(x)\}^T = \{N_k(x)\ \ Q_{yk}(x)\ \ Q_{zk}(x)\ \ M_{xk}(x)\ \ M_{yk}(x)\ M_{zk}(x)\}$ – internal force vector at section $k$ of the spatial $FE$ model.

The equilibrium (state) equation of the system in terms of the nodal displacements is given by:

$$[K(x)]\ \{\delta(x)\} = \{F\},$$

where $[K(x)]$ – is the stiffness matrix of the system; $\{F\}$ – is the vector of external loads.

For a spatial pin-jointed truss system:

$$\{\delta_i(x)\}^T = \{u_i(x)\ v_i(x)\ w_i(x)\},$$
$$\{s_k(x)\}^T = \{N_k(x)\}.$$

The most resource-intensive are the constrained extremum solver module and the finite-element analysis module.

To solve the constrained optimization problem, we will use the Lagrangian function $F_L$

$$F_L = f(x) + \{Y\}^T[\delta]\{g\}. \qquad (4)$$

Here $\{Y\}$ – is the vector of Lagrange multipliers; $[\delta]$ – is a diagonal matrix of Boolean variables, where $\delta_{jj}$ =1, if $j \in M_{ПА}$, and $\delta_{jj}$ =0 otherwise, where $M_{ПА}$ – denotes the set of potentially active constraints.

To expand the convergence domain of the search algorithm, we introduce a modification of the Lagrangian function, denoted as *Fp*:

$$FP = k_f F_L + 0{,}5\{g\}^T[\delta][k]\{g\}, \qquad (5)$$

The search algorithm for solving problem (1–3) includes two main operations at each iteration: searching for the parameter set $\{X\}$ by minimizing the modified Lagrangian function *Fp* and updating the dual variables $\{Y\}$, which are determined from the stationarity condition of the Lagrangian function $F_L$ and the modified function *Fp* with respect to *X*:

$$y_j^{t+1} = \max\left(0, y_j^t + \frac{k_{jj}^t}{k_f^t} g^*\left(X^{t+1}\right)\right). \qquad (6)$$

In expression (5), [k] – is the penalty coefficients matrix, and $k_f$ – is the scaling factor for the Lagrange function. Figure 1 shows a flowchart of the sequence of operations within the iterations of the search algorithm, a full description of which is given in [12].

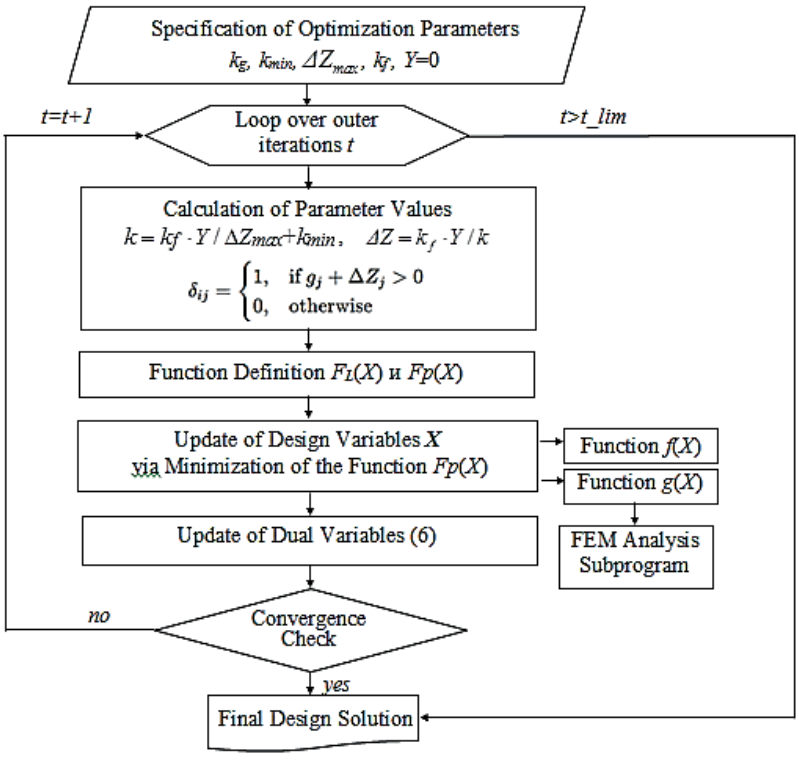


*Figure 1. Flowchart of the sequence of computational operations during the iterations*

If the structure is statically indeterminate, determining the cross-sectional parameters at each iteration requires recalculating internal forces and displacements by invoking the *FE* analysis subprogram. In this subprogram, the stiffness matrix is assembled using the system's equilibrium matrix [*A*] and flexibility matrix [*B*].

$$[K]=[A][B]^{-1}[A]^{T}$$

Consequently, if node positions are not varied, the equilibrium matrix [*A*] requires no reassembly during the iterative process. The iteration exit criteria at step t are:

$$\left|X^{t+1}-X^{t}\right|\le\varepsilon_{x}\left|X^{t}\right|,\qquad \left|\overline{g}\right|\le\varepsilon_{g}, \tag{7}$$

where $\left|\overline{g}\right|$ – is the set of potentially active constraints; $\varepsilon_x$, $\varepsilon_g$ – denote specified convergence tolerances.

Let us consider the specifics of implementing this algorithm in the MathCAD software environment. The minimization of the modified Lagrangian function *Fp*(*X*) is performed using the methods embedded in this package. The automatic termination is controlled by the user according to condition (7).

This approach to the solution offers several advantages: the sequence of operations is clear and logically structured, the algorithm can be reproduced without programming skills, and its implementation only requires knowledge of MathCAD operation principles [13].

**Example of frame optimization in the MATHCAD system**

To verify the functionality and reliability of the optimization method, a sample problem of optimal design for a 36-bar timber frame structure was solved. The task requires selecting cross-sectional areas for elements of the timber frame structure shown in Figure 2, where the structure is displayed with coordinate axes

Input data: *d*=3 m, *h*=3 m. The material is Grade 1 pine, with an elastic modulus along the grain *E* = 10000 MPa, allowable compressive strength $R_c$ =13,365 MPa, and allowable tensile strength $R_t$ =8 MPa.

Two loading cases are specified (see Figure 3):

- first case: force *P* = 25 kN applied in the directions of the *x, y, z* axes at node 1;
- second case: force: *P* = 25 kN applied in the negative *z*-direction at nodes 1, 2, 3, and 4.

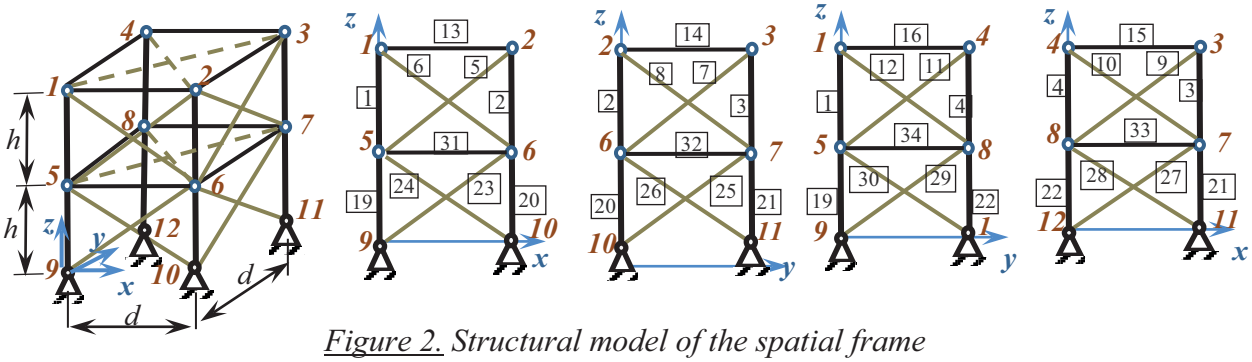


*Figure 2. Structural model of the spatial frame*

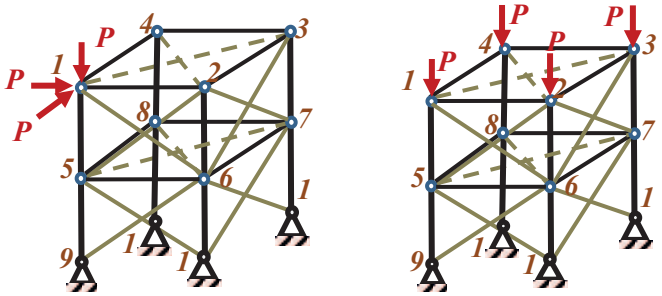


*Figure 3. First and second loading cases*

The structural elements are grouped by cross-sectional types, as shown in Table 1. On each floor, four types of elements are considered: 4 columns, 8 braces, 4 beams, and 2 horizontal ties.

*Table 1. Distribution of cross-sectional areas ($A_i$) of elements by groups*

| Variation parameters | | | | | | | |
|---|---|---|---|---|---|---|---|
| $x_1$ | $x_2$ | $x_3$ | $x_4$ | $x_5$ | $x_6$ | $x_7$ | $x_8$ |
| $A_1$:$A_4$ | $A_5$:$A_{12}$ | $A_{13}$:$A_{16}$ | $A_{17}$:$A_{18}$ | $A_{19}$:$A_{22}$ | $A_{23}$:$A_{30}$ | $A_{31}$:$A_{34}$ | $A_{35}$:$A_{36}$ |

*The cross-sectional areas in each group* were varied within the range of 6 to 90 cm$^2$.
The objective is *to minimize* the structure's volume

$$f = \sum_{k=1}^{nel} A_k l_k$$

where *nel* = 36; $A_k$ , $l_k$ – are the cross-sectional area and length of the *k*-th element.
The following constraint functions are adopted.
The strength check for the *i*-th group of structural cross-section types (8 constraints) is carried out according to the formulas of *«СП 64.13330.2017 Деревянные конструкции»*.

For compressed elements

$$g_i = \frac{|N_i|}{\varphi \cdot x_i \cdot R_c} - 1 \le 0,$$

For tensioned elements

$$g_i = \frac{N_i}{x_i \cdot R_t} - 1 \le 0.$$

Here, $x_i$ – is the design variable, $N_i$ – is the design axial force for the most heavily loaded member in the *i*-th group (taken as the maximum force from the two loading cases). $\varphi$ - is the buckling reduction factor, calculated per Formulas (13–16) of «*СП 64.13330.2017*».
For structural members satisfying $\lambda < 70$

$$\varphi = 1 - 0{,}8\left(\frac{\lambda}{100}\right)^2.$$

For structural members satisfying $\lambda > 70$

$$\varphi = \frac{3000}{\lambda^2}, \quad \text{where}$$

$$\lambda = \frac{l}{r}, \quad r = \sqrt{\frac{A_s}{12}}.$$

The stiffness check is based on the maximum displacement, which occurs at node 1. Therefore, one constraint from the first loading case along the *x-axis* is considered.

$$g_9 = \frac{\delta_1}{[\Delta]} - 1 \le 0. \qquad [\Delta]=1{,}4 \text{ cm}.$$

**Solution.** Computational operations during iterations of the search algorithm are illustrated in Figure 1. The minimization problem for function *Fp* was solved using built-in MathCAD methods:

- Levenberg-Marquardt method;
- Conjugate gradient method;
- Quasi-Newton method.

The program automatically switches between these methods until convergence is achieved by one of them.

## 2. RESULTS AND DISCUSSION

Optimization results (Figure 4) provide the cross-sectional areas for each member group in the frame structure.

*Figure 4. Optimization results*

| *Optimal parameters (cm²)* | |
|---|---|
| 1 | 74,46636995 |
| 2 | 88,78768792 |
| 3 | 42,26213826 |
| 4 | 78,17657518 |
| 5 | 82,57623377 |
| 6 | 78,06506049 |
| 7 | 6 |
| 8 | 6 |

| *Stress constraint thresholds* | |
|---|---|
| 1 | -3,89058E-08 |
| 2 | 1,78E-07 |
| 3 | 2,14E-07 |
| 4 | -1,03054E-06 |
| 5 | -1,06004E-06 |
| 6 | 3,09E-07 |
| 7 | -0,51288 |
| 8 | -0,51288 |

| *Displacement constraint at Node 1* |
|---|
| -0,76425 |

Analysis of constraint functions reveals that strength constraints for the first five member groups are active (critical).

Convergence plots for both the objective function and constraint functions across iterations are presented in Figure 5. The iterative cycle terminated based on condition (7). The constraint residuals demonstrated high precision ($10^{-7}$). The optimization yielded a final objective function value of $8.84109 \times 10$ cm$^3$.

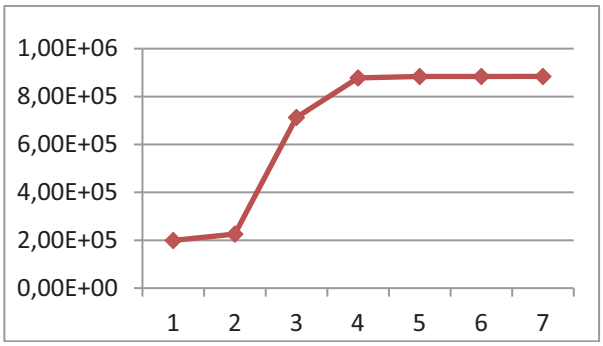


*Figure 5. Objective function evolution during iterations*

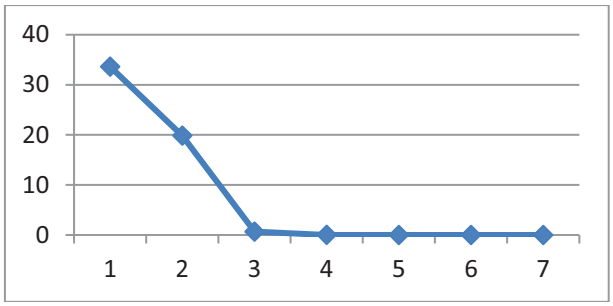


*Figure 6. Evolution of maximum constraint residuals during iterations*

To verify the calculation results, we will compute *the complete* vector of strength and stiffness constraints in the MathCAD program, where the obtained solution is checked. The cross-sectional area parameters here are taken from the optimization program..

Analysis of the obtained values shows that the strength constraints are active for second-floor columns under loading case 2. For all other element groups, the constraints are active under loading case 2. For first-floor beams and bracing elements, the constraints are satisfied with a safety margin.

*Table 2. Strength Verification*

| | | Elements | Loading Case 1 | Loading Case 2 |
|---|---|---|---|---|
| **Floor 2** | **Columns** | **1** | -0,791 | **-3,90E-08** |
| | | **2** | -0,966 | **-3,90E-08** |
| | | **3** | -0,415 | **-3,90E-08** |
| | | **4** | -0,966 | **-3,90E-08** |
| | **Braces** | **5** | -0,907 | -0,787 |
| | | **6** | **1,78E-07** | -0,787 |
| | | **7** | -0,88 | -0,787 |
| | | **8** | -0,617 | -0,787 |
| | | **9** | -0,617 | -0,787 |
| | | **10** | -0,88 | -0,787 |
| | | **11** | -0,907 | -0,787 |
| | | **12** | **1,78E-07** | -0,787 |
| | **Beams** | **13** | **2,15E-07** | -0,972 |
| | | **14** | -0,941 | -0,972 |
| | | **15** | -0,941 | -0,972 |
| | | **16** | **2,15E-07** | -0,972 |
| | **Bracings** | **17** | **-1,03E-06** | -0,972 |
| | | **18** | -0,956 | -0,972 |
| **Floor1** | **Columns** | **19** | -0,77 | -0,153 |
| | | **20** | -0,752 | -0,153 |

| | | | | |
|---|---|---|---|---|
| | | **21** | **-1,06E-06** | -0,153 |
| | | **22** | -0,752 | -0,153 |
| | **Braces** | **23** | -0,791 | -0,777 |
| | | **24** | -0,365 | -0,777 |
| | | **25** | -0,939 | -0,777 |
| | | **26** | **3,09E-07** | -0,777 |
| | | **27** | **3,09E-07** | -0,777 |
| | | **28** | -0,939 | -0,777 |
| | | **29** | -0,791 | -0,777 |
| | | **30** | -0,365 | -0,777 |
| | **Beams** | **31** | -0,946 | -0,513 |
| | | **32** | -0,763 | -5,13E-01 |
| | | **33** | -0,763 | -5,13E-01 |
| | | **34** | -0,946 | -0,513 |
| | **Main** | **35** | -0,956 | -0,513 |
| | | **36** | -0,753 | -0,513 |

The stiffness constraints are satisfied with significant safety margins for both loading cases.

**Verification Analysis of Spatial Frame in LIRA-SOFT Software**

Using the selected cross-sections, a verification analysis was performed in LIRA-SOFT software (Figs. 7, 8). The internal forces obtained in LIRA-SOFT and MathCAD calculations showed complete agreement. The results confirm the correctness of the finite element analysis implementation within the optimization algorithm.

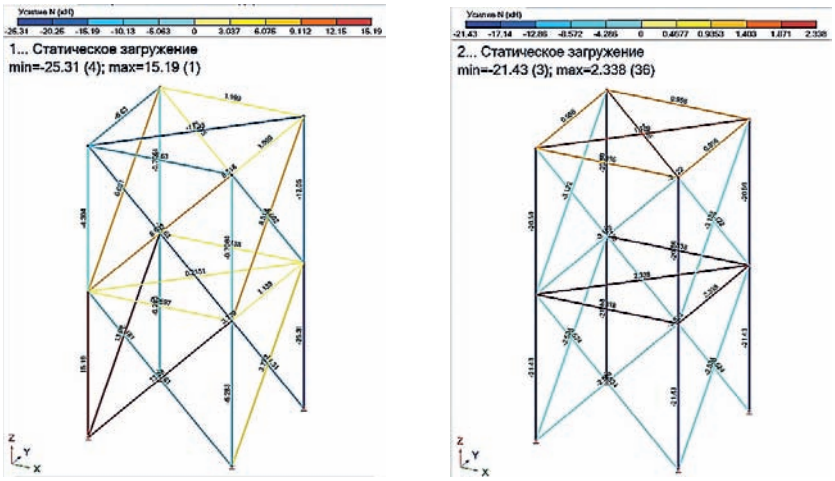


*Figure 7. Internal forces from Loading Cases 1 and 2 in LIRA-SOFT*

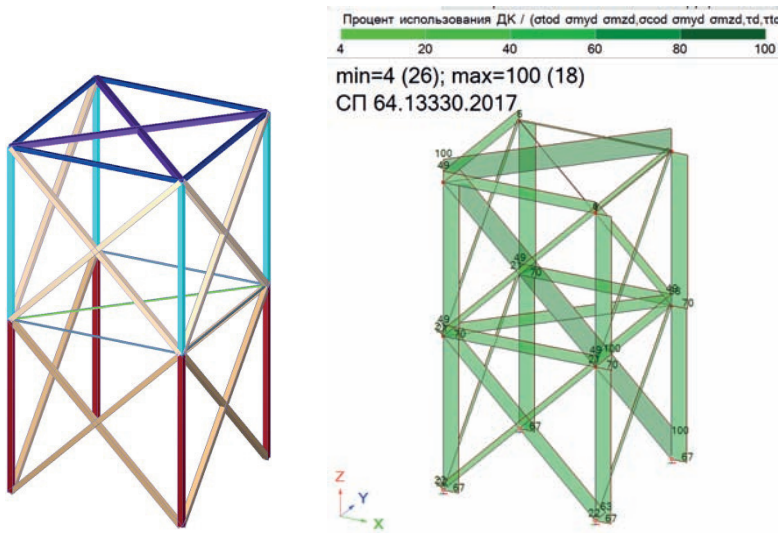


*Figure 8. Original Frame Model and Section Utilization Percentage in LIRA-SOFT*

An optimal design of a spatial timber frame has been obtained, with the optimization algorithm demonstrating stable convergence and high accuracy of results.

Factors affecting algorithm performance: structure size (number of members, nodes); degree of static indeterminacy; computer processing power; efficiency of finite element analysis implementation in MathCAD; choice of optimization method.

*Advantages*:

- Clear and logically transparent algorithm
- Implementation possible without specialized programming skills (basic MathCAD knowledge sufficient)
- Easy modification and adaptation to specific problems

*Limitations*:

- No automatic iteration exit (requires user monitoring) - inconvenient for large/complex problems
- Potentially lower performance compared to specialized optimization software
- Limited MathCAD functionality
- Implementation simplicity: relatively easy for MathCAD users, but lack of automation may hinder non-specialists
- Scalability: performs poorly for very large structures due to FEA computational complexity and lack of automated optimization

The timber material's influence on optimization algorithm development should be noted. The algorithm accounted for these parameters: design compressive strength, design tensile strength, and elastic modulus. Strength, stiffness, and stability verifications were completed.

However, comprehensive efficiency evaluation requires testing on more examples with variations in structure size, geometry, and loading conditions. Also necessary is comparing algorithm runtime against other known frame structure optimization algorithms.

## CONCLUSION

An optimization algorithm for designing frame structures has been developed and implemented in the MathCAD environment. The algorithm combines the finite element method for analyzing structural stress-strain states with a modified Lagrange function minimization method to determine optimal cross-sectional areas while satisfying strength, stiffness, and stability constraints.

The key advantage of this approach is its transparency and accessibility, enabling engineers with basic MathCAD knowledge to understand and control the optimization process, unlike complex commercial packages that function as "black boxes." Experimental results for a 36-bar structure demonstrated the algorithm's functionality.

However, it should be noted that the algorithm's performance is constrained by MathCAD's capabilities. The complexity of finite element analysis makes it unsuitable for optimizing large and complex structures within reasonable timeframes. Moreover, the need for manual convergence monitoring requires user expertise and may significantly increase design time.

Despite these limitations, the developed algorithm can be valuable for teaching structural optimization fundamentals to students and engineers, as well as for solving small-scale problems where transparency and manual adjustment capabilities are essential.

Future research should focus on improving this optimization algorithm, for example by automating the convergence process. Additionally, more extensive experimental studies are necessary to evaluate the algorithm's effectiveness across various timber structure types and compare it with existing approaches.

## REFERENCES

1. **Elbakry, H.M.F., Tarabia, M.A., & Diab, M.A.** Optimum design of reinforced concrete continuous beam and slab systems using genetic algorithms // Journal of Engineering and Applied Sciences. 2025. Vol. 72, No. 39. https://doi.org/10.1186/s44147-025-00597-w

2. **Etaati, B., Neshat, M., Abdollahi Dehkordi, A., Salami Pargoo, N., El-Abd, M., Sadollah, A., & Gandomi, A.H.** Shape and sizing optimisation of space truss structures using a new cooperative coevolutionary-based algorithm. // Results in Engineering. 2024. Vol. 21, 101859 p. https://doi.org/10.1016/j.rineng.2024.101859
3. **Kassem, R., Khalil, M., El Hayek, S., Ghannam, N., Hamdan, M., & Harb, A.** Unveiling the power of big data analytics in supply chain management: A comprehensive review // Digital Applications in Supply Chain Management. 2023. 100266 p. https://doi.org/10.1016/j.dajour.2023.100266
4. **Nicaise, A., Maier, G., De Donato, O., & Comi, M.** A finite element analysis of elastic-plastic scaled structures // Computers & Structures. 1984. Vol. 19, No. 5-6. pp. 571-580. https://doi.org/10.1016/0045-7949(84)90161-5
5. **Daneshvar, H., Cheshmehkaboodi, N., Qi, B., Chui, Y. H.** Enhanced particle swarm optimisation technique for parametrising the hysteresis response in wooden dowel-type connections // Structures. 2025. Vol. 79, 109312 p. https://doi.org/10.1016/j.istruc.2025.109312
6. **Seikot P., Aloisi A., Obradovic V., Iqbal A.** Experimental, finite element, and analytical characterization of the hysteresis response of ductile connections with pinned angle brackets for mass timber structures // Canadian Journal of Civil Engineering. 2024. Vol. 51, No. 7. pp. 803-811. https://doi.org/10.1139/cjce-2023-0394
7. **Huang Y., Ruan A., Yong Y., Su Y., Jin G., Xu H.** The influence of icing on the stress-strain behavior of concrete under uniaxial compression // Construction and Building Materials. 2013. Vol. 48. pp. 38-44. https://doi.org/10.1016/j.conbuildmat.2012.11.068
8. **Sukumar P., Alawadhi E., Mohammadi A., Colombo J., Ghanbari M., Moin U**. Investigating the mechanical properties of eco-friendly concrete incorporating palm oil fuel ash and ground granulated blast-furnace slag // Construction and Building Materials. 2021. Vol. 297. 123112 p. https://doi.org/10.1016/j.conbuildmat.2021.123112
9. **Li Y., Liu Y., Zhang X., Ma Y., Wang Y.** Seismic performance of reinforced concrete frame structures with low strength concrete in beam. Engineering Structures. 2020. Vol. 223. 110692 p. https://doi.org/10.1016/j.engstruct.2020.110692
10. **Xiao, Feng, Xiangwei Meng, Weiwei Zhu, Gang S. Chen, and Yu Yan**. Combined Joint and Member Damage Identification of Semi-Rigid Frames with Slender Beams Considering Shear Deformation // Buildings. 2023. Vol. 13. No. 7. 1631 p. https://doi.org/10.3390/buildings13071631
11. **Dmitrieva, T. L., Podshivalova, K. A., Molchanov, D. O., & Beloborodov, K. M.** Current approaches to the modeling and calculation of wood-frame buildings, accounting for the interaction of frame load-bearing elements and cladding // IOP Conference Series: Earth and Environmental Science. 2021. Vol. 751. No. 1. 12089 p.
12. **Dmitrieva T.L.** Parametric optimization in the design of structures subject to static and dynamic impact: monograph. Irkutsk: Irkutsk State Technical University, 2010, 176 p.
13. **Herhager, M. (2000).** MathCad 2000: The Complete Guide. BHV.

## СПИСОК ЛИТЕРАТУРЫ

1. **Elbakry, H.M.F., Tarabia, M. A., & Diab, M.A.** Optimum design of reinforced concrete continuous beam and slab systems using genetic algorithms // Journal of Engineering and Applied Sciences. 2025. Vol. 72, No. 39. https://doi.org/10.1186/s44147-025-00597-w
2. **Etaati, B., Neshat, M., Abdollahi Dehkordi, A., Salami Pargoo, N., El-Abd, M., Sadollah, A., & Gandomi, A.H.** Shape and sizing optimisation of space truss struc-

tures using a new cooperative coevolutionary-based algorithm. // Results in Engineering. 2024. Vol. 21, 101859 p. https://doi.org/10.1016/j.rineng.2024.101859
3. **Kassem, R., Khalil, M., El Hayek, S., Ghannam, N., Hamdan, M., & Harb, A.** Unveiling the power of big data analytics in supply chain management: A comprehensive review // Digital Applications in Supply Chain Management. 2023. 100266 p. https://doi.org/10.1016/j.dajour.2023.100266
4. **Nicaise, A., Maier, G., De Donato, O., & Comi, M.** A finite element analysis of elastic-plastic scaled structures // Computers & Structures. 1984. Vol. 19, No. 5-6. pp. 571-580. https://doi.org/10.1016/0045-7949(84)90161-5
5. **Daneshvar, H., Cheshmehkaboodi, N., Qi, B., Chui, Y. H.** Enhanced particle swarm optimisation technique for parametrising the hysteresis response in timber dowel-type connections // Structures. 2025. Vol. 79, 109312 p. https://doi.org/10.1016/j.istruc.2025.109312
6. **Seikot P., Aloisi A., Obradovic V., Iqbal A.** Experimental, finite element, and analytical characterization of the hysteresis response of ductile connections with pinned angle brackets for mass timber structures // Canadian Journal of Civil Engineering. 2024. Vol. 51, No. 7. pp. 803-811. https://doi.org/10.1139/cjce-2023-0394
7. **Huang Y., Ruan A., Yong Y., Su Y., Jin G., Xu H.** The influence of icing on the stress-strain behavior of concrete under uniaxial compression // Construction and Building Materials. 2013. Vol. 48. pp. 38-44. https://doi.org/10.1016/j.conbuildmat.2012.11.068
8. **Sukumar P., Alawadhi E., Mohammadi A., Colombo J., Ghanbari M., Moin U**. Investigating the mechanical properties of eco-friendly concrete incorporating palm oil fuel ash and ground granulated blast-furnace slag // Construction and Building Materials. 2021. Vol. 297. 123112 p. https://doi.org/10.1016/j.conbuildmat.2021.123112
9. **Li Y., Liu Y., Zhang X., Ma Y., Wang Y.** Seismic performance of reinforced concrete frame structures with low strength concrete in beam. Engineering Structures. 2020. Vol. 223. 110692 p. https://doi.org/10.1016/j.engstruct.2020.110692
10. **Xiao, Feng, Xiangwei Meng, Weiwei Zhu, Gang S. Chen, and Yu Yan**. Combined Joint and Member Damage Identification of Semi-Rigid Frames with Slender Beams Considering Shear Deformation // Buildings. 2023. Vol. 13. No. 7. 1631 p. https://doi.org/10.3390/buildings13071631
11. **Dmitrieva T. L., Podshivalova K. A., Molchanov D. O., Beloborodov K. M.** Current approaches to the modeling and calculation wood frame building, taking into account the joint work of the load-bearing elements of the frame and cladding // IOP Conference Series: Earth and Environmental Science, Volume 751, 2021, No. 1, p. 12089
12. **Дмитриева Т.Л.** Параметрическая оптимизация в проектировании конструкций, подверженных статическому и динамическому воздействию**:** монография. Иркутск: ИрГТУ, 2010, 176 с.
13. **Херхагер М. MathCad 2000**. Полное руководство. — BHV, 2000. — 416 с.

*Tatiana Lvovna Dmitrieva* - Doctor of Technical Sciences, Professor of the Department of Mechanics and Resistance of Materials, Federal State Budget Educational Institution of Higher Education «Irkutsk National Research Technical University» (INRTU), 83, Lermontov str., Irkutsk, 664074, Russia, dmitrievat@list.ru

*Татьяна Львовна Дмитриева* - д.т.н., зав. кавф. кафедры «Механика и сопротивление материалов», Федеральное государственное бюджетное образовательное учреждение высшего образования «Иркутский национальный исследовательский технический университет» (ФГБОУ ВО «ИРНИТУ»), 83, ул. Лермонтова, г. Иркутск, 664074, Россия, dmitrievat@list.ru

*Podshivalova Kristina Aleksandrovna* - Postgraduate student of the Center for Software Engineering, Senior Lecturer of the Department "Construction Production", Federal State Budget Educational Institution of Higher Education «Irkutsk National Research Technical University» (INRTU), 83, Lermontov str., Irkutsk, 664074, Russia, 1295536@mail.ru

*Botkhoev Alexander Evgenievich* - Department of Mechanics and Strength of Materials, Federal State Budget Educational Institution of Higher Education «Irkutsk National Research Technical University» (INRTU), 83 Lermontov Str., Irkutsk, 664074, Russia, botkhoev@ya.ru

*Подшивалова Кристина Александровна* - аспирант центра программной инженерии, старший преподаватель кафедры «Строительное производство», Федеральное государственное бюджетное образовательное учреждение высшего образования «Иркутский национальный исследовательский технический университет» (ФГБОУ ВО «ИРНИТУ»), 83, ул. Лермонтова, г. Иркутск, 664074, Россия, 1295536@mail.ru

*Ботхоев Александр Евгеньевич* – аспирант кафедры «Механика и сопротивление материалов» Федерального государственного бюджетного образовательного учреждения высшего образования «Иркутский национальный исследовательский технический университет» (ИРНИТУ), ул. Лермонтова, 83, г. Иркутск, 664074, Россия, botkhoev@ya.ru

DOI:10.22337/2587-9618-2025-21-3-33-40

# BIO-RESISTANT CEMENT COMPOSITES WITH ACTIVE MINERAL ADDITIVE

***Vladimir.T. Yerofeev [1], Margarita A. Goncharova [2], Vasily.F. Smirnov [1], Alexander. I. Rodin [1], Alexander P. Volkov [1]***

[1] Moscow State University of Civil Engineering (National Research University), Moscow, RUSSIA
[2]Lipetsk State Technical University, Lipetsk, RUSSIA

**Abstract:** Bio-damage is a serious problem affecting all stages of the life cycle of building materials, from the production and storage of raw materials to the transportation and operation of finished products. Bacteria and fungi, being the main agents of biodegradation, can significantly reduce the performance characteristics of materials, which leads to economic losses and a decrease in the quality of building structures. As part of this study, a comprehensive assessment of the biostability of cement composites was carried out. Special attention was paid to the study of the species composition of micromycetes colonizing the surface of composites, as well as the determination of fouling indices. The mechanisms of the effect of microorganisms on the physico-mechanical properties of composites, including their effect on mass content and strength characteristics, were studied in detail. The data obtained are important for the development of new strategies for protecting building materials from biodegradation, which will increase their durability and reliability under operating conditions.

**Keywords:** bio-resistance, physical and mechanical properties, biocidal cements, composites, active mineral additives, strength, biocorrosion

# БИОСТОЙКИЕ ЦЕМЕНТНЫЕ КОМПОЗИТЫ С АКТИВНОЙ МИНЕРАЛЬНОЙ ДОБАВКОЙ

***В.Т. Ерофеев [1], М.А. Гончарова [2], В.Ф. Смирнов [1], А.И. Родин [1], А.П. Волков [1]***

[1] Национальный исследовательский университет Московский государственный строительный университет, Москва, РОССИЯ
[2] Липецкий государственный технический университет, Липецк, РОССИЯ

**Аннотация:** Биоповреждения представляют собой серьезную проблему, затрагивающую все этапы жизненного цикла строительных материалов, начиная от производства и хранения сырья и заканчивая транспортировкой и эксплуатацией готовых изделий. Бактерии и грибы, являясь основными агентами биодеструкции, способны существенно снижать эксплуатационные характеристики материалов, что приводит к экономическим потерям и снижению качества строительных конструкций. В рамках данного исследования была проведена комплексная оценка биостойкости цементных композитов. Особое внимание уделялось изучению видового состава микромицетов, колонизирующих поверхность композитов, а также определению показателей обрастаемости. Были детально исследованы механизмы воздействия микроорганизмов на физико-механические свойства композитов, включая их влияние на массосодержание и прочностные характеристики. Полученные данные имеют важное значение для разработки новых стратегий защиты строительных материалов от биодеградации, что позволит повысить их долговечность и надежность в условиях эксплуатации.

**Ключевые слова:** биостойкость, физико-механические свойства, биоцидные цементы, композиты, активные минеральные добавки, прочность, биокоррозия

## INTRODUCTION

The problem of bio-damage covers a wide range of scientific and practical tasks related to the protection of raw materials, materials and goods from damage by bacteria and fungi, both in conditions of long-term storage, as well as during production, transportation and operation. Currently, one of the main tasks in building

materials science is to increase the durability of building materials and products. In this case, the problem of biological corrosion is given a primary role, since the negative effects of bacteria, mycelial fungi and actinomycetes in buildings and structures pose a serious danger to human health [1-3]. With insufficient resistance of materials to microbiological corrosion, the operational reliability of products and structures decreases, their appearance and the environmental situation in buildings and structures deteriorate. To date, a large number of facts of destruction of industrial buildings and structures under the influence of microorganisms have been established. For example, the destruction of reinforced concrete structures at Kievsky, Kirovogradsky, Kamenets-Podolsky and other meat processing plants, the canopy of the Sennaya Ploshchad metro station in St. Petersburg, the outer concrete walls of the Svir-HPP power and gateway stations, and other building structures fully proves the destructive ability of microorganisms [3-5]. Every year, huge amounts of money are spent all over the world on repairing damaged structures, treating patients, and preventing diseases.

Increasing the biosafety of building materials can be achieved through various measures, including the use of biocidal cements. Giving Portland cement, sulfate-resistant, hydrophobic, plasticized and other cements fungicidal and bactericidal properties, as well as the creation of special biocidal cements is the most important direction of modern construction [1, 3-5]. Recently, in world practice, preference has been given to various types of mixed cements [6-9]. The development of technology for the production and optimization of compositions of biocidal Portland cements with an active mineral additive for the manufacture of building composites with biocidal properties that have increased resistance in biological and chemical aggressive environments, resistance to various climatic factors, as well as improved physico-mechanical properties is one of the urgent tasks being solved in this work.

The purpose of the research was to evaluate the bio-stability of cement composites based on Portland cement with an active mineral additive, identify the dominant species of microorganisms on their surface, and study the effect of mycelial fungi on changes in the strength and mass content of materials.

## METHODS

The studies were carried out on samples of cement stone obtained from a solution of normal density. The following materials were used as binders in the manufacture of composites: portland cement M–500–D0-H Russia Standard GOST 10178-85 (CJSC Eurocement Group, Komsomolsky settlement, Russia) as a mineral additive, metallurgical plant slags of three types – blast furnace, granular and converter with a specific surface area of 2900-3000 $cm^2/g$, Russia Standard GOST 3476-74 (Novolipetsk Metallurgical Kombinat, Lipetsk, Russia). The samples were made in the form of beams with dimensions of 1×1×3 cm, which hardened for 28 days in humid conditions before testing.

Cement stone samples were tested for fungus resistance and fungicidal properties in accordance with Russia Standard GOST 9049-91. The following micromycete species were used as test organisms: *Aspergillus oryzae (Ahiburg) Cohn, Aspergillus nigerien Tieghem, Aspergillus terreus Thom, Chaetomium globosum Kunze, Paecilomyces varioti Bainier, Penicillium funiculosum Thom, Penicillium chrysogenum Thom, Penicillium cyclopium Westling, Trichoderma viride Pcis, e*x Fr.

The fouling of cement composites by mold fungi was determined by two methods. Method 1 (without additional sources of carbon and mineral nutrition) and method 3 (on solid nutrient medium of Chapek–Doks) with the establishment of fungal resistance and fungicidal activity, respectively. The coefficient of biological resistance was determined as the ratio of compressive and flexural strength of the samples soaked in the medium used for testing

for 6 months according to method 3. To determine the change in mass content, the samples removed from the medium were wiped with a cotton swab soaked in alcohol. Then the control samples and the samples kept in the medium were dried for 5 hours in a drying cabinet at a temperature of 50 °C, after which they were weighed. The number of tested samples ensured an experimental accuracy of at least 95%.

The identification of micromycetes was carried out based on their morphological and cultural characteristics.

## RESULTS AND DISCUSSION

Table 1 shows the studied formulations and test results. In the studied formulations, the content of slag fillers varied up to 60%. From the conducted fouling studies of cement stone (Table 1), the growth of fungi was established: by the method of 1-0 points, by the method of 3 – 1-3 points. In addition, the resistance of the cement composite to mycelial fungi was revealed, with a concentration of active mineral additives of 20-40%, these composites are fungicidal. Identification of micromycetes on the surface of cement stone after one month of testing according to Method 3 (see Table. 1) established the dominance of *Aspergillus terreus (1), Penicillium cyclopium (2) and Penicillium chrysogenum (3)* on almost all cement composites.

As research practice shows, it is the above-mentioned microorganisms that are the most dangerous and aggressive against reinforced concrete structures and are more common in the food and processing industry. Conditionally pathogenic strains capable of causing various human diseases are found among the destructive fungi isolated from the surface of composites. Thus, the fungus *Aspergillus terreus* (1) causes mycoses of the pulmonary and cardiovascular systems, cerebral mycoses, and also affects the musculoskeletal system. *Penicillium chrysogenum (3)* is capable of causing mycoses of the spleen, kidneys, heart, skin; ear inflammation, tongue and eye lesions. No less harmful are other micromycetes identified on the surface of cement composites.

*Table 1 Fouling of cement stone and species composition microorganisms on its surface*

| № Sample | Granular Slag (G), % | Blast Furnace Slag (D), % | Converter Slag (C), % | Portland Cement, % | Growth assessment | | Property: Fungicide (F) / Mushroom-resistant (MR) | The species composition of the dominant microorganisms (method 3) |
|---|---|---|---|---|---|---|---|---|
| | | | | | Method 1 | Method 3 | | |
| 1 | 5 | - | - | 95 | 0 | 2 | MR | *2,3* |
| 2 | 20 | - | - | 80 | 0 | 1 | F | *2* |
| 3 | 40 | - | - | 60 | 0 | 1 | F | *2* |
| 4 | 60 | - | - | 40 | 0 | 3 | MR | *1, 2* |
| 5 | - | 5 | - | 95 | 0 | 2 | MR | *1,2, 3* |
| 6 | - | 20 | - | 80 | 0 | 1 | F | *1* |
| 7 | - | 40 | - | 60 | 0 | 1 | F | *1, 2* |
| 8 | - | 60 | - | 40 | 0 | 2 | MR | *1, 2, 3* |
| 9 | - | - | 5 | 95 | 0 | 3 | MR | *1, 2, 3* |
| 10 | - | - | 20 | 80 | 0 | 1 | F | *2,3* |
| 11 | - | - | 40 | 60 | 0 | 1 | F | *1, 2, 3* |
| 12 | - | - | 60 | 40 | 0 | 3 | MR | *1, 2* |
| 13 | - | - | - | 100 | 0 | 2 | MR | *1, 2, 3, Penicillium funiculosum* |

According to a number of authors, the destructive effect of micromycetes on cement composites is due to the aggressive effects of fungal metabolites – organic acids, hydrolytic and redox enzymes - on individual components of materials [7, 8]. The results of changes in the mass content and strength characteristics of composites after exposure to standard mycelial fungi are shown below (Fig. 1, 4, 7).

From the results obtained (Fig. 2, 3, 5, 6, 8 and 9) It can be seen that after six months of exposure in a standard environment of mycelial fungi, the strength of cement stone samples from a dough of normal density changed depending on the slag content.

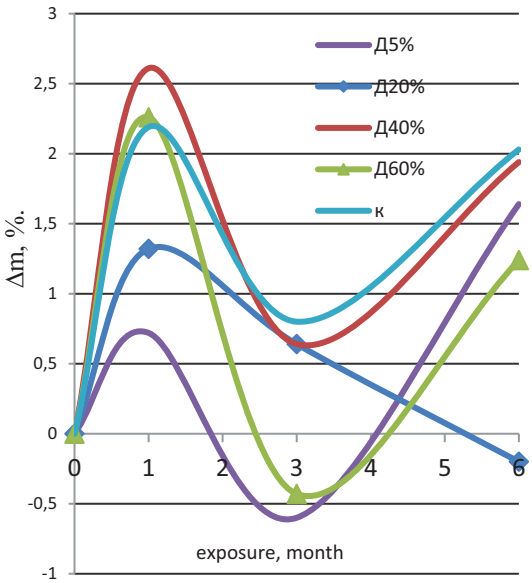


*Figure 1. Dependence of the change in the mass of cement composites modified with blast furnace slag in the medium of micellar fungi*

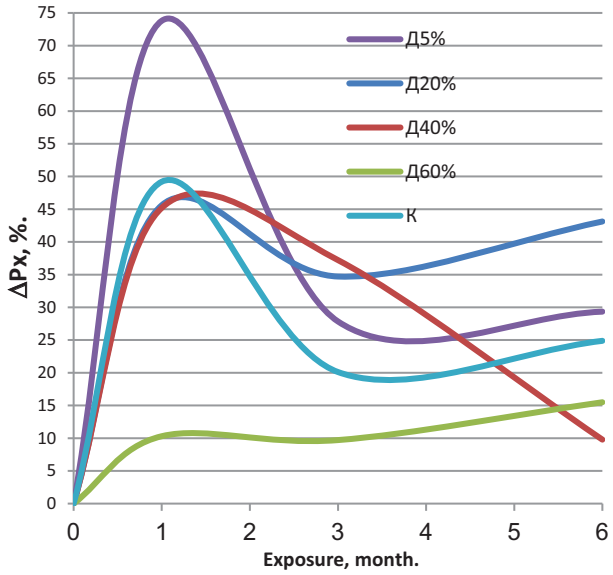


*Figure 2. Dependence of the change in compressive strength ($P_x$,%)of cement composites modified with blast furnace slag in the in the medium of mycelial fungi*

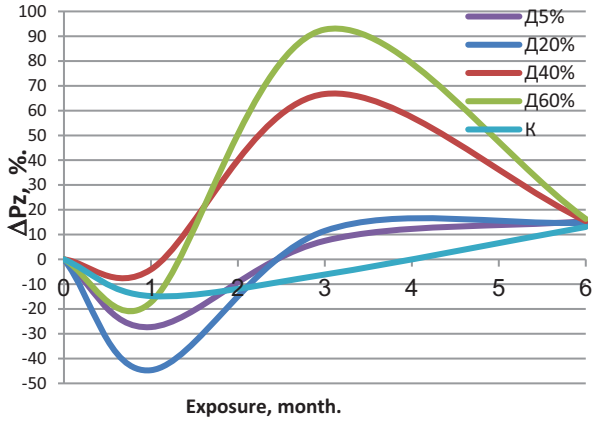


*Figure 3. Dependence of bending strength changes (Pz, %) of cement composites modified with blast furnace slag in the in the medium of mycelial fungi*

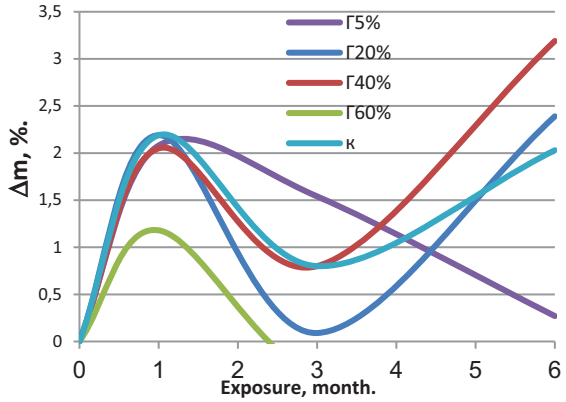


*Figure 4. Dependence of the change in the mass of cement composites modified with Granular slag in the medium of mycelial fungi*

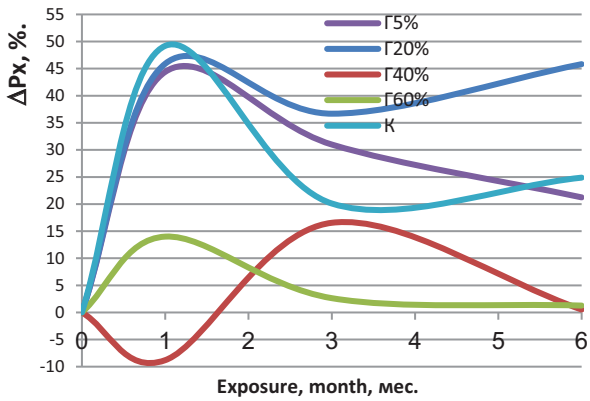


*Figure 5. Dependence of the change in compressive strength ($\Delta P_x$,%)of cement composites modified with Granular slag in the in the medium of mycelial fungi*

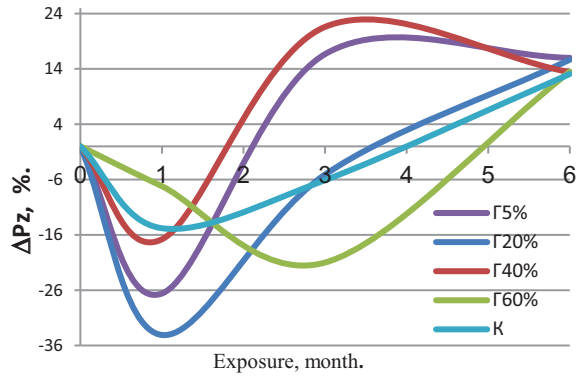


*Figure 6. Dependence of bending strength changes (ΔPz, %) of cement composites modified with Granular slag in the in the medium of mycelial fungi*

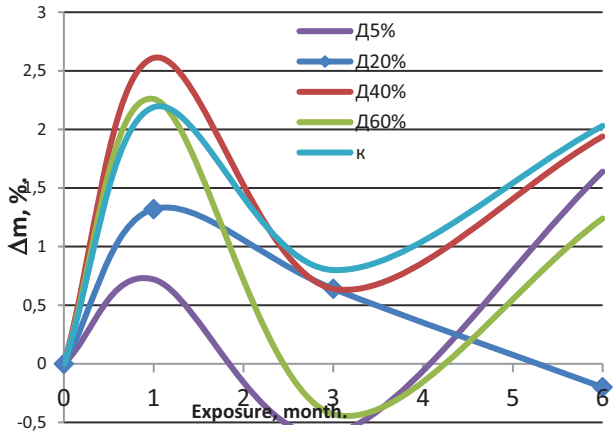


*Figure 7. Dependence of the change in the mass of cement composites modified with Converter Slag in the medium of mycelial fungi*

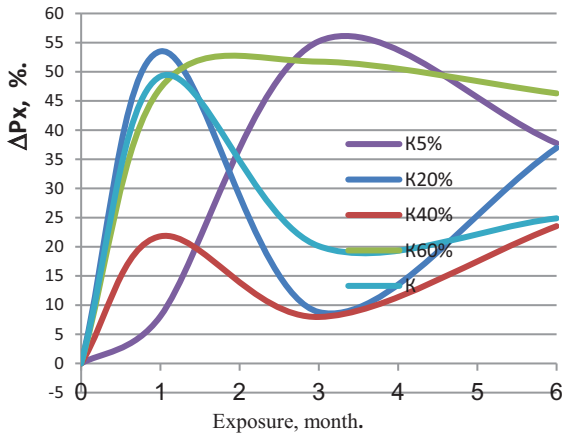


*Figure 8. Dependence of the change in compressive strength ($P_x$,%)of cement composites modified with Converter Slag in the in the medium of mycelial fungi*

It can be seen from the presented graphs that the change in the mass content of cement composite samples during exposure is not the same, which is expressed by the different content of mineral additives.

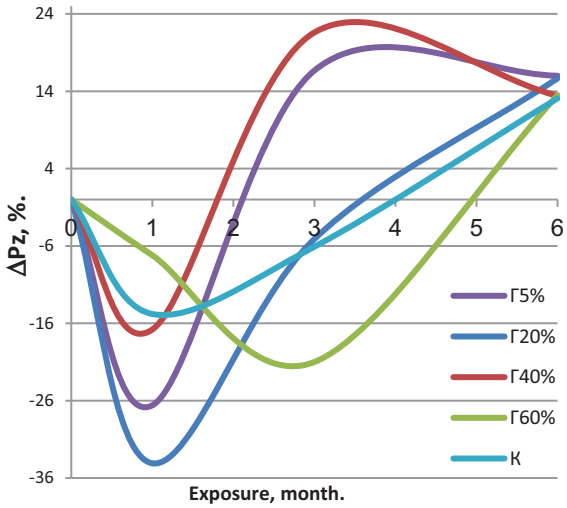


*Figure 9. Dependence of bending strength changes (Pz, %) of cement composites modified with Converter Slag in the in the medium of mycelial fungi*

This is probably expressed by the highest water absorption value of the mineral additive. Analyzing the changes in the mass content and strength characteristics of cement composites modified with active mineral additives, the following can be distinguished: after 30 days of holding samples in a standard environment of mycelial fungi, an increase in mass is observed, this is due to the fact that when samples are immersed in a biological medium, microorganisms sorption occurs in the pores of cement composite samples. At the same time, the presence of microorganisms also affects the strength characteristics, they increase. Further exposure of the samples leads to a decrease in strength characteristics. After three months, there is a decrease in strength and mass content, as the degradation of materials begins in the external diffusion-kinetic region, i.e. destruction occurs in the surface layer of the sample. Then, after six months, there is a second stage of

increasing the mass content and strength. The increase in characteristics begins due to the repeated adhesion of microorganisms to the pores of the already new surface of the samples.
Summing up these studies, it should be noted that one of the main factors affecting the biostability of cement composites, according to the conducted research, is the chemical and mineralogical composition of cements. It determines the nature of the structure formation of composites, the pore space, as well as the species composition of microorganisms on their surface at the first stages of operation, which in turn determines the aggressiveness of the operating environment. As a result of the interaction of the biologically active medium with the composite, the chemical composition of the surface and then the inner zones of the material changes, which leads to a change in the species composition of microorganisms and, as a result, the operating environment.

## CONCLUSION

The compositions of cement composites have been developed, characterized by increased resistance to the effects of microbiological aggressive media. Based on the research, the following cement compositions are recommended for the manufacture of composites: with an optimal content of active mineral additives: (20% and 40%) having fungal and fungicidal properties.
The identification of microorganisms inhabiting cement composites was carried out, after a month of testing in a standard environment of mycelial fungi, three dominant species of micromycetes of the genus *Penicillium* (*Penicillium cyclopium, Penicillium chrysogenum, Penicillium funiculosum*) were identified. In addition to the above-mentioned micromycetes of the genus *Penicillium*, one species of the genus *Aspergillus (Aspergillus terreus*) has been identified. The change in mass content and strength characteristics under the conditions of the standard environment of mycelial fungi (Russia Standard GOST 9.049-91, Method 3) was studied.

## ACKNOWLEDGEMENTS

The research was funded by the National Research Moscow State University of Civil Engineering (Grant for fundamental scientific research, project No. 05-661/130).

## REFERENCES

1. Biological resistance of materials / **V.I. Solomatov** [etc.] – Saransk: Publishing House of the muzzle. Unt., 2001. 196 p.
2. Influence of modifying additives on the durability of cement composites under conditions of a model bacterial protection / **V.T. Erofeev** [etc.] // Bulletin of the Dagestan State Technical University. Technical sciences. 2011. № 4. P. 121–126.
3. Problems of biological damage and biosecurity building materials, products and structures / **N.I. Karpenko** [etc.] // Biodeteriorations and biocorrosion in Construction: Materials Int. Scientific. tehn. Conf. Saransk, 2004. P. 6–11.
4. Biocidal cement composites with additives containing guanidine / **V.T. Erofeev** [etc.] // The list of scientific journal. 2010. № 4 (16). P. 87–94.
5. Biocidal Portland cement with improved physical and mechanical properties / **V.T. Erofeev** [etc.] // International Journal for Computational Civil and Structural Engineering. 2012.V. 8, Is. 3. P. 81–92.
6. **Hong M., Niu D., Fu Q., Hui Z., Wan Zh.** Insights into bio-deterioration of concrete exposed to sewer environment: A case study // Construction and Building Materials. 2024. V. 412. 134835.

7. **Pramanik S.K., Bhuiyan M., Robert D., Roychand R., Gao L., Cole I., Pramanik B.K.,** Bio-corrosion in concrete sewer systems: Mechanisms and mitigation strategies // Science of The Total Environment. 2024. V. 921. 171231.
8. **Georges M., Bourguiba A., Chateigner D., Sebaibi N., Boutouil M.** The study of long-term durability and bio-colonization of concrete in marine environment // Environmental and Sustainability Indicators. 2021. V. 10. 100120.
9. **Roghanian N., Banthia N.** Development of a sustainable coating and repair material to prevent bio-corrosion in concrete sewer and waste-water pipes // Cement and Concrete Composites. 2019. V. 100. P. 99-107.
10. **A.U. Adebanjo, N. Shafiq, V. Kumar, S. Ahmad Farhan, O.J. Olatoyan, T.I. Qureshi, S.N. Abd Razak, I.C. Adebanjo, L. Guillaumat**, Antimicrobial concrete for development: A critical review, Journal of Cleaner Production. 2024, V. 458. 142445.
11. **L. Stohl, T. Manninger, J. von Werder, F. Dehn, A. Gorbushina, B. Meng**, Bioreceptivity of concrete: A review, Journal of Building Engineering, 2023. V. 76. 107201.
12. **X. Li, I. Johnson, K. Mueller, S. Wilkie, L. Hanzic, P.L. Bond, L. O'Moore, Z. Yuan, G. Jiang,** Corrosion mitigation by nitrite spray on corroded concrete in a real sewer system, Science of The Total Environment. 2022. V. 806, P. 3, 151328.
13. **Y. Song, K. Chetty, U. Garbe, J. Wei, H. Bu, L. O'moore, X. Li, Z. Yuan, T. McCarthy, G. Jiang,** A novel granular sludge-based and highly corrosion-resistant bio-concrete in sewers, Science of The Total Environment. 2021. V. 791. 148270.

## СПИСОК ЛИТЕРАТУРЫ

1. Биологическое сопротивление материалов /**В.И. Соломатов, В.Т. Ерофеев, В.Ф. Смирнов** [и др.] Саранск: Изд-во Морд. ун-та. 2001. 196 с. Влияние модифицирующих добавок на стойкость цементных композитов в условиях воздействия модельной бактериальной среды / **В.Т. Ерофеев** [и др.] // Вестник Дагестанского государственного технического университета. Технические науки. 2011. № 4. С. 121–126.
2. Проблемы биоповреждений и биозащиты строительных материалов, изделий и конструкций / **Н.И. Карпенко** [и др.] // Биоповреждения и биокоррозия в строительстве: материалы Междунар. науч.-техн. конф. – Саранск, 2004. – С. 6–11.
3. Биоцидные цементные композиты с добавками, содержащими гуанидин /**В.Т. Ерофеев** [и др.] // Приволжский научный журнал. – 2010. – № 4 (16). – С. 87–94.
4. Биоцидный портландцемент с улучшенными физико-механическими свойствами / **В.Т. Ерофеев** [и др.] // International Journal for Computational Civil and Structural Engineering. 2012. V. 8, Is. 3. С. 81–92.
5. **Hong M., Niu D., Fu Q., Hui Z., Wan Zh.** Insights into bio-deterioration of concrete exposed to sewer environment: A case study // Construction and Building Materials. 2024. V. 412. -134835.
6. **Pramanik S.K., Bhuiyan M., Robert D., Roychand R., Gao L., Cole I., Pramanik B.K**., Bio-corrosion in concrete sewer systems: Mechanisms and mitigation strategies // Science of The Total Environment. 2024. V. 921. 171231.

7. **Georges M., Bourguiba A., Chateigner D., Sebaibi N., Boutouil M.** The study of long-term durability and bio-colonization of concrete in marine environment // Environmental and Sustainability Indicators. 2021. V. 10. 100120.
8. **Roghanian N., Banthia N.** Development of a sustainable coating and repair material to prevent bio-corrosion in concrete sewer and waste-water pipes // Cement and Concrete Composites. 2019. V. 100. P. 99-107.
9. **A.U. Adebanjo, N. Shafiq, V. Kumar, S.A. Farhan, O.J. Olatoyan, T.I. Qureshi, S.N. Abd Razak, I.C. Adebanjo, L. Guillaumat**, Antimicrobial concrete for development: A critical review, Journal of Cleaner Production, V. 458, 2024, 142445.
10. **L. Stohl, T. Manninger, J. von Werder, F. Dehn, A. Gorbushina, B. Meng**, Bioreceptivity of concrete: A review, Journal of Building Engineering, V. 76, 2023, 107201.
11. **X. Li, I. Johnson, K. Mueller, S. Wilkie, L. Hanzic, P.L. Bond, L. O'Moore, Z. Yuan, G. Jiang**, Corrosion mitigation by nitrite spray on corroded concrete in a real sewer system, Science of The Total Environment, V. 806, P. 3, 2022, 151328.
12. **Y. Song, K. Chetty, U. Garbe, J. Wei, H. Bu, L. O'moore, X. Li, Z. Yuan, T. McCarthy, G. Jiang**, A novel granular sludge-based and highly corrosion-resistant bio-concrete in sewers, Science of The Total Environment, V. 791, 2021, 148270.

---

*Vladimir Trofimovich Yerofeyev,* Doctor of Technical Sciences, Professor, Professor of the Department of Building Materials Science, National Research University of Moscow State University of Civil Engineering, 26 Yaroslavskoye Highway, Moscow, 129337, Russia, yarofeevvt@mail.ru

*Margarita Aleksandrovna Goncharova*, Doctor of Technical Sciences, Professor, Head of the Department of Building Materials Science and Road Technologies, Lipetsk State Technical University, 30 Moskovskaya St., Lipetsk, 398024, Russia, magoncharova777@yandex.ru

*Vasily Filippovich Smirnov*, Doctor of Biological Sciences, Professor, biodeg@mail.ru

*Rodin Alexander Ivanovich*, Candidate of Technical Sciences, Associate Professor, al_rodin@mail.ru

*Volkov Alexander Pavlovich*, postgraduate student of the Department of "Building Materials and Technologies", volkovap94@yandex.ru

*Владимир Трофимович Ерофеев*, доктор технических наук, профессор, профессор кафедры строительного материаловедения, Национальный исследовательский университет «Московский государственный строительный университета», д.26, Ярославское шоссе, Москва, 129337, Россия, yarofeevvt@mail.ru

*Маргарита Александровна Гончарова*, доктор технический наук, профессор, зав. кафедры строительного материаловедения и дорожных технологий, Липецкий государственный технический университет, д.30, ул Московская, г. Липецк, 398024, Россия, magoncharova777@yandex.ru

*Смирнов Василий Филиппович,* доктор биологических наук, профессор, biodeg@mail.ru

*Родин Александр Иванович*, Кандидат технических наук, доцент, al_rodin@mail.ru

*Волков Александр Павлович*, аспирант кафедры «Строительные материалы и технологии», volkovap94@yandex.ru

DOI:10.22337/2587-9618-2025-21-3-41-53

# SOLUTION TO FILTRATION PROBLEM WITH LINEAR POROSITY FUNCTION

***Galina L. Safina***

Moscow State University of Civil Engineering, Moscow, RUSSIA

**Abstract:** Injection techniques are an effective tool for road construction, repair and maintenance. They allow solving a wide range of problems related to soil reinforcement, pavement rehabilitation and drainage improvement, ensuring durability and reliability of road infrastructure. Injection of various compositions (cement, polymer, silicatized) into weak soils (peat, clay, silt) can increase their bearing capacity, reduce deformations and prevent roadway subsidence. In addition, injection compositions fill voids and cracks formed as a result of erosion, soil erosion or vibration from traffic, which prevents further destruction of the road base. The study of depth filtration in injectable soil reinforcement techniques is a key aspect for optimizing and improving the effectiveness of these technologies. It helps to understand how injection solutions penetrate the soil, how they interact with the soil, and how this process can be controlled to achieve the best results. In this paper, the problem of suspension filtration in a heterogeneous porous medium with a linear porosity function varying as a function of spatial coordinate is solved. The exact solution to the problem is found. Asymptotic solutions of the concentrations of suspended and retained particles for the case of insignificant porosity measurement are obtained.

**Keywords:** deep bed filtration, suspended and retained particles, suspension, porous medium, concentration function, asymptotic solution, porosity function

# РЕШЕНИЕ ЗАДАЧИ ФИЛЬТРАЦИИ С ЛИНЕЙНОЙ ФУНКЦИЕЙ ПОРИСТОСТИ

***Г.Л. Сафина***

Национальный исследовательский Московский государственный строительный университет, г. Москва, РОССИЯ

**Аннотация:** Инъекционные методы являются эффективным инструментом для строительства, ремонта и обслуживания автомобильных дорог. Они позволяют решать широкий спектр задач, связанных с укреплением грунта, восстановлением покрытия и улучшением дренажных свойств, обеспечивая долговечность и надежность дорожной инфраструктуры. Инъекции различных составов (цементных, полимерных, силикатизированных) в слабые грунты (торф, глина, ил) позволяют повысить их несущую способность, снизить деформации и предотвратить просадки дорожного полотна. Помимо этого, инъекционные составы заполняют пустоты и трещины, образовавшиеся в результате эрозии, размывания грунта или вибрации от транспорта, что предотвращает дальнейшее разрушение основания дороги. Изучение глубинной фильтрации при инъекционных методах укрепления грунтов является ключевым аспектом для оптимизации и повышения эффективности этих технологий. Оно помогает понять, как инъекционные растворы проникают в грунт, как происходит их взаимодействие с грунтом, и как можно контролировать этот процесс для достижения наилучших результатов. В работе решается задача фильтрации суспензии в неоднородной пористой среде с линейной функцией пористости, изменяющейся в зависимости от пространственной координаты. Найдено точное решение задания. Получены асимптотические решения концентраций взвешенных и осажденных частиц для случая незначительного измерения пористости.

**Ключевые слова:** глубинная фильтрация, взвешенные и осажденные частицы, суспензия, неоднородная пористая среда, асимптотическое решение, функция пористости

## INTRODUCTION

Injection reinforcement of roadbeds is a method of repairing and reinforcing an existing road surface by injecting special liquid compositions (injection materials) into the space under the roadbed or into its structure. It is an effective way to restore the bearing capacity of the road base, fill voids, stabilize cracks and prevent further deterioration [1-3].

The injected material is injected under pressure through small holes (injectors) drilled into the road surface (fig. 1). It fills voids, cracks and pores in the road base, strengthening its structure and increasing its bearing capacity. After curing, the injection material creates a strong bond between the road surface layers and the subgrade, preventing further deterioration.

*Figure 1. Injection of injectable material*

Currently, there are several types of injection materials such as cement mortars, polymeric materials, microcements, and composite materials [4-7]. Each of the above types has its own disadvantages and advantages. Thus, cement mortars have high strength and relatively low cost, but have limited penetration ability into small cracks and are prone to shrinkage and cracking [8]. Polymeric materials (polyurethanes, epoxy resins) are characterized by high penetration ability, elasticity, resistance to water and chemicals, the disadvantages include their high cost and complexity of application [9-11].

The study of solid suspension filtration in porous media is a complex problem. Road pavement and road base are porous media (asphalt, crushed stone, sand, soil). The injection material must penetrate these pores and cracks to strengthen the structure. During the filtration process, larger suspension particles can become trapped in the porous medium, while smaller particles can continue to move through. This causes the composition of the injected material to change as it spreads deep into the roadway. The change in composition can affect the strength, elasticity and other characteristics of the cured material, which ultimately affects the durability of the reinforced section [12]. Also fine particles of injection material and fragments that have separated from the pavement can clog microcracks and pores, which reduces the water permeability of the road surface. This can lead to accumulation of water inside the road structure, which in winter will cause deterioration due to freezing and thawing.

Underestimating the influence of seepage can lead to ineffective strengthening, shortening the service life of the pavement and even its destruction. It is therefore necessary to pay attention to all aspects of the interaction between the injection material and the porous structure of the pavement when designing and carrying out injection reinforcement works.

The concept of porosity is one of the most important in the study of deep filtration of suspension in porous media [13-15]. This characteristic determines many of its properties of porous media, including permeability, specific surface area, thermal conductivity, strength and sorption capacity. It characterizes the proportion of the volume occupied by pores (voids) in relation to the total volume of the material.

Homogeneous porosity is characterized by the uniform distribution of pores throughout the volume of the material, as well as the closeness of their size and shape. This means that the porosity (pore volume fraction) is almost the same at any point in the material, and that there are no significant differences in the size and shape of individual pores. Many articles are devoted to depth filtration of suspension in a homogeneous porous medium [16-20].

The study of filtration of porous medium with inhomogeneous porosity is of great interest [21-24]. Variable porosity is characterized by non-uniform distribution of pores, for example, there may exist regions with high and low porosity. In addition, the pore diameter can vary over a wide range. Both micropores and macropores may be present. There can also be differences in pore shape (e.g. prismatic, cylindrical).

In this paper the problem of depth filtration in a heterogeneous porous medium for the case of variable porosity function, linearly varying depending on the spatial coordinate $x$ is solved. Exact solutions for the concentrations of suspended and retained particles, as well as asymptotic solutions for the case of small changes in porosity are obtained.

## MATHEMATICAL MODEL

Let consider a dimensionless problem of depth filtration in a medium with variable porosity with unknown concentration functions of suspended particles $C(x,t)$ and retained particles $S(x,t)$:

$$\varphi(x)\frac{\partial C}{\partial t}+\frac{\partial C}{\partial x}+\frac{\partial S}{\partial t}=0, \qquad (1)$$

$$\frac{\partial S}{\partial t}=\Lambda(S)C. \qquad (2)$$

Here $\varphi(x)$ is a variable porosity function, $\Lambda(S)$ is a filtration function. The problem is solved in the domain $\begin{cases}0\le x\le 1,\\ t\ge 0.\end{cases}$

At the inlet of the filter at $x=0$ the concentration of suspended particles is equal to one, i.e.

$$C(0,t)=1, \qquad (3)$$

at the initial moment of time $t=0$ the concentrations of suspended and retained particles are equal to zero:

$$C(x,0)=0;\quad S(x,0)=0. \qquad (4)$$

Let the filtration function be of the form $\Lambda(S)=S_m-S$, where $S_m$ is the maximum value of sediment, and the porosity function be of the form $\varphi(x)=a+bx$. Then equations (1) and (2) take the form

$$(a+bx)\frac{\partial C}{\partial t}+\frac{\partial C}{\partial x}+\frac{\partial S}{\partial t}=0, \qquad (5)$$

$$\frac{\partial S}{\partial t}=(S_m-S)C. \qquad (6)$$

The curve $t=ax+b\frac{x^2}{2}$, called the concentration front, divides the domain $\begin{cases}0\le x\le 1,\\ t\ge 0\end{cases}$ into two subdomains. Before the front at $t<ax+b\frac{x^2}{2}$, the concentrations of both types of particles are zero. Behind the front, the concentrations of suspended and retained particles are positive values. At the front the concentrations are $C\left(x,ax+b\frac{x^2}{2}\right)>0$ and $S\left(x,ax+b\frac{x^2}{2}\right)=0$.

## EXACT SOLUTION TO THE PROBLEM

Taking into account that at the filter inlet $C(0,t)=1$, we obtain from equation (6)

$$\int_0^{S(0,t)}\frac{dS}{S_m-S}=\int_0^t dt,$$

from which we obtain

$$S(0,t)=S_m\left(1-e^{-t}\right).$$

Then from equation (6) we have $C = \frac{\partial S / \partial t}{S_m - S}$, let us substitute the obtained expression into equation (5):

$$(a+bx)\frac{\partial}{\partial t}\left(\frac{\partial S/\partial t}{S_m - S}\right)+\frac{\partial}{\partial x}\left(\frac{\partial S/\partial t}{S_m - S}\right)+\frac{\partial S}{\partial t}=0.$$

Taking into account that the obtained equality is equal to the equation

$$\frac{\partial}{\partial t}\left((a+bx)\frac{\partial S/\partial t}{S_m - S}\right)+\frac{\partial}{\partial t}\left(\frac{\partial S/\partial x}{S_m - S}\right)+\frac{\partial S}{\partial t}=0,$$

we obtain

$$(a+bx)\frac{\partial S/\partial t}{S_m - S}+\frac{\partial S/\partial x}{S_m - S}+\frac{\partial S}{\partial t}=0.$$

Moving on to the new variables $\begin{cases}\tau = t - ax - b\dfrac{x^2}{2},\\ x = x,\end{cases}$ we have

$$\frac{\partial S}{\partial x}+\left(S_m - S\right)S=0.$$

Solving the obtained equation with separating variables and taking into account the fact that $S_0(0,t)=S_0(0,\tau)$, we obtain the exact solution behind the concentration front

$$S(x,\tau)=\frac{S_m\left(e^{\tau}-1\right)}{e^{S_m x}+e^{\tau}-1}.$$

Then

$$S(x,t)=\frac{S_m\left(e^{t-ax-b\frac{x^2}{2}}-1\right)}{e^{S_m x}+e^{t-ax-b\frac{x^2}{2}}-1} \qquad (7)$$

and

$$C(x,t)=\frac{e^{t-ax-b\frac{x^2}{2}}}{e^{S_m x}+e^{t-ax-b\frac{x^2}{2}}-1}. \qquad (8)$$

## ASYMPTOTIC SOLUTION FOR SMALL CHANGES IN POROSITY

Let us consider the case of small porosity variation, i.e. let $\varphi(x)=a+\varepsilon x$, where $\varepsilon$ takes a small value. Let us decompose the concentrations of suspended and precipitated particles, as well as the filtration function by a small parameter

$$S(x,t)=S_0(x,t)+\varepsilon S_1(x,t)+\frac{\varepsilon^2}{2}S_2(x,t)+.., \quad (9)$$

$$C(x,t)=C_0(x,t)+\varepsilon C_1(x,t)+\frac{\varepsilon^2}{2}C_2(x,t)+..., (10)$$

$$\Lambda(S)=S_m - S_0(x,t)-\varepsilon S_1(x,t)-\frac{\varepsilon^2}{2}S_2(x,t)+...(11)$$

Substituting expressions (9) and (11) into (5) and grouping the summands by powers of $\varepsilon$, we obtain:

at $\varepsilon^0$: $$a\frac{\partial S_0(x,t)}{\partial t}+\frac{\partial S_0(x,t)}{\partial x}+\left(S_m - S_0(x,t)\right)S_0(x,t)=0; \qquad (12)$$

at $\varepsilon^1$: $$x\frac{\partial S_0(x,t)}{\partial t}+a\frac{\partial S_1(x,t)}{\partial t}+\frac{\partial S_1(x,t)}{\partial x}+\left(S_m - 2S_0(x,t)\right)S_1(x,t)=0; \qquad (13)$$

at $\varepsilon^2$: $$x\frac{\partial S_1(x,t)}{\partial t}+\frac{a}{2}\frac{\partial S_2(x,t)}{\partial t}+\frac{1}{2}\cdot\frac{\partial S_2(x,t)}{\partial x}+\frac{1}{2}\left(S_m - 2S_0(x,t)\right)S_2(x,t)-S_1^2(x,t)=0. \qquad (14)$$

To find $S_1(x,t)$, $S_2(x,t)$ and $S_3(x,t)$ in equations (12)-(14) we will make a transition to the variables $\begin{cases}\tau = t - ax, \\ x = x.\end{cases}$ Equation (12) is transformed to the form

$$\frac{\partial S_0(x,\tau)}{\partial x} + \left(S_m - S_0(x,\tau)\right) S_0(x,\tau) = 0,$$

Then

$$S_0(x,\tau) = \frac{S_m S_0(0,\tau)}{S_m e^{S_m x} - S_0(0,\tau) e^{S_m x} + S_0(0,\tau)}.$$

Passing to the old variables and taking into account that $S_0(0,\tau) = S_0(0,t) = S_m\left(1 - e^{-t}\right)$, we obtain

$$S_0(x,t) = \frac{S_m(e^{t-ax} - 1)}{e^{S_m x} + e^{t-ax} - 1}.$$

The transition to new variables in equation (13) leads it to the linear equation

$$\frac{\partial S_1(x,\tau)}{\partial x} + \left(S_m - 2S_0(x,\tau)\right) S_1(x,\tau) = $$
$$= -xS_m \frac{e^{\tau + S_m x}}{\left(e^{S_m x} + e^{\tau} - 1\right)^2}.$$

Given that $S_1(0,\tau) = 0$, we obtain the solution

$$S_1(x,\tau) = -\frac{S_m x^2 e^{S_m x + \tau}}{2\left(e^{S_m x} + e^{\tau} - 1\right)^2},$$

consequently,

$$S_1(x,t) = -\frac{S_m x^2 e^{S_m x + t - ax}}{2\left(e^{S_m x} + e^{t-ax} - 1\right)^2}.$$

After the transition to new variables equation (14) takes the form

$$\frac{\partial S_2(x,\tau)}{\partial x} + \left(S_m - 2S_0(x,\tau)\right) S_2(x,\tau) =$$
$$= 2S_1^2(x,\tau) - 2x\frac{\partial S_1(x,\tau)}{\partial \tau}.$$

Solving it as linear, substituting found $S_0(x,\tau)$, $S_1(x,\tau)$ and taking into account $S_2(0,\tau) = 0$, we obtain

$$S_2(x,\tau) = \frac{S_m e^{S_m x + \tau} x^4 \left(e^{S_m x} - e^{\tau} - 1\right)}{4\left(e^{S_m x} + e^{\tau} - 1\right)^3},$$

wherefrom

$$S_2(x,t) = \frac{S_m e^{S_m x + t - ax} x^4 \left(e^{S_m x} - e^{t-ax} - 1\right)}{4\left(e^{S_m x} + e^{t-ax} - 1\right)^3}.$$

Let us find $C_0(x,t)$, $C_1(x,t)$ and $C_2(x,t)$. For this purpose, we substitute expressions (9), (10) into equation (6) and equate the coefficients at the same degrees of $\varepsilon$:

$$\text{at } \varepsilon^0: \quad \frac{\partial S_0(x,t)}{\partial t} = \left(S_m - S_0(x,t)\right) C_0(x,t); \tag{15}$$

$$\text{at } \varepsilon^1: \quad \frac{\partial S_1(x,t)}{\partial t} = \left(S_m - S_0(x,t)\right) C_1(x,t) - S_1(x,t) C_0(x,t); \tag{16}$$

$$\text{at } \varepsilon^2: \quad \frac{1}{2}\frac{\partial S_2(x,t)}{\partial t} = \left(S_m - S_0(x,t)\right)\frac{C_2(x,t)}{2} - S_1(x,t) C_1(x,t) - \frac{1}{2} S_2(x,t) C_0(x,t). \tag{17}$$

Substituting already known $S_0(x,t)$, $S_1(x,t)$ and $S_2(x,t)$, we obtain

$$C_0(x,t)=\frac{e^{t-ax}}{e^{S_m x}+e^{t-ax}-1},$$

$$C_1(x,t)=-\frac{x^2e^{t-ax}\left(e^{S_m x}-1\right)}{2\left(e^{S_m x}+e^{t-ax}-1\right)^2},$$

$$C_2(x,t)=\frac{x^4e^{t-ax}\left(e^{S_m x}-1\right)\left(e^{S_m x}-e^{t-ax}-1\right)}{4\left(e^{S_m x}+e^{t-ax}-1\right)^3}.$$

Thus, the asymptotic solutions have the form

$$S(x,t)=\frac{S_m(e^{t-ax}-1)}{e^{S_m x}+e^{t-ax}-1}-\frac{\varepsilon}{2}\frac{S_m x^2e^{S_m x+t-ax}}{\left(e^{S_m x}+e^{t-ax}-1\right)^2}+\frac{\varepsilon^2}{8}\frac{S_m e^{S_m x+t-ax}x^4\left(e^{S_m x}-e^{t-ax}-1\right)}{\left(e^{S_m x}+e^{t-ax}-1\right)^3}+\ldots,$$

$$C(x,t)=\frac{e^{t-ax}}{e^{S_m x}+e^{t-ax}-1}-\frac{\varepsilon}{2}\frac{x^2e^{t-ax}\left(e^{S_m x}-1\right)}{\left(e^{S_m x}+e^{t-ax}-1\right)^2}+\frac{\varepsilon^2}{8}\frac{x^4e^{t-ax}\left(e^{S_m x}-1\right)\left(e^{S_m x}-e^{t-ax}-1\right)}{\left(e^{S_m x}+e^{t-ax}-1\right)^3}+\ldots$$

## RESEARCH RESULTS

Fig. 2 and fig. 4 show the exact (black lines) and asymptotic (red lines) solutions of suspended and retained particle concentrations, respectively, as a function of the *x* coordinate for $a=1$, $S_m=1$ and $\varepsilon=0.2$ at *t*=5. In fig. 3 and fig. 5 relative errors of asymptotic solutions of suspended and retained particle concentrations at the same parameters are shown.

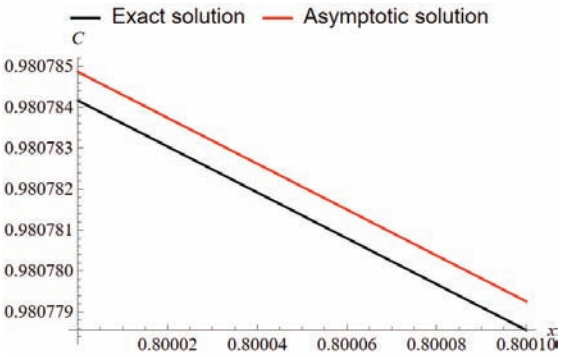


*Figure 2. Exact and asymptotic solution of suspended particle concentration at t=5*

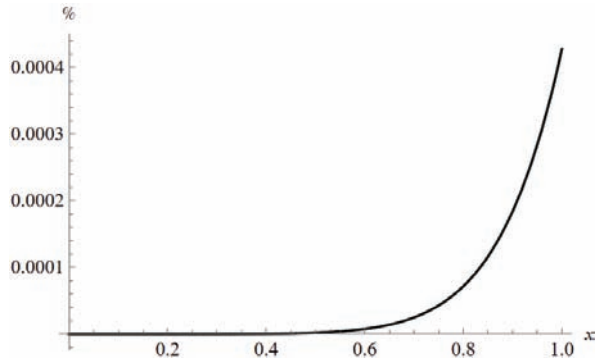


*Figure 3. Relative error of asymptotic solution of suspended particle concentration at t=5*

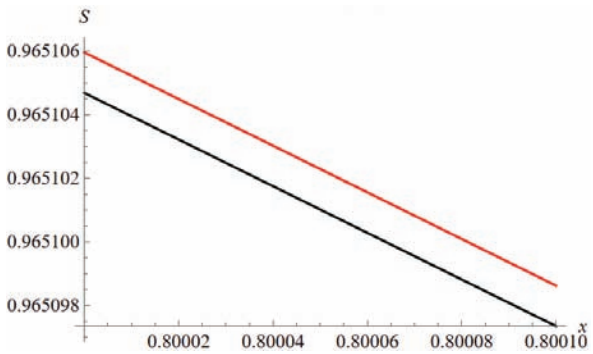


*Figure 4. Exact and asymptotic solution of retained particle concentration at t=5*

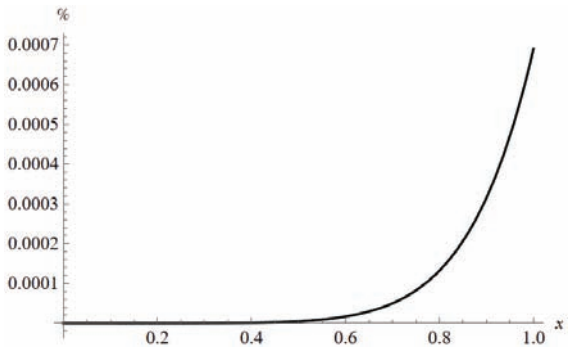


*Figure 5. Relative error of the asymptotic solution of the concentration of retained particles at t=5*

Figs. 6-9 are similar to Figs. 2-5 for $\varepsilon = 1$.

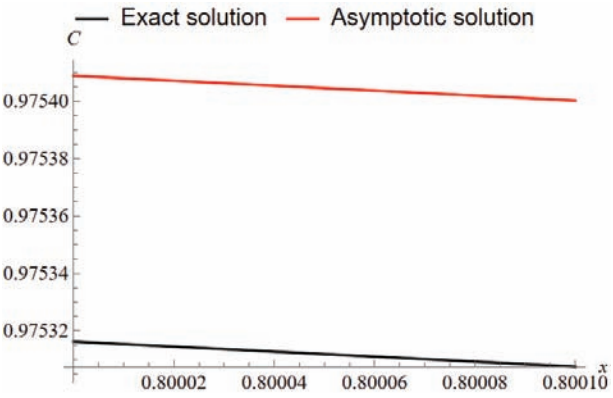


*Figure 6. Exact and asymptotic solution of suspended particle concentration at t=5*

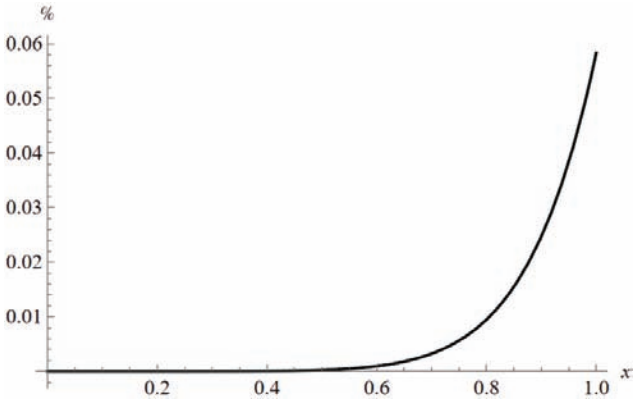


*Figure 7. Relative error of asymptotic solution of suspended particle concentration t=5*

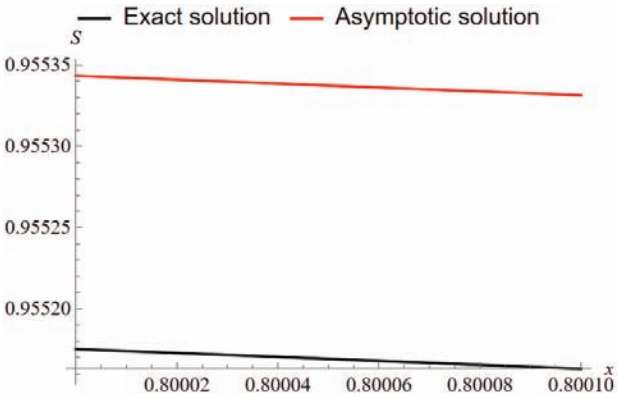


*Figure 8. Exact and asymptotic solution of retained particle concentration t=5*

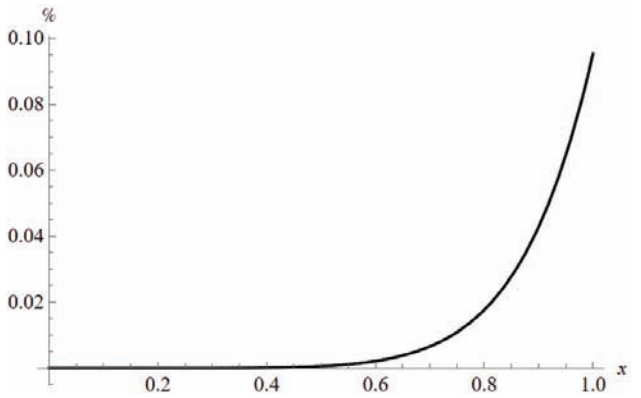


*Figure 9. Relative error of the asymptotic solution of the concentration of retained particles at t=5*

The obtained dependences show that with increasing parameter $\varepsilon$, the relative errors of asymptotic solutions of both suspended and retained particle concentrations increase significantly. The errors have a monotonically increasing character. It should be noted that the error of the asymptotic solution of the concentration of retained particles is higher than the error of the asymptotic solution of the concentration of suspended particles. Thus, at the filter output at $x$=1: for $\varepsilon = 0.2$ the relative error for $S(x,t)$ is 0.0007 %, for $C(x,t)$ is 0.0004 %, for the relative error for $S(x,t)$ is 0.0952 %, for $C(x,t)$ is 0.0584 %, which indicates the difference of these values in 1.6 times.

Fig. 10 and fig. 12 show the exact (black lines) and asymptotic (red lines) solutions of suspended and retained particle concentrations, respectively, as a function of time $t$ for $a = 1$, $S_m = 1$ and $\varepsilon = 0.2$ at $x$=0.5.

Fig. 11 and fig. 13 show the relative errors of asymptotic solutions of suspended and retained particle concentrations at the same parameters.

Figs. 14-17 are similar to figs. 10-13 and are obtained for the value $\varepsilon = 1$.

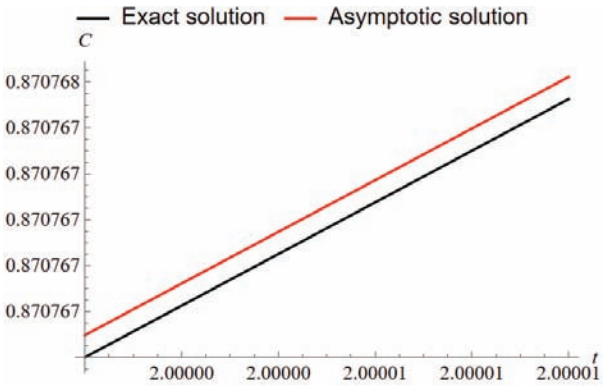


*Figure 10. Exact and asymptotic solution of suspended particle concentration at x=0.5*

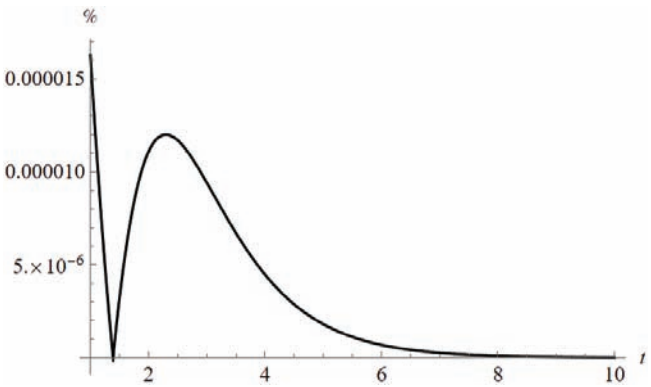


*Figure 11. Relative error of asymptotic solution of suspended particle concentration at x=0.5*

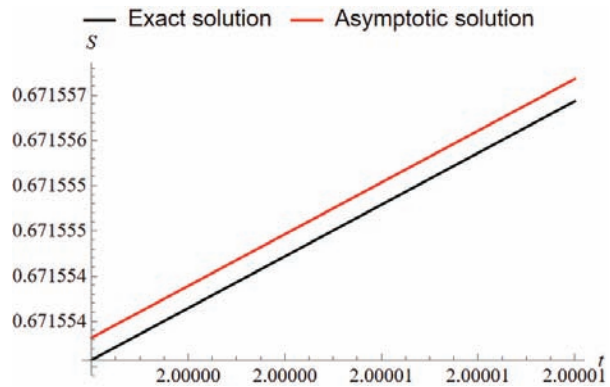


*Figure 12. Exact and asymptotic solution of retained particle concentration at x=0.5*

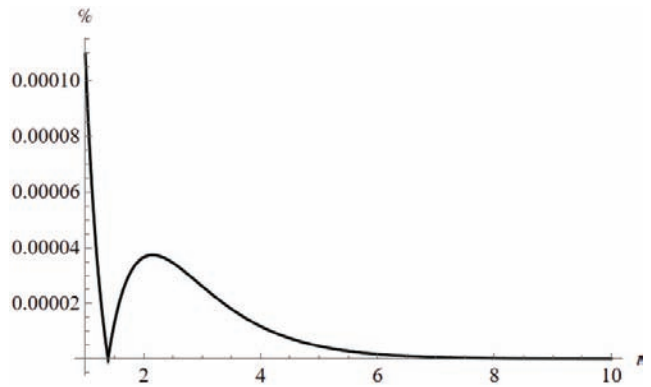


*Figure 13. Relative error of asymptotic solution of retained particle concentration at x=0.5*

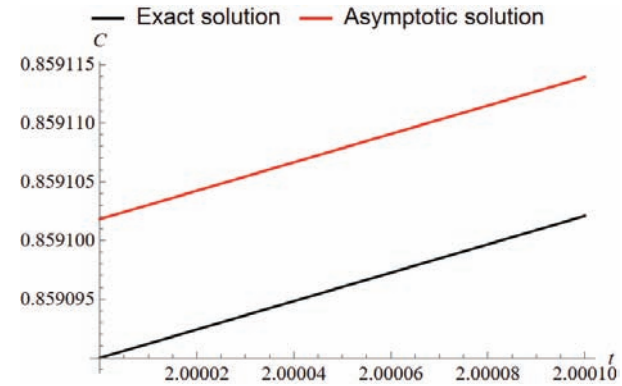


*Figure 14. Exact and asymptotic solution of suspended particle concentration at x=0.5*

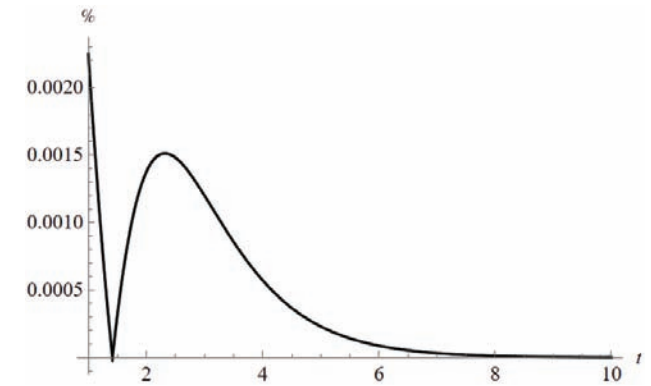


*Figure 15. Relative error of asymptotic solution of suspended particle concentration at x=0.5*

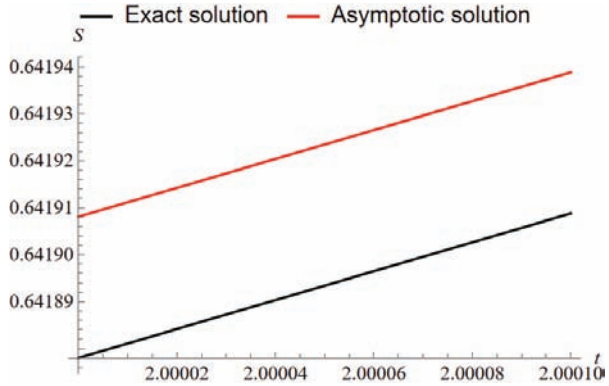


*Figure 16. Exact and asymptotic solution of retained particle concentration at x=0.5*

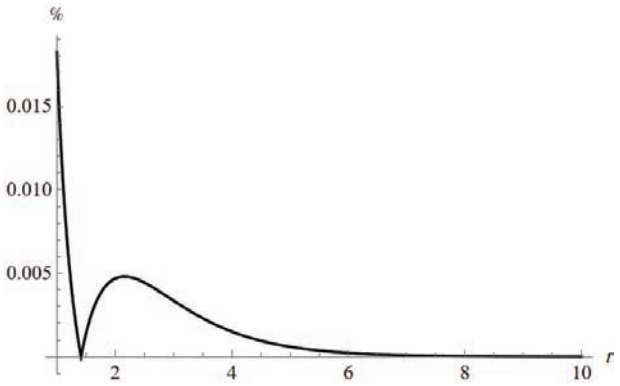


*Figure 17. Relative error of asymptotic solution of retained particle concentration at x=0.5*

The plots show that the relative errors of suspended and retained particles do not behave monotonically. At first, the errors decrease, reaching the zero value, then increase, reaching the maximum value, and then decrease again. At the same time, increasing the value of the parameter $\varepsilon$ does not affect the maximum point: for $C(x,t)$ at $\varepsilon = 0.2$ $t_{\max} = 2.3044$, at $\varepsilon = 1$ $t_{\max} = 2.3169$; for $S(x,t)$ at $\varepsilon = 0.2$ $t_{\max} = 2.1528$, at $\varepsilon = 1$ $t_{\max} = 2.1572$. The larger the value of the parameter $\varepsilon$, the larger the relative errors of the asymptotic solutions of both types of particles.

## CONCLUSION

The paper presents the solution of the problem of depth filtration with linear porosity function. Exact solutions of suspended $C(x,t)$ and retained $S(x,t)$ particle concentrations are obtained. With Taylor series expansion of functions $C(x,t)$ and $S(x,t)$ in powers of $\varepsilon$, the formulas of asymptotic solutions of suspended and retained particles concentrations with porosity function $\varphi(x) = a + \varepsilon x$, where $\varepsilon$ takes a small value, are derived. As the value of the parameter $\varepsilon$ increases, an increase in the relative errors of the asymptotic solutions for both types of particles is observed. As we move along the filter, the relative errors of the asymptotic solutions for the concentrations of suspended and retained particles monotonically increase, reaching the highest value at the filter outlet at $x=1$. The plots of relative errors as a function of time $t$ at a fixed value of $x$ have a non-monotonic character. Near the concentration front the errors reach their highest values, then there is their decrease to zero value, after which there is an increase in the error up to some value at $t_{\max}$, then again decrease to zero value. Thus, the use of asymptotic formulas for solutions of suspended and retained particle concentrations is reasonable for arbitrary time intervals.

## REFERENCES

1. **Fakhar A.M.M., Asmaniza A.** Road Maintenance Experience Using Polyurethane (PU) Foam Injection System and Geocrete Soil Stabilization as Ground Rehabilitation // *IOP Conf. Ser.: Materials Science and Engineering*, 2016, vol. 136, 012004. DOI: 10.1088/1757-899X/136/1/012004.
2. **Samodurova T.V., Volkov V.V., Sklyarov K.A.** Modelling the bearing properties of a road structure restored using interlayer injection by means of a repairing solution // *Russian Journal of Building Construction and Architecture*, 2019, vol. 42, no. 2, pp. 44-48. DOI: 10.25987/VSTU.2019.42.2.006.
3. **Boonsung A., Phunpeng V., Horpibulsuk S., Pathompongpairoj A.,**

**Sawatwutichaikul A., Choenklang P., Hoy M., Udomchai A., Arulrajah A.** Performance of the polyurethane foam injection technique for road maintenance applications // *Transportation Geotechnics*, 2024, vol. 49, 101411. DOI: 10.1016/j.trgeo.2024.101411.

4. **Panasyuk V.V., Marukha V.I., Sylovanyuk V.P.** Injection materials: technological, mechanical, and service characteristics // *Injection Technologies for the Repair of Damaged Concrete Structures*, 2013, pp. 97-114. DOI: 10.1007/978-94-007-7908-2_5.
5. **Sabri M.M.S., Vatin N.I., Alsaffar K.A.M.** Soil injection technology using an expandable polyurethane resin: a review // *Polymers*, 2021, vol. 13, 3666. DOI: 10.3390/polym13213666.
6. **Kharchenko I.Y., Grishin A.N., Panchenko I.Y., Bazhenov M.I.** Finely dispersed composite binder for reinforcing soils by injection method // *Vestnik MGSU*, 2017, vol. 12, iss. 11, pp. 1289-1298. DOI: 10.22227/1997-0935. 2017.11.1289-1298.
7. **Fediuk R.S., Lesovik V.S., Vavrenyuk S.V.m Zaiakhanov A.Ye., Bituyev A.V., Klyuev S.V., Lesovik K.Yu., Bakatov K.A.** Composite cement materials for structures foundation strengthening // *Magazine of Civil Engineering*, 2024, vol. 17, no. 3, 12701. DOI: 10.34910/MCE.127.1.
8. **Kalach F.N.** Performance evaluation of using injection reinforcement technology with self-expanding grout of soft soils at the sub-base of shallow foundations // *Construction and Geotechnics*, vol. 11, no. 2, pp. 2-67. DOI: 10.15593/2224-9826/2020.2.06.
9. **Chun B.S., Ryu D.S.** A study on applications of polyurethane injection material for ground improvement // *KSCE Journal of Civil Engineering*, 2000, vol. 19, no. , 4 pp. 113-118. DOI: 10.1007/ BF02830823.
10. **Anagnostopoulos C.A.** Laboratory study of an injected granular soil with polymer grouts // *Tunnelling and Underground Space Technology*, 2005, vol. 20, iss. 6, pp. 525-533. DOI: 10.1016/j.tust.2005.04. 005.
11. **Wang C., Guo C., Du X., Shi M., Liu Q., Xia Y.** Reinforcement of silty soil with permeable polyurethane by penetration injection // *Construction and Building Materials*, 2021, vol. 310, 124829. DOI: 10.1016/j.conbuildmat. 2021.124829.
12. **Liu Q., Cui X., Zhang C., Huang S.** Experimental investigation of suspended particles transport through porous media: particle and grain size effect // *Environmental Technology*, 2016, vol. 37, iss. 7, pp. 854-864. DOI: 10.1080/ 09593330.2015.1088578.
13. **Tsiberkin K.** Porosity effect on the linear stability of flow overlying a porous medium // *The European Physical Journal E*, 2020, vol. 43. DOI: 10.1140/epje/ i2020-11959-6.
14. **Sibiryakov B., Leite L.W.B., Sibiriakov E.** Porosity, specific surface area and permeability in porous media // *Journal of Applied Geophysics*, 2021, vol. 186, 104261. DOI: 10.1016/j.jappgeo.2021. 104261.
15. **Mehmani A., Prodanovic M.** The effect of microporosity on transport properties in porous media // *Advances in Water Resources*, 2014, vol. 63, pp. 104-119. 10.1016/j.advwatres.2013.10.009.
16. **Kuzmina L.I., Osipov Yu.V., Pesterev A.R.** Non-linear filtration model with splitting front // *International Journal of Non-Linear Mechanics*, 2024, vol. 167, 104905. DOI: 10.1016/j.ijnonlinmec. 2024.104905.
17. **Kuzmina, L., Osipov, Y.** Model of cake filtration in porous medium // *International Journal for Computational Civil and Structural Engineering*, 2024, vol. 20, no. 3, pp. 116-124. DOI: https://doi.org/10.22337/2587-9618-2024-20-3-116-124.

18. **Kuzmina, L., Osipov, Y.** Inverse filtration problem of multiparticle suspension // *Advances in Transdisciplinary Engineering*, 2024, vol. 62. DOI:10.3233/ATDE240966.
19. **Safina G.L.** Modelling of a three-dispersed suspension filtration // *International Journal for Computational Civil and Structural Engineering*, 2023, vol. 19, no. 1, pp. 14-30. DOI: 10.22337/2587-9618-2023-19-2-14-30.
20. **Safina G.L.** Filtration problem with nonlinear filtration and concentration functions // *International Journal for Computational Civil and Structural Engineering*, 2022, vol. 18, no. 1, pp. 129-140. DOI: 10.22337/2587-9618-2022-18-1-129-140.
21. **Kuzmina L.I., Osipov Yu.V.** Exact solution to non-linear filtration in heterogeneous porous media // *International Journal of Non-Linear Mechanics*, 2023, vol. 150, 104363. DOI: 10.1016/j.ijnonlinmec.2023.104363.
22. **Bradford S.A., Bettahar M., Simunek J., Van Genuchten M.T.** Straining and attachment of colloids in physically heterogeneous porous media // *Vadose Zone Journal*, 2004, vol. 3, no. 2, pp. 384-394. DOI: 10.2113/3.2.384.
23. **Galaguz Y.P., Safina G.L.** Calculation of the filtration in a heterogeneous porous medium // *MATEC Web of Conferences*, 2017, vol. 117, 00052. DOI: 10.1051/matecconf/201711700052.
24. **Safina G.L.** Numerical solution of filtration in porous rock // E3S Web of Conferences, 2019, vol. 97, 05016. DOI: 10.1051/e3sconf/20199705016.

## СПИСОК ЛИТЕРАТУРЫ

1. **Fakhar A.M.M., Asmaniza A.** Road Maintenance Experience Using Polyurethane (PU) Foam Injection System and Geocrete Soil Stabilization as Ground Rehabilitation // *IOP Conf. Ser.: Materials Science and Engineering*, 2016, vol. 136, 012004. DOI: 10.1088/1757-899X/136/1/012004.
2. **Samodurova T.V., Volkov V.V., Sklyarov K.A.** Modelling the bearing properties of a road structure restored using interlayer injection by means of a repairing solution // *Russian Journal of Building Construction and Architecture*, 2019, vol. 42, no. 2, pp. 44-48. DOI: 10.25987/VSTU.2019.42.2.006.
3. **Boonsung A., Phunpeng V., Horpibulsuk S., Pathompongpairoj A., Sawatwutichaikul A., Choenklang P., Hoy M., Udomchai A., Arulrajah A.** Performance of the polyurethane foam injection technique for road maintenance applications // *Transportation Geotechnics*, 2024, vol. 49, 101411. DOI: 10.1016/j.trgeo.2024.101411.
4. **Panasyuk V.V., Marukha V.I., Sylovanyuk V.P.** Injection materials: technological, mechanical, and service characteristics // *Injection Technologies for the Repair of Damaged Concrete Structures*, 2013, pp. 97-114. DOI: 10.1007/978-94-007-7908-2_5.
5. **Sabri M.M.S., Vatin N.I., Alsaffar K.A.M.** Soil injection technology using an expandable polyurethane resin: a review // *Polymers*, 2021, vol. 13, 3666. DOI: 10.3390/polym13213666.
6. **Kharchenko I.Y., Grishin A.N., Panchenko I.Y., Bazhenov M.I.** Finely dispersed composite binder for reinforcing soils by injection method // *Vestnik MGSU*, 2017, vol. 12, iss. 11, pp. 1289-1298. DOI: 10.22227/1997-0935. 2017.11.1289-1298.
7. **Fediuk R.S., Lesovik V.S., Vavrenyuk S.V.m Zaiakhanov A.Ye., Bituyev A.V., Klyuev S.V., Lesovik K.Yu., Bakatov K.A.** Composite cement materials for structures foundation strengthening // *Magazine of Civil Engineering*, 2024, vol. 17, no. 3, 12701. DOI: 10.34910/MCE.127.1.
8. **Kalach F.N.** Performance evaluation of using injection reinforcement technology

with self-expanding grout of soft soils at the sub-base of shallow foundations // *Construction and Geotechnics*, vol. 11, no. 2, pp. 2-67. DOI: 10.15593/2224-9826/2020.2.06.

9. **Chun B.S., Ryu D.S.** A study on applications of polyurethane injection material for ground improvement // *KSCE Journal of Civil Engineering*, 2000, vol. 19, no. , 4 pp. 113-118. DOI: 10.1007/ BF02830823.
10. **Anagnostopoulos C.A.** Laboratory study of an injected granular soil with polymer grouts // *Tunnelling and Underground Space Technology*, 2005, vol. 20, iss. 6, pp. 525-533. DOI: 10.1016/j.tust.2005.04. 005.
11. **Wang C., Guo C., Du X., Shi M., Liu Q., Xia Y.** Reinforcement of silty soil with permeable polyurethane by penetration injection // *Construction and Building Materials*, 2021, vol. 310, 124829. DOI: 10.1016/j.conbuildmat. 2021.124829.
12. **Liu Q., Cui X., Zhang C., Huang S.** Experimental investigation of suspended particles transport through porous media: particle and grain size effect // *Environmental Technology*, 2016, vol. 37, iss. 7, pp. 854-864. DOI: 10.1080/ 09593330.2015.1088578.
13. **Tsiberkin K.** Porosity effect on the linear stability of flow overlying a porous medium // *The European Physical Journal E*, 2020, vol. 43. DOI: 10.1140/epje/ i2020-11959-6.
14. **Sibiryakov B., Leite L.W.B., Sibiriakov E.** Porosity, specific surface area and permeability in porous media // *Journal of Applied Geophysics*, 2021, vol. 186, 104261. DOI: 10.1016/j.jappgeo.2021. 104261.
15. **Mehmani A., Prodanovic M.** The effect of microporosity on transport properties in porous media // *Advances in Water Resources*, 2014, vol. 63, pp. 104-119. 10.1016/j.advwatres.2013.10.009.
16. **Kuzmina L.I., Osipov Yu.V., Pesterev A.R.** Non-linear filtration model with splitting front // *International Journal of Non-Linear Mechanics*, 2024, vol. 167, 104905. DOI: 10.1016/j.ijnonlinmec. 2024.104905.
17. **Kuzmina, L., Osipov, Y.** Model of cake filtration in porous medium // *International Journal for Computational Civil and Structural Engineering*, 2024, vol. 20, no. 3, pp. 116-124. DOI: https://doi.org/10.22337/2587-9618-2024-20-3-116-124.
18. **Kuzmina, L., Osipov, Y.** Inverse filtration problem of multiparticle suspension // *Advances in Transdisciplinary Engineering*, 2024, vol. 62. DOI:10.3233/ATDE240966.
19. **Safina G.L.** Modelling of a three-dispersed suspension filtration // *International Journal for Computational Civil and Structural Engineering*, 2023, vol. 19, no. 1, pp. 14-30. DOI: 10.22337/2587-9618-2023-19-2-14-30.
20. **Safina G.L.** Filtration problem with nonlinear filtration and concentration functions // *International Journal for Computational Civil and Structural Engineering*, 2022, vol. 18, no. 1, pp. 129-140. DOI: 10.22337/2587-9618-2022-18-1-129-140.
21. **Kuzmina L.I., Osipov Yu.V.** Exact solution to non-linear filtration in heterogeneous porous media // *International Journal of Non-Linear Mechanics*, 2023, vol. 150, 104363. DOI: 10.1016/j.ijnonlinmec.2023.104363.
22. **Bradford S.A., Bettahar M., Simunek J., Van Genuchten M.T.** Straining and attachment of colloids in physically heterogeneous porous media // *Vadose Zone Journal*, 2004, vol. 3, no. 2, pp. 384-394. DOI: 10.2113/3.2.384.
23. **Galaguz Y.P., Safina G.L.** Calculation of the filtration in a heterogeneous porous medium // *MATEC Web of Conferences*, 2017, vol. 117, 00052. DOI: 10.1051/matecconf/201711700052.
24. **Safina G.L.** Numerical solution of filtration in porous rock // E3S Web of Conferences, 2019, vol. 97, 05016. DOI: 10.1051/e3sconf/20199705016.

*Galina L. Safina,* Ph. D, Head of the Department of Fundamental Education, branch of Moscow State University of Civil Engineering in Mytishchi, Associate Professor of the Department of Computer Science and Applied Mathematics, Moscow State University of Civil Engineering; 129337, Russia, Moscow, Yaroslavskoe Shosse, 26, tel. +7(499)1835994, e-mail: minkinag@mail.ru.

*Сафина Галина Леонидовна*, кандидат технических наук, заведующий кафедрой фундаментального образования филиала НИУ МГСУ в г. Мытищи, доцент кафедры информатики и прикладной математики Национального исследовательского Московского государственного строительного университета; 129337, Россия, г. Москва, Ярославское шоссе, д. 26, тел. +7(499)1835994, e-mail: minkinag@mail.ru.

International Journal for Computational Civil and Structural Engineering, 21(3) 54–66 (2025)

DOI:10.22337/2587-9618-2025-21-3-54-66

# WARPING EFFECT IN A STEEL BOX GIRDER BRIDGE STRUCTURE

***Trong Chuc Nguyen*** [1], ***Ba Thang Phung*** [2]

[1] Le Quy Don Technical University, Hanoi 100000, VIETNAM

[2] University of Transport Technology, Hanoi 100000, VIETNAM

**Abstract:** In recent years, the construction of steel box girder bridges has become a widespread and standard practice in many major cities across Vietnam. These types of bridges are favored due to their structural strength, durability, and ability to accommodate modern traffic demands. Despite their increasing use, one important aspect often overlooked in current research is the distortion that occurs in the cross-sections of steel box girders, particularly during buckling. This distortion can significantly affect the structural performance and safety of the bridge over time. To address this research gap, this study focuses on analyzing how three critical factors—the size of the cross-section, the type of longitudinal link used, and the distance between longitudinal links—affect the buckling deformation behavior of steel box beam cross-sections. The analysis is conducted using the finite element method (FEM), a powerful simulation tool that enables detailed modeling of structural behavior under load. Through a series of simulations and evaluations, the study reveals that these parameters have a substantial influence on the deformation patterns and overall stability of the steel box girder. The results of this research contribute valuable insights that can assist engineers in designing more efficient and safer steel box bridges. Furthermore, the findings serve as a useful technical reference for current and future bridge design projects in Vietnam, helping to enhance both design standards and construction practices across the country's transportation infrastructure.

**Keywords:** Warping the section, steel box bridges, girder bridge, deformation, torsion

# ЭФФЕКТ КОРОБЛЕНИЯ В КОНСТРУКЦИИ МОСТА С КОРОБЧАТОЙ СТАЛЬНОЙ БАЛКОЙ

***Нгуен Чонг Чык*** [1], ***Пхунг Ба Тханг*** [2]

[1] Вьетнамский государственный технический университет имени Ле Куй Дона, Ханой 100000, ВЬЕТНАМ

[2] Университет транспортных технологий, Ханой 100000, ВЬЕТНАМ

**Аннотация:** В последние годы строительство мостов с коробчатыми стальными балками стало широко распространённой и стандартной практикой во многих крупных городах Вьетнама. Эти типы мостов пользуются популярностью благодаря своей высокой прочности, долговечности и способности удовлетворять требованиям современного транспортного движения. Несмотря на растущую распространённость таких конструкций, в существующих исследованиях часто упускается из виду один важный аспект — деформации, возникающие в поперечном сечении коробчатых балок, особенно при потере устойчивости (буртообразовании). Эти искажения могут существенно повлиять на несущую способность и безопасность мостовой конструкции в процессе эксплуатации. С целью восполнения данного научного пробела в настоящем исследовании проводится анализ влияния трёх ключевых факторов — размеров поперечного сечения, типа продольных связей и расстояния между ними — на поведение коробчатых стальных балок при потере устойчивости. Анализ осуществляется с использованием метода конечных элементов (МКЭ), который представляет собой мощный инструмент численного моделирования напряжённо-деформированного состояния конструкций под действием нагрузки. В результате серии численных экспериментов установлено, что указанные параметры оказывают значительное влияние на форму деформации и общую устойчивость коробчатых балок. Полученные результаты представляют собой ценный вклад в проектирование более эффективных и безопасных мостов с коробчатыми стальными балками. Кроме того, они могут служить надёжной технической основой для текущих и будущих проектов мостового строительства во Вьетнаме, способствуя улучшению проектных норм и строительных практик в транспортной инфраструктуре страны.

**Ключевые слова:** Деформация сечения, стальные коробчатые мосты, балочные мосты, деформация, кручение

## INTRODUCTION

Although Hanoi and Ho Chi Minh City in Vietnam have many steel bridges, there have been few domestic studies on how these structures function, particularly their effectiveness and response to warping in the cross-section of steel beams. Steel bridges' primary cross-sections are the I-section and the box-section. Intersections are bridges with a lot of torque when used on curved bridges, and the steel box girder bridge has the advantage of torsion stiffness. Depending on the width of the deck, the cross-section of a steel box girder bridge can take the form of a single box, several individual boxes, or a box with multiple partitions [1-3].

Bridge decks, reinforced concrete slabs combined with steel beams, and orthogonal slab decks are the most common types of steel bridges. Shear studs (Shear Stud) connect the reinforced concrete slab deck to the steel beams. Large bridges use steel orthogonal slab structures to reduce deck static load and save materials. The orthogonal slab functions as a deck slab as well as a main girder component. Because the orthogonal plate connects the main beam branches, the upper longitudinal connection system can be removed [4].

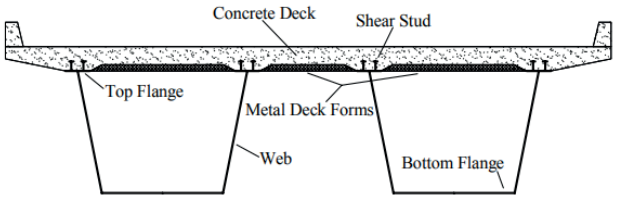


*Figure 1. Cross section of steel box beam [4]*

The bottom slab (Bottom Flange), web, top flange, and reinforced concrete deck (concrete deck) are the basic components of a composite steel box girder bridge shown in the cross-section. The bridge's box-shaped cross-section was closed. Anchor connection (Shear Stud) to ensure the unity of the steel beam and the reinforced concrete slab against sliding force and separation (Figure 1) [4-6].

The vertical and horizontal connection systems are both components of the box girder bridge's connection system. Figure 2.a depicts the internal bracing system as a K-frame. The connection system regulates the warping deformation of the box girder. Because of the shape of this K-frame connection system, it is easy to travel inside the box during construction or inspection while in use. The upper wing of the beam should have the truss form shown in Figure 2.b to control torsion during construction and erection [4].

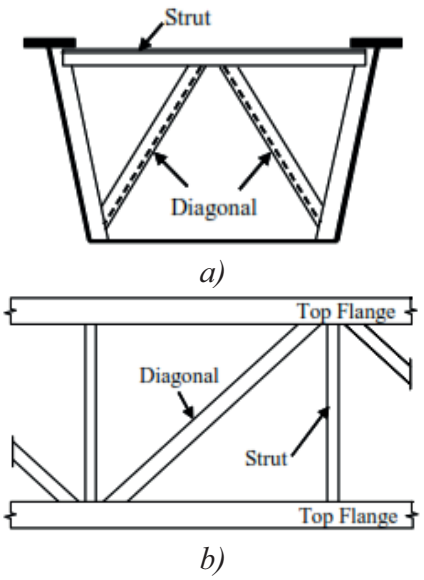


*Figure 2. Typical connection system in steel box girder bridges [4]*

The combined steel box girder solution satisfies the aforementioned criteria with exceptional benefits in span, high torsional stiffness, high aesthetics, durability, and good maintainability. The steel box girder is better for longer spans than the I-beam because it has higher flexural strength. The actual span is roughly 45-100m. This structure's span is 160 meters (Kanawha River bridge in Virginia state - USA). Because the steel box girder's structural form is more intricate than the I- beam's, manufacturing and installation of one call for highly skilled labor. Additionally, the weight of each steel box girder unit is typically higher than that of an I-beam, increasing the cost of construction. However, when compared to the I-beam span system, the steel box girder span system uses fewer main girders, transverse beams, and bracing systems, which lowers manufacturing costs as well as site labor costs. The characteristic of this type of beam is its high torsional rigidity,

so it is very suitable for curved bridges in intersections and ramps. Two bridges built in the US have a very small curvature of 45m (in the state of Massachusetts-1960) and 55m (the airport jetty at Dallas-1970). In contrast to other types of bridges, however, it should be noted that manufacturing vertical, horizontal, extremely high, and diagonal bridges can be challenging. Aesthetics are a notable benefit of steel box girder bridges. The bracing system, reinforcing ribs, utilities, and other components are "hidden" in the box, not being exposed and causing "distractions," while minimizing the risk of dust and dirt. This is in contrast to the integrated I-beam bridge. The direct corrosive effects of the environment are because they are "protected" inside the box, which lowers the cost of the coating system and makes it easy to conduct inspection and maintenance work inside the box [7].

## METHODS

### Research subjects

A steel beam structure with a span length of l = 50 m, a height of H = 1 m, a bottom plate width of beam B varying from 1.6 m to 4.6 m, and a box beam with a spaced horizontal connection system of 10 m connecting the two beam ribs is modeled and analyzed (Figure 3).

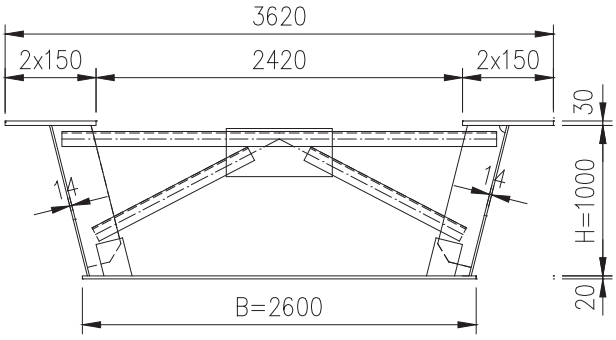


*Figure 3. Cross-section of the steel box beam surveyed*

Steel according to ASTM standards, elastic modulus E= 1.9995 kN/m$^3$; Poisson's coefficient is 0.3; thermal expansion coefficient is 1.17x10$^{-5}$; specific gravity is 77.09 kN/m$^3$.

### Working characteristics of steel box girder bridge.

Consider the cross-section of the eccentrically loaded box-shaped steel box girder P, which is analyzed into bending and torsion components (Figure 4) [8, 9].

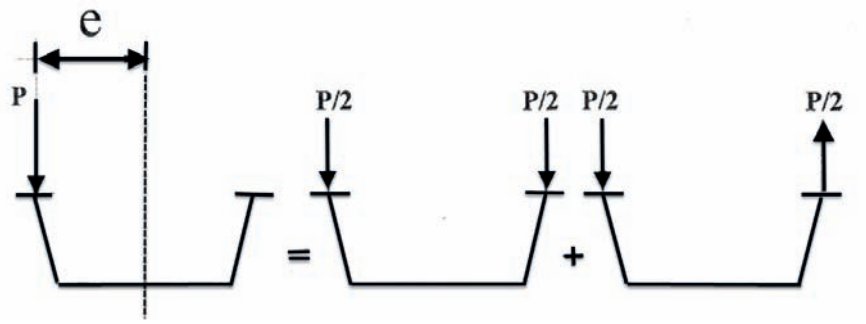


*a) Analysis of load components acting on the steel box girder cross-section*

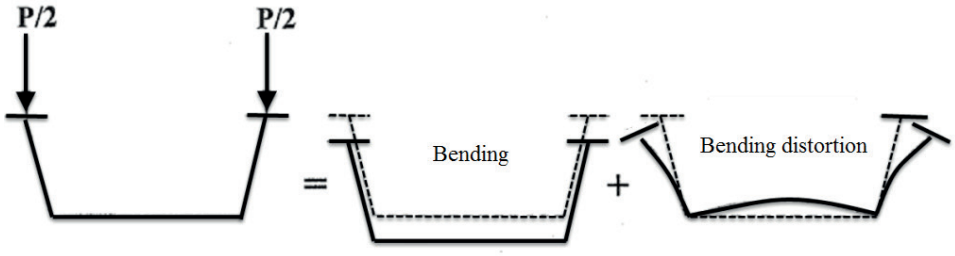


*b) Bending action*

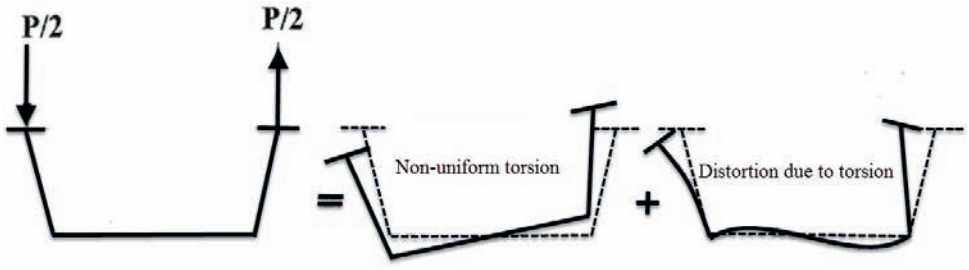


*c) Torsion effect*

*Figure 4. Analysis of load components P in open box girders according to the co-operative principle [10,11]*

Bending loads can warp and buckle sections (Figure 4.b). When impact loads are applied to beams, a common phenomenon known as longitudinal bending takes place. The cross-section is frequently assumed to always be flat when performing the calculation. When loads are applied to open boxes, deformation occurs. This distortion leads to bending in the ribs, lower flange, and upper flange of open box girders. The cross-sectional shape of the slabs is altered by the out-of-plane bending of the beams that make up the slabs. For this reason, investigating the displacement of points on the cross-section will produce conclusive findings about the phenomenon [12, 13].

The torsional load was induced on the section (Figure 4.c). Due to the curvature of the bridge, lateral loads acting on a box girder cause torsion with the girder's longitudinal axis. The cross-section is frequently assumed to always be flat when performing the calculation. Steel plates are bent and their cross-sections are deformed by torsion. In order to clearly see the effects of this phenomenon, one should study the displacement of points on the cross-section [14,15].

**Numerical method for determining the stress and strain states of steel box girders.**

The finite element method is the most popular numerical approach. With this technique, large, complex engineering problems can be solved quickly and accurately as needed. By using this technique, the texture is discretized into finite elements, linked by nodes, and supported by boundary and continuity conditions, among other conditions. Unknowns regarding Deformation and displacement at the nodes are the structural issue. Create differential equations by using fundamental mechanical principles, such as the energy principle, the virtual displacement principle, etc. This method is now available in commercial structural calculation programs like Midas, RM, Sap, Ansys, Abaqus, etc. that are frequently used in bridge construction. The elements used in the method include single-dimensional elements such as beams and bars as well as two-dimensional elements such as plates, shells, and solids (Figures 5, 6) [16-18].

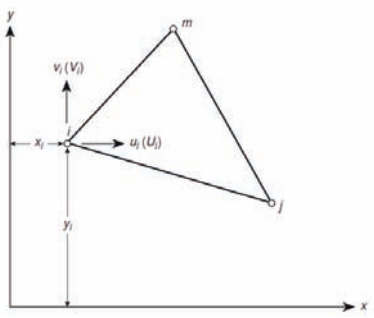


*Figure 5. Plate element*

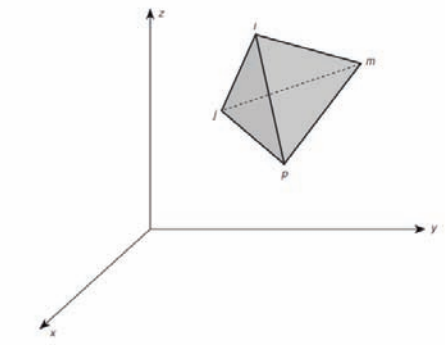


*Figure 6. Solid element*

The finite element method is regarded as a contemporary, all-encompassing approach that is currently widely used. It has demonstrated its benefits in quickly providing solutions to large-scale, complex problems. If using bar elements (6 degrees of freedom per node), the analysis will not clearly demonstrate the phenomenon of warping as well as distortion of the section based on the operation of curved steel box girders and the above-presented stress calculation formula. Therefore, the topic will analyze in detail the steel box girder structure using the plate element by the finite element method [19, 20].

## RESULTS AND DISCUSSION

**Effect of cross-sectional dimensions on section warping.** Modeling of the steel box girder section with nodes on the cross section is shown in Figure 7.

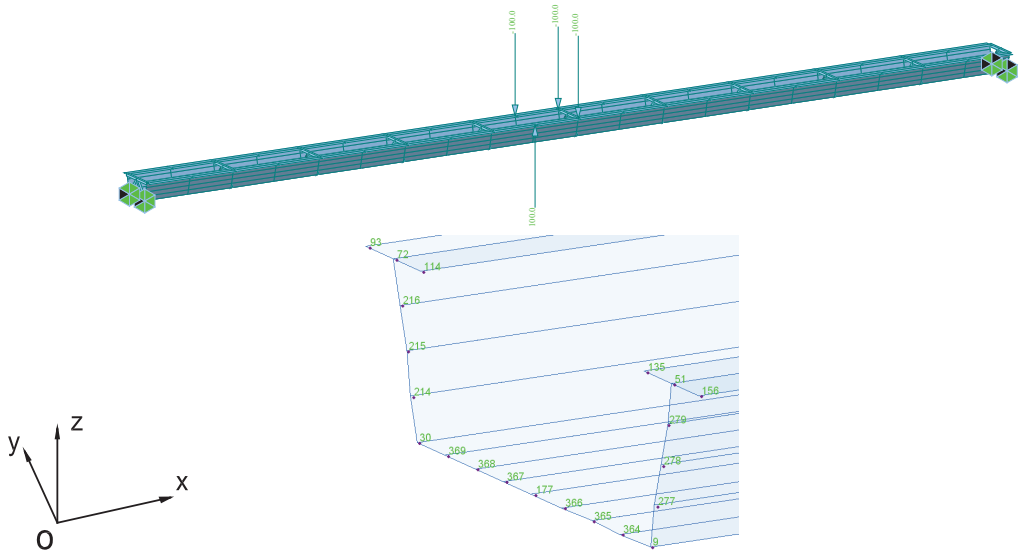


*Figure 7. Modeling the box girder segment and the nodes on the cross-section*

Surveying the width of the beam bottom plate (B) varies from 1.6m to 4.6m, the deformation results of the nodes on the beam cross section are shown in Figure 8.

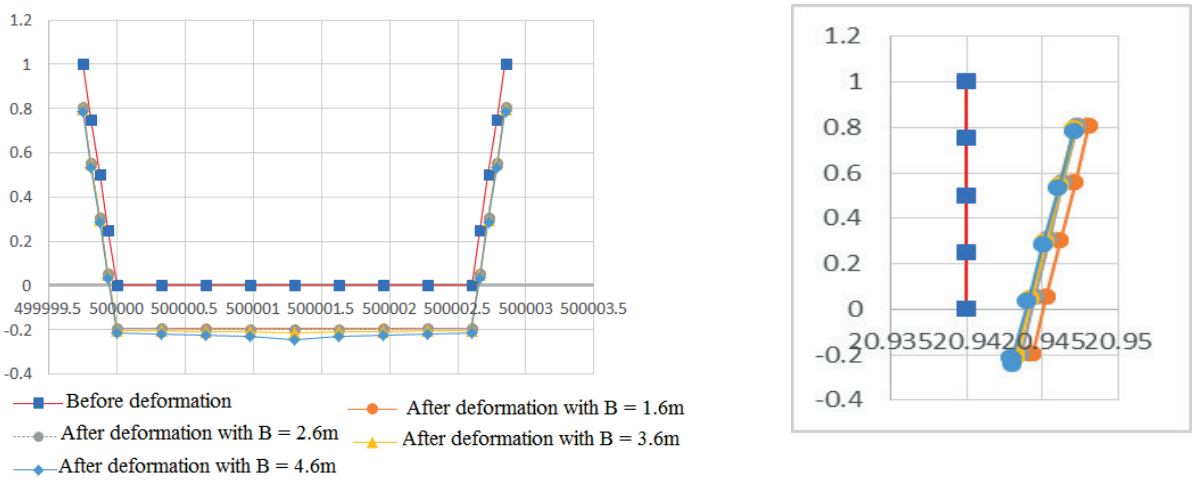


*Figure 8. Deformation due to self-load: a) deformation in the y-z plane; b) deformation in the x direction*

Figure 8 shows the deformation of the steel box girder cross-section due to the self-load. Figure 8.a shows the deformation in the y-z plane (the view is opposite to the x-axis). Figure 8.b shows the deformation in the x direction due to the change of cross section. Obviously, the deformation in the y-z plane under the effect of self-load reaches the maximum when the width of the beam bottom plate B = 4.6m. Besides, the deformation in the x direction is greatest when the width of the beam bottom plate B = 1.6m.

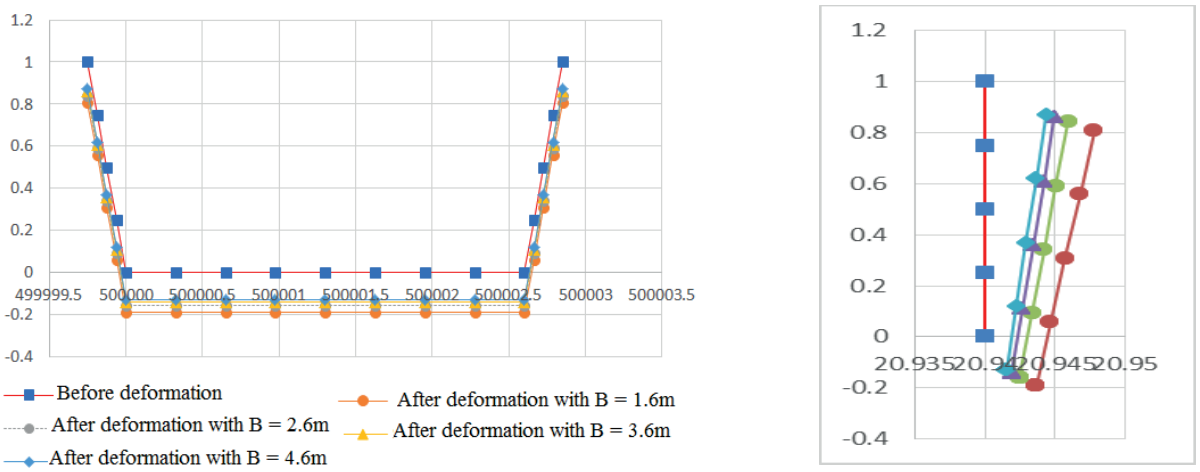


*Figure 9. Cross-sectional deformation of steel box girder under symmetrical load: a) deformation in the y-z plane; b) deformation in the x direction*

Figure 9 shows the deformation of the steel box girder cross-section under the application of symmetrical concentrated loads. Figure 9.a shows the deformation change in the y-z plane (the view is opposite to the x-axis). Figure 9.b shows the change of deformation in the x direction due to the change in cross section of the steel box girder. From Figure 9, we can see that the deformation of the cross-section in the y-z plane and in the x direction reaches the maximum value when the width of the beam bottom plate B = 1.6m.

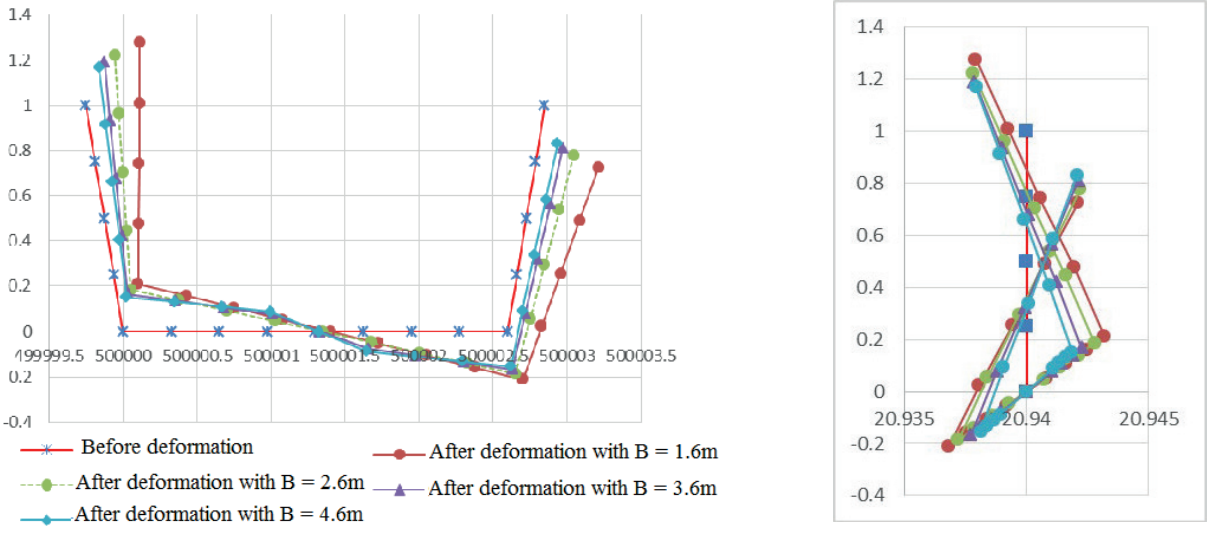


*Figure 10. Cross-sectional deformation of steel box girder due to eccentric load: a) deformation in the y-z plane; b) deformation in the x direction*

Figure 10 depicts the displacement change of the steel box girder cross-section due to eccentric load when the width of the beam bottom plate is changed. The results show that the displacement of the cross sectional nodes is significantly affected by the width of the beam bottom plate.

**Effect of distance of steel box girder cross-linking system on section warping**.

Look into how the steel box girder's cross-section warps in relation to the cross-linking system. Consider the case with and without cross-linking of steel box girders. When using a cross-linking system, the distance between them varies from 2.5m to 7.5m and as shown in Figure 11.

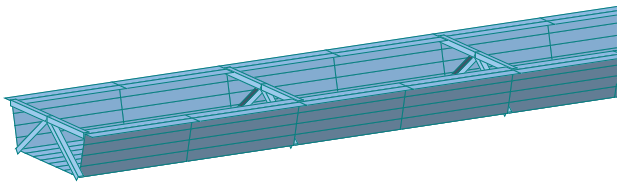

*Figure 11. Cross-linked beam model*

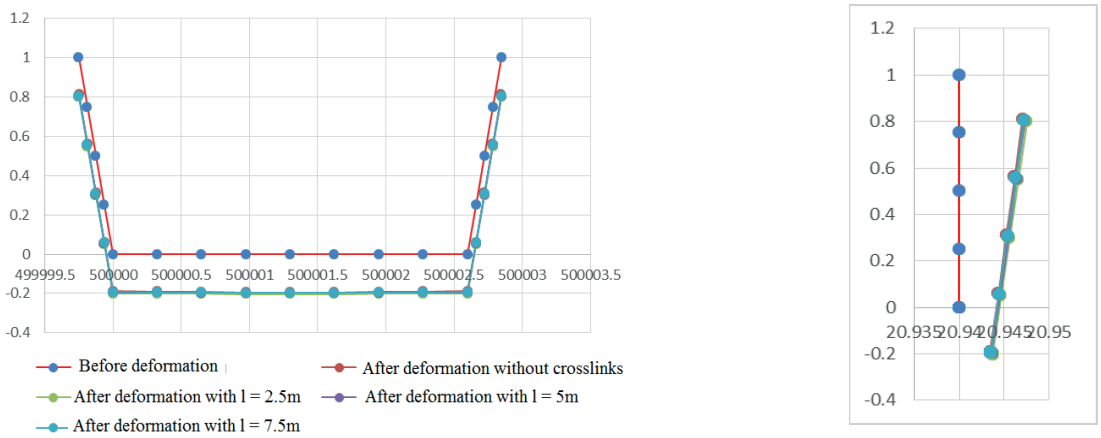


*Figure 12. Deformation due to self-load: a) deformation in the y-z plane; b) deformation in the x direction*

Figure 12 is the deformation diagram of the steel box girder cross-section caused by the self-load. Figure 12.a depicts the change in deformation in the y-z plane (opposite the x-axis view) as the crosslink spacing varies from 2.5m to 7.5m. Figure 12.b depicts the change in strain in the cross-section's x-direction as the distance between the cross-links increases from 2.5m to 7.5m.

Figure 13 is the deformation diagram of the steel box girder cross-section due to symmetrical concentrated loads.

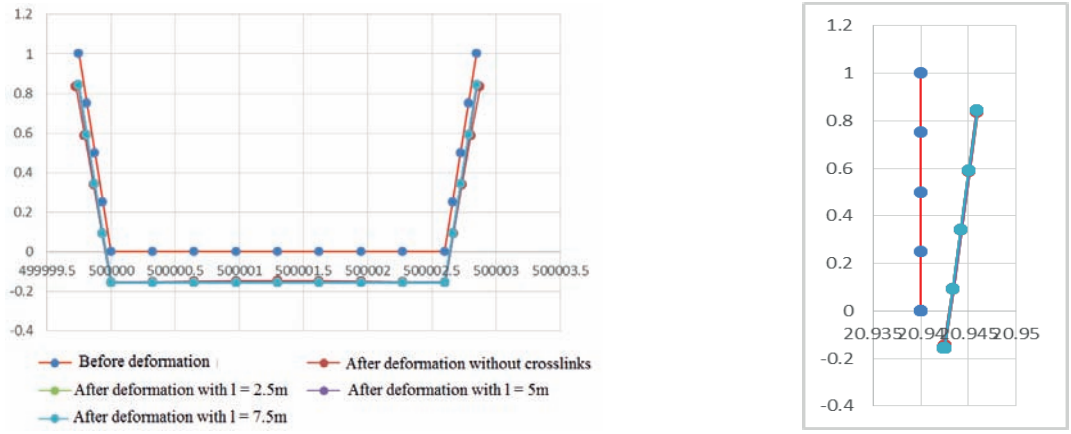


*Figure 13. Cross-sectional deformation of steel box girder under symmetrical load: a) deformation in the y-z plane; b) deformation in the x direction*

Figure 13.a shows the deformation change in the y-z plane (opposite of the x-axis view) when the crosslink distance varies from 2.5m to 7.5m. Figure 13.b demonstrates the change in strain in the x-direction of the cross-section when the cross-linking distance varies from 2.5m to 7.5m. When changing the cross-link distance of the steel box girder, the cross-sectional deformation in the y-z plane and in the x direction does not change significantly.

The deformation diagram of the steel box girder cross-section due to eccentric load is shown in Figure 14.

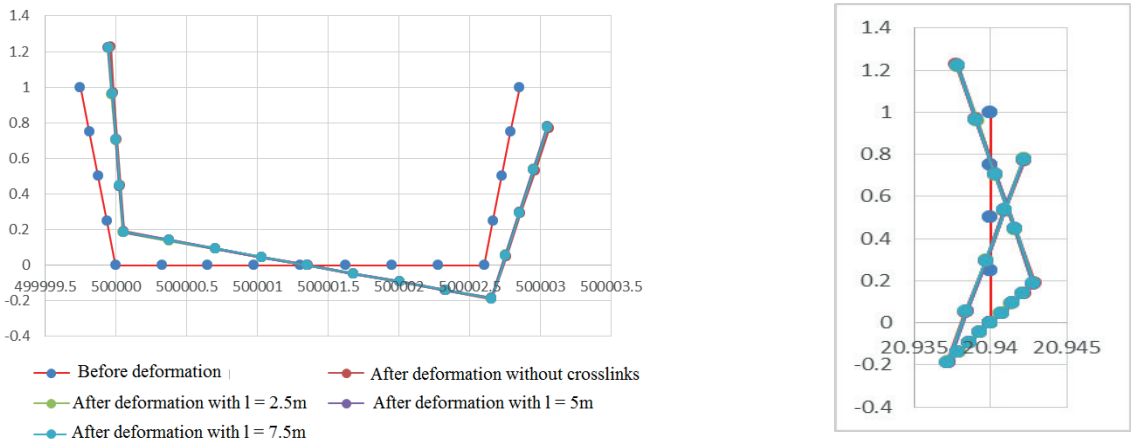


*Figure 14. Cross-sectional deformation of steel box girder due to eccentric load: a) deformation in the y-z plane; b) deformation in the x direction*

Figure 14.a shows how the deformation in the y-z plane (opposite the x-axis view) changes as the crosslink spacing varies from 2.5m to 7.5m. Figure 14.b depicts the x-direction strain change as the distance between the cross-links increases from 2.5m to 7.5m. The amount of deformation along the x-axis of the steel box girder cross-section depends greatly on the distance between the cross-beams.

**Effects of types of longitudinal connection systems on steel box girder bridges on section warping.**

Investigate the effect of longitudinal connections on cross-sectional warping in steel box girders. In this paper, we consider the cases where there is no bridge longitudinal linkage system, as well as type 1 (Figure 15.a) and type 2 (Figure 15.b) bridge longitudinal linkages.

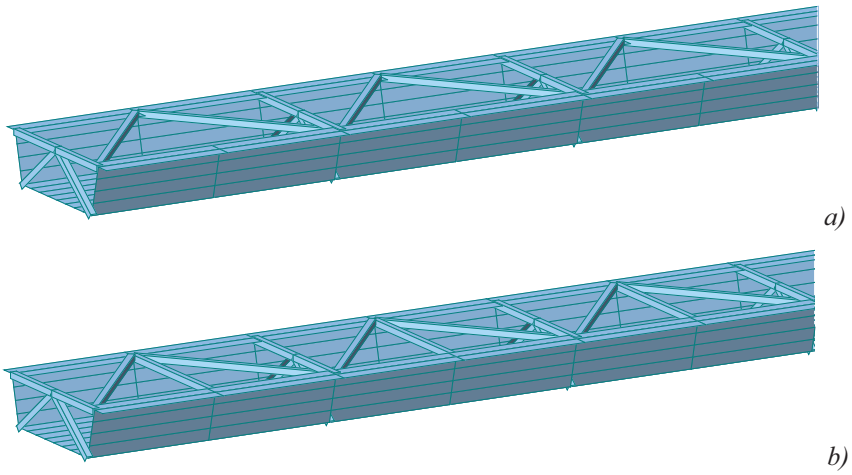


*Figure 15. Model of steel box girder with bridge longitudinal connection system*

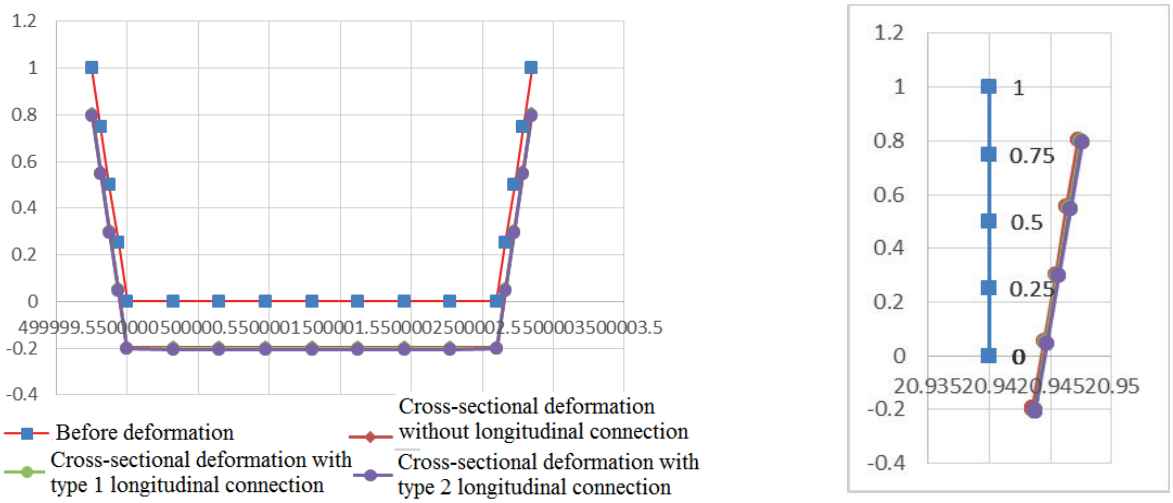


*Figure 16. Deformation due to self-load: a) deformation in the y-z plane; b) deformation in the x direction*

The self-load deformation diagram of the steel box beam cross-section is displayed in Figure 16. Figure 16.a illustrates how the strain has changed in the yx plane (the view direction is perpendicular to the x-axis), and Figure 16.b illustrates how the cross-section has changed and how the strain has changed in the x direction.

Figure 17 is the deformation diagram of the steel box beam cross-section due to symmetrical concentrated load. Figure 17.a shows the change in strain in the yx plane (view direction is opposite to the x axis), figure 17.b shows the change in strain in the x direction due to changing the cross section.

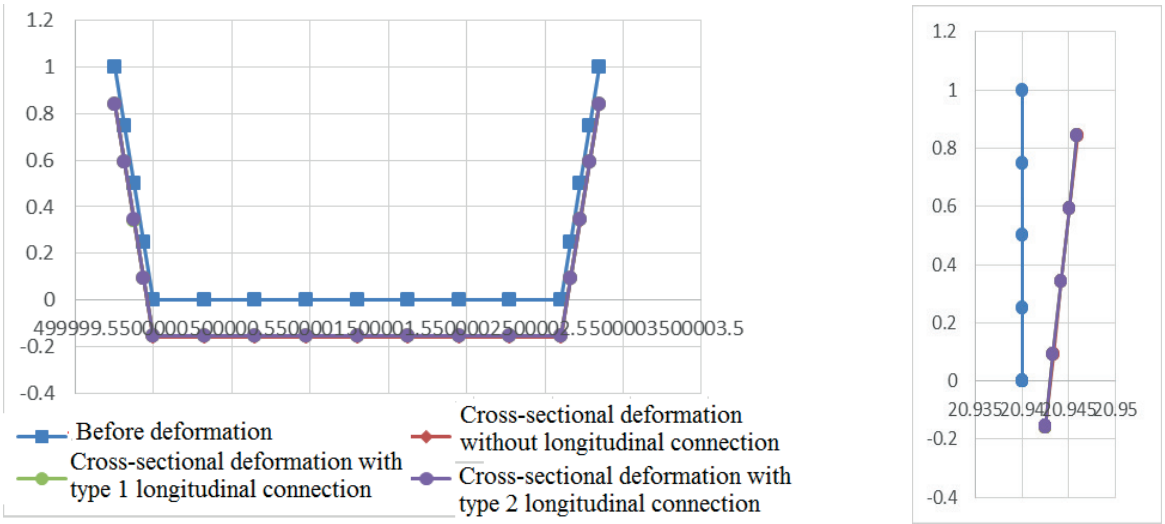


*Figure 17. Deformation due to symmetrical loading: a) deformation in the yz plane; b) deformation in the x direction*

Figure 18 shows the deformation diagram of the cross-section of a steel box beam due to eccentric loading causing torsion. Figure 18.a shows the change in strain in the yx plane (view direction is opposite to the x axis), figure 18.b shows the change in strain in the x direction due to changing the cross section.

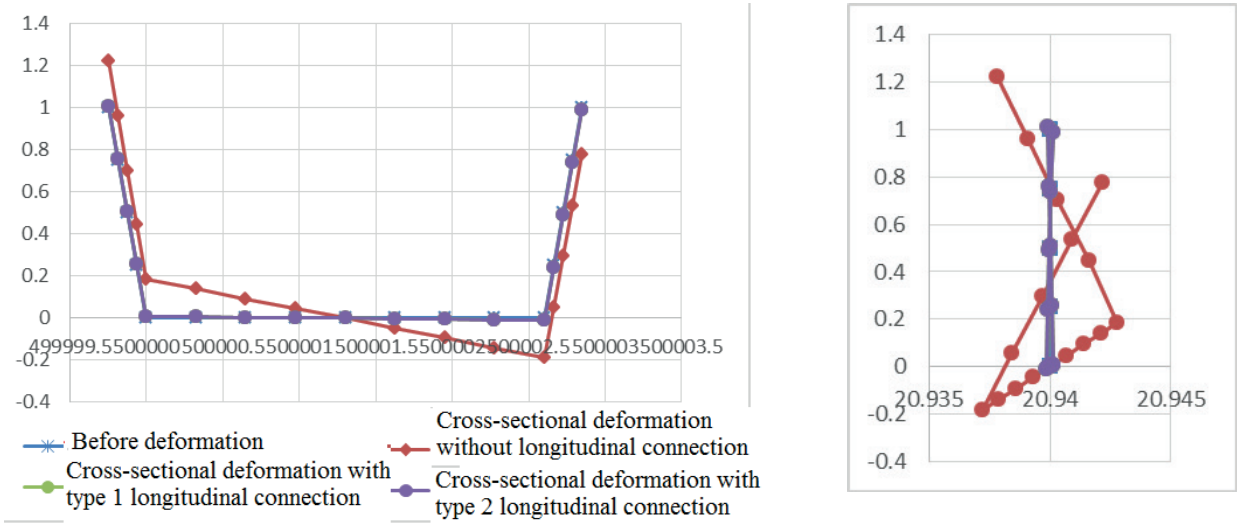


*Figure 18. Deformation due to eccentric loading: a) deformation in the yz plane; b) deformation in the x direction*

The findings displayed in the tables and graphics demonstrate how the longitudinal connection system affects warping deformation in steel box beams. It is evident how much more deformation can be prevented when the longitudinal connection system is used as opposed to not using a vertical linkage system.

## CONCLUSION

Based on the research results obtained, the following conclusions can be drawn:

1. The internal forces and displacements in a steel box girder bridge structure are significantly affected by the warping effect, which arises due to torsional deformation. This effect alters the distribution of stresses and strains, potentially compromising the structural integrity and serviceability of the bridge over time.
2. To effectively reduce the warping effect in the cross-section of a steel box beam, it is essential to carefully select an appropriate B/H ratio, determine the optimal number of horizontal beams, and choose a suitable type of vertical connection based on structural requirements.
3. The findings of this study can serve as a valuable reference for the design and optimization of steel box girder bridges in Vietnam. However, to ensure structural safety and long-term performance, the phenomenon of cross-sectional warping must be thoroughly evaluated and carefully incorporated into the design process.

## REFERENCES

1. **Nguyen Huu Hung**. (2015). Research and analyze in detail the performance of curved steel box girder bridges. *Vietnam Transport Magazine*. Vol.9(3). Pp. 46-56.
2. **Dang Viet Duc**. (2021). analyses and investigations of torsional resistance on prestressed concrete continuous box girder bridges with horizontally curved alignment. *Transport and Communications Science Journal*. Vol 72(3). Pp. 356-368. https://doi.org/10.47869/tcsj.72.3.10
3. **Nguyen Viet Trung, Hoang Ha, Le Quang Hanh**. (2005). Steel bridge structure. Construction Publishing House, Hanoi, Vietnam.
4. **Todd Helwig, Joseph Yura, Reagan Herman, Eric Williamson, Dawei Li**. (2007). Design Guidelines for Steel Trapezoidal Box Girder Systems. *Texas Department of Transportation.*
5. **Donald, W. White et al.** (2012). Guidelines for Analysis Methods and

Construction Engineering of Curved and Skewed Steel Girder Bridges. *Transportation Research Board, WASHINGTON, D.C.*

6. **Zakia B.** (2010). Analysis and Behavior Investigations of Box Girder Bridge. *M. Tech. thesis, Indian Institute of Technology Roorkee, India.*
7. **Manjula R., Amrutha A.** (2021). Parametric analysis of single-cell box girder bridge. *IOP Conf. Series: Materials Science and Engineering, Vol. 1197(012047). DOI* 10.1088/1757-899X/1197/1/012047
8. **Tauheed Reyaz, M.D., Syeda Nikhat Fathima**. (2018). Analysis and design of segmental box girder bridge. *International Research Journal of Engineering and Technology (IRJET)*. Vol. 5(3). Pp. 1912-1919.
9. **Sennah K.M., Kennedy J.B**. (2002). Literature review in analysis of box-girder bridges. *Journal of Structural Engineering ASCE*. Vol. 1061(10). Pp.1084-702. https://doi.org/10.1061/(ASCE)10840702(2002)7:2(134)
10. **Bien J., Kuzawa M., Kaminski T.** (2015). Validation of numerical models of concrete box bridges based on load test results. *Archieves of Civil and Mechanical Engineering.* Vol.15. Pp. 1046-1060. 10.1016/j.acme.2015.05.007
11. **Ayman M. Okeil, Sherif El-Tawil**. (2004). Warping Stresses in Curved Box Girder Bridges: Case Study. *Journal of Bridge Engineering*. Vol. 9(5). https://doi.org/10.1061/(ASCE)1084-0702(2004)9:5(487)
12. **Fernando A. Branco, Roger Green A**. (1985). Composite Box Girder Bridge Behavior During Construction. *Journal of Structural Engineering*. Vol. 111(3). https://doi.org/10.1061/(ASCE)0733-9445(1985)111:3(57)
13. **Ghani Razaqpur A., Hangang Li**. (1991). Thin-Walled Multicell Box-Girder Finite Element. *Journal of Structural Engineering*.Vol. 117(10). https://doi.org/10.1061/(ASCE)0733-9445(1991)117:10(295)
14. **Rajendra Thakai, Raghunath Deshpande, Shantinath Bedkihal**. (2016). Parametric study on behavior of box-girder bridges using finite element method. *International Research Journal of Engineering and Technology (IRJET).* Vol. 3(1). Pp. 211-218.
15. **John B. Kennedy, Magdy Samnna, Khaled M. Sennah**. (2007). Dynamic analysis of curved continuous multiple-box girder bridges. *ASCE Journal of Bridge Engineering*. Vol.12. Pp.184-193.
16. **Martin Alenius.** (2003). Finite element modelling of composite bridge stability. *MSc. Thesis , Department of Mechanics., Royale Institute of Technology*.
17. Gupta P.K., Singh K K., Mishra A. (2010). Parametric study on behaviour of box-girder bridges using finite element method. *Asian journal of civil engineering*. Vol. 11(1). Pp. 135-148.
18. **SAP2000**.(2012). Integrated software for structural analysis and design structural modelling and analysis. *LRFD; Bridge Design Practice.*
19. **Ibrahim A., Salim** H. (2013). Finite-element analysis of reinforced-concrete box girder bridges under close-in detonation. *Journal of Structural Engineering ASCE*, No.10.1061, pp. 1943-5509. https://doi.org/10.1061/(ASCE)CF.1943-5509.0000360
20. **Zhang Y.H., Lin L.X**. (2014). Shear lag analysis of thin-walled box girders adopting additional deflection as generalized displacemen. *Journal of Structural Engineering ASCE*, No.10.1061. Pp. 1943-7889. https://doi.org/10.1061/(ASCE)EM.1943-7889.000070

## СПИСОК ЛИТЕРАТУРЫ

1. **Nguyen Huu Hung**. (2015). Research and analyze in detail the performance of curved

steel box girder bridges // *Vietnam Transport Magazine*. Vol.9(3). Pp. 46-56.
2. **Dang Viet Duc**. (2021). analyses and investigations of torsional resistance on prestressed concrete continuous box girder bridges with horizontally curved alignment // *Transport and Communications Science Journal*. Vol 72(3). Pp. 356-368. https://doi.org/10.47869/tcsj.72.3.10
3. **Nguyen Viet Trung, Hoang Ha, Le Quang Hanh**. (2005). Steel bridge structure // Construction Publishing House, Hanoi, Vietnam.
4. **Todd Helwig, Joseph Yura, Reagan Herman, Eric Williamson, Dawei Li**. (2007). Design Guidelines for Steel Trapezoidal Box Girder Systems // *Texas Department of Transportation.*
5. **Donald, W. White et al.** (2012). Guidelines for Analysis Methods and Construction Engineering of Curved and Skewed Steel Girder Bridges // *Transportation Research Board, WASHINGTON, D.C.*
6. **Zakia B.** (2010). Analysis and Behavior Investigations of Box Girder Bridge // *M. Tech. Thesis, Indian Institute of Technology Roorkee, India.*
7. **Manjula R., Amrutha A.** (2021). Parametric analysis of single-cell box girder bridge // *IOP Conf. Series: Materials Science and Engineering*, Vol. 1197(012047). DOI 10.1088/1757-899X/1197/1/012047
8. **Tauheed Reyaz, M.D., Syeda Nikhat Fathima**. (2018). Analysis and design of segmental box girder bridge // *International Research Journal of Engineering and Technology (IRJET)*. Vol. 5(3). Pp. 1912-1919.
9. **Sennah K.M., Kennedy J.B**. (2002). Literature review in analysis of box-girder bridges // *Journal of Structural Engineering ASCE*. Vol. 1061(10). Pp.1084-702. https://doi.org/10.1061/(ASCE)10840702(2002)7:2(134)
10. **Bien J., Kuzawa M., Kaminski T.** (2015). Validation of numerical models of concrete box bridges based on load test results // *Archieves of Civil and Mechanical Engineering.* Vol.15. Pp. 1046-1060. 10.1016/j.acme.2015.05.007
11. **Ayman M. Okeil, Sherif El-Tawil**. (2004). Warping Stresses in Curved Box Girder Bridges: Case Study // *Journal of Bridge Engineering*. Vol. 9(5). https://doi.org/10.1061/(ASCE)1084-0702(2004)9:5(487)
12. **Fernando A. Branco, Roger Green A**. (1985). Composite Box Girder Bridge Behavior During Construction // *Journal of Structural Engineering*. Vol. 111(3). https://doi.org/10.1061/(ASCE)0733-9445(1985)111:3(57)
13. **Ghani Razaqpur A., Hangang Li**. (1991). Thin-Walled Multicell Box-Girder Finite Element // *Journal of Structural Engineering*.Vol. 117(10). https://doi.org/10.1061/(ASCE)0733-9445(1991)117:10(295)
14. **Rajendra Thakai, Raghunath Deshpande, Shantinath Bedkihal**. (2016). Parametric study on behavior of box-girder bridges using finite element method // *International Research Journal of Engineering and Technology (IRJET).* Vol. 3(1). Pp. 211-218.
15. **John B. Kennedy, Magdy Samnna, Khaled M. Sennah**. (2007). Dynamic analysis of curved continuous multiple-box girder bridges // *ASCE Journal of Bridge Engineering*. Vol.12. Pp.184-193.
16. **Martin Alenius.** (2003). Finite element modelling of composite bridge stability // *MSc. Thesis , Department of Mechanics., Royale Institute of Technology.*
17. **Gupta P.K., Singh K K., Mishra A.** (2010). Parametric study on behaviour of box-girder bridges using finite element method // *Asian journal of civil engineering*. Vol. 11(1). Pp. 135-148.
18. **SAP2000**.(2012). Integrated software for structural analysis and design structural

modelling and analysis // *LRFD; Bridge Design Practice.*

19. **Ibrahim A., Salim** H. (2013). Finite-element analysis of reinforced-concrete box girder bridges under close-in detonation // *Journal of Structural Engineering ASCE*, No.10.1061, pp. 1943-5509. https://doi.org/10.1061/(ASCE)CF.1943-5509.0000360
20. **Zhang Y.H., Lin L.X**. (2014). Shear lag analysis of thin-walled box girders adopting additional deflection as generalized displacemen // *Journal of Structural Engineering ASCE*, No.10.1061. Pp. 1943-7889. https://doi.org/10.1061/(ASCE)EM.1943-7889.000070

---

*Trong Chuc Nguyen* — PhD, Lecturer and Researcher; Le Quy Don Technical University; 236 Hoang Quoc Viet Street, Hanoi, Vietnam; Scopus: 57214830825, ORCID: 0000-0001-9723-5161; trongchuc.nguyen@lqdtu.edu.vn

*Ba Thang Phung* — PhD, Lecturer and Researcher; University of Transport Technology, Hanoi 100000, Vietnam; thangpb@utt.edu.vn

*Нгуен Чонг Чык* — кандидат технических наук, преподаватель-исследователь; Вьетнамский государственный технический университет имени Ле Куй Дона; Вьетнам, г. Ханой, ул. Хоанг Куок Вьет, д. 236; Scopus: 57214830825, ORCID: 0000-0001-9723-5161; trongchuc.nguyen@lqdtu.edu.vn

*Пхунг Ба Тханг* — кандидат технических наук, преподаватель-исследователь; Университет транспортных технологий, Ханой 100000, Вьетнам.

International Journal for Computational Civil and Structural Engineering, 21(3) 67–79 (2025)

DOI:10.22337/2587-9618-2025-21-3-67-79

# AUTOMATED ANALYSIS OF ELECTRICITY CONSUMPTION DURING WATER TRANSPORTATION THROUGH A PIPELINE AFTER ITS RENOVATION BY ALTERNATIVE TECHNOLOGIES WITH CONSIDERATION OF TEMPERATURE FACTOR

***Vladimir A. Orlov, Sergey P. Zotkin, Maria A. Bolshakova***

National Research Moscow State University of Civil Engineering, Moscow, RUSSIA

**Abstract**. The article considers the causes of energy consumption increase during operation of pressure pipeline networks of water supply systems and possibilities for their control. In an automated mode using mathematical modeling, an analysis was carried out of energy saving ways during water transportation in dilapidated pressure pipelines subjected to trenchless repair with alternative materials. The most effective repair options include applying a flexible polymer sleeve, multilayer hoses, polyethylene pipes and sprayed protective coatings to the inner wall of the pipeline, as well as pulling pipes made of unplasticized polyvinyl chloride into the pipeline. The role of information technologies is shown that allow us to solve problems of prompt planning of works on pipeline transport renovation with finding the optimal option by reducing energy consumption during water transportation taking into account the temperature factor when laying surface and underground pipelines.

**Keywords**: modeling, energy costs, temperature factor, pipelines, reconstruction technologies, protective materials, design assessment

# АВТОМАТИЗИРОВАННЫЙ АНАЛИЗ ПОТРЕБЛЕНИЯ ЭЛЕКТРОЭНЕРГИИ С УЧЕТОМ ТЕМПЕРАТУРНОГО ФАКТОРА ПРИ ТРАНСПОРТИРОВКЕ ВОДЫ ПО ТРУБОПРОВОДУ ПОСЛЕ ЕГО РЕМОНТА АЛЬТЕРНАТИВНЫМИ ТЕХНОЛОГИЯМИ

***Владимир А. Орлов, Сергей П. Зоткин, Мария А. Большакова***

Национальный исследовательский Московский государственный строительный университет, г. Москва, РОССИЯ

**Аннотация**. Рассмотрены причины увеличения энергетических затрат при эксплуатации напорных трубопроводных сетей систем водоснабжения и возможности управления ими. В автоматизированном режиме с использованием математического моделирования проведен анализ путей экономии электроэнергии при транспортировке воды в ветхих напорных трубопроводах, подвергнутых бестраншейному ремонту альтернативными материалами. В качестве вариантов ремонта рассматриваются наиболее эффективные технологии нанесения на внутреннюю стенку трубопровода гибкого полимерного рукава, многослойных рукавов-шлангов, полиэтиленовых труб и напыляемых (набрызгиваемых) защитных покрытий, а также протаскивания в трубопровод труб из непластифицированного поливинилхлорида. Показана роль информационных технологий, позволяющих решать задачи оперативного проектирования работ по реновации трубопроводного транспорта с отысканием оптимального варианта за счет снижения потребления электроэнергии при транспортировке воды с учетом температурного фактора при наземной и подземной прокладке трубопроводов

**Ключевые слова**: моделирование, энергозатраты, температурный фактор, трубопроводы, технологии реконструкции, защитные материалы, проектная оценка

## INTRODUCTION

Effective management of energy consumption in various industries today is an important tool for achieving key goals in the field of energy efficiency and environmental protection [1-3].
For urban water utilities, the tasks of saving material and financial resources during the construction and repair of pressure pipelines made of alternative materials, as well as maintaining or reducing the cost of electricity during the transportation of liquids are a priority [4, 5]. These tasks become even more important if the temperature factor, which is typical for different regions with warm, moderate and cold climates, as well as the methods of laying the pipeline (underground, ground or above the ground), are taken into account [6, 7].
To successfully solve the problems of reducing energy costs in the case of pipeline repair, a significant role is given to the assessment of their technical condition and the selection of optimal materials for reconstruction or modernization. The required qualitative and quantitative indicators of water and maintaining energy costs during the operation of the engineering pipeline network should be ensured by the following requirements [8, 9]:
- an appropriate degree of reliability for uninterrupted water supply to consumers at any time of day or night in the required quantity;
- the ability to resist corrosion, as well as various other influences (stray currents, aggressive soils, etc.);
- using network elements made from modern building materials that have a long service life and lower hydraulic resistance coefficients;
- minimal amount of damage to ensure a high degree of tightness of the pipeline system.

In order to reduce capital costs, the network is designed according to the principle of having minimal costs for construction and further efficient operation. The above requirement can be met provided that the diameter and material of pipelines with the appropriate hydraulic characteristics are correctly selected, ensuring the preservation or reduction of energy costs for transporting water, as well as maintaining its organoleptic characteristics.
Numerous water losses in the system, as well as an increase in energy costs in water supply system pipelines, occur for the following reasons [10]:
- due to significant losses of liquid in the network caused by improper use of water in buildings and structures;
- impossibility of efficient operation of pumping equipment;
- unsatisfactory quality of urban water supply networks;
- low level of control over the operating parameters of pipeline system elements.

Foreign researchers note that the efficiency of hydrophore station control (i.e. pumping stations with several parallel pumps) plays a significant role in energy consumption in water distribution systems, when modeling is necessary by correlation between the amount of water supplied and electricity [11]. The proposed method has proven itself as a useful tool for assessing the daily consumption of electrical energy, taking into account the flow rate and growth of water pressure in the form of fuzzy numbers. The results obtained show that it is theoretically possible and reliable to use trapezoidal fuzzy numbers in the calculation to assess the daily consumption of electricity by hydrophore stations. The error in the assessment is less than 6%.
According to domestic experience, the maximum energy saving effect at pumping stations of water supply systems is achieved by implementing a set of measures, including equipment modernization, the use of energy-saving pumping equipment, monitoring the hydraulic mode of water supply in the pumping station area, the use of a set of tools to improve the hydraulic mode of the networks, as well as a system for optimal control of the water supply mode [12].
For the implementation of labor-intensive technical, economic and hydraulic calculations of construction projects and renovation of pipeline networks, domestic practice, for the purpose of optimizing hydraulic modes and thereby reducing energy consumption during

water transportation, widely uses automated software packages of the Samara State University of Architecture and Civil Engineering (SamGASU), Bentley WaterGEMS V8, VNII VODGEO, etc. The informational operation of the above programs is based on the principles of calculations (hydraulic, economic) of certain network elements taking into account the operation of pumping equipment and spare tanks [13-15].

The priority tasks of public utilities include correct and clear management of water supply systems in urban areas. The main goal of improving management systems is to develop cost-effective and efficient technologies that provide automatic control over the thermal state of pipelines and optimization of thermal conditions of water mains and distribution networks [16]. The scientific community has repeatedly emphasized the need to use low-roughness pipelines that operate within certain temperature ranges to minimize energy consumption during water transportation [17, 18].

Some researchers have come to the conclusion that the use of information technologies based on automated programs allows for the efficient operation of water supply networks under various influences that occur in real operating conditions of the facility during various repair and restoration work on the network [19, 20]. The information technologies listed above are capable of performing various tasks, which can be quite broad. For example, conducting analysis, as well as optimization of the parameters of elements of urban water supply systems, taking into account the issues in the field of energy conservation [21].

As an example, we can note the experience of laying pipelines in various areas of the northern territories of the country, where the soil contains ice (permafrost soils), and the average annual temperature is below zero. Ensuring the reliability of water supply and preventing freezing of pipes, which consists in preventing internal icing of the pipeline during operation and transportation of water for all types of pipeline laying, remains an important technological task [22].

At the same time, researchers note that internal icing of water pipelines that occurs during emergency shutdowns not only does not disrupt their operation, but also has in a number of cases the following advantages and economic benefits [23, 24]:

-a crust of ice that forms on the inner surface of the pipe acts as a protective film, preventing direct contact of water with steel; this potentially reduces the rate of corrosion of pipes, increases their service life and improves water quality;

- the formation of ice on the inner surface of the pipe smooths out its roughness, which leads to a significant reduction in pressure losses, which allows energy costs for liquid supply to be reduced by 18-20%.

It should be noted that icing is only possible when the water temperature is close to 0°C.

Certain patterns regarding the influence of the temperature parameters of the environment and the supplied liquid on the hydraulic characteristics of pipelines were noted by researchers in the middle of the last century [25]. The main tasks were to determine the friction pressure losses along the length of the flow during hydraulic and aerodynamic calculations of pipelines of all types, especially for the supply of water, oil and gas over long distances.

In recent years, in foreign practice, one of the types of forecasting the electrical load of a water supply pipeline system for the purpose of its effective management also uses the principle of combining weather (temperature) conditions as input variables. Foreign researchers propose calculating a complex parameter - a thermal index, where two types of weather parameters are incorporated (temperature and relative humidity) [17].

The issues of saving and maintaining energy costs are on the agenda in regions with cold and hot climates. For example, the northern part of our country, called the Far North, has the peculiarity of having permafrost soils on almost the entire territory. They can be found in the Arctic, part of the Arkhangelsk Region, the Komi Republic and a large area of the Siberian

region. The average annual temperature in this area is below zero. Thus, this will obviously affect the efficiency of the pipeline [26].
In the southern regions where liquids such as oil are pumped, increasing the energy efficiency of the pipeline-pumping station system requires a comprehensive approach based on mathematical modeling that incorporates the influence of both the temperature factor and changes in the characteristics of centrifugal pumps [27].

## METHODS

The research consists of assessing the energy costs for transporting water when restoring the transport capacity of an old steel pipeline with a diameter of 325 mm and a length of 1,45 km for underground and above-ground installation options and for the corresponding temperature conditions.
The research method consists in the analysis of design solutions for selecting an optimal method of trenchless repair of an underground pipeline in an automated mode, in which, taking into account the temperature factor, the possibility of reducing energy costs for transporting water is assessed. Several automated complexes were subject to operation [28].
The following trenchless technologies were considered as methods for restoring the capacity of an old steel pipeline:
- pulling pipes made of unplasticized polyvinyl chloride UPVC SDR 41 (with an outer diameter of 225 mm, an inner diameter of 214 mm and a socket diameter of 265 mm) into a steel pipeline, followed by filling the intertube space with mortar; SDR is the ratio of the pipe diameter to its wall thickness;
- pulling and securing in an old steel pipeline a multilayer polymer sleeve-hose Primus Line, pre-deformed in the factory and fastened with tape, followed by its straightening within the old pipeline after inflation with steam under pressure;
- pulling deformed polyethylene pipes into an old pipeline using Swagelining technology without forming an intertube space;
- applying a sprayed Scotchkote coating with an appropriate wall thickness that ensures the load-bearing capacity of the pipeline system after repair;
- application of a sprayed Subcote coating with an appropriate layer thickness, which guarantees an increase in the load-bearing capacity of the repaired section of the pipeline after restoration work;
- use of a thin polymer sleeve as an internal lining that ensures the load-bearing capacity of the pipeline being restored.
Figure 1 shows in general terms fragments of the implementation of some of the listed trenchless technologies that are adopted to solve the problems of renovation of steel pipelines. Primus Line (top left), Swagelining (top right), Subcote and Scotchkote spraying (bottom left), and polymer sleeve pulling by method of air blowing and UV polymerization (bottom right).
Figure 2 shows the internal surfaces of an old pipeline after treatment with protective coatings Subcote (left) and Scotchkote (right).
Scotchkote protective coating is a non-soluble aliphatic isocyanate polyurethane that cures after application to the internal surface of the pipeline within 8-10 minutes.
The Subcote material is based on a polyurethane resin that quickly polymerizes on the inner wall of the pipeline being restored. This coating has a wide range of applications, allowing for effective spraying on the inner surface of pipes made of steel, cast iron, concrete, chrysotile cement and even old polymer pipes.
For the technology of inserting a flexible polymer sleeve into a pipeline and fixing it, in relation to its wall thickness, as well as strength characteristics, materials were used indicated in [29].
The costs of electrical energy for transporting water to the point of consumption are determined by automated programs, where 9 parameters characterizing the operation of the pipeline system are highlighted in the dialog box [30].
The type of dialog box is presented in Table 1.

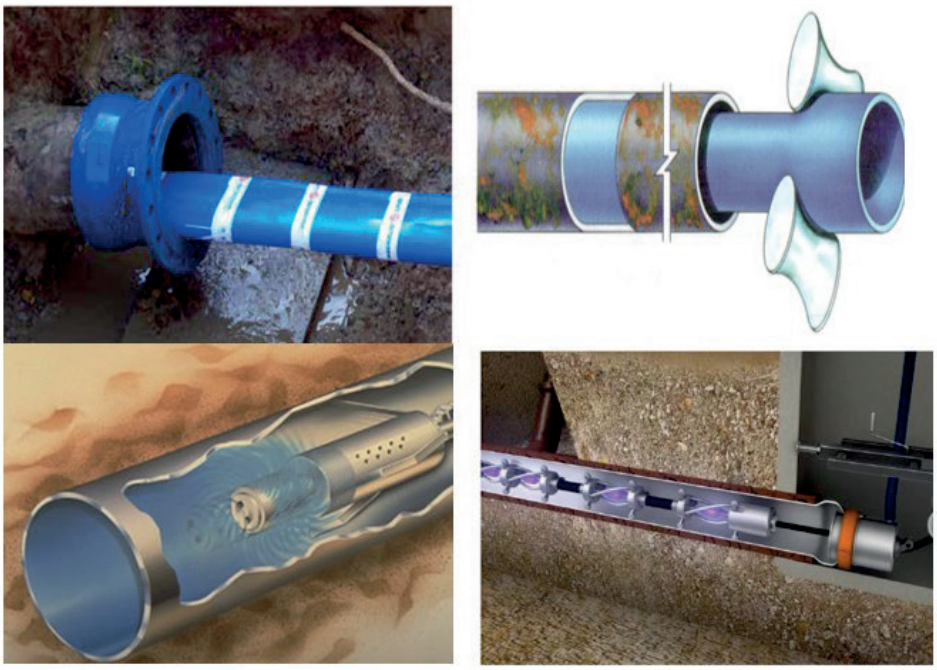

*Figure 1. Selective methods of pipeline renovation using technologies*

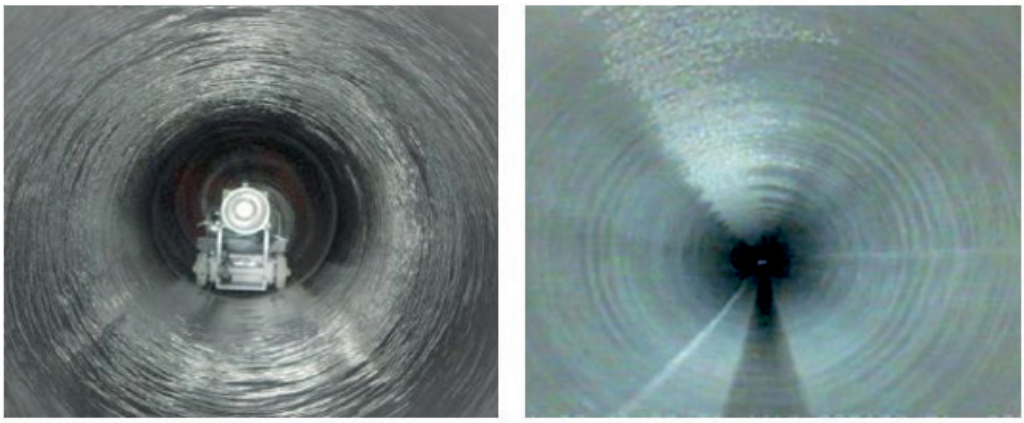

*Figure 2. Illustration of the internal surfaces of a restored steel pipeline with spray coatings applied*

*Table 1. Input information of the dialog box of the program for calculating energy costs for underground steel pipeline conditions*

| | |
|---|---|
| 1. Pipeline material | steel |
| 2. Inner diameter of the pipeline, m | 0,315 |
| 3. Length of the pipeline, m | 1450 |
| 4. Water flow rate, m3/s | 0,072 |
| 5. Efficiency of the pumping unit | 0,95 |
| 6. Temperature of the liquid flow | 10 |
| 7. Temperature of the pipe wall | 10 |
| 8. Coefficient in the formula for specific resistance of the pipe material K | 0,0017 |
| 9. Power n for diameter in the formula for specific resistance | 5,1359 |

The temperature of water transported from an underground water source, as well as the temperature of the steel pipeline wall for two installation options are taken as follows:
-10 oC, and the pipe temperature is 30 oC (for ground installation in a hot climate);
-10 oC, and the pipe temperature is 10 oC (for underground installation, i.e., when the pipe temperature is identical to the temperature of water from an underground water supply source).
The base water flow rate for all cases is taken to be 0,072 m3/s (or 72 l/s), and the specific hydraulic resistance for a steel pipe is calculated using the formula
A = 0,0017·d-5,1359.
A preliminary analysis of the printouts for two installation options for a steel pipeline at a flow rate of 0,072 m3/s showed that the power consumption is, respectively,:
Eu = 31,397 thousand kWh/year (underground installation)
Eo = 29,191 thousand kWh/year (ground installation)
Thus, owing to the change (decrease) in the viscosity of the transported liquid during ground laying, due to the increase in the temperature of the pipeline wall and the change in the coefficient of hydraulic friction λ from 0,015247 to 0,013867, the values of electricity consumption differ by 1,0701 times (or 7,01%).
With regard to the use of the technology of pulling a PVC-U pipe into the steel pipeline for its repair, a preliminary strength calculation of a two-layer pipe structure was performed using an automated program with a dialog box presented in Table 2 [31].
The resulting two-layer structure after repair and construction work meets the strength conditions. In particular, it ensures:
- compliance with the conditions of maximum permissible deformation in the pipe cross-section;
- resistance to floating, i.e. overcoming the Archimedes force of the round shape of the polymer pipe pulled into the restored pipeline.
The calculated data for the "steel + PVC-U" structure showed that the resulting two-layer pipe structure meets the listed strength requirements.

*Table 2. Input information of the dialog box of the program for strength calculation of a two-layer structure "steel + PVC-U"*

| | |
|---|---|
| 1. Diameter of the pipeline to be renovated, m | 0,315 |
| 2. Diameters of the new pipeline pulled into the old one:<br>outer, m<br>inner, m | <br><br>0,225<br>0,214 |
| 3. Volumetric weights, N/m3:<br>cement mortar<br>pulled pipe<br>transported water | <br>25000,0<br>9500,0<br>9800,0 |
| 4. Internal pressure of the transported medium corresponding to the reduced design stress | 0,00 |
| 5. Value of possible vacuum in the inter-pipe space, MPa | 0,00 |
| 6. Standard service life of the pulled pipeline, years | 50,0 |
| 7. Maximum operating temperature of the pulled pipeline, degrees Celsius | 30,00 |
| 8. Maximum permissible value of ovalization of the cross-section, % | 5,0 |

As far as the renovation using Primus Line technology is concerned, two versions of the pulled-through sleeve-hose were subject to analysis:
- two-layer aramid fabric with a thickness of 9,0 mm with an outer diameter of 315 mm and an inner diameter of 297 mm;
- similar single-layer fabric with a layer thickness of 6,5 mm; while the outer and inner diameters are 315 and 302 mm, respectively.
According to the calculated data obtained as a result of using the software package [32], when using the Swagelining technology with a polymer pipe SDR 50 with a diameter of 355 mm, subjected to preliminary thermomechanical compression and subsequent expansion after pulling into the old steel pipeline, the internal diameter of the two-layer pipe structure will be 300,73 mm (Table 3). Table 3, as an example, also provides data on pipes with a wide range of SDR values, which can be considered as an alternative to the selected option.

*Table 3. Output summary information with data on pipeline diameters and pressure losses at different SDR values*

| | Values of SDR | | | | | | |
|---|---|---|---|---|---|---|---|
| Calculated values | 11 | 17 | 21 | 26 | 33 | 41 | 50 |
| Internal diameter after renovation, mm | 248,77 | 272,16 | 280,76 | 287,45 | 292,96 | 297,54 | 300,73 |
| Head loss after renovation, m | 2,995 | 1,791 | 1,498 | 1,309 | 1,174 | 1,074 | 1,011 |

As follows from the calculated data in Table 3, when using Swagelining technology with SDR 50 pipeline, pressure losses are minimal, which will allow achieving the greatest energy saving effect during water transportation.

## RESULTS AND DISCUSSION

Below is a comparative analysis of alternative methods for renovating an old steel pipeline.
A. Calculation of energy savings for transporting water in a two-layer pipe structure "steel + PVC-U" for underground installation and an efficiency of 0,95.
Value of the coefficient of specific resistance of a PVC-U pipe: APVC-U = 0,0008·d-5,1977 [4].
Energy savings for a two-layer ground pipeline are negative equal to -16.965 thousands kWh per year.
Thus, it should be noted that this reconstruction option using a PVC-U pipe is unacceptable due to the increase in energy costs due to a significant narrowing of the flow cross-section of the pipeline after repair.

B. Calculation of energy savings for transporting water in a two-layer pipe structure "steel + Primus Line sleeve-hose" for underground installation and an efficiency of 0,95.
Option 1. Using a two-layer aramid fabric 9.0 mm thick (outer diameter is 315 mm, inner diameter is 297 mm) as a protective coating, the specific resistance coefficient is A = 0.0004·d-5.7276.
The energy savings for a two-layer ground pipeline are 10.899 thousands kWh per year.
Thus, it should be noted that, despite the slight narrowing of the flow cross-section of the pipeline after repair, this reconstruction option using the coating is acceptable because of the reduction in energy costs due to the reduction in hydraulic resistance of the pipeline wall.
Option 2. Using a single-layer aramid fabric 6,5 mm thick (outer diameter is 315 mm, inner diameter is 302 mm), the specific resistance coefficient is A = 0,0004·d-5,7276.
The energy savings for a two-layer ground pipeline are 12.768 thousands kWh per year.

Thus, we note that this renovation option is not expensive in terms of energy savings.

C. Calculation of energy savings for water transportation in a two-layer pipe structure "steel + pre-compressed polyethylene" (Swagelining) for underground installation and an efficiency of 0,95.

The possibility of using SDR 50 polymer pipes (outer diameter is 355 mm, inner one is 300,73 mm) as a protective coating is considered, the coefficient of specific resistance is A = 0.0009·d-5.2146.

The energy savings for a two-layer ground pipeline are 7.919 thousands kWh per year.

Therefore, it can be concluded that this reconstruction option is somewhat inferior to the above-mentioned renovation options in terms of energy savings.

D. Calculation of energy savings for water transportation in a two-layer pipe structure “steel + spray coating” (Scotchkote) for underground installation.

When applying the coating, the internal diameter of the steel two-pipe pipeline will be 315-2·5=305 mm, and the specific resistance coefficient is A=0,0008d-5,1883.

Energy savings on a two-layer ground pipeline amount to 12.84 thousands kWh per year.

This reconstruction option is not expensive in terms of energy savings.

E. Calculation of energy savings for water transportation in a two-layer pipe structure "steel + spray coating (Subcote)" for underground installation and efficiency of 0,95.

After carrying out repair and restoration work, the internal diameter of the steel two-pipe pipeline will change and become 315-2·4=307 mm, and the specific resistance coefficient is A=0,0008d-5,19.

Energy savings on a two-layer ground pipeline amount to 13.423 thousands kWh per year.

This reconstruction option is also not expensive in terms of energy savings.

F. Calculation of energy savings for water transportation in a two-layer pipe structure “steel + polymer sleeve” for underground installation and efficiency of 0,95.

When inserting and fixing a thin polymer sleeve into a pipeline, the internal diameter of the steel pipeline will become 315-2·3=309 mm, and the specific resistance coefficient is A=0,0007d-5,2791.

The wall thickness of the thin-wall polymer pipeline equal to 3 mm was selected based on the results of the automated calculation [33].

The energy savings for the two-layer ground pipeline is 14.513 thousands kWh per year.

Thus, it should be noted that this reconstruction option is the most acceptable in comparison with the others in terms of energy savings.

Table 4 presents the summary calculation results for underground installation, which allow the designer to assess the degree of potential reduction in energy costs for water transportation after renovation work on the steel pipeline (base option) with alternative trenchless methods has been executed.

*Table 4. Summary data on reduction in electricity costs for underground installation after execution of renovation work (without the unacceptable option of renovation with PVC-U pipe)*

| Name of the double-layer pipeline | Reduction in electricity consumption compared to the base case, % |
|---|---|
| Steel + sleeve-hose (Primus Line)<br>Option 1<br>Option 2 | <br>34,0<br>40,7 |
| Steel + pre-compressed polyethylene (Swagelining) | 25,2 |
| Steel + spray coating (Scotchkote) | 40,9 |
| Steel + spray coating (Subcote) | 42,7 |
| Steel + polymer sleeve | 46,2 |

Taking into account the data in Table 4, the method of pulling a polymer sleeve into a steel pipeline and fixing it inside the pipeline can be adopted as the most acceptable trenchless renovation technology in terms of the energy costs, among other methods under consideration, for which the energy consumption can be reduced by 46,2%. According to calculations, given the cost of 1 kWh equal to 5,25 rubles for industry, the monetary costs for renovation options for the case of underground pipeline laying with a pump efficiency of 0,95 and a flow rate of 0,072 m3/s will amount to the values presented in Table 5.

*Table 5. Comparative data on the values of energy costs and savings in money when transporting water through a renovated pipeline depending on the repair method*

| Name of the double-layer pipeline | Energy savings on water transportation per year in thousands of kWh | Reduction of water transportation costs per year in thousands of rubles. |
|---|---|---|
| Steel + sleeve-hose (Primus Line)<br>Option 1<br>Option 2 | <br>10,899<br>12,768 | <br>57,22<br>67,03 |
| Steel + pre-compressed polyethylene (Swagelining) | 7,919 | 41,57 |
| Steel + spray coating (Scotchkote) | 12,84 | 67,41 |
| Steel + spray coating (Subcote) | 13,423 | 70,47 |
| Steel + polymer sleeve | 14,513 | 76,19 |

Thus, the cheapest option for savings on electricity when transporting water can be considered as the "steel + polymer sleeve" method. This trenchless technology is considered the least expensive in terms of money savings. Other technologies can also be used, but they provide a slightly smaller effect on energy savings. It should be noted that the use of any other methods of pipeline renovation among the trenchless technologies used in practice is not excluded after assessing the values of possible energy savings when using them.

## CONCLUSIONS

1. Based on the results of modeling using automated programs, a project assessment of the possible reduction in electricity costs (taking into account the temperature factor) during the transportation of water through an old pressure pipeline, after repair and restoration work has been executed, was obtained using a specific example.
2. Based on the analysis of calculated data, the dynamics of the reduction in energy costs for transporting water through a restored pipeline, as well as savings in funds for several alternative methods for pipeline repair, are presented.
3. The technology of applying a protective coating in the form of a polymer sleeve has been identified as the most effective method of trenchless pipeline renovation in terms of the possibility of achieving energy saving effects.
4. It has been proposed that the management of the operating parameters of the pipeline system should be carried out at the design stage by selecting the most cost-effective option for its construction and repair, taking into account cost estimates, temperature conditions of the ambient environment and the transported water, as well as the minimum cost of electricity consumption.

## REFERENCES


1. **Leznov B.S.** Energosberezheniye i reguliruyemyy privod v nasosnykh i vozdukhoduvnykh ustanovkakh // M.: Energoatomizdat. 2006. 359 p.
2. **Heber Pimentel Gomes, Pedro Augusto Silva Sabino de Farias, Saulo de Tarso Marques Bezerra, Sabrina da Silva** Efficiency indicator for assessment of water distribution networks carrying capacity //Environmental Engineering and Management Journal. May 2020, Vol. 19, No. 5, 747-753
3. **Mihai Toderaşc, Vlad Iordache, Cristian Petcu, Horia Petran** Real time monitoring of indoor environment quality and energy consumption in a residential building //Environmental Engineering and Management Journal. July 2019, Vol. 18, No. 7, 1391-1620
4. **Orlov V.A.** Bestransheynyye tekhnologii i energosberezheniye.-M: ASV. 2021. 123 p.
5. **Chupin R.V., Melekhov E.S.** Justification of the parameters of developing water supply and sanitation systems based on their electronic models // IOP Conference Series: Materials Science and Engineering, 2020. DOI: 10.1088/1757-899X/880/1/012050
6. **Vladimir Orlov, Dmitry Peterburgsky** Temperature as a factor of energy consumption in pipeline network operation. // AIP Conference Proceedings 2791, 050016 (AUGUST 02 2023) DOI: https://doi.org/10.1063/5.0143462
7. **Houghtalen R., Osman A., Akan A., Hwang N.** Fundamentals of Hydraulic Engineering Systems, 5th edition. Pearson. 2016. 528 p.
8. **Dobromyslov A.YA.** Problema dolgo-vechnosti i nadezhnosti truboprovodnykh sistem // Zhurnal «Santekhnika». 2003. No. 5. p. 2-4.
9. **Otstavnov A.A., Ustyugov V.A., Dmitriyev A.N.** K voprosu minimizatsii zatrat na ustroystvo i ekspluatatsiyu podzemnykh vodoprovodov // Zhurnal «Santekhnika». 2006. No. 9. p. 38-43
10. **Gal'perin Ye.M.** Opredeleniye nadezhnosti funktsionirovaniya kol'tsevoy vodo-provodnoy seti // Zhurnal «Vodo-snabzheniye i sanitarnaya tekhnika». 1999. No. 6. s. 23-28
11. **Grigoras G. Istrate M.** Energy consumption estimation in water distribution systems using fuzzy techniques // Environmental Engineering and Management Journal, 2008, Vol. 9, Nr. 2, ISSN: 1843-3707
12. Vodosnabzheniye Sankt-Peterburga // Pod redaktsiyey F.V.Karmazinova. Izd. «Novyy mir». SPb. 2003. 322 p.
13. **Govindan SH., Val'ski T., Kuk D.** Resheniya Bentley Systems: gidravlicheskiye modeli. Pomogaya prinimat' luchshiye resheniya // Zhurnal «SAPR i grafika». 2009. No 4. p. 36-38
14. **Borisov D.A.** Bentley Systems – modelirovaniye i ekspluatatsiya naruzhnykh setey vodosnabzheniya i kanalizatsii // Zhurnal «SAPR i grafika». 2009. No. 5. p. 64-68
15. **Seleznev V.Ye., Aleshin V.V., Pryamov S.M.** Matematicheskoye modelirovaniye truboprovodnykh setey i sistem kanalov //M.: Maks-Press. - 2007. 695 p.
16. **Khramenkov S.V., Primin O.G.** Reglament ekspluatatsii vodoprovodnoy seti.-M.: //Miklosh. 2007. 223 p.
17. **Gilda Gavrilaş, Mihai Gavrilas, Ovidiu Ivanov** /Electricity load prediction for water supply systems // Environmental Engineering and Management Journal, July/August 2008, Vol. 7, Nr. 4, ISSN: 1843 – 3707 c.
18. **Khramenkov S.V., Primin O.G**. Rekonstruktsiya truboprovodnykh sistem.-M: ASV. 2008. 215 p.
19. **Bogdasarov N.V.** Obobshcheniye opyta ekspluatatsii vodovodov v yuzhnykh rayonakh vechnoy merzloty. / Vodosnabzheniye i kanalizatsiya naselennykh mest v rayonakh Vostochnoy

Sibiri Kraynego Severa. Materialy k Vsesoyuznoy konferentsii/ L.: LISI, 1966.
20. **Bondarev E.A.** Teplovoye i mekhanicheskoye vozdeystviye inzhenernykh sooruzheniy s merzlymi gruntami. Novosibirsk: Nauka, 1977. 140 p.
21. **Vdovin Yu.I.** Water supply in the north. L.: Stroyizdat, Leningrad department, 1987. 166 p..
22. Instruktsiya po proyektirovaniyu setey vodosnabzheniya i kanalizatsii dlya rayonov rasprostraneniya vechnomerzlykh gruntov. SN 510-78. M.: Stroyizdat, 1979. 72 p.
23. **Zenger N.N.** Osobennosti ustroystva truboprovodov v usloviyakh vechnoy merzloty. M.: Stroyizdat. 1964.99 s.
24. **Stegantsev V.P.** Issledovaniya raboty vodovodov v surovykh klimaticheskikh usloviyakh Vostochnoy Sibiri. Avtoreferat dissert. na soiskaniye uch. stepeni. kand. tekhn. nauk. Krasnoyarsk, KrasNPSNIIP. 1965.-28 p.
25. **Al'tshul' A.D.** Gidravlicheskiye soprotivleniya, − 2-ye izd. pererab. i dop. M., Nedra, 1982, p. 224.
26. **Terekhov L.D.** Tekhnologicheskiye osnovy energosberezheniya pri podache vody po vodovodam na Severe: monografiya / L.D. Terekhov. – Khabarovsk: Izd-vo DVGUPS, 2008
27. **Kuspanov A.B.** Povysheniye energo-effektivnosti truboprovodnoy sistemy v sluchaye goryachey perekachki vysokovyazkikh neftey //Molodoy uchenyy. 2017. No 18 (152). p. 45-48
28. **Orlov V.A.** Instrumenty tsifrovizatsii v praktike proyektirovaniya truboprovodnykh sistem-Moskva-Vologda.: Izdatel'stvo «Infra-Inzheneriya». 2024. 125 p.
29. **Zakharov Yu.S., Orlov V.A.** Remont i vosstanovleniye samotechnykh vodo-otvodyashchikh setey.-M.: Izdatel'stvo ASV. 2023. 265 p.
30. **Orlov V.A., Zotkin S.P., Inshakova M.A., Gerasimov V.A.** Analiz potrebleniya elektroenergii pri transportirovke vody po napornym truboprovodam iz al'ternativnykh materialov. Svidetel'stvo o gosudarstvennoy registratsii programmy dlya EVM No. 2021615221 (06.04.2021).
31. **Khurgin R.Ye., Orlov V.A., Zotkin S.P**. Programma opredeleniya nagruzok na truboprovod s proverkoy yego nesushchey sposobnosti pri rekonstruktsii. Svidetel'stvo o gosudarstvennoy registratsii programmy dlya EVM No 201361544 (10.06.2013).
32. **Orlov V.A., Zotkin S.P., Zotkina I.A., Khrenov K.Ye.** Raschet parametrov raboty napornykh truboprovodov, vosstanav-livayemykh predvaritel'no szhatymi polimernymi trubami. Svidetel'stvo o gosudarstvennoy registratsii programmy dlya EVM No. 2014612753 (06.03.2014).
33. **Orlov V.A., Zotkin S.P., Pelipenko A.A.** Raschet tolshchiny stenki gibkogo polimernogo rukava pri renovatsii truboprovodov. Svidetel'stvo o gosudarstvennoy registratsii programmy dlya EVM No. 2017615864 (30.05.2017).

## СПИСОК ЛИТЕРАТУРЫ

1. **Лезнов Б.С.** Энергосбережение и регулируемый привод в насосных и воздуходувных установках // М.: Энергоатомиздат. 2006. 359 с.
2. **Heber Pimentel Gomes, Pedro Augusto Silva Sabino de Farias, Saulo de Tarso Marques Bezerra, Sabrina da Silva** Efficiency indicator for assessment of water distribution networks carrying capacity //Environmental Engineering and Management Journal. May 2020, Vol. 19, No. 5, 747-753
3. **Mihai Toderaşc, Vlad Iordache, Cristian Petcu, Horia Petran** Real time monitoring of indoor environment quality and energy consumption in a residential building //Environmental Engineering and Management Journal. July 2019, Vol. 18, No. 7, 1391-1620
4. **Орлов В.А.** Бестраншейные технологии и энергосбережение.-М: АСВ. 2021. 123 с.

5. **Chupin R.V., Melekhov E.S.** Justification of the parameters of developing water supply and sanitation systems based on their electronic models // IOP Conference Series: Materials Science and Engineering, 2020. DOI: 10.1088/1757-899X/880/1/012050
6. **Vladimir Orlov, Dmitry Peterburgsky** Temperature as a factor of energy consumption in pipeline network operation. // AIP Conference Proceedings 2791, 050016 (AUGUST 02 2023) DOI: https://doi.org/10.1063/5.0143462
7. **Houghtalen R., Osman A., Akan A., Hwang N.** Fundamentals of Hydraulic Engineering Systems, 5th edition. Pearson. 2016. 528 p.
8. **Добромыслов А.Я.** Проблема долговечности и надежности трубопроводных систем // Журнал «Сантехника». 2003. № 5. с. 2-4.
9. **Отставнов А.А., Устюгов В.А., Дмитриев А.Н.** К вопросу минимизации затрат на устройство и эксплуатацию подземных водопроводов // Журнал «Сантехника». 2006. № 9. с. 38-43
10. **Гальперин Е.М.** Определение надежности функционирования кольцевой водопроводной сети // Журнал «Водоснабжение и санитарная техника». 1999. № 6. с. 23-28
11. **Grigoras G. Istrate M**. Energy consumption estimation in water distribution systems using fuzzy techniques // Environmental Engineering and Management Journal, 2008, Vol. 9, Nr. 2, ISSN: 1843-3707
12. Водоснабжение Санкт-Петербурга // Под редакцией Ф.В.Кармазинова. Изд. «Новый мир». СПб. 2003. 322 с.
13. **Говиндан Ш., Вальски Т., Кук Д.** Решения Bentley Systems: гидравлические модели. Помогая принимать лучшие решения // Журнал «САПР и графика». 2009. № 4. с. 36-38
14. **Борисов Д.А.** Bentley Systems – моделирование и эксплуатация наружных сетей водоснабжения и канализации // Журнал «САПР и графика». 2009. № 5. с. 64-68
15. **Селезнев В.Е., Алешин В.В., Прямов С.М.** Математическое моделирование трубопроводных сетей и систем каналов //М.: Макс-Пресс. - 2007. 695 с.
16. **Храменков С.В., Примин О.Г**. Регламент эксплуатации водопроводной сети.-М.: //Миклош. 2007. 223 с.
17. **Gilda Gavrilaş, Mihai Gavrilas, Ovidiu Ivanov** /Electricity load prediction for water supply systems // Environmental Engineering and Management Journal, July/August 2008, Vol. 7, Nr. 4, ISSN: 1843 – 3707 с.
18. **Храменков С.В., Примин О.Г.** Реконструкция трубопроводных систем.-М: АСВ. 2008. 215 с.
19. **Богдасаров Н.В.** Обобщение опыта эксплуатации водоводов в южных районах вечной мерзлоты. / Водоснабжение и канализация населенных мест в районах Восточной Сибири Крайнего Севера. Материалы к Всесоюзной конференции/ Л.: ЛИСИ, 1966. 175 с.
20. **Бондарев Э.А.** Тепловое и механическое воздействие инженерных сооружений с мерзлыми грунтами. Новосибирск: Наука, 1977. 140 с.
21. **Вдовин Ю.И.** Водоснабжение на севере. Л.: Стройиздат, Ленинградское отд., 1987. 166 с.
22. Инструкция по проектированию сетей водоснабжения и канализации для районов распространения вечномерзлых грунтов. СН 510-78. М.: Стройиздат, 1979. 72 с.
23. **Зенгер Н.Н.** Особенности устройства трубопроводов в условиях вечной мерзлоты. М.: Стройиздат. 1964. 99 с.
24. **Стеганцев В.П.** Исследования работы водоводов в суровых климатических условиях Восточной Сибири. Автореферат диссерт. на соискание уч. степени. канд. техн. наук. Красноярск, КрасНПСНИИП. 1965.-28 с.

25. **Альтшуль А.Д.** Гидравлические сопротивления, − 2-е изд. перераб. и доп. М., Недра, 1982, с. 224.
26. **Терехов Л.Д.** Технологические основы энергосбережения при подаче воды по водоводам на Севере: монография / Л.Д. Терехов. – Хабаровск: Изд-во ДВГУПС, 2008
27. **Куспанов А.Б.** Повышение энерго-эффективности трубопроводной системы в случае горячей перекачки высоковязких нефтей //Молодой ученый. 2017. № 18 (152). С. 45-48
28. **Орлов В.А.** Инструменты цифровизации в практике проектирования трубопроводных систем - Москва-Вологда.: Издательство «Инфра-Инженерия». 2024. 125 с.
29. **Захаров Ю.С., Орлов В.А**. Ремонт и восстановление самотечных водо-отводящих сетей. - М.: Издательство АСВ. 2023. 265 с.
30. **Орлов В.А., Зоткин С.П., Иншакова М.А., Герасимов В.А.** Анализ потребления электроэнергии при транспортировке воды по напорным трубопроводам из альтернативных материалов. Свидетельство о государственной регистрации программы для ЭВМ № 2021615221 от 06.04.2021
31. **Хургин Р.Е., Орлов В.А., Зоткин С.П.** Программа определения нагрузок на трубопровод с проверкой его несущей способности при реконструкции. Свидетельство о государственной регистрации программы для ЭВМ № 201361544 от 10.06.2013
32. **Орлов В.А., Зоткин С.П., Зоткина И.А., Хренов К.Е.** Расчет параметров работы напорных трубопроводов, восстанавливаемых предварительно сжатыми полимерными трубами. Свидетельство о государственной регистрации программы для ЭВМ № 2014612753 от 06.03.2014
33. **Орлов В.А., Зоткин С.П., Пелипенко А.А.** Расчет толщины стенки гибкого полимерного рукава при реновации трубопроводов. Свидетельство о государственной регистрации программы для ЭВМ № 2017615864 от 30.05.2017

---

*Orlov Vladimir A.,* Professor, Doctor of Technical Sciences; National Research Moscow State University of Civil Engineering (NRU MGSU), Russia, 129337, Moscow, 26 Yaroslavskoe Shosse, E-mail: OrlovVA@mgsu.ru.

*Zotkin Sergey P.,* Professor, Candidate of Technical Sciences; Russia, National Research Moscow State University of Civil Engineering (NRU MGSU), Russia, 129337, Moscow, 26 Yaroslavskoe Shosse; E-mail: ZotkinSP@mgsu.ru.

*Bolshakova Maria A.,* PhD student; National Research Moscow State University of Civil Engineering (NRU MGSU), Russia, 129337, Moscow, 26 Yaroslavskoe Shosse; E-mail: haritonova_mariy@mail.ru.

*Орлов Владимир Александрович*, профессор, доктор технических наук; Федеральное государственное бюджетное образовательное учреждение высшего образования «Национальный исследовательский Московский государственный строительный университет» (НИУ МГСУ), Россия, 129337, Москва, Ярославское шоссе, 26; E-mail: OrlovVA@mgsu.ru

*Зоткин Сергей Петрович*, профессор, кандидат технических наук; Россия, Федеральное государственное бюджетное образовательное учреждение высшего образования «Национальный исследовательский Московский государственный строительный университет» (НИУ МГСУ), 129337, Москва, Ярославское шоссе, 26; E-mail: ZotkinSP@mgsu.ru.

*Большакова Мария Анатольевна,* аспирант; Федеральное государственное бюджетное образовательное учреждение высшего образования «Национальный исследовательский Московский государственный строительный университет» (НИУ МГСУ), Россия, 129337, Москва, Ярославское шоссе, 26; E-mail: haritonova_mariy@mail.ru

International Journal for Computational Civil and Structural Engineering, 21(3) 80–92 (2025)

DOI:10.22337/2587-9618-2025-21-3-80-92

# DEFORMATION OF COMPOSITE SHELLS DILATING MATERIALS BEYOND ELASTIC LIMITS

***Alexander A. Treshchev***

Tula State University, Tula, RUSSIA

**Annotation.** A mathematical model is proposed for the deformation of a thin flat shell of positive Gaussian curvature with a rectangular contour loaded with a transverse load. The model takes into account the deformation of the shell both at the elastic stage of the material's operation and at the plastic stage. The model is developed for shells made of initially isotropic composite and polymer materials, for which physical linearity corresponding to the generalized Hooke's law is valid in the elastic stage of deformation. During the transition to the plastic region of deformation for these materials, the manifestation of dilatation and the dependence of the yield strength on the type of stress state are taken into account. The model describes all stages of deformation of the elastic shell, the stage of the initial appearance of plastic zones up to the formation of plastic hinges. The model is applicable to dilating materials whose plastic properties can be interpreted as ideal without hardening. In this regard, two plasticity conditions, specially developed for isotropic composites, are considered. The first of them was proposed in the works of E.V. Lomakin, and the second - in the publications of the author of the presented study. At the same time, the disadvantages of the first version of the condition are noted. In addition, the developed model can naturally function with the classical von Mises plasticity condition. Therefore, for quantitative and qualitative comparison of the results obtained, calculations were carried out using three variants of plasticity conditions. To construct the model, technical hypotheses traditional for thin shells were used within the framework of geometrically nonlinear representations of the Karman deformation components. Nonlinear resolving differential equations for the bending of shallow shells were obtained, which were processed by V.V. Petrov's two-step method of successive perturbations of parameters with subsequent numerical implementation. For specific calculations, a shell with a square plan, hinged along the entire contour and loaded with a distributed transverse load of constant intensity, was adopted. As a result of applying the developed mathematical model, the dependences of the calculated maximum deflections of a shell made of polymethyl methacrylate on the load intensity are presented. The fields of propagation of plasticity over the surfaces and through the thickness of the shell are constructed at individual load values. In addition, the values of the loads at which plasticity first develops on the surfaces of the shell and the ultimate loads corresponding to the formation of plastic hinges are given in tabular form. It is shown that when dilating materials go beyond the elastic limits, traditional theories of plasticity lead to significant errors in determining the states and ultimate loads for shallow shells. Considering the obvious advantages for the calculation of such structures, it is advisable to apply the plasticity conditions proposed by the author.

**Keywords:** plasticity conditions, shallow shell, dilatation, ideal plasticity, dependence of yield stress on the type of stress state, limit states, geometric nonlinearity

# ДЕФОРМИРОВАНИЕ ОБОЛОЧЕК ИЗ КОМПОЗИТНЫХ ДИЛАТИРУЮЩИХ МАТЕРИАЛОВ ЗА ПРЕДЕЛАМИ УПРУГОСТИ

***А.А. Трещев***

Тульский государственный университет, Тула, РОССИЯ

**Аннотация.** Предложена математическая модель деформирования тонкой пологой оболочки положительной Гауссовой кривизны с прямоугольным контуром загруженной поперечной нагрузкой. В модели учтено деформирование оболочки как упругой стадии работы материала, так и в пластической. Модель разработана для оболочек, выполненных из начально изотропных композитных и полимерных материалов, у которых в упругой стадии деформирования справедлива физическая линейность, соответствующая обобщенному закону Гука. При переходе в пластическую область деформирования для

этих материалов учтено проявление дилатации и зависимость пределов текучести от вида напряженного состояния. Модель описывает все стадии деформирования оболочки упругую, стадию начального появления пластических зон вплоть до образования пластических шарниров. Модель применима для дилатирующих материалов, пластические свойства, которых можно интерпретировать как идеальные без упрочнения. В связи с этим рассмотрены два условия пластичности, специально разработанные применительно к изотропным композитам. Первое из них предложено в работах Е.В.Ломакина, а второе – в публикациях автора представленного исследования. При этом отмечены недостатки первого варианта условия. Кроме того, разработанная модель естественным образом может функционировать с классическим условием пластичности Мизеса. Поэтому для количественного и качественного сравнения получаемых результатов проведены расчеты с использованием трех вариантов условий пластичности. Для построения модели использованы традиционные для тонких оболочек технические гипотезы в рамках геометрически нелинейных представлений компонентов деформаций по Карману. Получены нелинейные разрешающие дифференциальные уравнения изгиба пологих оболочек, которые были обработаны двухшаговым методом последовательных возмущений параметров В.В.Петрова с последующей численной реализацией. Для конкретных расчетов принята квадратная в плане оболочка, шарнирно закрепленная по всему контуру и загруженная распределенной поперечной нагрузкой постоянной интенсивности. Как результат применения разработанной математической модели приведены зависимости рассчитанных максимальных прогибов оболочки, выполненной из полиметилметакрилата, от величины интенсивности нагрузки. Построены поля распространения пластичности по поверхностям и по толщине оболочки при отдельных величинах нагрузок. Кроме того в табличной форме приведены величины нагрузок, при которых впервые развивается пластичность на поверхностях оболочки и предельных нагрузок, соответствующих образованию пластических шарниров. Показано, что при выходе за пределы упругости дилатирующих материалов традиционные теории пластичности приводят к существенным погрешностям определения состояний и предельных нагрузок для пологих оболочек. Учитывая явные преимущества для расчета подобных конструкций целесообразно применять предложенные автором условия пластичности.

**Ключевые слова:** условия пластичности, пологая оболочка, дилатация, идеальная пластичность, зависимость пределов текучести от вида напряженного состояния, предельные состояния, геометрическая нелинейность

## 1. INTRODUCTION

In construction and other branches of technology, polymer, composite and similar materials are increasingly being used as structural materials. The physical and mechanical behavior of these materials in most cases contradicts traditional theories of elastoplastic deformation. This is especially evident after the stresses reach the yield strength. As a result of experimental studies, the dependence of the yield strength of composites on the type of stress state, accompanied by plastic compressibility or loosening, called dilatation (dilatancy) was established [1 – 7]. Even widely known and long-used materials in technology, such as concrete and cast iron, have similar properties [8 – 11]. To determine the plastic states of dilating materials, a number of phenomenological conditions were proposed [11 – 17], and directly for modern composites, the relations of limit states proposed by Corresponding Member of the Russian Academy of Sciences E.V. Lomakin have found wide application. [3]:

$$F(\sigma_{ij}) = f(\xi^*)\sigma_i = k\,, \qquad (1)$$

where $f(\xi^*)$ – a function determined depending on the type of stress state; $k = \sqrt{3}\tau_s$; $\tau_s$ – yield strength established at pure shear; $\xi^* = \sigma / \sigma_i$ – parameter of the type of stress state; $\sigma = \delta_{ij}\sigma_{ij} / 3$ – medium stress; $\sigma_i = \sqrt{3S_{ij}S_{ij} / 2}$ – stress intensity; $S_{ij} = \sigma_{ij} - \delta_{ij}\sigma$ – stress tensor deviator; $\delta_{ij}$ – Kronecker symbol.

In this case, the type of function $f(\xi^*)$ was established as a result of processing experimental data on the yield strength of a particular material under a wide range of types of stress states. For some specific types of this function, condition (1) can be reduced to the previously considered criteria of strength and ductility, that is, it partially has a generalizing character in relation to previously known ones [6, 11, 14]. The parameter $\xi^* = \sigma / \sigma_i$ or its deformation analogue, apparently, was first used in the works of A.V. Berezin, Yu.N. Rabotnov, E.V. Lomakin. and V.M. Panferov [2, 18, 19]. However, recently, separate publications have appeared [20], in which these parameters are characterized as those proposed by their authors. The plasticity condition (1) was repeatedly used to solve many applied problems, the results of which were often quite acceptable.

## 2. RECOMMENDED CONDITION OF PLASTICITY

Obviously, the parameter $\xi^* = \sigma / \sigma_i$ has a variation interval $\pm\infty$, and this can lead to mathematical uncertainties. This parameter has been repeatedly criticized even at the level of deformation theories [21 – 24]. When using this parameter, the approximation of experimental data on determining the yield strengths corresponding to various types of stress states, the function $f(\xi^*)$ often exists in a limited interval $\xi^*$, that is, the plasticity condition (1) does not work in many cases. Therefore, the author of the presented work at one time proposed a different plasticity condition [23, 24], free from such shortcomings, to determine the limiting states of dilating composites:

$$F(\sigma_{ij}) = f(\xi)\tau = k_\tau, \qquad (2)$$

where $\xi = \sigma / S_0$ – is the normalized normal stress on the octahedral site (parameter change interval $\pm 1$); $\tau = \sqrt{S_i S_i / 3}$ – tangential octahedral stress ($\tau = \sigma_i \sqrt{2} / 3$); $S_0 = \sqrt{\sigma^2 + \tau^2}$ – norm of the vector space associated with the octahedral area; $k_\tau = \sqrt{2/3}\tau_S$.

Condition (2) has undergone deep experimental testing and theoretical testing. Optimal options for the function $f(\xi)$, that approximates experimental data for a wide range of composites are presented in [23, 24]. In particular, materials such as polymethyl methacrylate, phenol plastic AG-4V, graphite composites VPP and MPG-6, cast iron MSCh38-60 are considered, for which options for linear, exponential, piecewise linear and piecewise exponential approximation of the function $f(\xi)$ are adopted, respectively.

Based on the associated law technique, plastic flow equations are formulated. Therefore, in the presented work, this condition (2) was used to construct a model of transverse bending of flat shells of positive Gaussian curvature beyond the elasticity limit.

## 3. PROBLEM STATEMENT AND SHELL CALCULATION

Thin shells of a square outline with a constant surface curvature are considered, such that a mathematical model of their mechanics was built using the Kirchhoff–Love hypotheses and the Karman formalism [25]. In this case, the connections between the significant components of the shell deformation at any point of its body with the displacements of the middle surface were determined in the traditional way:

$$e_{11} = \varepsilon_{11} - z\frac{\partial^2 w}{\partial x_1^2}; \quad e_{22} = \varepsilon_{22} - z\frac{\partial^2 w}{\partial x_2^2};$$

$$e_{12} = \varepsilon_{12} - z\frac{\partial^2 w}{\partial x_1 \partial x_2}, \qquad (3)$$

where $w$ – is the deflection of the middle surface; $x_1$, $x_2$ – Cartesian coordinates of the plan of the middle surface; $\varepsilon_{ij}$ – straines in the middle surface:

$$\varepsilon_{11} = \frac{\partial u}{\partial x_1} - k_1 w + \frac{1}{2}\left(\frac{\partial w}{\partial x_1}\right)^2;$$

$$\varepsilon_{22} = \frac{\partial \upsilon}{\partial x_2} - k_2 w + \frac{1}{2}\left(\frac{\partial w}{\partial x_2}\right)^2;$$

$$2\varepsilon_{12} = \frac{\partial \upsilon}{\partial x_1} + \frac{\partial u}{\partial x_2} + \frac{\partial w}{\partial x_1}\frac{\partial w}{\partial x_2};$$

$u$, $\upsilon$ – displacement of the middle surface in the direction of the corresponding axes $x_1$ and $x_2$; $k_1$, $k_2$ – curvature of the middle surface of the shell in the corresponding directions.

It should be noted here that, in contrast to the elastic scheme of the shell, the resulting straines $\varepsilon_{ij}$, п appear not only due to the influence of membrane forces, but are also further aggravated due to the displacement of its neutral surfaces relative to the middle, caused by the difference in stress values reaching the yield strength in opposite zones of the section.

Considering that the materials considered [23, 24], when deformed within the elastic range, do not exhibit a dependence of mechanical properties on the kind of stress state, the relationship equations between stresses and strains were established according to the generalized Hooke's law [25]:

$$\sigma_{11} = \frac{E}{1-\nu^2}(e_{11} + \nu \cdot e_{22});$$

$$\sigma_{22} = \frac{E}{1-\nu^2}(e_{22} + \nu \cdot e_{11});$$

$$\tau_{12} = \frac{E}{1+\nu} e_{12}, \qquad (4)$$

where $E$ – is the elastic modulus of the material; $\nu$ – Poisson's ratio.

During the transition of the shell deformation process from the elastic stage to the plastic fluidity of the material, the material can develop in one zone of sections, or in two (stretched and compressed). Such shell conditions are aggravated due to the dependence of the yield strength on the type of stress state, as shown in Fig. 1.

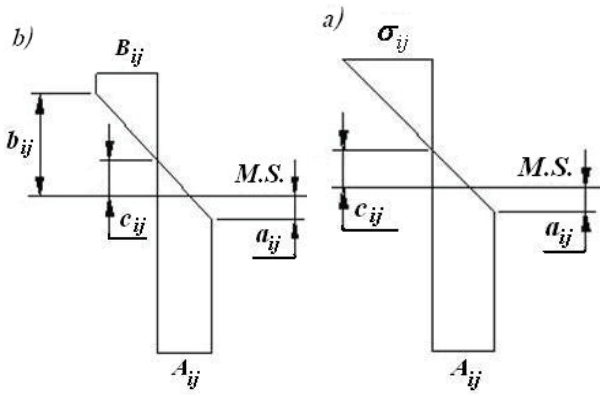


*Figure 1. Diagrams of stress distribution across shell sections beyond elasticity: а – one-sided plasticity; б – bilateral plasticity*

In Fig. 1 $A_{ij}$ indicates the stresses that cause plasticity in the lower zone, and through $B_{ij}$ – in the upper zone. The functions $A_{ij}$ and $B_{ij}$ are calculated in accordance with the plasticity condition (2). In the process of plastic deformation of the shell material, it can be distinguished into two stages: the state of one-sided plasticity and the state of two-sided plasticity (Fig. 1). The plasticity condition is first triggered in the outer fibers of one surface of the shell, and with increasing load, bilateral plasticity develops.

The problem of transverse bending of the shell is formulated within the framework of the theory of small elastoplastic deformations. In this case, as shown above, the traditional fundamentals of the technical theory of thin shells are used, and the stress-strain diagrams of materials have a physical yield strength (there is a yield plateau), which allows the use of a

model of an ideal elastoplastic body. In addition, the loading of the shell is assumed to be simple.

Considering that the bending of the shell is considered at all stages of elastoplastic deformation, it is convenient to present the dependence of stresses on strains in a single general form:

$$\sigma_{ij} = F_{ij}(r_{ij} - z\Delta_{ij}); \quad i,j = 1, 2, \qquad (4^*)$$

where $F_{11} = F_{22} = \frac{E}{1-\nu^2}$; $F_{12} = \frac{E}{1+\nu}$;

$r_{11} = \varepsilon_{11} + \nu\varepsilon_{22}$; $r_{22} = \varepsilon_{22} + \nu\varepsilon_{11}$; $r_{12} = \varepsilon_{12}$;

$\Delta_{11} = w,_{11} + \nu w,_{22}$; $\Delta_{22} = w,_{22} + \nu w,_{11}$;

$\Delta_{12} = w,_{12}$; $\chi_{11} = w,_{11}$; $\chi_{22} = w,_{22}$; $\chi_{12} = w,_{12}$.

The coordinates of the neutral surface of the shell $x_3 = c_{ij}$ are determined based on the stress being equal to zero $\sigma_{ij} = 0$. Then we have $c_{ij} = r_{ij} / \Delta_{ij}$. The positions of the boundaries of the plastic zones in terms of stresses $a_{ij}$ and $b_{ij}$ are determined from the obvious conditions, that $\sigma_{ij} = A_{ij}$ at $x_3 = a_{ij}$ and $\sigma_{ij} = B_{ij}$ at $x_3 = b_{ij}$ (see Fig. 1), from which we obtain

$$a_{ij} = \frac{F_{ij} \cdot r_{ij} - A_{ij}}{F_{ij} \cdot \Delta_{ij}}; \; b_{ij} = \frac{F_{ij} \cdot r_{ij} - B_{ij}}{F_{ij} \cdot \Delta_{ij}}. \qquad (5)$$

In the general case, in the process of elastoplastic deformation of the shell, its mechanical behavior, taking into account the accepted assumptions, is reduced to solving a system of three nonlinear differential equilibrium equations [25]:

$$N_{11},_1 + N_{12},_2 = 0; \quad N_{12},_1 + N_{22},_2 = 0;$$
$$M_{11},_{11} + 2M_{12},_{12} + M_{22},_{22} +$$
$$N_{11}(w,_{11} + k_1) + 2N_{12}w,_{12} + N_{22}(w,_{22} + k_2) + q = 0, \qquad (6)$$

where $q$ – is the intensity of the transverse load; $N_{ij}$, $M_{ij}$ – membrane forces, bending and torque moments.

Forces and moments are determined by integrating stresses over the thickness of the shell according to known rules:

$$N_{ij} = \int_{-h/2}^{h/2} \sigma_{ij} dx_3; \; M_{ij} = \int_{-h/2}^{h/2} \sigma_{ij} x_3 dx_3. \qquad (7)$$

In the elastic stage of shell deformation, system (6), taking into account traditional concepts (3), (4) and (7), is reduced to three nonlinear differential equations for displacements $u$, $\upsilon$ and $w$, the solution of which is known from the literature [25].

Taking into account the transformation of the equations of state to a general form that is valid at all stages of shell deformation (4), the parameters $r_{ij}$ will be determined by the equal areas of stress diagrams distributed over the thickness of the shell, corresponding to forces (7). Thus, with the development of one-sided plasticity, we have

$$N_{ij} = \int_{-h/2}^{a_{ij}} \sigma_{ij} dx_3 + \int_{a_{ij}}^{h/2} A_{ij} dx_3, \qquad (8)$$

and with bilateral plasticity –

$$N_{ij} = \int_{-h/2}^{b_{ij}} B_{ij} dx_3 + \int_{b_{ij}}^{a_{ij}} \sigma_{ij} dx_3 + \int_{a_{ij}}^{h/2} A_{ij} dx_3. \qquad (9)$$

Obviously, the moments will be determined in accordance with rules (7) as follows:

with the development of one-sided plasticit –

$$M_{ij} = \int_{-h/2}^{a_{ij}} \sigma_{ij} x_3 dx_3 + \int_{a_{ij}}^{h/2} A_{ij} x_3 dx_3 ; \quad (10)$$

when bilateral plasticity occurs –

$$M_{ij} = \int_{-h/2}^{b_{ij}} B_{ij} x_3 dx_3 + \int_{b_{ij}}^{a_{ij}} \sigma_{ij} x_3 dx_3 + \int_{a_{ij}}^{\frac{h}{2}} A_{ij} x_3 dx_3 . \quad (11)$$

The set of equations (4*), (10), (11) with the simplest transformations gives expressions for moments in the form:

$$M_{ij} = R_{ij} + S_{ij} \cdot \Delta_{ij}, \quad (12)$$

where

$$R_{ij} = \frac{A_{ij}}{2}\left(\frac{h^2}{4} - a_{ij}^{\ 2}\right) + \frac{F_{ij} \cdot r_{ij}}{2}\left(a_{ij}^{\ 2} - \frac{h^2}{4}\right),$$

$$S_{ij} = -\frac{F_{ij}}{3}\left(a_{ij}^{\ 3} + \frac{1}{8} b_{ij}^{\ 3}\right)$$ – with one-sided plasticit;

$$R_{ij} = \frac{A_{ij}}{2}\left(\frac{h^2}{4} - a_{ij}^2\right) + \frac{B_{ij}}{2}\left(b_{ij}^2 - \frac{h^2}{4}\right) +$$

$$+ \frac{F_{ij}}{2} r_{ij}(a_{ij}^2 - b_{ij}^2), \; S_{ij} = -F_{ij}(a_{ij}^3 - b_{ij}^3)/3$$

– with bilateral plasticity.

In this case, the set of dependencies (4*), (8), (9) after transformations allows us to obtain expressions for membrane forces:

$$N_{ij} = T_{ij} + C_{ij} \cdot \Delta_{ij}, \quad (13)$$

where

$$T_{ij} = A_{ij}\left(\frac{h}{2} - a_{ij}\right) + F_{ij} \cdot r_{ij}\left(a_{ij} + \frac{h}{2}\right),$$

$$C_{ij} = -\frac{F_{ij}}{2}\left(a_{ij}^{\ 2} - \frac{h^2}{4}\right)$$ – with one-sided plasticit;

$$T_{ij} = A_{ij}\left(\frac{h}{2} - a\right) + B_{ij}\left(b - \frac{h}{2}\right) + ;$$

$$+ F_{ij} r_{ij}(a_{ij} - b_{ij}); \; C_{ij} = -F_{ij} \cdot (a_{ij}^2 - b_{ij}^2)$$

– with bilateral plasticity.

Considering dependencies (3), (4), (4*), (5), (12), (13) together, and introducing them into the equilibrium equations (6), we obtain a mathematical model that describes the deformation of the shell from dilating materials in all three stages. This model is represented by a system of three nonlinear differential equations:

$$\frac{\partial(T_{11} + C_{11} \cdot \Delta_{11})}{\partial x_1} + \frac{\partial(T_{12} + C_{12} \cdot \Delta_{12})}{\partial x_2} = 0;$$

$$\frac{\partial(T_{12} + C_{12} \cdot \Delta_{12})}{\partial x_1} + \frac{\partial(T_{22} + C_{22} \cdot \Delta_{22})}{\partial x_2} = 0;$$

$$\frac{\partial^2(R_{11} + S_{11} \cdot \Delta_{11})}{\partial x_1^2} + \frac{\partial^2(R_{22} + S_{22} \cdot \Delta_{22})}{\partial x_2^2} +$$

$$+ \frac{\partial^2(R_{12} + S_{12} \cdot \Delta_{12})}{\partial x_1 \partial x_2} =$$

$$= -[q + (T_{11} + K_{11} \cdot \Delta_{11}) \cdot \frac{\partial^2 w}{\partial x_1^2} +$$

$$+ (T_{22} + K_{22} \cdot \Delta_{22}) \cdot \frac{\partial^2 w}{\partial x_2^2} +$$

$$+ 2(T_{12} + K_{12} \cdot \Delta_{12}) + K_1(T_{11} + K_{11} \cdot \Delta_{11}) +$$

$$+ K_2(T_{22} + K_{22} \cdot \Delta_{22})]. \quad (14)$$

It should be noted that the dimensions of the depths of development of plastic deformations along the thickness of the shell $a_{ij}$ and $b_{ij}$ do not depend on the direction ($a_{11} = a_{22} = a_{12}$, $b_{11} = b_{22} = b_{12}$), since these parameters are

determined by the totality of stresses $\sigma_{ij}$ arising in accordance with the plasticity condition (2), and not by a separate stress component. Therefore, you can easily omit the indices in these parameters, using the general notations $a$ and $b$ for them. In order for system (14) to be closed, it is necessary to add boundary conditions, which in the presented work are assumed to be the same along the entire support contour as for hinged fastening (for example, with: $x_1 = l$: $w = 0$, $\upsilon = 0$, $u = 0$, $M_{11} = 0$ ($l$ – the length of the support contour along the corresponding axis)).

The solution of the system of nonlinear differential equations was carried out within the framework of the two-step method of successive perturbations of parameters proposed by V.V. Petrov [26]. Before applying the two-step method procedure, it is necessary to linearize the resolving differential equations (14) and boundary conditions using the method of successive loadings [26]. The numerical implementation of the considered model was carried out using the finite-difference method. When assigning mesh sizes, the convergence of the numerical procedure was assessed.

For specific calculations, a flat shell, square in plan, 1000×1000 mm in size, 10 mm thick, made of polymethyl methacrylate, was adopted. The lifting boom of the middle surface of the shell in the center of the plan was taken to be 100 mm. For polymethyl methacrylate, the following mechanical characteristics were accepted: elastic modulus $E$=3300 MPa; Poisson's ratio $\nu$=0,3; plasticity constant $k_\tau$=58,9 MPa. A function that depends on the kind of stress state $f(\xi)$, and is included in the plasticity condition (2) was adopted in accordance with the data on processing experimental studies of limit states [23, 24] in exponential form:

$$f(\xi) = \exp(A_1 \xi), \qquad (15)$$

where $A_1$=0,424.

The calculation of the shell was carried out taking into account three variants of plasticity conditions: 1) use of condition (2); 2) according to condition (1) taking into account the corresponding function $\xi^*$ and constant $k = \sqrt{3}\tau_s$ [3]; 3) application of the Mises condition, which does not take into account the dependence of the yield strength on the type of stress state. The load on the shell was assumed to be uniformly distributed over the entire surface. The load step interval was taken for all calculation options at a constant 5 kPa in the elastic stage of deformation, and when the yield strength was reached – 5 kPa, decreasing to 100 Pa as the intensity of deflections increased. Taking into account the symmetry of the load case and the geometry of the shell in plan, its fourth part was calculated, covered with a mesh of size 15×15, which ensured the necessary accuracy of the solution.

As the results of the calculations in Fig. 2 shows the processes of increase in the maximum relative deflections of the shell in its plan center $w/h$ as the intensity of the transverse load $q$ increases using three models of plasticity conditions. The solid line shows the dependence of the growth of deflections obtained using condition (2), the dashed line - in accordance with the E.V. Lomakin model (1), and the dash-dotted line - with the classical Mises model. In Fig. 2, the following designations for the characteristic states of the shell are introduced: I.1 – the occurrence of plastic deformations during calculations using the plasticity condition (2); I.2 – moment of formation of a plastic hinge when calculating according to condition (2); II.1 – the occurrence of plastic deformations during calculations using the plasticity condition (1); II.2 – moment of formation of a plastic hinge when calculating according to condition (1); III.1 – the occurrence of plastic deformations during calculations using the von Mises limit state; III.2 – formation of a plastic hinge when calculating using the von Mises limit state.

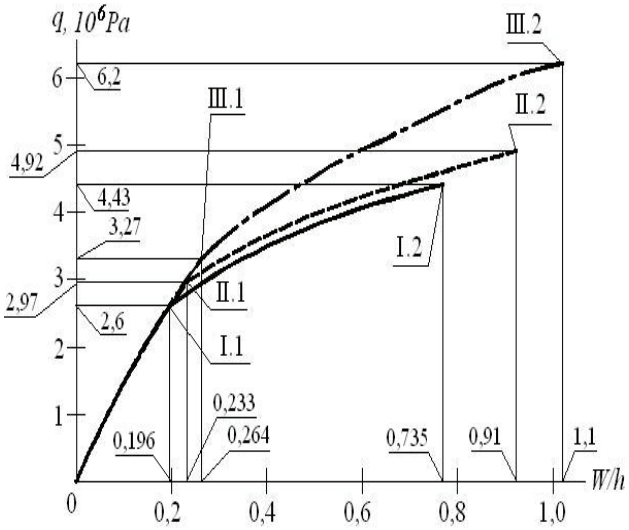


*Figure 2. Increase in maximum deflections depending on load intensity*

In Fig. 3 and 4 demonstrate the trends in the propagation of areas of plastic deformation along the surfaces of the shell (upper and lower). Pictures of plasticity zones are also calculated for three variants of plasticity conditions and are presented at two characteristic values of load intensity. The areas of the shell surfaces in which plastic deformations occurred are shaded.

Fig. 5 and 6 illustrate the deep distribution of zones of plastic deformation along the thickness of the shell along the axis of symmetry, which is the coordinate axis and along the diagonal. Pictures of the depth penetration of plasticity zones are also calculated for three variants of plasticity conditions and are presented at two characteristic values of load intensity. The areas of deep development of plastic deformations along the thickness of the shell are shaded as follows: solid lines characterize the boundaries of plasticity zones corresponding to condition (2); dashed lines – condition (1); dash-dotted lines – to the Mises condition.

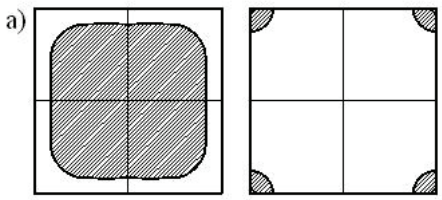


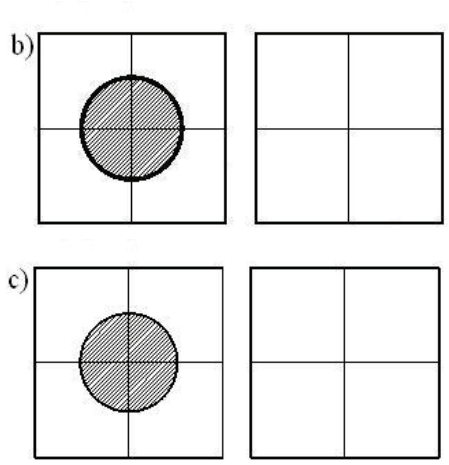


*Figure 3. Development of plastic zones along the lower and upper surfaces of the shell at a load intensity of 3,85 MPa: a) – calculation according to condition (2); b) – calculation according to condition (1); c) – calculation according to the Mises condition*

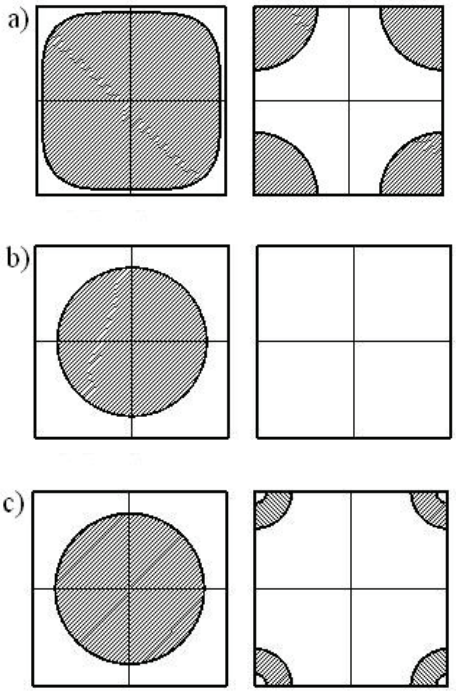


*Figure 4. Development of plasticity zones along the lower and upper surfaces of the shell at a load intensity of 4,12 MPa: a) – calculation according to condition (2); b) – calculation according to condition (1); c) – calculation according to the Mises condition*

Additionally, to illustrate the characteristic states in the process of elastoplastic deformation of a shell made of polymethyl methacrylate, Table 1 shows numerical parameters for the intensity of loads that first cause plasticity and the formation of plastic hinges, calculated for three variants of limit state conditions. The percentages of discrepancy between the values of limit states when calculating using conditions (1) and (2) in comparison with the Mises theory are given in parentheses.

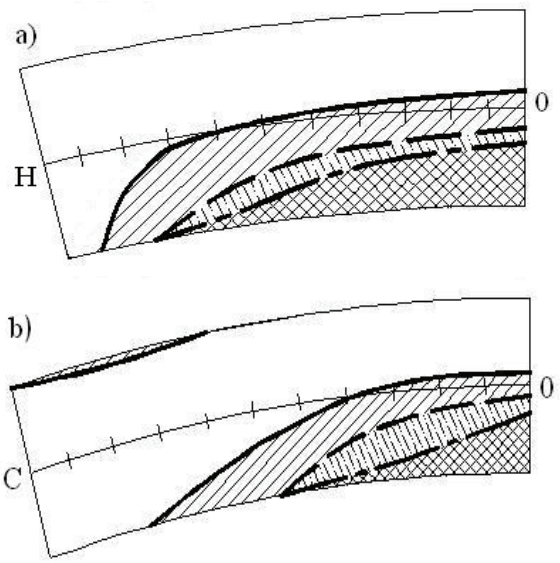


*Figure 5. Development of plasticity zones along the thickness of the shell at a value load intensity 3,85 MPa: a) along the axis of symmetry along the coordinate $x_1$; b) along the diagonal of the shell (0 – center of the shell plan; H – boundary hingedly supported contour; C – corner point of the shell plan)*

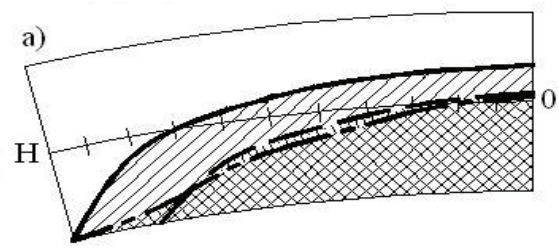


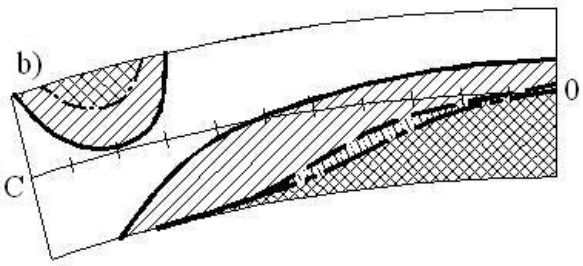


*Figure 6. Development of plasticity zones along the thickness of the shell at a value load intensity 4,12 MPa: a) along the axis of symmetry along the coordinate $x_1$; b) along the diagonal of the shell (0 – center of the shell plan; H – boundary hingedly supported contour; C – corner point of the shell plan)*

*Table 1*

| Variant of the plasticity condition | Load intensity at appearance of plasticity, MPa | | Load intensity upon the onset of plastic hinges, MPa |
|---|---|---|---|
| | On the top surface | On the bottom surfaces | |
| Treshchev (2) | 3,85 (28,1%) | 2,6 (25,8%) | 4,43 (40,0%) |
| Lomakin (1) | 4,82 (2,3%) | 2,97 (10,0%) | 4,92 (26,0%) |
| Mises | 4,93 | 3,27 | 6,20 |

## 4. ANALYSIS OF THE RESULTS OBTAINED

Analysis of the results of calculating the elastic-plastic states of the shell shown in Fig. 2 shows that when plastic deformations appear at the initial stage, the values of maximum deflections obtained using conditions (2) and (1) differ insignificantly and do not exceed 9%. With increasing load, the discrepancy between these values tends to maintain the specified interval. At the same time, there are significant differences in the values of deflections calculated with conditions (2) and (1) in relation to the calculation results taking into account the Mises theory. These differences with developed plasticity zones reach 30%. To prevent violation of the rigor of the calculation, changes in the parameters of the stress-strain states of the shell

were analyzed in order to detect local unloadings, which were not established until the formation of plastic hinges. Additional data from Table 1 demonstrate the fact that the load intensity causing the appearance of plasticity in the lower fibers of the shell, calculated using equation (2) differs from option (1) by 14,2%. The difference in calculating maximum deflections according to model (2) in comparison with the classical Mises theory reaches 25,8%, and for model (1) – 10%. Similar differences in the magnitude of the loads causing the appearance of plastic deformations in the upper fibers of the shell are 25,2%, 28,1% and 2,3%, respectively (see Table 1).

The intensity of the load causing the formation of plastic hinges, calculated using condition (2), differs from the data of the Mises theory by 40%, and for the version using equation (1) – by 26%. Between themselves, the values of the indicated loads calculated on the basis of conditions (2) and (1) differ by 11,1%.

Analyzing the areas of development of plasticity on the surfaces and along the thickness of the shell at a load of 3,85 MPa, it can be noted that the patterns calculated using condition (1) and Mises are close to each other, differing in the depth of penetration (see Fig. 3 and 5). In this case, condition (2) gives qualitative differences from the previous two options, since plastic deformations already occur in the corner sections of the upper fibers, and on the lower surface the plasticity region is more developed. An increase in load does not lead to significant changes in the qualitative patterns of plasticity development on surfaces, but numerical discrepancies are found in the sizes of these zones between the calculation options under conditions (2) and (1). At the same time, the qualitative and quantitative pictures of the areas occupied by plasticity in the upper surfaces of the shell differ when calculated with condition (2) and according to the Mises theory. This can be detected in particular at 4,12 MPa, when, when calculating using condition (2), plasticity extends completely to the corner zones of the shell, while the Mises theory predicts that plastic deformations, developing from the corner regions to the central ones, retain elasticity directly in the corners.

## 5. CONCLUSION

The presented mathematical model of the deformation of thin shells made of dilating materials and the calculations carried out using the example of polymethyl methacrylate clearly show that when determining the states of such structures beyond elasticity, traditional theories of plasticity lead to significant errors. These errors manifest themselves when determining the limiting states of the formation of plastic hinges, when the Mises theory leads to an error in the values of the maximum loads on a hinged shell of up to 40% (polymethyl methacrylate material), and in the values of deflections – up to 49,7%.

It should also be noted that due to the advantages of the plasticity condition (2), its use is more appropriate for calculating shells beyond elasticity, which has been confirmed experimentally.

## REFERENCES

1. **Ainbinder S.B.** The influence of hydrostatic pressure on the mechanical properties of polymer materials / S.B. Ainbinder, M.G. Laka, I.Yu. Majors // Polymer Mechanics. 1965. No. 1. P. 65 – 75.
2. Resistance to deformation and fracture of isotropic graphite materials under complex stress conditions / **A.V. Berezin** et al. // Problems of strength. 1979. No. 2. P. 60 – 65.
3. **Lomakin E.V.** Dependence of the limiting state of composite and polymer materials on the type of stress state / E.V. Lomakin // Mechanics of composite materials. – 1988. – No. 1. P. 3 – 9.
4. **Fridman A.M.** Study of the destruction of carbon-graphite materials under complex stress conditions / A.M. Fridman, Yu.P. Anufriev, V.N. Barabanov // Problems of strength. – 1973. – No. 1. – pp. 52–55.

5. **Zhukov A.M.** Strength properties of polymethyl methacrylate under biaxial tension / A.M. Zhukov // Ing. Sat. – 1960. – Vol. 1. – Issue. 2. – P. 200 – 204.
6. **Goldman A.Ya**. Strength of structural plastics / A.Ya. Goldman. – L.: Mechanical Engineering, 1979. – 320 p.
7. **Ainbinder S.B.** Properties of polymers at high pressures / S.B. Einbinder, K.I. Alksne, E.L. Tyupina, M.G. Laka. – M., 1973.
8. **Bazant Z.P.** Endochronic Theory of Inelasticity and Failure of Concrete / Z.P.Bazant, P.D.Bhat // Journal of the Engineering Mechanics Division, ASCE. – 1976. – Vol. 102. – No. EM4. – P. 701–722.
9. **Tasuji M.E.** Stress-Strain Response and Fracture of Concrete in Biaxial Loading / M.E.Tasuji, F.O.Slate, A.H.Nilson // ACI Journal. – 1979. – No. 7. – P. 806 – 812.
10. **Leonov M.Ya.** Dependences between strains and stresses for semi-brittle bodies / M.Ya. Leonov, V.A. Panyaev, K.N. Rusinko // Ing. magazine MSB. – 1967. – No. 6. – P. 26 – 32.
11. **Yagn Yu.I.** Strength and ductility of modified cast iron under various stress states / Yu.I.Yagn, V.V. Evstratov // Reports Academy of Sciences of the USSR. – 1957. – Vol. 113. – No. 3. – P. 573 – 575.
12. **Goldenblat I.I.** Strength criteria for structural materials / I.I.Goldenblat, V.A.Kopnov. – M.: Mashinostroenie, 1968. – 192 p.
13. **Pisarenko G.S.** Deformation and strength of materials under complex stress state / G.S. Pisarenko, A.A. Lebedev. – Kyiv: Naukova Dumka, 1976. – 416 p.
14. **Balandin P.P.** On the issue of strength hypotheses / P.P. Balandin // Bulletin of engineers and technicians. – 1937. – No. 1. – P. 37 – 41.
15. **Geniev G.A.** On the issue of generalizing the theory of concrete strength / G.A.Geniev, V.N.Kissyuk // Concrete and reinforced concrete. – 1965. – No. 2. – P. 16 – 19.
16. **Tolokonnikov L.A.** On the shape of the limiting surface of an isotropic body / L.A.Tolokonnikov // Applied mechanics. – 1969. – Issue. 10. – Vol. 5. – P. 123 – 126.
17. **Green R.J.** A plasticity theory for porous solid / R.J.Green // Int. J. Mech. Sci. – Vol. 14. –1972. – P. 215 – 227.
18. **Lomakin E.V.** Relations of the theory of elasticity for an isotropic body of different moduli / E.V. Lomakin, Yu.N. Rabotnov // News Academy of Sciences of the USSR. MSB. – 1978. – No. 6. – P. 29–34.
19. **Panferov V.M.** Theory of elasticity and deformation theory of plasticity for bodies with different properties for compression, tension and torsion / V.M. Panferov // Reports Academy of Sciences of the USSR. – 1968. – Vol. 180. – No. 1. – P. 41 – 44.
20. Relationships between stresses and strains in a nonlinearly deformable body. Part 1. Basic principles and relationships of the mechanics of a deformable solid body / **V.M. Kruglov**, S.V. Bakushev, A.I. Shein, V.T. Erofeev, S.D.S. Al Dulaimi, A.A. Tomilov // Expert: Theory and practice. – 2023. – No. 4(23). – P. 154 – 163.
21. **Treshchev A.A.** Theory of deformation and strength of materials with initial and induced sensitivity to the type of stress state. Defining relations / A.A. Treshchev. – M.; Tula: RAACS; Tula State University, 2016. – 326 p.
22. **Treshchev A.A.** Theory of deformation and strength of differently resistant materials / A.A.Treshchev. – Tula: Tula State University, 2020. – 359 p.
23. **Treshchev A.A.** Dependence of limit states of structural materials on the type of stress state / A.A.Treshchev // News of higher educational institutions. Construction. – 1999. – No. 10. – P. 9–18.
24. **Treshchev A.A.** On the theory of plasticity of dilating materials of different resistance / A.A. Treshchev // Problems of mechanical

engineering and automation. – International magazine. – 2003. – No. 2. – pp. 58–62.
25. **Timoshenko S.P.** Plates and shells / S.P. Timoshenko, S. Voinovsky–Krieger. – M.: Fizmatgiz, 1966. – 636 p.
26. **Petrov V.V.** Methods for calculating structures made of nonlinear deformable material / V.V. Petrov, I.V. Krivoshein. – M.: ASV, 2009. – 208 p.

## СПИСОК ЛИТЕРАТУРЫ

1. **Айнбиндер С.Б.** Влияние гидростатического давления на механические свойства полимерных материалов / С.Б.Айнбиндер, М.Г.Лака, И.Ю.Майорс // Механика полимеров. 1965. № 1. С. 65 – 75.
2. Сопротивление деформированию и разрушению изотропных графитовых материалов в условиях сложного напряженного состояния / **А.В.Березин** и др. // Проблемы прочности. 1979. № 2. С. 60 – 65.
3. **Ломакин Е.В.** Зависимость предельного состояния композитных и полимерных материалов от вида напряженного состояния / Е.В.Ломакин // Механика композитных материалов. – 1988. – № 1. С. 3 – 9.
4. **Фридман А.М.** Исследование разрушения углеграфитовых материалов в условиях сложного напряженного состояния / А.М.Фридман, Ю.П.Ануфриев, В.Н.Барабанов // Проблемы прочности. – 1973. – №1. – С. 52–55.
5. **Жуков А.М.** Прочностные свойства полиметилметакрилата при двухосном растяжении / А.М.Жуков // Инж. сб. – 1960. – Т. 1. – Вып. 2. – С. 200 – 204.
6. **Гольдман А.Я.** Прочность конструкционных пластмасс / А.Я.Гольдман. – Л.: Машиностроение, 1979. – 320 с.
7. **Айнбиндер С.Б**. Свойства полимеров при высоких давлениях / С.Б.Айнбиндер, К.И.Алксне, Э.Л.Тюпина, М.Г.Лака. – М., 1973.
8. **Bazant Z.P.** Endochronic Theory of Inelasticity and Failure of Concrete / Z.P.Bazant, P.D.Bhat // Journal of the Engineering Mechanics Division, ASCE. – 1976. – Vol. 102. – № EM4. – P. 701–722.
9. **Tasuji M.E.** Stress-Strain Response and Fracture of Concrete in Biaxial Loading / M.E.Tasuji, F.O.Slate, A.H.Nilson // ACI Journal. – 1979. – №7. – P. 806–812.
10. **Леонов М.Я.** Зависимости между деформациями и напряжениями для полухрупких тел / М.Я.Леонов, В.А.Паняев, К.Н.Русинко // Инж. журн. МТТ. – 1967. – № 6. – С. 26 – 32.
11. **Ягн Ю.И.** Прочность и пластичность модифицированного чугуна при различных напряженных состояниях / Ю.И.Ягн, В.В. Евстратов // Докл. АН СССР. – 1957. – Т. 113. - №3. – С. 573-575.
12. **Гольденблат И.И.** Критерии прочности конструкционных материалов / И.И.Гольденблат, В.А.Копнов. – М.: Машиностроение, 1968. – 192 с.
13. **Писаренко Г.С.** Деформирование и прочность материалов при сложном напряженном состоянии / Г.С.Писаренко, А.А.Лебедев. – Киев: Наукова думка, 1976. – 416 с.
14. **Баландин П.П.** К вопросу о гипотезах прочности / П.П.Баландин // Вестник инженеров и техников. – 1937. – № 1. – С. 37 – 41.
15. **Гениев Г.А.** К вопросу обобщения теории прочности бетона / Г.А.Гениев, В.Н.Киссюк // Бетон и железобетон. – 1965. – № 2. – С. 16 – 19.
16. **Толоконников Л.А.** О форме предельной поверхности изотропного тела / Л.А.Толоконников // Прикладная механика. – 1969. – Вып. 10. – Том 5. – С. 123 – 126.

17. **Green R.J.** A plasticity theory for porous solid / R.J.Green // Int. J. Mech. Sci. – Vol.14. –1972. – P. 215 – 227.
18. **Ломакин Е.В.** Соотношения теории упругости для изотропного разномодульного тела / Е.В.Ломакин, Ю.Н.Работнов // Изв. АН СССР. МТТ. – 1978. – №6. – С. 29–34.
19. **Панферов В.М.** Теория упругости и деформационная теория пластичности для тел с различными свойствами на сжатие, растяжение и кручение / В.М.Панферов // Докл. АН СССР. – 1968. – Т. 180. – №1. – С. 41–44.
20. Зависимости между напряжениями и деформациями в нелинейно деформируемом теле. Часть 1. Основные принципы и соотношения механики деформируемого твердого тела / **В.М.Круглов**, С.В.Бакушев, А.И.Шеин, В.Т.Ерофеев, С.Д.С. Аль Дулайми, А.А.Томилов // Эксперт: Теория и практика. – 2023. – №4(23). – С. 154 – 163.
21. **Трещев А.А.** Теория деформирования и прочности материалов с изначальной и наведенной чувствительностью к виду напряженного состояния. Определяющие соотношения / А.А.Трещев. – М.; Тула: РААСН; ТулГУ, 2016. – 326 с.
22. **Трещев А.А.** Теория деформирования и прочности разносопротивляющихся материалов / А.А.Трещев. – Тула: ТулГУ, 2020. – 359 с.
23. **Трещев А.А.** Зависимость предельных состояний конструкционных материалов от вида напряженного состояния / А.А.Трещев // Известия высших учебных заведений. Строительство. – 1999. – №10. – С. 9–18.
24. **Трещев А.А.** К теории пластичности дилатирующих разносопротивляющихся материалов / А.А.Трещев // Проблемы машиностроения и автоматизации. – Международный журнал. – 2003. – №2. – С. 58–62.
25. **Тимошенко С.П.** Пластинки и оболочки / С.П.Тимошенко, С.Войновский–Кригер. – М.: Физматгиз, 1966. – 636 с.
26. **Петров В.В.** Методы расчета конструкций из нелинейно-деформируемого материала / В.В.Петров, И.В.Кривошеин. – М.: АСВ, 2009. – 208 с.

---

*Aleksander Anatolyevich Treshchev*, Doctor of Technical Sciences, Professor, Head of the Department of Construction, Building Materials and Structures, Tula State University, Corresponding Member of RAACS; 300012, Russia, Tula, Lenin Avenue. 92. E-mail: taa58@yandex.ru.

*Александр Анатольевич Трещев*, доктор технический наук, профессор, заведующий кафедрой «Строительство, строительные материалы и конструкции» Тульского государственного университета, член-корреспондент РААСН; 300012, г. Тула, Проспект Ленина, 92. E-mail: taa58@yandex.ru

International Journal for Computational Civil and Structural Engineering, 21(3) 93–104 (2025)

DOI:10.22337/2587-9618-2025-21-3-93-104

# COMPREHENSIVE INTELLECTUAL AND STATISTICAL ANALYSIS OF WATER CONSUMPTION

***Elena V. Ignatova, Elena Kh. Kitaytseva***

National Research Moscow State University of Civil Engineering, Moscow, RUSSIA

**Abstract:** This article deals with the water consumption regime in a residential building. The study is based on data of cold and hot water hourly consumption in a multi-storey apartment building. The measurement period is one month. The study comprehensively uses statistical analysis of water consumption and data mining of group outliers. Statistical data analysis is designed to determine the distribution pattern of different data samplings. The analysis is carried out for three different samplings of apartment water consumption data. As a result, group outliers of hourly water consumption are identified. Machine learning methods are used to identify group outliers. The task boils down to clustering the hours of the day to find hours with reduced (nighttime) water consumption. Clustering is carried out using five methods, and clustering quality is assessed by three metrics. As a result, nighttime consumption periods are determined for different samplings of water consumption data in apartment buildings. In general, comprehensive intellectual and statistical analysis of water consumption is useful for solving the tasks of designing water supply and sanitation systems, adjusting the operating modes of engineering equipment, and clarifying the calculated parameters of water consumption in apartment buildings.

**Keywords:** statistical analysis, data mining, machine learning, clustering, hourly water consumption, apartment building

# КОМПЛЕКСНЫЙ ИНТЕЛЛЕКТУАЛЬНО-СТАТИСТИЧЕСКИЙ АНАЛИЗ ВОДОПОТРЕБЛЕНИЯ

***Е.В. Игнатова, Е.Х. Китайцева***

Национальный исследовательский Московский государственный строительный университет, г. Москва, РОССИЯ

**Аннотация:** В статье исследуется режим водопотребления в многоквартирном доме. Исследование основано на данных о почасовом потреблении холодной и горячей воды в многоэтажном жилом здании. Период измерения – один месяц. Исследование в комплексе использует статистический анализ водопотребления и интеллектуальный анализ групповых выбросов данных. Статистический анализ данных предназначен для определения характера распределения различных выборок данных. Анализ проводится для трех различных выборок данных водопотребления квартирами. В результате выявляются групповые выбросы почасового потребления воды. Для выделения групповых выбросов используются методы машинного обучения. Задача сводится к кластеризации часов суток для поиска часов с пониженным (ночным) потреблением воды. Кластеризация проводится пятью методами, качество кластеризации оценивается тремя метриками. В результате определяются периоды ночного потребления для разных наборов данных водопотребления в доме. В целом комплексный интеллектуально-статистический анализ водопотребления полезен для решения задач проектирования систем водоснабжения и водоотведения, настройки режимов эксплуатации инженерного оборудования, уточнения расчетных параметров водопотребления в многоквартирных домах.

**Ключевые слова:** статистический анализ, интеллектуальный анализ данных, машинное обучение, кластеризация, почасовое водопотребление, многоквартирный дом

## INTRODUCTION

The object of the study is the consumption of cold and hot water in an apartment building. The subject of the study is the mode of water consumption depending on the time of day and day of the week. The purpose of the study is to obtain reliable characteristics of water consumption modes in a house based on the integrated use of various data analysis methods.

The problem of determining the regime and volume of water consumption is relevant for all countries. Digitalization programs are being implemented in Russia, which should turn apartment buildings into high-tech and energy-efficient digital facilities. A mandatory component of such facilities is a smart resource consumption telemetry system.

It is possible to take meter readings daily (hourly, every second), store digital information in data centers, quickly compile reports and transmit data to interested authorities and relevant information systems. It should be noted that telemetry data is collected for statistics and is mainly used in financial settlement services for automatic accrual of payments for used resources [1].

An analysis of the scientific literature in the field of water consumption research shows that water consumption monitoring data can be used to solve other important tasks, including to refine engineering calculations, adjust regulatory indicators, and make recommendations on resource conservation [2].

It should be noted that when designing water supply systems, overestimated design loads lead to an increase in pipeline diameters, an increase in heat loss of hot water pipes, and an overestimation of the required characteristics of pumping equipment. In addition, overestimated values of estimated water consumption led to an unjustified increase in the diameters of drainage systems.

Despite the common goals facing the researchers, the study of the process relies on diverse information. For example, article [3] analyzes the second flow rate passing through different devices installed in the same apartment, article [4] analyzes the hourly flow rate in an 80-apartment residential building. The article [5] examines hourly expenses in an urban-type settlement, the article [6] deals with the daily water consumption of a city where about one hundred thousand inhabitants live in apartment buildings. In all these articles, the object of research is water consumption in residential apartment buildings. It is noted in [7] that there is practically no data on water consumption in public buildings.

A commonly used method of data analysis is visualization of water consumption. Graphs help to understand the process on a qualitative level, but they do not provide accurate quantitative characteristics.

In the article [5], based on graphs, the maximum water consumption in an urban-type settlement is analyzed depending on the day of the week. The nighttime water consumption period is allocated for different days of the week. As a result, the schedules of the actual daily consumption do not coincide with the schedules of the standard daily uneven water consumption.

A similar study is conducted in the article [8]. The telemetry data of water consumption in a multi-storey residential building is used. Nighttime hours of reduced consumption of hot and cold water are defined for weekdays and weekends. The graphs show a significant difference between night and day water consumption.

The main characteristics of water consumption in a house (average, median, minimum, maximum, and standard deviation) are determined using descriptive statistics.

In the article [9], based on a statistical analysis of data on water consumption in an apartment building, it is concluded that the actual average daily water consumption per inhabitant is less than recommended by standards for calculating internal water supply systems. A similar conclusion is found in the article [4].

Several papers attempt to describe empirical samplings using a theoretical distribution law. The intensity of water consumption using individual devices is described by a Gamma distribution [3]. The intensity of water consumption by a building is estimated by a normal distribution [4], the number of simultaneously operating appliances in the building is described by a binomial distribution [7].

The least squares method was used to determine the time of intensive consumption of hot water during the day in apartment buildings [10]. The total time of intensive consumption of hot water

per day is defined as 18-21 hours. However, the specific hours are not specified. From this study, it can be concluded that the period of reduced water consumption lasts 3-5 hours per day.

The tasks of identifying trends, seasonality, or cyclicity in water consumption can be solved based on time series analysis [11, 12]. Artificial intelligence methods are increasingly being used to solve classification, clustering, optimization, and forecasting problems [13]. Machine learning methods make it possible to recover missing data [14].

If we consider the volume of nighttime water consumption to be significantly different from the volume of water consumption at other hours of the day, then they can be considered as a group data outlier. Searching for group outliers involves identifying abnormal patterns or behaviors within datasets. Unlike individual outliers, group outliers exhibit anomalies common to a subset of observations within a larger population. Statistical methods or machine learning algorithms can be used to detect group outliers [15]. Data clustering methods can be considered suitable intelligent machine learning algorithms.

In the article [16], the DBSCAN machine learning method was used to identify uneven water consumption in an apartment building, designed to cluster data considering their distribution density. Unfortunately, the quality of clustering was not discussed. A variety of density-based clustering methods are described in [17]. It is important to note that the choice of clustering quality assessment metrics is of great importance. Metrics make it possible to identify the most suitable methods for the available data set [18].

Research [19] shows the complex use of various analysis methods to study water consumption patterns and search for anomalies based on payment documents of water consumers with mechanical meters. The DBSCAN clustering method and time series analysis were used together. The integrated use of various data analysis methods helps to solve tasks more effectively.

## METHODS

The numerical experiment is used in the research. Water consumption data is processed and analyzed based on the integrated use of statistical analysis and data mining. The units of measurement of water consumption are liters.

At the first step of the study the data is cleaned.

At the second step of the study statistical analysis is carried out on various samplings to determine patterns of water use by apartments.

At the third step of the study the task of clustering the hours of the day is solved to determine the periods of reduced (nighttime) consumption of cold and hot water in the house. Machine learning methods are used.

### Data preprocessing

The first stage of data processing is its cleaning. Each data set requires an individual approach, but the general rule of data validation remains the search for impossible or unlikely events.

Equal hourly water consumption by different apartments at different times is a regular event. The same daily water consumption by different apartments is a possible event. The same hourly water consumption during the day for the entire observation period is an unlikely event. A composite key was used to search for duplicate information for the entire observation period. This key includes:

– total water consumption for the entire observation period;
– number of hours with no consumption;
– maximum flow rate;
– average consumption;
– standard deviation;
– the number of cases with an hourly consumption of more than 100 l/h.

All the above parameters are determined for the entire observation period separately for the consumption of cold and hot water. Several apartments are excluded from the analysis as duplicate data. Apartments with zero water consumption for the entire measurement period are excluded from the analysis.

Data preprocessing is performed in an Excel environment.

**Statistical data analysis**

Preliminary data analysis includes the calculation of the main sampling parameters: minimum (min), maximum (max), mean (m), standard deviation (s), quartiles ($Q_1$, $Q_2$, $Q_3$), coefficient of skewness (A) and kurtosis (E), mode (Mo).

The consumption of cold and hot water during the entire observation period is considered as samplings:

– hourly consumption by apartments (sampling 1);

– average hourly consumption for all apartments (sampling 2);

– average daily hourly consumption of apartments (sampling 3).

The frequency distribution of cold and hot water consumption for each sampling is visualized.

Statistical data analysis is performed in the Excel environment.

**Clusterization**

To identify the hours of reduced (night) water consumption, the task of clustering the hours of the day is solved. Clustering is understood as an algorithm that divides data into clusters, that is, groups of elements with similar characteristics. Similarity is determined by calculating the conditional "distance" between the elements. Machine learning methods for clustering are tailored to the characteristics of the source data. The use of clustering methods is often associated with setting the required number of clusters or other necessary algorithm parameters. To identify the hours of reduced (nighttime) water consumption, 5 clustering methods are used: Affinity Propagation, DBSCAN, Agglomerative Clustering, K-means, Spectral Clustering.

At first the Affinity Propagation method is used, because it does not require specifying the number of clusters. Then the DBSCAN method is used, which also does not require specifying the number of clusters. It requires specifying the minimum number of elements in clusters ($Nb_{min}$) and the conditional distance between cluster elements (ε). Three options for parameter values are considered for this method. Then Agglomerative Clustering method, K-means method, and the Spectral Clustering method are used consistently. These three methods require setting the number of clusters. Several numerical experiments were conducted with different numbers of clusters. The initial approximation is the number of clusters determined by the Affinity Propagation method.

Three metrics were selected to assess the quality of clustering [11].

The Davies-Bouldin (*DB*) index is based on the distance from cluster objects to their centroids, and separability is based on the distance between the centroids:

$$DB = \frac{1}{K}\sum_{k=1}^{K} max\left\{\frac{S(c_k) + S(c_l)}{\|\overline{c_k} - \overline{c_l}\|}\right\} \quad (1)$$

Where:

$$S(c_k) = \frac{1}{n_k}\sum_{x_i \in c_k} \|x_i - \overline{c_k}\|$$

$K$ – number of clusters,

$n_k$ – size of cluster,

$\overline{c_k}$ - centroid of cluster *k.*

As the clustering result improves, the *DB* index should decrease.

The Calinsky-Harabasz (*CH*) index is based on the distance from cluster points to their centroids, and separability is based on the distance from cluster centroids to the global centroid.

$$CH = \frac{N-K}{K-1} \cdot \frac{\sum_{k=1}^{K} n_k \left\|\overline{c_k} - \overline{C}\right\|}{\sum_{k=1}^{K} \sum_{x_i \in c_k} \|x_i - \overline{c_k}\|} \quad (2)$$

Where:

$K$ – number of clusters,

$n_k$ – size of cluster $k$,

$\overline{c_k}$ - centroid of cluster *k*,
$\overline{C}$ - global centroid of sampling,
*N* – sample size.
The CH index should increase.
Silhouette (*Sil*) coefficient defined as the average of silhouettes across all elements.
The silhouette of an element shows the difference between the average distance with elements inside its cluster and the average distance with elements of another cluster:

$$Sil = \frac{1}{N}\sum_{k=1}^{K}\sum_{x_i \in c_k}\frac{b(x_i, c_k) - a(x_i, c_k)}{max\{a(x_i, c_k), b(x_i, c_k)\}} \quad (3)$$

Where:

$$a(x_i, c_k) = \frac{1}{n_k}\sum_{x_j \in c_k}\|x_i - x_j\|$$

- average distance from $x_i \in c_k$ to other objects in the $c_k$ cluster,

$$b(x_i, c_k) = min_{k \neq j}\left\{\frac{1}{n_k}\sum_{x_j \in c_j}\|x_i - x_j\|\right\}$$

- distance from $x_i \in c_k$ to objects from another cluster $c_j$,
$n_k$ – size of cluster *k*,
*N* – sample size.
The *Sil* index should aim at 1.
Clusterization is performed using Python programming language libraries.

## RESULTS AND DISCUSSION

### Data preprocessing

Using a composite key allows you to detect duplicates in the measurement results of both cold and hot water. The results are presented in table 1.
The first three data blocks contain information that is completely repetitive throughout the entire observation period. The first two blocks include 2 apartments each, the third block includes 3 apartments. The fourth block contains one apartment, where the information about the consumption of cold water completely coincides with the information about the consumption of hot water. The fifth block includes apartment numbers in which no consumption of cold and/or hot water was recorded during the entire observation period.

*Table 1. Apartment numbers with duplicated information on cold and hot water consumption*

| Block | Cold water | | | Hot water | | |
|---|---|---|---|---|---|---|
| | apartment | duplicate | | apartment | duplicate | |
| 1 | 1 | 2 | - | 4 | 5 | - |
| 2 | 4 | 5 | - | 26 | 28 | - |
| 3 | 50 | 51 | 53 | 50 | 51 | 53 |
| 4 | 62 | - | - | - | 62 | - |
| 5 | 7 | - | - | 7 | 38 | 61 |

Further analysis will provide information on the consumption of cold and hot water in these 9 apartments. (№ 2, 5, 51, 53, 62, 7, 38, 61) it is not counted. As a result, the sampling consists of the hourly water consumption for 73 apartments for 32 days.
The analysis of daily water consumption shows that out of 2336 (73*32) cases, in 26 cases (1.1%) there is no consumption of cold and hot water, in 105 cases (4.5%) there is no consumption of hot water, in 28 cases (1.2%) cold water. Hourly readings for those apartments where there is no consumption of cold and/or hot water during the day are removed from the initial sampling. The volume (n) of the final sampling of hourly cold and hot water costs is 52248.

### Statistical data analysis

The results of the statistical analysis are presented in Table 2. It should be noted that the values are similar or practically identical to the average values of m for all 3 samplings for cold and hot water, while the standard deviations of s for samplings 2 and 3 are several times smaller than for sampling 1.
Averaging during the organization of samplings 2 and 3 makes it possible to offset the error in determining hourly costs, the values of which are less than 10 liters. Unlike Sampling 1, the quartiles $Q_1$ and $Q_2$ of samplings 2 and 3 have values other than 0.

The values of the skewness indicators A and kurtosis E for sampling 2 are less than the corresponding values for samplings 1 and 3. The values of A and E for this sampling indicate that the distribution tends to a normal distribution.

*Table 2. Statistical analysis*

| Param. | Cold Water (CW) | | | Hot Water (HW) | | |
|---|---|---|---|---|---|---|
| | Samplings | | | | | |
| | CW1 | CW1 | CW1 | HW1 | HW2 | HW3 |
| n | 52248 | 768 | 2177 | 52248 | 768 | 2177 |
| Min, l/h | 0 | 0,1 | 0,4 | 0 | 0 | 0,4 |
| Max, l/h | 420 | 21,1 | 91,3 | 820 | 33,2 | 79,6 |
| m, l/h | 8,2 | 7,6 | 8,2 | 11,5 | 10,7 | 11,5 |
| s, l/h | 17,9 | 3,9 | 7,7 | 34,2 | 6,5 | 10,5 |
| $Q_1$, l/h | 0 | 5 | 3 | 0 | 6 | 4 |
| $Q_2$, l/h | 0 | 8 | 6 | 0 | 10 | 9 |
| $Q_3$, l/h | 10 | 10 | 11 | 10 | 15 | 16 |
| Mo, l/h | 0 | 7 | 1 | 0 | 9 | 3 |
| A | 5,3 | 0,3 | 3,0 | 6,7 | 0,4 | 1,9 |
| E | 55,7 | -0,2 | 18,2 | 69,4 | -0,1 | 5,5 |
| m+ 3s, l/h | 62 | 19 | 31 | 114 | 30 | 43 |
| Out-liers % | 893 | 2 | 35 | 1040 | 4 | 37 |
| | 1,7 | 0,3 | 1,6 | 2 | 0,5 | 1,7 |
| $Q_1$+ 3($Q_3$-$Q_1$), l/h | 30 | 20,5 | 27,9 | 30 | 32,2 | 40 |
| Out-liers % | 5290 | 1 | 53 | 6357 | 1 | 52 |
| | 10,1 | 0,1 | 2,4 | 12,2 | 0,1 | 2,4 |

Regardless of the method of estimating anomalous values, the number of outliers in samplings 2 and 3 is lower both absolutely and relative to the size of sampling 1.

Figures 1-3 show the frequency distribution of hourly consumption of cold (CW) and hot (HW) water by apartments for 3 samplings.

The distribution pattern is the same for samplings 1 and 3 (figures 1 and 3). The distribution of hourly water consumption averaged across apartments (sampling 2) differs (figure 2).

Visualization of the average hourly consumption of all apartments (figure 2) allows us to identify two consumption modes, regardless of whether the consumption of cold or hot water is considered.

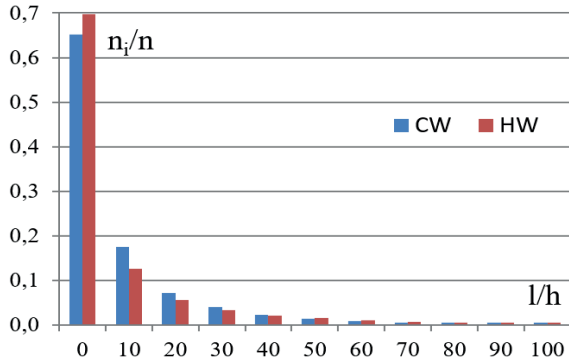


*Figure 1. Frequency distribution of cold (CW) and hot (HW) water consumption - sampling 1*

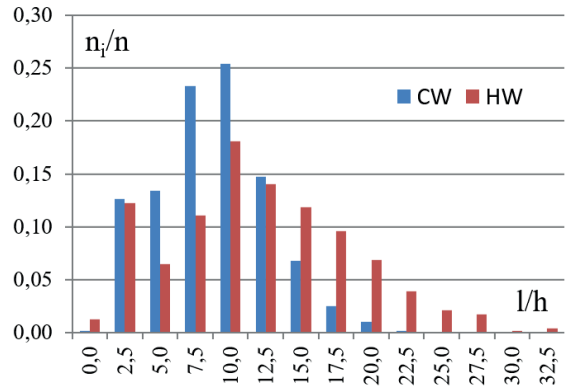


*Figure 2. Frequency distribution of cold (CW) and hot (HW) water consumption - sampling 2*

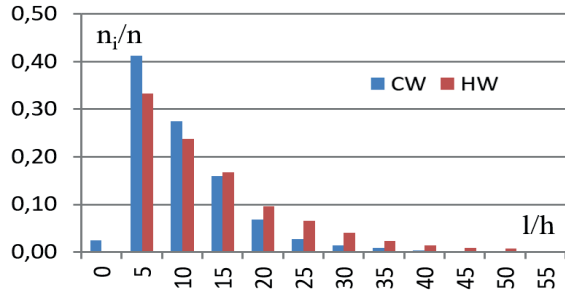


*Figure 3. Frequency distribution of cold (CW) and hot (HW) water consumption - sampling 3*

The first mode corresponds to the mode occurring at a flow rate of 2.5 l/h, the second

mode corresponds to the mode occurring at a flow rate of 10 l/h. The points forming the first mode are a group outlier for the sampling. Identifying a group outlier is equivalent to dividing a sampling into two subsets. Solving this problem is laborious, and clusterization methods must be used to automate this process.

**Clusterization**

Clustering is performed for the hours of total water consumption by the apartments in the house. The data is converted into datasets in which hourly water consumption is assigned to one of the 24 hours of the day (from 0 to 23). In addition, subsets of data are generated separately for weekends and weekdays of the measurement period.

The results of using various clustering methods, considering experiments with the number of clusters, are evaluated for quality. As a result, the number of clusters with the best clustering quality is determined for each method. Table 3 shows five clustering methods and three measures of the quality of their results.

*Table 3. Results of quality assessment of clusterization of hot water consumption*

| Methods | Para-meter | Metrics (index) | | |
|---|---|---|---|---|
| | | DB | CH | Sil |
| Affinity Propagation | - | 0,93 | 14,00 | 0,33 |
| DBSCAN | ε =2000 | 1,12 | 17,15 | 0,33 |
| | ε =2100 | 1,09 | 17,20 | 0,35 |
| | ε =2200 | 1,17 | 11,25 | 0,30 |
| Agglomerative Clustering | K =3 | 1,15 | 16,95 | 0,33 |
| | K =4 | 0,97 | 13,78 | 0,32 |
| | K =5 | 0,90 | 11,99 | 0,31 |
| K-means | K =3 | 1,09 | 17,20 | 0,35 |
| | K =4 | 1,10 | 14,10 | 0,33 |
| | K =5 | 1,37 | 11,82 | 0,19 |
| Spectral Clustering | K =3 | 1,16 | 16,91 | 0,32 |
| | K =4 | 1,50 | 11,01 | 0,19 |
| | K =5 | 1,33 | 12,01 | 0,21 |

The Affinity Propagation method allocates four clusters. Based on the metrics for the DBSCAN method, the parameters ε=2100 and $Nb_{min}$=2.

Four clusters are defined for the Agglomerative Clustering method, three for the K-means method, and three for the Spectral Clustering method.

As an example, Figures 4-8 show the results of clustering the hours of hot water consumption in a house over the entire measurement period. The hours of the day are shown on the horizontal axis, and the volume of hot water consumption is shown on the vertical axis. For clarity, there is one dot corresponding to each hour. The ordinate of the point is calculated as the median of a set of values for hourly hot water consumption over the entire observation period. The point color is selected automatically depending on the cluster number. Different methods give different numbering and number of clusters.

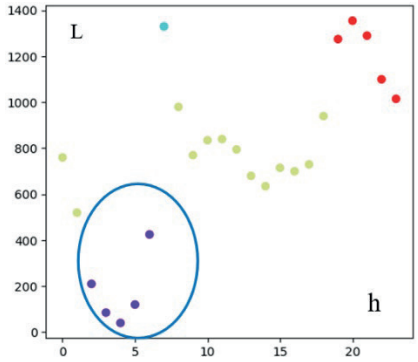


*Figure 4. Affinity Propagation method result*

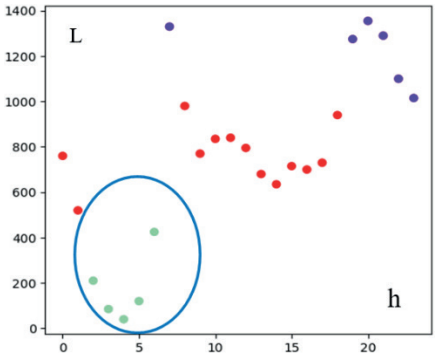


*Figure 5. DBSCAN method result*

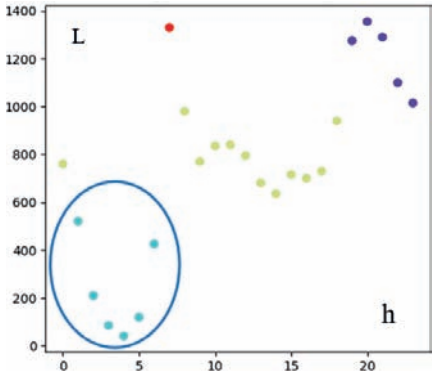


*Figure 6. Agglomerative Clustering method result*

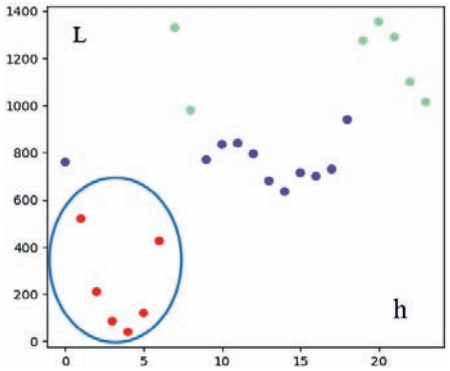


*Figure 7. K-means method result*

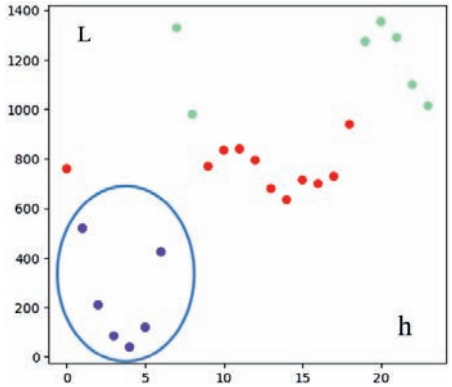


*Figure 8. Spectral Clustering method result*

The results of clustering using different methods are presented in Table 4. The method numbers match their enumeration above.

The table shows that the results obtained by different methods for different samplings are in most cases close or identical. The final conclusion about the period of nighttime (reduced) water consumption is based on the results obtained by most methods.

*Table 4. Hours of reduced (overnight) consumption of cold and hot water: 1-Affinity Propagation, 2-DBSCAN, 3-Agglomerative Clustering, 4-K-means, 5-Spectral Clustering*

| Water | Days of week | Methods | | | | | Result , Hours |
|---|---|---|---|---|---|---|---|
| | | 1 | 2 | 3 | 4 | 5 | |
| Cold Water | All days | 1-6 | 1-6 | 2-6 | 1-6 | 1-6 | 1–6 |
| | Weekdays | 1-6 | 1-6 | 1-6 | 1-6 | 1-6 | 1–6 |
| | Weekends | 1-6 | 2-6 | 2-6 | 1-6 | 1-6 | 1–6 |
| Hot Water | All days | 2-7 | 2-7 | 1-7 | 1-7 | 1-7 | 1–7 |
| | Weekdays | 2-6 | 2-6 | 2-6 | 2-6 | 1-7 | 2–6 |
| | Weekends | 1-9 | 1-9 | 2-8 | 1-9 | 1-9 | 1–9 |

## CONCLUSION

1. The scale of water consumption facilities, methods, and conditions for obtaining source data, as well as the structure and format of data storage, are important for analyzing water consumption.
2. To solve various problems, it is usually necessary to transform data values (normalization, averaging) and change the data structure.
3. Improving data quality involves removing duplicates, anomalies, deviations from the norm, and zeros. However, in data related to hourly water consumption, it is necessary to carefully study anomalies and outlines, including analyzing them as group outlines.
4. Data samplings for analyzing water consumption in an apartment building can be formed for various objects (the building, apartments, appliances, tenants) and for different time periods (the entire observation period, days of the week, hours of the day). Samplings for statistical analysis can be formed based on averaged data values.
5. Different data samplings may have different distribution laws. The choice of further data analysis methods depends on the identified distribution function.
6. Intelligent machine learning methods for clustering differ in cluster formation algorithms, control parameters, and the quality of the result.

During the research, it is necessary to use a set of clustering methods and evaluate their quality.
7. Most clustering methods have yielded consistent results. The Agglomerative Clustering method has shown special results in many cases and has not been considered.
8. The results of the study can be used in the design of water supply and sanitation systems, setting operating modes of engineering equipment, clarifying the regulatory parameters of water consumption in apartment buildings.

## REFERENCES


1. **Ignatova E.V., Kruglova L.V.** Information systems for accounting and data analysis of housing and communal services of apartment buildings. J. Construction and Architecture Vol. 4, 2023, p. 38. DOI:10.29039/2308-0191-2023-11-4-38-37
2. **Kitaytseva E.H., Ignatova E.V.** Trends in the use of water supply systems telemetry data. J. Construction and Architecture Vol. 4, 2023, p. 22. DOI:10.29039/2308-0191-2023-11-4-22-22
3. **Polivanov D.E., Semenov A.A., Yarkova O.N.** Mathematical modeling of the intensity of water consumption by various types of water collecting devices. J. Information and mathematical technologies in science and management. 2024 Vol. 1 (33)
4. **Andreenko A.A., Sharipov T.R.** Analysis of hourly water consumption in a residential building. Modern problems of water supply and sanitation : collection of materials of the Interuniversity scientific and practical conference [December 1-3, 2021]. St. Petersburg : SPbGASU, 2022, p.3-11
5. **Ignatchik V.S., Sarkisov S.V., Obvintsev V.A.** Research of water consumption hour inequality coefficients. J. Water and ecology Vol.2 (70), 2017. p. 27-39. DOI:10.23968/2305-3488.2017.20.2.27–39
6. **Kermany E., Mazzawi H., Baras D., Naveh Y., Michaelis H.** Analysis of advanced meter infrastructure data of water consumption in apartment Buildings. 19th ACM SIGKDD international conference on Knowledge discovery and data mining. 2013, p.1159-1167. DOI:10.1145/2487575.2488193
7. **Josey B.M., Buchberger S.G., Jinzhe G.J.** Comparing Actual and Designed Water Demand in Australian Multilevel Residential Buildings. Water Resour. Plann. Manage., 2023, 149(1): 05022013. DOI:10.1061/(asce)wr.1943-5452.0001625
8. **Kitaytseva E.H.** Numerical analysis of hourly consumption of hot and cold water. International Journal for Computational Civil and Structural Engineering. Vol. 8, Issue 4, 2012 - M. : DIA Publishing House, p. 78-84. Library ID: 18973119 EDN: https://www.elibrary.ru/pzexll
9. **Zhulin A.G., Aminova A.Kh., Belova L.V.** Determination of the amount of water consumed by various water users of the residential sector. Arkhitektura, stroitel'stvo, transport [Architecture, construction, transport], 2021 (1), p. 47-57. (in Russia)
10. **Nejranowski J., Szaflik W.** Hot water consumption time in multi-apartment buildings. Journal of Ecological Engineering. 2020, 21(4), p.199–202. DOI:10.12911/22998993/119906
11. **Surendra P., Deka H., Rajakumara N.** Application of Mamdani model-based fuzzy inference system in water consumption estimation using time series. J.Soft Computing - A Fusion of Foundations, Methodologies and Applications. 2022, 5. DOI:10.1007/s00500-022-06966-4
12. **Lee S.S., Lee H.H., Lee Y.J.** Prediction of Minimum Night Flow for Enhancing Leakage Detection Capabilities in Water Distribution Networks. Appl. Sci. 2022, 12, 6467. DOI:10.3390/app12136467
13. **Kim J., Lee H., Lee M., Han H., Kim D., Kim H.S.** Development of a Deep Learning-Based Prediction Model for Water Consumption at the Household Level. Water 2022, 14, 1512. DOI:10.3390/w14091512

14. **Heydari Z., Cominola A., Stillwell A.S**. Is smart water meter temporal resolution a limiting factor to residential water end-use classification? A quantitative experimental analysis. Environmental Research: Infrastructure and Sustainability, 2022, Vol.2, Num.4, 045004. DOI:10.1088/2634-4505/ac8a6b
15. **Vedishcheva E.V., Kapyrin A.S., Vasilenko M.S.** Analiz i utochnenie klassifikatsii anomalij i vybrosov na economicheskih dannyh [Analysis and refinement of classification of anomalies and outliers on economic data] // Bulletin of the Altai Academy of Economics and Law. 2019, Vol. 6-1. P. 41-46 (in Russia) URL: https://vaael.ru/ru/article/view?id=589
16. **Ignatova E.V.** Water supply telemetry data processing in apartment buildings. BIO Web of Conferences Volume 107 01004 (2024) (YRC-2024). DOI:10.1051/bioconf/202410701004
17. **Bhattacharjee P., Mitra P.** A survey of density-based clustering algorithms, Frontiers of Computer Science. (2021) 15, 151308, DOI:10.1007/s11704-019-9059-3.
18. **Sivogolovko E.V.** Metody otsenki kachestva chotkoj klasterizatsii [Methods for assessing the quality of clear clusterization] // Computer tools in education, Tver', 2011, Issue 4(96), p. 14-31. (in Russia)
19. **Ghamkhar H., Ghazizadeh J.M., Mohajeri S.H., Moslehi I., Yousefi-Khoshqalb E.** An unsupervised method to exploit low-resolution water meter data for detecting end-users with abnormal consumption: Employing the DBSCAN and time series complexity. Sustainable Cities and Society, Volume 94, 2023, 104516 DOI:10.1016/j.scs.2023.104516

## СПИСОК ЛИТЕРАТУРЫ

1. **Игнатова Е.В., Круглова Л.В.** Информационные системы учета и анализа данных жилищно-коммунального хозяйства многоквартирных домов/ Строительство и архитектура № 4 2023. стр. 38 DOI:10.29039/2308-0191-2023-11-4-38-37
2. **Китайцева Е.Х., Игнатова Е.В.** Тренды использования данных телеметрии систем водоснабжения. Строительство и архитектура № 4, 2023. стр. 22. DOI:10.29039/2308-0191-2023-11-4-22-22
3. **Поливанов Д.Е., Семенов А.А., Яркова О.Н.** Математическое моделирование интенсивности водопотребления различными типами водоразборных устройств / Информационные и математические технологии в науке и управлении. 2024. № 1(33). С. 78-92. DOI:10.25729/esi.2024.33.1.007
4. **Андреенко А.А., Шарипов Т.Р.** Анализ почасового водопотребления в жилом доме. Современные проблемы водоснабжения и водоотведения : сборник материалов межвузовской научно-практической конференции [1–3 декабря 2021 года]– Санкт-Петербург : СПбГАСУ, 2022, С.3-11
5. **Игнатчик В.С., Саркисов С.В., Обвинцев В.А.** Исследование коэффициентов часовой неравномерности водопотребления / Вода и экология: проблемы и решения. 2017. №2 (70). С. 27-39 DOI:10.23968/2305-3488.2017.20.2.27–39
6. **Kermany E., Mazzawi H., Baras D., Naveh Y. and Michaelis H.** Analysis of advanced meter infrastructure data of water consumption in apartment Buildings 19th ACM SIGKDD international conference on Knowledge discovery and data mining. 2013, P.1159-1167 DOI:10.1145/2487575.2488193
7. **Josey B.M., Buchberger S.G. and Jinzhe G.J.** Comparing Actual and Designed Water Demand in Australian Multilevel Residential Buildings. Water Resour. Plann. Manage., 2023, 149(1): 05022013 DOI:10.1061/(asce)wr.1943-5452.0001625

8. **Китайцева Е.Х.** Численный анализ часового потребления горячей и холодной воды. International Journal for Computational Civil and Structural Engineering. Volume 8, Issue 4, 2012. M. : Издательство ACB, С. 78-84. elibrary ID: 18973119 EDN: https://www.elibrary.ru/pzexll
9. **Жулин А.Г., Аминова А.Х., Белова Л.В.** Определение количества расходуемой воды различными водопотребителями жилого сектора./ Архитектура, строительство, транспорт. № 1 (95). 2021. С. 47–57 elibrary ID: 46409679 EDN: https://www.elibrary.ru/njfcvo
10. **Nejranowski J., Szaflik W.** Hot water consumption time in multi-apartment buildings. Journal of Ecological Engineering. (2020) 21(4), pp.199–202. DOI:10.12911/22998993/119906
11. **Surendra P., Deka H., Rajakumara N.** Application of Mamdani model-based fuzzy inference system in water consumption estimation using time series. J.Soft Computing - A Fusion of Foundations, Methodologies and Applications. 2022, 5. DOI:10.1007/s00500-022-06966-4
12. **Lee S.S., Lee H.H., Lee Y.J.** Prediction of Minimum Night Flow for Enhancing Leakage Detection Capabilities in Water Distribution Networks. Appl. Sci. 2022, 12, 6467. DOI:10.3390/app12136467
13. **Kim J., Lee H., Lee M., Han H., Kim D., Kim H.S.** Development of a Deep Learning-Based Prediction Model for Water Consumption at the Household Level. Water 2022, 14, 1512. DOI:10.3390/w14091512
14. **Heydari Z., Cominola A., Stillwell A.S**. Is smart water meter temporal resolution a limiting factor to residential water end-use classification? A quantitative experimental analysis. Environmental Research: Infrastructure and Sustainability, 2022, Vol.2, Num.4, 045004. DOI:10.1088/2634-4505/ac8a6b
15. **Видищева Е.В., Копырин А.С., Василенко М.С.** Анализ и уточнение классификации аномалий и выбросов на экономических данных // Вестник Алтайской академии экономики и права. 2019. № 6-1. С.41-46 URL: https://vaael.ru/ru/article/view?id=589
16. **Ignatova E.V.** Water supply telemetry data processing in apartment buildings. BIO Web of Conferences Volume 107 01004 (2024) (YRC-2024). DOI:10.1051/bioconf/202410701004
17. **Bhattacharjee P., Mitra P.** A survey of density-based clustering algorithms, Frontiers of Computer Science. (2021) 15, 151308, DOI:10.1007/s11704-019-9059-3.
18. **Сивоголовко Е.В.** Методы оценки качества четкой кластеризации. // Компьютерные инструменты в образовании. Тверь, 2011, Вып. 4(96), С. 14-31
19. **Ghamkhar H., Ghazizadeh J.M., Mohajeri S.H., Moslehi I., Yousefi-Khoshqalb E.** An unsupervised method to exploit low-resolution water meter data for detecting end-users with abnormal consumption: Employing the DBSCAN and time series complexity. Sustainable Cities and Society, Volume 94, 2023, 104516. DOI:10.1016/j.scs.2023.104516

*Elena V. Ignatova* — Candidate of Technical Sciences, Associate Professor, Department of Information Systems, Technologies and Automation in Construction, National Research Moscow State University of Civil Engineering (NRU MGSU), 26 Yaroslavskoe Shosse, Moscow, 129337, Russia, Email: IgnatovaEV@mgsu.ru

*Елена Валентиновна Игнатова* — кандидат технических наук, доцент кафедры Информационных систем, технологий и автоматизации в строительстве, Федеральное государственное бюджетное образовательное учреждение «Национальный исследовательский Московский государственный строительный университет» (НИУ МГСУ), 26, Ярославское шоссе, Москва, 129337, Россия, E-mail: IgnatovaEV@mgsu.ru

*Elena Kh. Kitaytseva* — Candidate of Technical Sciences, Associate Professor, Department of Information Systems, Technologies and Automation in Construction, National Research Moscow State University of Civil Engineering (NRU MGSU), 26 Yaroslavskoe Shosse, Moscow, 129337, Russia, E-mail: KitaytsevaEH@mgsu.ru

*Елена Халиловна Китайцева* — кандидат технических наук, доцент, доцент кафедры Информационных систем, технологий и автоматизации в строительстве, Федеральное государственное бюджетное образовательное учреждение «Национальный исследовательский Московский государственный строительный университет» (НИУ МГСУ), 26, Ярославское шоссе, Москва, 129337, Россия, E-mail: KitaytsevaEH@mgsu.ru

International Journal for Computational Civil and Structural Engineering, 21(3) 105–120 (2025)

DOI:10.22337/2587-9618-2025-21-3-105-120

# ANALYTICAL EVALUATION OF BASE CONTROL SYSTEM EFFECTIVENESS FOR REGULATION SEISMIC RESPONSE OF SUSPENDED EQUIPMENT BRACED WITH METAL FRAMES BY HYSTERESIS DAMPERS

***Aleksandr M. Anushchenko***

CKTI-VIBROSEISM Co. Ltd., Saint-Petersburg, RUSSIA

**Abstract:** Equipment suspended from metal frames, such as steam boilers, usually has a bracing system that reduces the oscillation amplitude of equipment during an earthquake to technologically acceptable values. Hysteresis dampers are often used as bracing elements, the installation of which affects frame dynamic response. If frame stress-strain state worsens when dampers are used, it is advisable to additionally use a Base Control System (BCS), the optimal parameters of which must be selected during the design process. This ensures both the strength and reliability of building structures in case of an earthquake, and the most financially economical technical solution. BCS includes elastic spring elements that carry the load from the frame and equipment, and viscous dampers that decrease vibrations and increase the overall damping of the structural system. Detailed finite element models are not applicable for optimization analysis purposes. It requires significant time and computing resources in conditions of the nonlinear nature of the constructive system. In this paper an analytical model of the "suspended equipment – frame" system with bracing hysteresis dampers and BCS is proposed. This model is easily implemented using MathCAD software programming tools. The paper also analyzes the possibility of implementing BCS for the purpose of seismic insulation of frames and boilers during seismic impacts of various frequency compositions. It is shown how different parameters of the seismic insulation elements can affect the efficiency of its installation. It is noted that it is necessary to determine the most optimal number of viscous dampers, at which the maximum decrease in the seismic response is observed.

**Keywords:** metal frame, suspended steam boiler, hysteresis damper, base control system, seismic response, earthquake, analytical model

# АНАЛИТИЧЕСКАЯ ОЦЕНКА ЭФФЕКТИВНОСТИ ПРИМЕНЕНИЯ СИСТЕМЫ КОНТРОЛЯ ПЕРЕМЕЩЕНИЙ (BCS) ДЛЯ РЕГУЛИРОВАНИЯ СЕЙСМИЧЕСКОГО ОТКЛИКА ПОДВЕШЕННОГО ОБОРУДОВАНИЯ, РАСКРЕПЛЕННОГО УПРУГОПЛАСТИЧЕСКИМИ ДЕМПФЕРАМИ С МЕТАЛЛИЧЕСКИМИ КАРКАСАМИ

***А.М. Анущенко***

Общество с ограниченной ответственностью «ЦКТИ-ВИБРОСЕЙСМ», г. Санкт-Петербург, РОССИЯ

**Аннотация:** Оборудование, подвешенное к опорным металлических каркасам, например, паровые котлоагрегаты, обычно имеет систему раскрепления, которая снижает амплитуду сейсмических колебаний до технологически приемлемых значений. В качестве элементов раскрепления используются упругопластические демпферы, установка которых влияет на динамические характеристики конструктивной системы. Если напряженно-деформированное состояние элементов металлического каркаса ухудшается при использовании демпферов, рекомендуется дополнительно использовать систему контроля перемещений (BCS), оптимальные параметры которой должны быть определены в процессе проектирования. При этом одновременно обеспечиваются требования к сейсмостойкости конструкций и экономичности принимаемых технических решений. BCS включает в себя блоки пружин – опоры,

воспринимающие нагрузку от каркаса и оборудования, и вязкие демпферы, повышающие общее демпфирование системы. Подробные конечно-элементные модели не применимы для целей оптимизационного анализа эффективности BCS, поскольку в условиях нелинейного характера работы системы они требуют значительных временных и программно-вычислительных ресурсов. В данной статье предлагается аналитическая модель системы "подвесное оборудование – каркас" с упругопластическими демпферами и системой BCS, которая легко реализуется алгоритмами программы MathCAD. В статье также анализируется возможность применения BCS с целью сейсмоизоляции подвешенного оборудования (котлов) и каркасов при воздействиях различного частотного состава. Показано, как различные параметры элементов BCS могут влиять на эффективность. Отмечается, что необходимо определить наиболее оптимальное количество вязких демпферов, при котором наблюдается максимальное снижение сейсмического отклика.

**Ключевые слова:** металлический каркас, подвесной паровой котел, упругопластический демпфер, система контроля перемещений (BCS), сейсмическая реакция, землетрясение, аналитическая модель

## INTRODUCTION

Large-sized suspended equipment can oscillate with considerable amplitude during an earthquake. As a rule, its displacements are limited to small values for technological reasons. First of all, it is possible to destroy pipelines and cables that ensure the normal operation of the equipment. In addition, significant displacements cause a high level of bending stresses in suspension system, which can lead to plastic deformations, suspension breakage and equipment collapse. Any of the above situations are considered emergencies. A minimal consequence of these is a temporary equipment failure. The most significant consequences are technogenic disasters, which can be accompanied by environmental damage, destruction of infrastructure, and loss of life. To ensure safe operation in case of earthquakes, various means of seismic isolation, energy dissipation and vibration damping are used [1-4].

Thermal power plants (TPP) are danger objects. Most of them are equipped with high-energy steam boilers suspended from freestanding metal frames inside TPP buildings (fig. 1). In this paper, boilers suspended from frames are considered as one of the most common types of sus-pended equipment.

Boilers and frames have weights up to several tens of thousands of tons, dimensions in plan and height up to 100 m [3-6]. The dynamic characteristics of the frames and boilers are well studied, and regardless of the standard sizes they have a number of similar characteristics [6]:

– the predominant oscillation frequencies of the frame in both horizontal directions are approximately the same and are in the range of 1 – 2 Hz;
– the predominant oscillation frequencies of suspended boilers are in the range of 0.1 – 0.5 Hz;
– the modal mass of the first oscillation frequency for the frame is 60 – 80%, the type of vibration is flexural, similar to a single-mass oscillator; the ratios between the frame mass ($M_f$) and boiler mass ($M_b$) as a rule, the ratio of $M_f / M_b = 1/4$ is observed.
– the torsional forms of natural oscillations are of little importance.

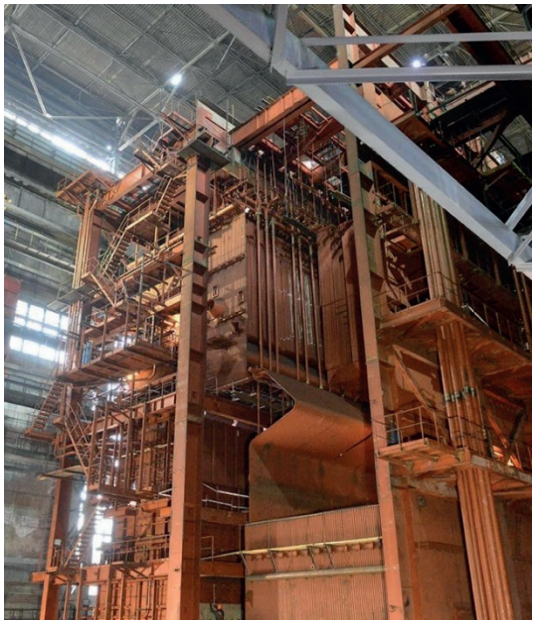

*Figure 1. Metal frame with suspended equipment (steam boiler)*

Studies [7-11] have shown that hysteresis dampers of various types, for example, cantilever type dampers and axial dampers (fig. 2) with a localized zone of plastic deformations, can be effective to reduce the amplitude of boiler vibrations and prevent emergencies. These structures have passed cyclic dynamic tests (fig. 3) showed stable hysteresis operation for a large number of loading cycles up to maximum operating amplitudes without failure. The hysteresis is reproduced qualitatively in numerical simulation programs (fig. 4). This allows you to carry out design work without additional expensive full-scale tests.

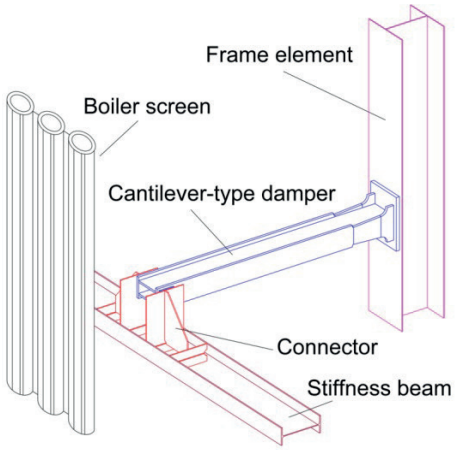


*a) cantilever-type damper (installation scheme)*

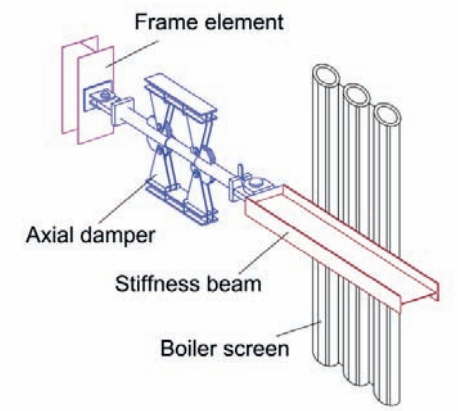


*b) axial damper (installation scheme)*

*Figure 2. Hysteresis dampers for antiseismic bracing frame and boiler*

*Figure 3. Full-scale experiment for axial damper*

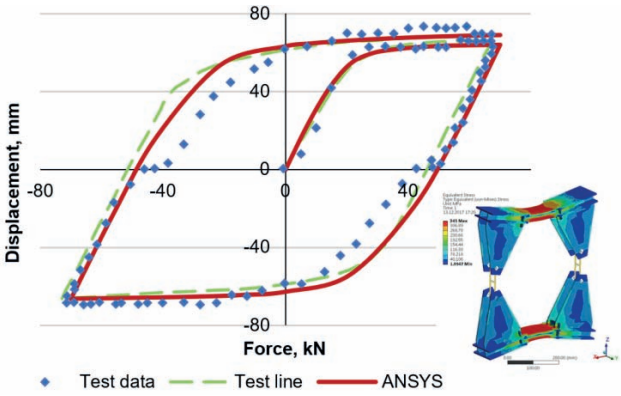


*Figure 4. Comparison of test and numerical results for hysteresis damper*

Hysteresis dampers reduces boiler displacements effectively during an earthquake. It is established that their introduction corrects the dynamic characteristics of the structural system "frame-boiler". Therefore, it is required to perform an optimization analysis of the effectiveness of the solution being developed. This makes it possible to reduce the movements of the frame elements and reduce the momentary load on the supporting zones of the frame columns, which ensures its earthquake resistance.

However, in some cases, the optimal parameters of hysteresis dampers cannot be selected. The introduction of these elements leads to a deterioration of the stress-strain state of the building structures of the frame. In this case, the design solutions of the frame are adjusted [12] (changes in the cross-sections of the elements; the device of additional connections and

stiffness elements) or traditional seismic insulation systems are used [8,13,14].
Among all of the existing spatial passive 3D developments of isolation devices, the most effective and reliable system seems to be the Base Control System (BCS) [15-18]. The application of the base control system for various NPP equipment [17,18] and for massive turbine foundations [19,20] has been widely studied at the present time. However, possibilities of effective use BCS for the "frame-boiler" system have not been studied in detail before. This work is intended to fill this gap.
It is proposed to consider the possibility of using BCS that includes elastic elements – spring supports and viscous dampers (fig. 3 – a). Due to the application of spring elements the mode shape of the isolation structure is changed and fundamental period of vibration increases. The second measure is based on the increase of damping that may be combined with the reduction of the frequency. More other, BCS provides vibration damping in both the horizontal and vertical directions of seismic vibrations. It is known that most traditional means of seismic isolation increase the vertical response due to their significant rigidity. This is unacceptable for the frame-boiler system, since it is possible to significantly redistribute the forces in the suspensions and overload them, which requires compensatory measures. BCS has been experimentally tested and its effectiveness has been confirmed by CKTI-VIBROSEISM Co. Ltd. (fig. 3 – b) [13].

*a) viscous damper and spring (BCS elements)*

*b) BCS full-scale test*

*Figure 5. Base Control System for regulating seismic response [13]*

## METHODS AND MATERIALS

It is impractical to perform full-scale tests or detailed finite element calculations for preliminary estimates of the effectiveness of BCS. Therefore, in this work, an analytical model of the structural system "suspended equipment (boiler) – hysteresis dampers – metal frame – BCS" is being developed.
The analytical model makes it possible to estimate the acceleration and displacement of its components, which are used as basic parameters for evaluating the effectiveness of the developed seismic insulation solutions. It is impossible to perform a direct assessment of the stress-strain state of building structures; however, an indirect qualitative assessment can be given.
The analytical model assumes the use of simplified models of dampers. One of the most widely accepted differential model Bouk-Wen [21-23] is used to describe the hysteresis nature of dampers. In this model, the restoring force and deformation are related by a nonlinear first-order differential equation containing a number of parameters that refine the shape of hysteresis loops in accordance with experimental data [24-26]. According to [21,24], a hysteresis damper can be represented as elastic post yielding spring ($F^{el}$) and hysteretic spring (Z), giving in total a full restoring force ($F_{u,Z}$):

$$F_{u,Z} = F^{el} + Z. \quad (1)$$

The hysteresis force Z is expressed as

$$\frac{dZ}{dt} = \left\{Ak_d - \left[\gamma + \beta sign\left(Z\frac{du}{dt}\right)\right]|Z|^n\right\}\frac{du}{dt}, \quad (2)$$

there $u$ – displacement;
$t$ – time;
$A$, $\beta$, $\gamma$ – parameters regulating the duration of plastic deformations and the shape of the hysteresis loop;
$n$ – parameter regulating the sharpness of the transition from the elastic to the plastic stage;
$k_d$ – a parameter equal to the difference between elastic $k_i$ and plastic $k_f$ stiffness according to a characteristic bilinear diagram:

$$k_d = k_i - k_f. \quad (3)$$

Parameters A, β, γ, n are determined individually for each designed device with hysteresis according to experimental or calculated graphs of material deformation for one full cycle of operation.
Focusing on the researches of Aida, Nishida et al. [9,27] and decoupling criteria in regulatory documents (ASCE 4-16, ASN guide 2006, CEA 2008, ETC-C 2012) [28-30], it was previously proposed to idealize the "frame – N hysteresis dampers – boiler" system to 3DOF oscillator (fig. 5) [6,7], where:
– the subsystem approximating vertical load-bearing frame structures below the level of the mass center consists of mass $m_1$ and connection elastic bonds to the base with stiffness $k_1$ and damping $c_1$;
– the subsystem approximating the frame overlap with adjacent vertical structures consists of mass $m_2$ connected by elastic bonds (stiffness $k_2$ and damping $c_2$) with mass $m_1$;
– masses $m_1$ and $m_2$ with elastic bonds $k_1$, $c_1$ and $k_2$, $c_2$ provide the first modal response of the frame;
– the subsystem approximating a boiler consists of mass $m_3$, elastic bond with mass $m_2$ (a model of a boiler suspension system with stiffness $k_3$ and damping $c_3$) and hysteresis bond with mass $m_1$ (a model of dampers).

The features of $k_1$, $k_2$, $c_1$, $c_2$ parameter determination are presented in detail in the study [6].
The analytical model is determined by solving a system of 4 differential equations of motion, which is written as follows for 3DOF oscillator:

$$\begin{aligned}
&m_1\frac{d^2x_1}{dt^2} + c_1\frac{dx_1}{dt} + k_1x_1 - c_2\frac{d(x_2 - x_1)}{dt} - \\
&-k_2(x_2 - x_1) - Nk_f(x_3 - x_1) - NZ = -m_1y''(t), \\
&m_2\frac{d^2x_2}{dt^2} + c_2\frac{d(x_2 - x_1)}{dt} + k_2(x_2 - x_1) - \\
&-c_3\frac{d(x_3 - x_2)}{dt} - k_3(x_3 - x_2) = -m_2y''(t), \\
&m_3\frac{d^2x_3}{dt^2} + c_3\frac{d(x_3 - x_2)}{dt} + k_3(x_3 - x_2) + \\
&+Nk_f(x_3 - x_1) + NZ = -m_3y''(t), \\
&\frac{dZ}{dt} = \left\{Ak_d - \left[\gamma + \beta sign\left(Z\frac{d(x_3 - x_1)}{dt}\right)\right]|Z|^n\right\}\frac{d(x_3 - x_1)}{dt},
\end{aligned} \quad (4)$$

there $y''(t)$ – ground acceleration;
$x_i$ – mass displacements (i = 1, 2, 3).

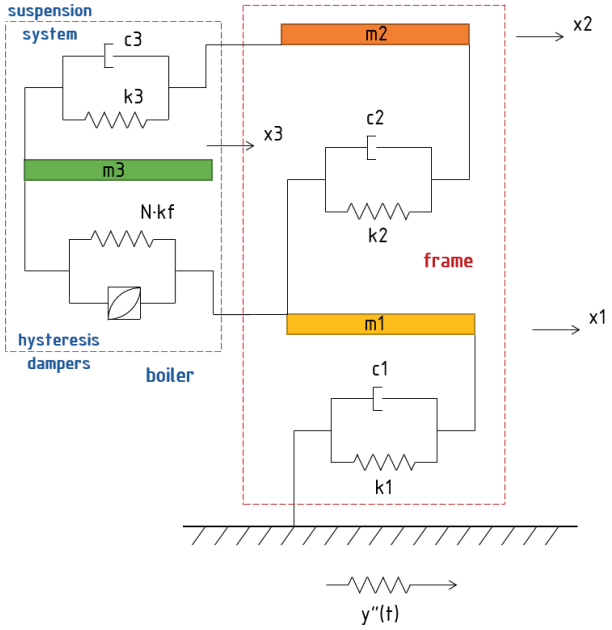


*Figure 6. 3DOF oscillator – an analytical model of the "frame – N hysteresis dampers – boiler" system*

3DOF model provides quantitative and qualitative matching of results with finite element calculations (the discrepancy between the results is up to 10%), which allows to use this model at the pre-initial design stages [6,7].

BCS is mounted to the foundation. To support the frame with a suspended boiler on it, it is necessary to arrange an intermediate plate (MS). Its load-bearing capacity should be sufficient to wear loads from higher structures.
According to experimental data [16], BCS spring elements (fig. 7) can be considered as elastic bonds (fig. 8) with a linear relationship between the applied force and the acquired displacement.

*Figure 7. BCS spring block*

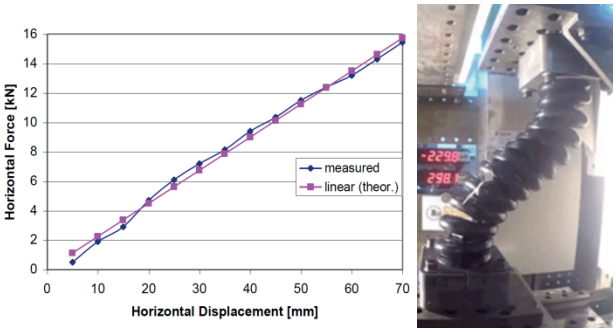


*Figure 8. BCS spring test and theory results*

Viscous dampers (fig. 9) are widely used for their essential advantages [31,32]:
– reducing vibration and dynamic response of systems in all degrees of freedom by tremendous increasing of system's damping with possibility to tune to optimal damping;
– developing high damping forces under any dynamic impact whereas slow motions are free;
stability to high temperature, humid, toxic and radiation environment.

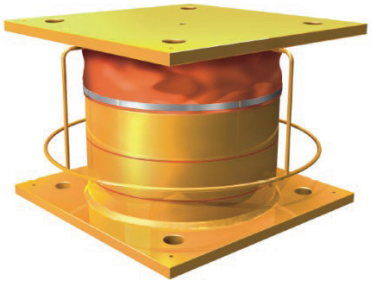

*Figure 9. Viscous damper*

Viscous liquid defines damper viscous-elastic behavior. The simplest mathematical model describing such behavior is a Maxwell Model consists of ideal viscous damper and spring element chain (2-parameters Maxwell Model). This model demonstrates the following typical features:
– reaction at the low frequency range is considered as viscous;
– reaction at the high frequency range is considered as essentially elastic.
Dynamic characteristics of viscous dampers derived from the experiments are more complex than 2-parameters Maxwell Model. It was recognized that a set of two parallel Maxwell chains, or 4-parameters Maxwell Model demonstrates quite appropriate results (fig. 10). This model is used in regulatory document [33] in the present time.

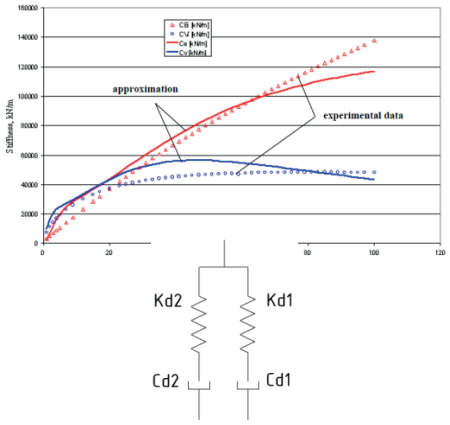


*Figure 10. Approximation of test data with 4-parameters Maxwell Model for viscous damper*

Considering BSC modeling features, 3DOF analytical model (fig. 6) can be supplemented and represented as in Figure 11.

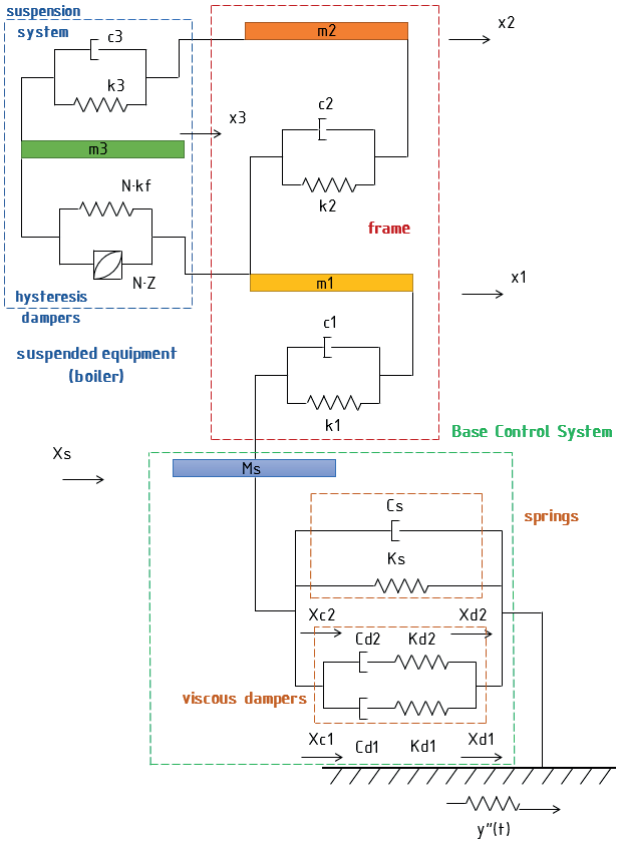


*Figure 11. The "suspended equipment (boiler) – hysteresis dampers – metal frame – BCS" analytical model*

The system of 7 differential equations of motion [34] for the "suspended equipment (boiler) – hysteresis dampers – metal frame – BCS" system is written as:

$$
\begin{gathered}
m_s\frac{d^2x_s}{dt^2}+c_s\frac{dx_s}{dt}+k_sx_s+k_{d1}(x_s-x_{d1})+\\
+k_{d2}(x_s-x_{d2})-c_1\frac{d(x_1-x_s)}{dt}-k_1(x_1-x_s)=\\
=-m_sy^{"}(t),\\
k_{d1}x_{d1}=c_{d1}\frac{dx_{c1}}{dt},\\
k_{d2}x_{d2}=c_{d2}\frac{dx_{c2}}{dt},\\
m_1\frac{d^2x_1}{dt^2}+c_1\frac{d(x_1-x_s)}{dt}+k_1(x_1-x_s)\\
-c_2\frac{d(x_2-x_1)}{dt}-\\
-k_2(x_2-x_1)-Nk_f(x_3-x_1)-NZ=-m_1y^{"}(t),
\end{gathered}
\tag{5}
$$

$$
\begin{gathered}
m_2\frac{d^2x_2}{dt^2}+c_2\frac{d(x_2-x_1)}{dt}+k_2(x_2-x_1)-\\
-c_3\frac{d(x_3-x_2)}{dt}-k_3(x_3-x_2)=-m_2y^{"}(t),\\
m_3\frac{d^2x_3}{dt^2}+c_3\frac{d(x_3-x_2)}{dt}+k_3(x_3-x_2)+\\
+Nk_f(x_3-x_1)+NZ=-m_3y^{"}(t),\\
\frac{dZ}{dt}=\left\{Ak_d-\left[\gamma+\beta sign\left(Z\frac{d(x_3-x_1)}{dt}\right)\right]|Z|^n\right\}\frac{d(x_3-x_1)}{dt},
\end{gathered}
$$

there $k_{d1}$, $k_{d2}$, $c_{d1}$, $c_{d2}$ – stiffness and damping parameters of viscous dampers (4-parameters Maxwell Model);

$x_{d1}$, $x_{d2}$, $x_{c1}$, $x_{c2}$ – viscous damper model element displacements;

$x_s$ – intermediate plate (Ms) displacements.

The solution of eq. (5) is performed automatically in the MathCAD program according to the algorithms described in [6].

## RESULTS AND DISCUSSION

In this paper an analysis of the effect of adding BCS on boiler and frame response is performed (seismic displacements are compared as the main parameters regulated by the norms). The "frame - boiler" system without hysteresis dampers is considered as a basic situation. The first design situation considers the installation of hysteresis dampers only. These situations are analyzed using eq. (4). Next, the BCS parameters are varied (the number of dampers and the stiffness of spring supports). To analyze a system with an additional mounted BSC a model according to eq. (5) is used.

The "frame – N hysteresis dampers – boiler" system described in detail in the dissertation work was chosen as the research object [6]. The main parameters of the object for analytical models are:

– the first natural frequency – $f_1$ = 1.25 Hz;

– the total horizontal stiffness of the suspension system – 2202000 N/m;

– the frame mass – 1053138.1 N·s$^2$/m; the overlap mass – 401355.7 N·s$^2$/m; the frame mass below the level of the mass center of the boiler – 513720.2 N·s$^2$/m; the boiler mass – 921238.4 N·s$^2$/m;

– $m_1$ = 513720.2 N·s$^2$/m, $k_1$ = 95238095 N/m, $c_1$ = 699500 N·s/m;
– $m_2$ = 539417.9 N·s$^2$/m, $k_2$ = 81300812 N/m, $c_2$ = 662200 N·s/m;
– $m_3$ = 921238.4 N·s$^2$/m, $k_3$ = 2202000 N/m, $c_3$ = 142400 N·s/m;
– characteristics of hysteresis dampers: $k_i = 4.24 \cdot 10^6$ N/m, $k_f = 1.27 \cdot 10^5$ N/m, n = 2.0, A = 1.45, $\gamma = \beta = 0.00013$ N$^{-1}$/m;
– hysteresis damper number – 6 pcs (constant value).

3 variants of seismic impact spectrum (fig. 12) with different frequency compositions are considered:
– low-frequency spectrum (Bukharest, 1977) with maximum response below 1 Hz (the zone of the main oscillation frequencies for boilers);
– medium-frequency spectrum (synthesized [6]) with maximum response in the range of 1...2 Hz (characteristic range of the main oscillation frequencies for frames);
– high-frequency spectrum (Valparaiso, 1985) with maximum response in the range of 2...10 Hz (range of higher oscillation frequency forms for frames).

To perform calculations using eq. (4) and eq. (5), accelerograms of impacts were generated in the CVSpec program.

For the analysis, considering significant frame and boiler masses, viscous dampers of large standard size VD 630/325-15 were selected. Damper characteristics are shown in Table 1. In the work, the number of dampers is varied (the range from 2 to 42 pieces is considered).

The mass of the additional base plate is assumed to be no more than 5% of the total mass of the frame and boiler ($M_s$ = 100000 N·s$^2$/m).

The total stiffness of spring supports varies 4 times (10000 kN/m, 20000 kN/m, 40000 kN/m, 60000 kN/m).

Further, all calculated results will be presented in figures, including cases when BCS seismic displacements exceed the acceptable parameter (Table 1). This makes it possible to analyze the effect of the introduction of additional damping on the seismic response of the system. In the tables such results are highlighted in red, and in figures they are indicated by unshaded markers.

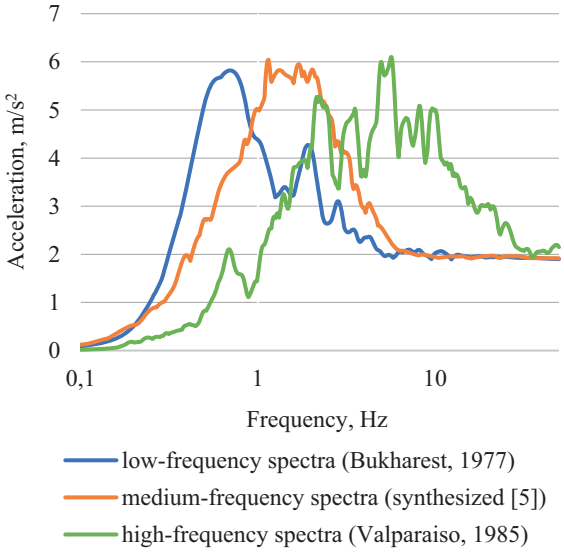


*Figure 12. Seismic impact spectra*

*Table 1. VD 630/325-15 characteristics*

| $K_1$, kN/m | $K_2$, kN/m | $C_1$, rad/sec | $C_2$, rad/sec | Acceptable displacement, mm |
|---|---|---|---|---|
| 8479.9 | 14635.6 | 32.4 | 179.6 | 122 |

The first series of 42 calculations was performed for the low-frequency spectrum. Figure 13 shows the change nature in maximum seismic displacements for boiler (a) and frame overlap (b).

As we can see, the first design situation provides a relatively small (20%) decrease in boiler displacements and a sharp (up to 2 times) increase in frame overlap displacements, which significantly increases the loss probability of its overall stability and stresses in the frame columns. The addition of hysteresis dampers can increase the rigidity of the connections between the boiler and the frame. In the end, this requires consideration of a different system, when the frame and the boiler oscillate together. In this case, the oscillation frequency of the system will decrease significantly, which will lead to operation in the peak zone of the low-frequency spectrum.

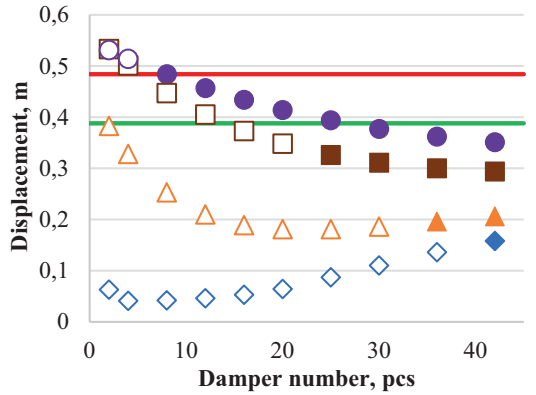


*a) boiler displacement*

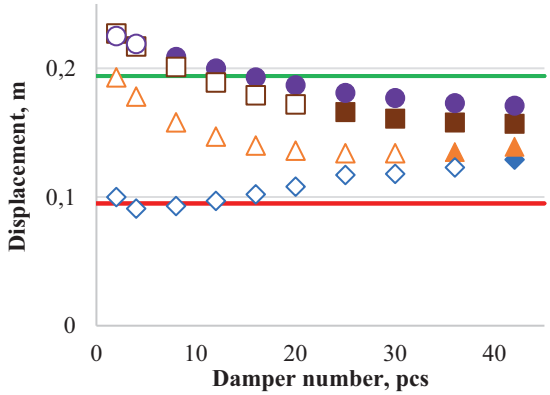


*b) frame overlap displacement*

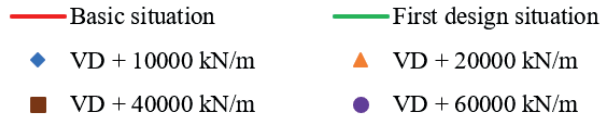


*Figure 13. Results for the low-frequency spectrum (Bukharest, 1977)*

With a low level of rigidity and additional damping of the seismic insulation, it becomes possible to significantly enhance the effect of the seismic insulation of the boiler. Its displacements are reduced many times, providing a technologically safe level. At the same time, the seismic response of the frame remains or slightly exceeds the basic situation level, and the dynamic factor is in the range of 1...1.4. However, this positive effect is achieved due to the possibility of significant movements of the seismic insulation, which in the case of BCS have limitations for both spring supports and viscous dampers. I.e. it is not feasible in practice and it is necessary to consider other means of seismic isolation. Increasing the rigidity of the seismic insulation significantly reduces the positive effects. It is known that BCS causes a decrease in the predominant oscillation frequency of the structure. For boiler frames with the first frequency at the level of 1...2 Hz, this leads to operation in the peak zone of low-frequency spectrum. Accordingly, in almost all cases, there is an increase in the response of the system in comparison with the basic situation.

The second series of 42 calculations was performed for the medium-frequency spectrum. Figure 14 shows the change nature in maximum seismic displacements for boiler (a) and frame overlap (b).

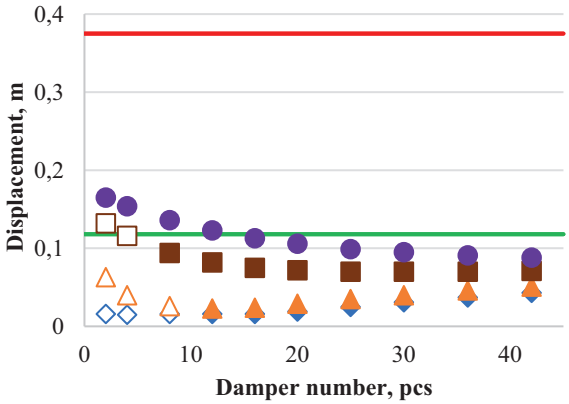


*a) boiler displacement*

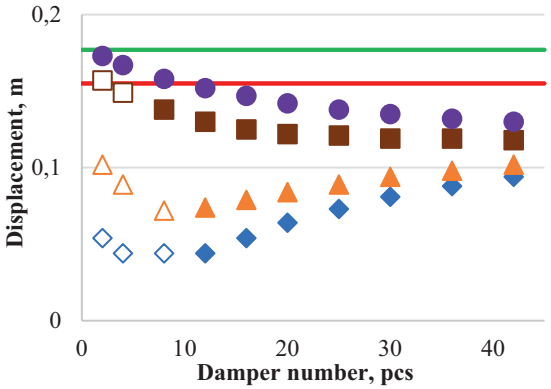


*b) frame overlap displacement*

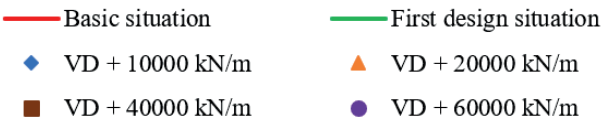


*Figure 14. Results for the medium-frequency spectrum (synthesized [5])*

In almost all cases, BCS shows effectiveness. Reduction in the frame seismic response can reach 70% in comparison with the basic situation. BSC spring elements with low rigidity (up to 20% of rigidity for vertical frame structures below the level of the mass center) ensures maximum effect. For more rigid BSC spring elements, there is a significant decrease in efficiency (with a low level of damping, the dynamic factor is in the range of 1...1.2). This positive effect is logical, since a decrease in the frame predominant oscillation frequency ensures operation in the zone to the left of the peak acceleration values of the spectrum. In addition, BSC spring elements with low rigidity provides an additional reduction in the seismic response of the boiler compared to the first design situation by an amount from 40 to 90%.

With low stiffness of the BCS spring elements, the zone of the optimum number of viscous dampers (additional damping) is clearly visible, after which an increase in their number leads to a tightening of the BCS and a decrease in the positive effect. For cases of high rigidity of BCS spring elements, the optimum is determined by the asymptote. The required optimal number of viscous dampers increases, making this solution both technically and economically impractical.

The third series of 42 calculations was performed for the high-frequency spectrum. Figure 15 shows the change nature in maximum seismic displacements for boiler (a) and frame overlap (b).

For seismic impacts with predominant high frequencies (compared to the system frequency), the seismic isolation effect is maximal in the absence of additional damping or at a relatively low level (combined with low BCS rigidity). As damping and stiffness of BCS increase, seismic insulating effect decreases. With very high damping or significant rigidity, the system acquires signs of a rigid connection between the object and the base, as a result of which a negative effect of amplifying the seismic response of structures is possible. The dynamic factor can reach 1.2...1.8 relative to the basic situation. Adjusting the BCS stiffness has the least effect on the seismic response of the boiler. Basically, the introduction of BSC provides an additional reduction in the seismic response of the boiler.

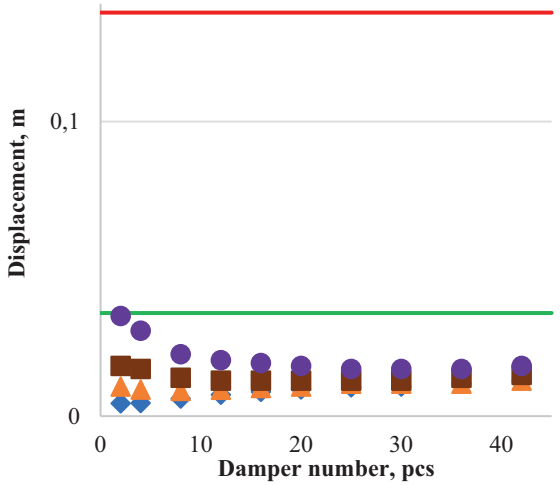


*a) boiler displacement*

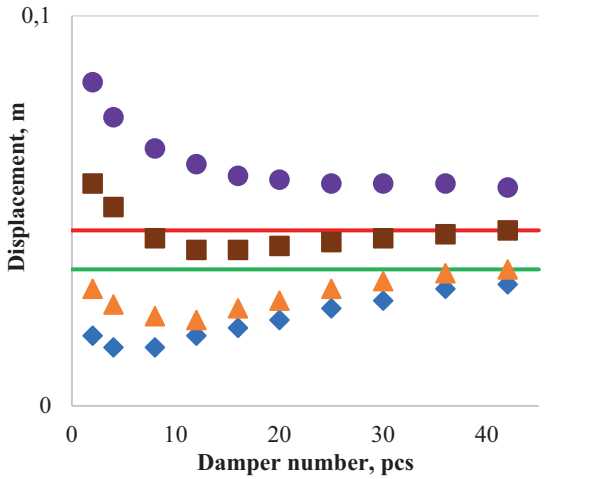


*b) frame overlap displacement*

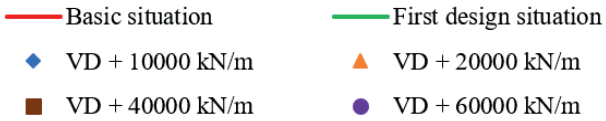


*Figure 15. Results for the high-frequency spectrum (Valparaiso, 1985)*

## CONCLUSION

In this article, a nonlinear analytical model of the "suspended equipment (boiler) – hysteresis dampers – frame – BCS" system is developed. It

allows you to make a preliminary assessment of the effectiveness for developed seismic insulation system to ensure the required level of earthquake resistance of metal frames and boilers suspended from them. This model is implemented by the algorithms of the MathCAD program. It allows optimization analysis by varying parameters (characteristics of hysteresis dampers, types and number of viscous dampers, stiffness of spring supports) to select the most technically and economically reasonable seismic insulation system.

Using BSC for seismic insulation of frames and boilers braced by hysteresis dampers is possible and can have significant positive effects on the seismic response both frame and boiler.

Significant limitations are observed only for low-frequency seismic impacts with peak accelerations up to 1 Hz, which is due to the design features of the "frame-boiler" systems. For such impacts, an additional tightening of the frame can be proposed as a recommendation, which can increase the predominant oscillation frequency.

BSC is most effective for seismic impacts with peak accelerations above 1 Hz. At the same time, there may be both a significant decrease in the frame response and an additional decrease in the boiler response (relative to a system with hysteresis dampers only). This is important because there may be restrictions on the number of hysteresis dampers or their standard sizes, when using only hysteresis dampers does not provide the required response of either the boiler or the frame.

There are optimal combinations of BCS stiffness and damping to maximize seismic response reduction.

## REFERENCES


1. **Fan, F., Zhi, X., Li,W.** (2022) Analysis of the Acceleration Response Spectra of Single-Layer Spherical Reticulated Shell Structures. *Applied Sciences.* 12(4):2116. https:// doi.org/10.3390/app12042116
2. **Chiba, T., Fujita, S.** (2004) Seismic proving test of equipment and structures in thermal conventional power plant. Journal of Japan Association for Earthquake Engineering. Volume 4, Issue 3. pp. 457-464. https://doi.org/10.5610/jaee.4.3_457
3. **Anuschenko, A.M.** (2024). Ensuring Earthquake Resistance of Fossil Power Plants Steel Frames and Steam Boilers. In: Sigaher, A.N., Sutcu, F., Yenidogan, C. (eds) Seismic Isolation, Energy Dissipation and Active Vibration Control of Structures. WCSI 2023. Lecture Notes in Civil Engineering, vol 412. Springer, Cham. https://doi.org/10.1007/978-3-031-71048-3_14
4. **Anushchenko, A.M.** (2023) *Problemy i osobennosti raschetov metallicheskih karkasov podvesnyh kotlov TES na sejsmicheskie vozdejstviya* [Problems and features of calculations of metal frames of suspended boilers of thermal power plants for seismic effects]. Sejsmostojkoe stroitel'stvo. Bezopasnost' sooruzhenij. №6. pp. 53-73.
5. **Muto, K., Shibata, K., Tsugawa, T., Yamada, K.** (1988) Earthquake resistant design of boiler building of thermal power plant. Proceedings of 9 World Conference on Earthquake Engineering. Vol.VI. 10-6-7. P. 855-860.
6. **Anushchenko, A.M.** (2024) *Sejsmostojkost' metallicheskih karkasov podvesnyh parovyh kotlov s uprugoplasticheskimi elementami raskrepleniya* [Earthquake resistance of metal frames of suspended steam boilers with elastoplastic release elements]. Dissertation for the degree of Candidate of Sciences. P. 168.
7. **Anushchenko, A.M.** (2024) *Effektivnye konstruktivnye meropriyatiya i osobennosti inzhenernyh raschetov pri reshenii zadach obespecheniya sejsmostojkosti energeticheskoj infrastruktury na primere kotel'nyh agregatov TEC* [Effective constructive measures and features of engineering calculations in solving the tasks

of ensuring the seismic resistance of energy infrastructure using the example of boiler units of thermal power plants]. Prirodnye i tekhnogennye riski. Bezopasnost' sooruzhenij. 5(72). pp. 40-47.

8. **Kasai, K., Nakai, M., Nakamura, Y., Asai, H., Suzuki, Y., Ishii, M.** (2009) Building Passive Control in Japan. *J. Disaster Res*. Vol.4, No.3, pp. 261-269. https://doi.org/10.20965/jdr.2009.p0261
9. **Nishida, E., Suzuki, K., Yasuda, T., Ohwa, Y.** (1992) Optimum design of connecting elements in complex structures and its application to seismic design of boiler plant structures. *Proceedings of the Earthquake Engineering, Tenth World Conference*. Rotterdam. P.2167-2172. Corpus ID: 173984235
10. **Aida, K, Kawate, K, Hiyoshi, Y, Kawamura, K, Fujita, S.** (2014) Earthquake Load Reduction Effects of Boiler Structures by High Energy Absorbing Seismic Ties. *Proceedings of the ASME 2014 Pressure Vessels and Piping Conference. Volume 8: Seismic Engineering. V008T08A048*. https://doi.org/10.1115/PVP2014-28351
11. **Aida, K., Morikawa, S., Shimono, M., Kato, M., Morishita, K., Amano, T.** (2017) Elasto-Plastic Finite Element Analysis of Long-Lived Seismic Ties for Thermal Power Boiler Structure // *Proceedings of the ASME 2017 Pressure Vessels and Piping Conference*. *Volume 8: Seismic Engineering. V008T08A036*. ASME. https://doi.org/10.1115/PVP2017-65665
12. **Harikrishna, T., Baskar, K.** (2015). Comparative Study on Response of Boiler Supporting Structure Designed Using Structural Steel I-Columns and Concrete Filled Square Steel Tubular Columns. In: Matsagar, V. (eds) Advances in Structural Engineering. Springer, New Delhi. https://doi.org/10.1007/978-81-322-2187-6_161
13. **Saito, T.** (2015) Behavior of response controlled and seismically isolated buildings during severe earthquakes in Japan. Energia, Ambiente e Innovazione. pp. 31-37. DOI 10.12910/EAI2015-078
14. **Belash, T.A., Smirnova, L.N., Bubis, A.A., Zvezdov, A.I.** (2023) *Ob osobennostyah ispol'zovaniya special'nyh sredstv sejsmozashchity dlya povysheniya sejsmostojkosti ekspluatiruemyh sooruzhenij* [On the specifics of using special seismic protection equipment to increase the seismic resistance of operated structures]. Promyshlennoe i grazhdanskoe stroitel'stvo. № 12. pp. 10-16.
15. **Belyaev, V.S., Kostarev, V.V., Vasil'ev, P.S., Kultcep, A.V., Bondarev, D.E.** (2023) *Sovremennye metody sejsmozashchity zdanij, uchityvayushchie prostranstvennyj harakter sejsmicheskogo vozdejstviya* [Modern methods of seismic protection of buildings, taking into account the spatial nature of seismic impact]. Prirodnye i tekhnogennye riski. Bezopasnost' sooruzhenij. 4(65). pp. 38-45.
16. **Kostarev, V., Kultsep, A., Vasilyev, P.** (2024). Analysis, Testing and Application of the 3D BCS Base Control Isolation System with 3D Viscodampers. In: Sadan, B., Tuzun, C., Erdik, M. (eds) Seismic Isolation, Energy Dissipation and Active Vibration Control of Structures. WCSI 2023. Lecture Notes in Civil Engineering, vol 533. Springer, Cham. https://doi.org/10.1007/978-3-031-66888-3_20
17. **Nawrotzki, P., Siepe, D.** (2015) Seismic protection of machinery, buildings and equipment of nuclear power plants by using 3-D base control systems. *Transactions, SMiRT-23*. Manchester, United Kingdom - August 10-14, 2015. Division VI.
18. **Parsi, S.S., Lal, K.M., Kosbab, B.D., Ingersoll, E.D., Shirvan, K., Whittaker, A.S.** (2022) Seismic isolation: A pathway to standardized advanced nuclear reactors // *Nuclear Engineering and Design.* Volume 387. 111445. https://doi.org/10.1016/j.nucengdes.2021.111445

19. **Tarasov, V.A.** (2020) Double Seismic Insulation System of Turbine Unit Foundation. Construction of Unique Buildings and Structures. Volume 91. Article No 9101. DOI: 10.18720/CUBS.91.1
20. **Babskij, A.E., Lalin, V.V., Olejnikov, I.I., Tarasov, V.A.** (2021) *Sejsmostojkost' vibroizolirovannyh fundamentov turboagregatov v zavisimosti ot chastotnogo sostava sejsmicheskogo vozdejstviya* [Seismic resistance of vibration-insulated foundations of turbine units, depending on the frequency composition of the seismic impact]. Stroitel'naya mekhanika inzhenernyh konstrukcij i sooruzhenij. Tom. 17. 1. pp. 30-41.
21. **Charalampakis, A.E.** (2015) The response and dissipated energy of Bouc - Wen hysteretic model revisited. *Arch Appl Mech*. 85. pp. 1209–1223. https://doi.org/10.1007/s00419-014-0937-8
22. **Grimmer, M.** (2017) Analysis of Hysteretic Systems: Preisach Formalism and Bouk-Wen Modeling. A thesis submitted in partial fulfillment of the requirements for the degree Master of Science. Texas. 91 p.
23. **Wen, Y.K.** (1976) Method of random vibration of hysteretic systems. ASCE J. Eng. Mech. 102(2). pp. 249-263.
24. **Boccamazzo, A., Carboni, B., Quaranta, G., Lacarbonara, W.** (2020). Optimization Strategies of Hysteretic Tuned Mass Dampers for Seismic Control. In: Lacarbonara, W., Balachandran, B., Ma, J., Tenreiro Machado, J., Stepan, G. (eds) Nonlinear Dynamics and Control. Springer, Cham. https://doi.org/10.1007/978-3-030-34747-5_10
25. **Maldonado, G.O., Singh, M.P., Casciati, F., Faravelli, L.** (1987) Stochastic response of single degree of freedom hysteretic oscillators. Technical Report of Research Supported by The National Science Foundation Under Grant Number CEE-8412830. Department of Engineering Science and Mechanics Virginia Polytechnic Institute and State University Blacksburg. VA 24061. 85 p.
26. **Noori, M.** (1984) Random Vibration of Degrading Systems with General Hysteretic Behavior: Doctoral dissertation. University of Virginia. 206 p.
27. **Aida, K., Kawamura, K., Maruyama, N., Suzuki, K., Fujita, S., Chiba, T.** (2000) Proving Tests of Energy Absorbing Seismic Ties for Aseismic Design of Boiler Plant Structures. 12th World Conference on Earthquake Engineering. New Zealand. Paper No. 2588.
28. **Chen, B.G., Wu. J.** (1999) Transfer-Function-Based Criteria for Decoupling of Secondary Systems. Journal of engineering mechanics. Vol. 125. Issue 3. pp. 340-346. https://doi.org/10.1061/(ASCE)0733-9399(1999)125:3(340)
29. **Chaudhuri, S.R., Gupta, V.K.** (2002) A response-based decoupling criterion for multiply-supported secondary systems. Earthquake engineering and structural dynamics. 31. pp. 1541–1562. https://doi.org/10.1002/eqe.175
30. **Fouquiau, P.-V., Frederic, B., Chatzigogos, C.T.** (2018). New dynamic decoupling criteria for secondary systems // Proceedings of 16th European Conference on Earthquake Engineering.
31. **Kostarev, V.V., Petrenko, A.V., Vasilyev, P.S., Reinsch, K.-H.** (2005) Adaptation of high viscous dampers (HVD) for essential decreasing of in-structure floor response spectra. Proceedings of SMiRT18-K11-6. pp. 3423-3434. https://api.semanticscholar.org/CorpusID:55256766
32. **Tamura, I., Kuramasu, M., Barutzki, F., Fischer, D., Kostarev, V., Berkovskiy, A., Vasiliev, P., Inoue, T., Okita, S., Namita, Y.** (2016) Dynamic Analysis of NPP Piping Systems and Components With Viscoelastic Dampers Subjected to Severe Earthquake Motions. Proceedings of the ASME 2016 Pressure Vessels and Piping

Conference. Volume 8: Seismic Engineering. Vancouver, British Columbia, Canada. July 17–21, 2016. V008T08A022. ASME. https://doi.org/10.1115/PVP2016-64029
33. **Technical specifications TU 4192-001-20503039-01** (2011) Viscoelastic dampers of the VD series. Technical specifications. CKTI-VIBROSEISM Co. Ltd. Saint-Petersburg.
34. **Bondarev, D.E.** (2023) Stenovoj dempfer «WD CVS» kak effektivnoe sredstvo povysheniya sejsmostojkosti karkasnyh metallicheskih zdanij [Wall damper "WD CVS" as an effective means of increasing the seismic resistance of framed metal buildings]. Sejsmostojkoe stroitel'stvo. Bezopasnost' sooruzhenij. №5. pp.74-90.

## СПИСОК ЛИТЕРАТУРЫ

1. **Fan, F., Zhi, X., Li,W.** Analysis of the Acceleration Response Spectra of Single-Layer Spherical Reticulated Shell Structures // *Applied Sciences*. 2022. 12(4):2116. https:// doi.org/10.3390/app12042116
2. **Chiba, T., Fujita, S.** Seismic proving test of equipment and structures in thermal conventional power plant // Journal of Japan Association for Earthquake Engineering. 2004. Volume 4, Issue 3. pp. 457-464. https://doi.org/10.5610/jaee.4.3_457
3. **Anuschenko, A.M.** (2024). Ensuring Earthquake Resistance of Fossil Power Plants Steel Frames and Steam Boilers. In: Sigaher, A.N., Sutcu, F., Yenidogan, C. (eds) Seismic Isolation, Energy Dissipation and Active Vibration Control of Structures. WCSI 2023. Lecture Notes in Civil Engineering, vol 412. Springer, Cham. https://doi.org/10.1007/978-3-031-71048-3_14
4. **Анущенко, А.М.** Проблемы и особенности расчетов металлических каркасов подвесных котлов ТЭС на сейсмические воздействия // Сейсмостойкое строительство. Безопасность сооружений. 2023. 6. С. 53-73.
5. **Muto, K., Shibata, K., Tsugawa, T., Yamada, K.** Earthquake resistant design of boiler building of thermal power plant. Proceedings of 9 World Conference on Earthquake Engineering. 1988. Vol.VI. 10-6-7. P. 855-860.
6. **Анущенко, А.М.** Сейсмостойкость металлических каркасов подвесных паровых котлов с упругопластическими элементами раскрепления : дисс. … канд. тех. наук : 2.1.1 / Анущенко Александр Михайлович. – СПб., 2024. – 168 с.
7. **Анущенко, А.М.** Эффективные конструктивные мероприятия и особенности инженерных расчетов при решении задач обеспечения сейсмостойкости энергетической инфраструктуры на примере котельных агрегатов ТЭЦ. Природные и техногенные риски. Безопасность сооружений. 2024. 5(72). С. 40-47.
8. **Kasai, K., Nakai, M., Nakamura, Y., Asai, H., Suzuki, Y., Ishii, M.** Building Passive Control in Japan // *J. Disaster Res*. 2009. Vol.4, No.3, pp. 261-269. https://doi.org/10.20965/jdr.2009.p0261
9. **Nishida, E., Suzuki, K., Yasuda, T., Ohwa, Y.** Optimum design of connecting elements in complex structures and its application to seismic design of boiler plant structures // *Proceedings of the Earthquake Engineering, Tenth World Conference*. Rotterdam. 1992. P.2167-2172. Corpus ID: 173984235
10. **Aida, K, Kawate, K, Hiyoshi, Y, Kawamura, K, Fujita, S.** (2014) Earthquake Load Reduction Effects of Boiler Structures by High Energy Absorbing Seismic Ties // *Proceedings of the ASME 2014 Pressure Vessels and Piping Conference. Volume 8: Seismic Engineering. V008T08A048*. https://doi.org/10.1115/PVP2014-28351
11. **Aida, K., Morikawa, S., Shimono, M., Kato, M., Morishita, K., Amano, T.**

(2017) Elasto-Plastic Finite Element Analysis of Long-Lived Seismic Ties for Thermal Power Boiler Structure // *Proceedings of the ASME 2017 Pressure Vessels and Piping Conference*. *Volume 8: Seismic Engineering*. *V008T08A036*. ASME. https://doi.org/10.1115/PVP2017-65665

12. **Harikrishna, T., Baskar, K.** (2015). Comparative Study on Response of Boiler Supporting Structure Designed Using Structural Steel I-Columns and Concrete Filled Square Steel Tubular Columns. In: Matsagar, V. (eds) Advances in Structural Engineering. Springer, New Delhi. https://doi.org/10.1007/978-81-322-2187-6_161
13. **Saito, T.** Behavior of response controlled and seismically isolated buildings during severe earthquakes in Japan // Energia, Ambiente e Innovazione. 2015. 5. P. 31-37. DOI 10.12910/EAI2015-078
14. **Белаш, Т.А., Смирнова, Л.Н., Бубис, А.А., Звездов, А.И.** Об особенностях использования специальных средств сейсмозащиты для повышения сейсмостойкости эксплуатируемых сооружений // Промышленное и гражданское строительство. 2023. № 12. С. 10-16.
15. **Беляев, В.С., Костарев, В.В., Васильев, П.С., Кульцеп, А.В., Бондарев, Д.Е.** Современные методы сейсмозащиты зданий, учитывающие пространственный характер сейсмического воздействия // Природные и техногенные риски. Безопасность сооружений. 2023. 4(65). С. 38-45.
16. **Kostarev, V., Kultsep, A., Vasilyev, P.** (2024). Analysis, Testing and Application of the 3D BCS Base Control Isolation System with 3D Viscodampers. In: Sadan, B., Tuzun, C., Erdik, M. (eds) Seismic Isolation, Energy Dissipation and Active Vibration Control of Structures. WCSI 2023. Lecture Notes in Civil Engineering, vol 533. Springer, Cham. https://doi.org/10.1007/978-3-031-66888-3_20
17. **Nawrotzki, P., Siepe, D.** Seismic protection of machinery, buildings and equipment of nuclear power plants by using 3-D base control systems // *Transactions, SMiRT-23*. Manchester, United Kingdom - August 10-14, 2015. Division VI.
18. **Parsi, S.S., Lal, K.M., Kosbab, B.D., Ingersoll, E.D., Shirvan, K., Whittaker, A.S.** Seismic isolation: A pathway to standardized advanced nuclear reactors // *Nuclear Engineering and Design.* 2022. Volume 387. 111445. https://doi.org/10.1016/j.nucengdes.2021.111445
19. **Tarasov, V.A.** Double Seismic Insulation System of Turbine Unit Foundation // Construction of Unique Buildings and Structures. 2020. Volume 91. Article No 9101. DOI: 10.18720/CUBS.91.1
20. **Бабский, А.Е., Лалин, В.В., Олейников, И.И., Тарасов, В.А.** Сейсмостойкость виброизолированных фундаментов турбоагрегатов в зависимости от частотного состава сейсмического воздействия // Строительная механика инженерных конструкций и сооружений. 2021. Том 17. 1. С. 30-41.
21. **Charalampakis, A.E.** The response and dissipated energy of Bouc - Wen hysteretic model revisited. *Arch Appl Mech*. 2015. 85. P. 1209–1223. https://doi.org/10.1007/s00419-014-0937-8
22. **Grimmer, M.** Analysis of Hysteretic Systems: Preisach Formalism and Bouk-Wen Modeling. A thesis submitted in partial fulfillment of the requirements for the degree Master of Science. Texas. 2017. 91 p.
23. **Wen, Y.K.** Method of random vibration of hysteretic systems // ASCE J. Eng. Mech. 102(2). 1976. pp. 249-263.
24. **Boccamazzo, A., Carboni, B., Quaranta, G., Lacarbonara, W.** (2020). Optimization Strategies of Hysteretic Tuned Mass Dampers for Seismic Control. In: Lacarbonara, W., Balachandran, B., Ma, J., Tenreiro Machado, J., Stepan, G. (eds)

Nonlinear Dynamics and Control. Springer, Cham. https://doi.org/10.1007/978-3-030-34747-5_10

25. **Maldonado, G.O., Singh, M.P., Casciati, F., Faravelli, L.** Stochastic response of single degree of freedom hysteretic oscillators. Technical Report of Research Supported by The National Science Foundation Under Grant Number CEE-8412830. Department of Engineering Science and Mechanics Virginia Polytechnic Institute and State University Blacksburg. VA 24061. 1987. 85 p.
26. **Noori, M.** Random Vibration of Degrading Systems with General Hysteretic Behavior: Doctoral dissertation. University of Virginia. 1984. 206 p.
27. **Aida, K., Kawamura, K., Maruyama, N., Suzuki, K., Fujita, S., Chiba, T.** Proving Tests of Energy Absorbing Seismic Ties for Aseismic Design of Boiler Plant Structures. 12th World Conference on Earthquake Engineering. New Zealand. Paper No. 2588. 2000.
28. **Chen, B.G., Wu. J.** Transfer-Function-Based Criteria for Decoupling of Secondary Systems // Journal of engineering mechanics, 1999. Vol. 125. Issue 3. PP. 340-346. https://doi.org/10.1061/(ASCE)0733-9399(1999)125:3(340)
29. **Chaudhuri, S.R., Gupta, V.K.** A response-based decoupling criterion for multiply-supported secondary systems // earthquake engineering and structural dynamics. 2002; 31. pp. 1541–1562. https://doi.org/10.1002/eqe.175
30. **Fouquiau, P.-V., Frederic, B., Chatzigogos, C.T.** (2018). New dynamic decoupling criteria for secondary systems // Proceedings of 16th European Conference on Earthquake Engineering, 2018.
31. **Kostarev, V.V., Petrenko, A.V., Vasilyev, P.S., Reinsch, K.-H.** Adaptation of high viscous dampers (HVD) for essential decreasing of in-structure floor response spectra. Proceedings of SMiRT18-K11-6. 2005. P. 3423-3434. https://api.semanticscholar.org/CorpusID:55256766
32. **Tamura, I., Kuramasu, M., Barutzki, F., Fischer, D., Kostarev, V., Berkovskiy, A., Vasiliev, P., Inoue, T., Okita, S., Namita, Y.** Dynamic Analysis of NPP Piping Systems and Components With Viscoelastic Dampers Subjected to Severe Earthquake Motions. Proceedings of the ASME 2016 Pressure Vessels and Piping Conference. Volume 8: Seismic Engineering. Vancouver, British Columbia, Canada. July 17–21, 2016. V008T08A022. ASME. https://doi.org/10.1115/PVP2016-64029
33. **ТУ 4192-001-20503039-01** Вязкоупругие демпферы серии ВД. Технические условия. ООО «ЦКТИ-ВИБРОСЕЙСМ». Санкт-Петербург. 2011.
34. **Бондарев, Д.Е.** Стеновой демпфер «WD CVS» как эффективное средство повышения сейсмостойкости каркасных металлических зданий // Сейсмостойкое строительство. Безопасность сооружений. 2023. 5. С.74-90.

*Aleksandr Mikhailovich Anushchenko* — PhD in Engineering, Lead Engineer, CKTI-VIBROSEISM Co. Ltd., 9, Gzhatskaya str., Saint-Petersburg, 195220, Russia, AAnushchenko@cvs.spb.su

*Александр Михайлович Анущенко* — кандидат технических наук, ведущий инженер, Общество с ограниченной ответственностью «ЦКТИ-ВИБРОСЕЙСМ» (ООО «ЦВС»), 9, Гжатская ул., г. Санкт-Петербург, 195220, Россия, AAnushchenko@cvs.spb.su

DOI:10.22337/2587-9618-2025-21-3-121-134

# RESISTANCE OF STEEL FRAMES WITH RIGID AND HINGED JOINTS TO PROGRESSIVE COLLAPSE

***Anatoly V. Alekseytsev, Valentina M. Tusnina***

National Research Moscow State University of Civil Engineering, Moscow, RUSSIA

**Abstract.** This paper addresses a significant and current issue in the field of improving the mechanical safety of buildings and structures with metal frames subjected to specific types of impact. Based on experimental tests and numerical verification, it studies the behavior of a steel frame in an emergency. The rapid removal of the central column was considered as an example of such an accidental action. To increase the frame's resistance to progressive collapse, the structure incorporates tie rods, which redistribute additional loads. Two types of frames were considered: those with hinged beam-column connections and those with similar rigid units. The experiments revealed the nature of the change in strains over time under dynamic loading and determined the characteristics of vibrational processes for frames with different joint designs. The role of tie rods in stabilizing frames against progressive collapse was determined. The displacement variation over time was also determined. The approach to modelling the accident situation was found to be in satisfactory agreement with experimental data. It was established that frames with hinged joints have a lower load-bearing capacity at the joint connections than frames with rigid joints. However, they have a predictable failure mechanism and a shorter transient dynamic process duration following an accident impact.

**Keywords:** dynamics, steel frames, progressive collapse, deformations, damping, mechanical safety, robustness, accidental action

# ОЦЕНКА СОПРОТИВЛЕНИЯ ПРОГРЕССИРУЮЩЕМУ РАЗРУШЕНИЮ СТАЛЬНЫХ РАМ С ШАРНИРНЫМИ И ЖЕСТКИМИ СОЕДИНЕНИЯМИ ЭЛЕМЕНТОВ

***А.В. Алексейцев, В.М. Туснина***

Национальный исследовательский Московский государственный строительный университет, г. Москва, РОССИЯ

**Аннотация.** В работе рассматривается важный и актуальный в настоящее время аспект повышения механической безопасности зданий и сооружений с металлическими рамными каркасами при особых воздействиях. На основе экспериментальных испытаний и численной верификации изучено поведение стальной рамы при аварийном воздействии. В качестве такого аварийного действия рассматривалось быстрое удаление средней стойки из расчетной схемы. Для повышения устойчивости к прогрессирующему разрушению рамы в ее схему были включены страховочные элементы в виде тяжей, перераспределяющих дополнительные нагрузки от аварийного динамического нагружения. Рассматривалось два типа рам: с шарнирными соединениями балки и колонны, а также с аналогичными жесткими узлами. В результате экспериментов выявлен характер изменения продольных деформаций во времени при динамическом нагружении, определены характеристики колебательных процессов для рам с различными конструктивными исполнениями узлов. Определена роль тяжей в обеспечении устойчивости рам к прогрессирующему разрушению. Установлен характер изменения перемещений во времени. Достигнуто удовлетворительное соответствие экспериментальным данным подхода к моделированию аварийной ситуации. Установлено, что рама с шарнирными узлами обладает более низкой несущей способностью по узловым соединениям по сравнению с жесткими узлами, однако имеет прогнозируемый механизм разрушения и меньшую длительность переходного динамического процесса аварийного воздействия.

**Ключевые слова:** динамика, стальная рама, прогрессирующее разрушение, деформации, демпфирование, механическая безопасность, живучесть, аварийное воздействие

## 1. INTRODUCTION

Mechanical safety of buildings under accidental actions is one of the main chalanges in construction science. A significant number of studies addressing this issue makes it possible to identify one of the urgent tasks of increasing the resistance of buildings to progressive collapse. This is the incorporation into the design scheme of additional structural elements, which are sometimes called safety elements. Such elements, e.g., struts, ties, prestressed ropes, rods with adjustable stress, diaphragms, wall fillings, suspenders, etc. redistribute loads, participate in the perception of dynamic loading and significantly increase the robustness of buildings and structures under accidental actions.

For industrial facilities, the robustness enhancement aspect is discussed in [1]. Based on the analysis of the stress-strain state of the structures of the existing reconstructed facility, possible accidental situations are related both to the structural features of the building and to the specifics of the technological process carried out in the considered metallurgical facility.

The concept of collapse resistance design of a steel framed system with members in which internal forces are controlled is outlined in [2]. These members are designed considering the range of forces that may appear during progressive collapse. Their presence allows to regulate the area of the structural system in which the failure of structural elements occurs.

The paper [3] presents the results of the study of robustness of damaged steel trusses, as well as the release time during which local failure occurs. Based on experimental and theoretical studies, the influence of local failure on load-bearing structures as a whole is studied. Numerical analysis shows that the shorter the failure time of a truss member, the greater the dynamic forces arising in the structure. Based on the obtained results, the failure time of the damaged rod and the redistribution of forces on the neighboring members of the truss have been calculated.

Study [4] has been dedicated to the investigation of the collapse resistance of steel frames with prestressed tie rods. The authors developed a macromodel of a typical connection for static nonlinear analysis of structural performance using finite element modeling with OpenSees. The model was validated against experimental data and applied to a six-story framed building. The scenarios of extreme and mid-column removal at the first floor have been considered. The results of the analysis showed that the steel braced frame has a fairly high resistance to collapse. The structure did not collapse if the middle column failed, and the probability of collapse if the outermost column failed was 2%.

The work [5] deals with the study of the relationship between the dynamic coefficient and the collapse resistance of a structure under the column removal scenario. It was found that the influence of medium and high strain rates on the ultimate displacement of structures under column removal can be ignored. It confirmed that the static FEM analysis of structures under column removal can be used to determine the ultimate limit state of the structure under medium and high strain rates.

The paper [6] considers an approach to the calculation of steel framed structures taking into account structural nonlinearity, including the removal of supports, accidental impacts, etc. This approach is based on the direct method of integration balanced by static equivalents of reactions.

The paper [7] analyzes the performance of the steel frame during the removal of the inner column and determines the critical deformations at collapse. The analysis was performed using finite element modeling employing the ABAQUS program. It considered the influence of beam span and height, thickness and side ratio of the floor slab of the building on the magnitude of these deformations due to the removal of the internal column of the considered steel frame of the building. Comparison of deformations of steel frame showed that the presence of floor slab significantly reduces the magnitude of deformations. At the same time, increasing the side ratio of the floor slab from 1:1 to 1:2 increases their magnitude by 20%.

The finite element analysis as pointed out in [8] is a general approach to perform nonlinear dynamic analysis of steel frame collapse with semi-rigid joints. The numerical results showed that the real performance of the assemblies has a significant effect on the dynamic reactions and subsequently on the failure process of the framed structures. It was marked that the failure of members and their joints, as well as the nonlinearities of material and joint behavior, should be accounted for in the analysis of structural failure. It was found that at the ends of beams in rigid and linear semi-rigid frames only element failures have been observed, while in nonlinear semi-rigid frame only joint failure has been identified.

The paper [9] presents a method for quantitative assessment of dynamic effects on a steel frame structure as a result of instantaneous removal of an internal column. This method allows us to calculate the value of the dynamic factor at the moment of reaching the limit state of structural failure and to predict its deformations under such a scenario. Similar to [7], a comprehensive parametric analysis was carried out in [9] to study the influence of various structural parameters such as beam span and depth, slab thickness and side ratio on the dynamic factor, including at the moment of structural collapse.

The paper [10] presents the results of experimental and theoretical studies of steel frames with reinforced concrete slab against progressive collapse. Finite element modeling of the structure was verified according test data for joints. The developed models were verified by the results of displacement tests, forces in the members. The failure regimes were established. Particular attention was paid to the development of resistance mechanisms of the floor slabs and the influence of beam-column assembly types on the behavior of the structure. In addition, the influence of the spacer system in the structure on the resistance to progressive collapse was investigated.

The results of the study of a modular steel structure are presented in [11]. Based on experimental data and numerical simulation, the failure mechanisms and force redistribution were studied for a four-story, nine-span modular steel structure under different failure scenarios. It was emphasized that the redistribution of forces occurs only within the span of the failed member or block and has little effect on the other part of the structure.

A comprehensive analysis of the influence parameters on the failure mechanism and failure resistance action of a typical bolted beam-to-column connection on angles in steel frames subjected to fire is given in [12]. The results of numerical analysis showed that all steel frame structures with different types of beam-to-column connections exhibits the arch action after the heating phase due to the thermal expansion of the beams. Based on the results, a theoretical method was proposed to predict the failure mechanism of steel frames with bolted beam-to-column connections subjected to fire under progressive collapse conditions.

The paper [13] investigates the influence of dynamics in progressive collapse by analyzing the dynamic factor for steel structures considering the increase in the number of floors. A numerical algorithm including static and dynamic analysis was proposed. This algorithm is applied to evaluate five framed structures with seismic design. An accurate finite element model was developed, taking into account imperfections and geometric nonlinearity, using the OpenSees software.

In order to increase the resistance to progressive collapse of steel frames, the authors of [14] have developed and investigated the beam-column interface, strengthened with a folding plate welded to the inner side of the I-beam flange and to the column. The load-carrying capacity of such a connection for progressive collapse was evaluated based on the results of tests and numerical analysis using the ABAQUS program. A comparative analysis of the performance of two types of assemblies: standard and reinforced with welded plates showed that the load-bearing capacity of the plate- strengthened specimen is 21.1% higher, indicating that such assemblies have the ability to increase the resistance to failure of steel framed structures.

The paper [15] presents the results of experimental and numerical analysis of the

mechanism of progressive collapse of a steel frame with beam-column connections made of L-profiles. According to the results of the research, the deformations of the connecting elements allow a better assessment of the process of failure and deformation of structures during the progressive collapse of the frame, as well as the performance mechanism of the damaged frame and the redistribution of forces between the load-bearing structures occurring at damage.

In [16], the effect of vertical ties on the load-bearing capacity of steel frames under progressive collapse was investigated. The test results showed that ties can increase the ultimate load-bearing capacity of frames by 102.3%.

The study [17] of steel frames with masonry infilling walls in the plane of the frames with smaller beam cross-sections demonstrate an increase in the load-bearing capacity of such structures compared to frames without such infilling. The supporting effect of the double strut that is formed inside the infilled diaphragm wall during the collapse phase, steel frame structures with infilled walls better resist to large displacements in accidental design situation than the corresponding frames without infilling.

The article [18] presents the results of static and dynamic tests of frames with bolted beam-column assemblies equipped with additional structural details to prevent progressive collapse. The results of tests of such assemblies showed that their load-bearing capacity is ensured even at rotations of the beam support part of more than 0.2 rad.

The paper [19] is dedicated to experimental and theoretical studies of beam-column assemblies of steel frames with lightweight frame-clad walls for progressive collapse at the removal of the inner column. Based on parametric analysis, the influence of key design variables on the resistance to progressive collapse of the structure was examined. The results emphasize that the influence contributed by the wall cladding of the frame on the load carrying capacity of the steel frame is significant.

The objective of this study is to investigate the load-bearing capacity of a steel frame with tie rods against progressive collapse.

## 2. METHODS

***2.1 General provisions.*** As part of the problem statement, the resistance to progressive collapse of an experimental specimen of a framed structure with rigid and hinge joints of beams and columns and safety suspender elements was investigated experimentally. The purpose of the research was to identify the deformation regimes of the frame and determine the characteristics of its stress-strain state (STS). The initiation of progressive collapse was performed by removing the middle column. The release time was assumed to be small. Physically the removal was performed by horizontal impact. The experimental results were used to verify the accuracy of modeling the progressive collapse of steel frames.

***2.2 Experimental designs and experimental plan.*** The specimens are frames whose beams and columns consist of 10B I-beams (GOST 26020-83) (Figure 1). Two variants of joints were considered. In the first variant the joints of beams with columns at supports and between each other in the spans were rigid, and in the second variant it was hinged. The connection of the columns to the power floor was rigid in all cases. To ensure that the frame deformed predominantly in its plane, a structure including additional columns and beams was used. Beams made of 51x3 round pipes (GOST 10704-91) connected the outermost joints of the frame to the force floor.

The frame was loaded with concrete blocks fastened to the beams by a steel cage consisting of plates tightened with studs. The mass of each of the blocks was 195 kg. The models and types of assemblies in rigid and hinged versions are shown in Figure 2. The general view of the experimental specimens is shown in Figure 3.

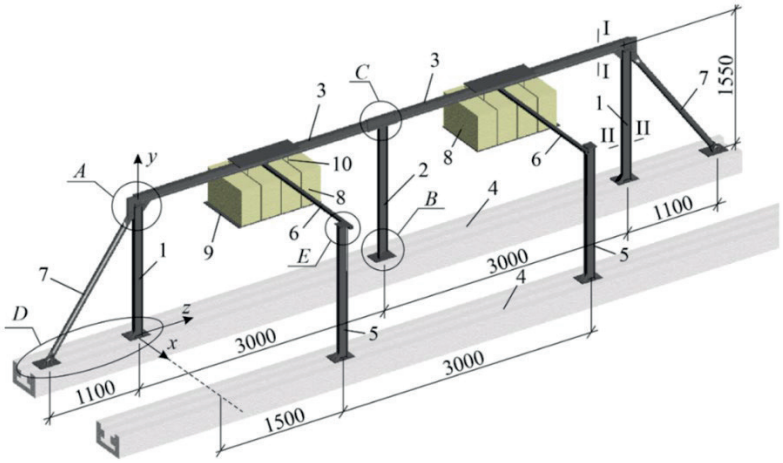


*Figure 1. Specimen of the framed structure with rigid joints: 1 - end columns, 2 - middle (removable) column, 3 - beams, 4 - power floor, 5 - additional columns, 6 - beams, 7 - tie rods, 8 - load blocks, 9 - support plates, 10 - studs; A-E marking of joints; I-I, II-II - cross-sections for measuring values of stress-strain state*

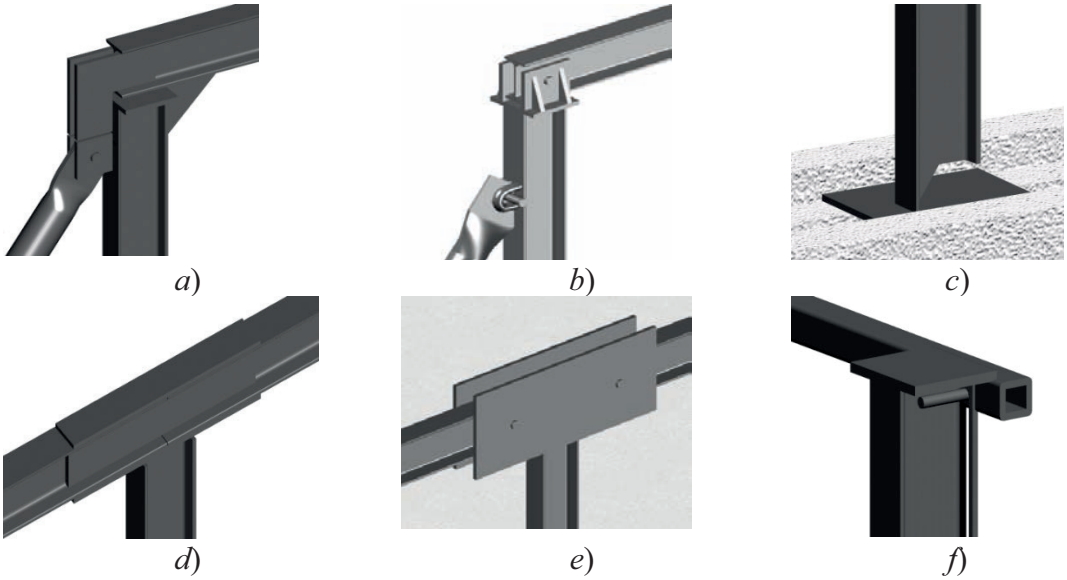

*a*) *b*) *c*)

*d*) *e*) *f*)

*Figure 2. Joints of the experimental frames (labeled in Figure 1): (a) joint A; (b) hinged joint A; (c) hinged jointB; (d ) hinged jointC; (e) hinged joint C; (f) hinged joint D*


*a*) *b*)

*Figure 3. General view of experimental specimens: (a) with rigid assemblies; (b) with hinged assemblies (showing the erecting supports used before installing the middle column)*

The experimental investigations were planned according to the following scenario. For a frame structure with rigid and hinged joints, 3 loading stages were performed. In the first stage, one load was placed in each span of the frame. In the second stage, one more load was added and in the third stage yet another load was added. At each of the stages, the middle column RC was removed using a rod striker T (Figure 3, a). During the removal, the displacements and deformations of the frame were measured. Here, the tie rods are safety elements that increase the robustness of the frame at an accidental action. If the removal of the column resulted in plastic deformations, the frame specimen was replaced with a new one for the subsequent test. The recorded displacements and deformations were compared with each other and with the simulation results.

***2.3. Displacement and deformation measurement in time.*** KF 5P1-3-200B12 strain gauges were glued for the beam and column in the cross sections shown in Figure 1 and Figure 4. Cold-curing cyanoacrylate was used for gluing. There were measured longitudinal strains in the beam and column flanges. To transfer data to the computer, an analog-to-digital converter LTR-212 with a sampling frequency of up to 3kHz was used. The frequency of 1.5 kHz was considered as sufficient for the experiment. An electronic recorder Lgraph was used for plotting deformation histories. Linear displacements of the frame beam in the vertical direction were measured at point D (Figure 4).

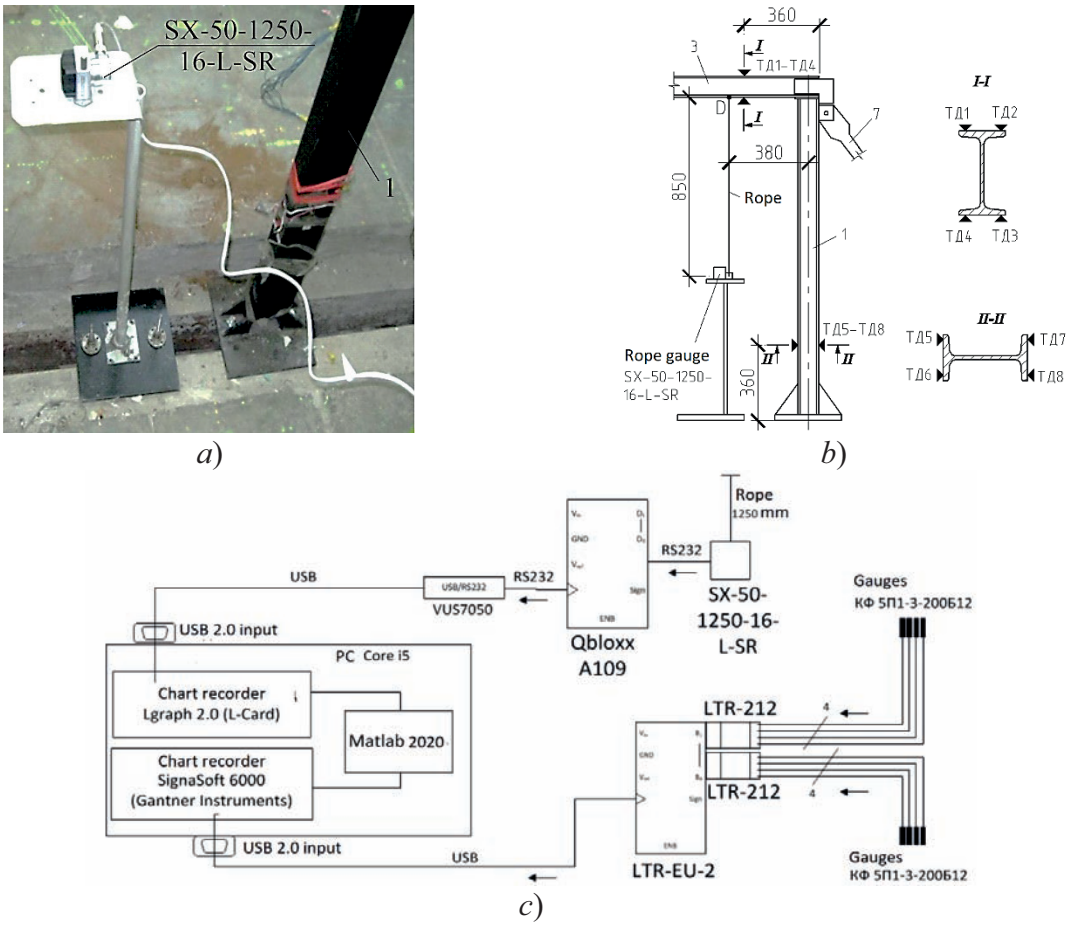


*Figure 4. Measurement of stresses and strains in time: general view of the rope gauge (a), diagram of installation of the rope gauge and strain gauges (b); 1 - column, 3 - beam, 7 -rod; schematic diagram of data acquisition and processing in the experiment (c)*

After stabilization of the system subjected to an accidental impact, the displacements of other points were measured with a laser rangefinder. The data obtained during the tests had to be cleaned from noise. For this purpose the data were exported to MATLAB software, where the values of strains and displacements were subjected to one-dimensional Meyer wavelet transformation by polynomials of 6 and 7 orders. The general scheme of information processing is shown in Figure 4, c.

***2.4 Preparation for the experiment.*** Before the dynamic tests, the properties of the steel of the frame I-beams were determined experimentally. Plane specimens were cut from the I-beam wall and tested for uniaxial tension in compliance with the standard methodology. As a result of statistical processing of the data it was found that the I-beams were made of steel with physical yield strength of $349 \pm 13$ *MPa* and ultimate tensile strength of $522 \pm 15$ *MPa*. Strain of the specimens corresponding to the yield strength was, and corresponding to the tensile strength was $0,0018 \pm 0,0002$ , and the strain of the specimens corresponding to the tensile strength was $0,233 \pm 0,026$.

***2.5 Numerical analysis.*** The frame was calculated using the finite element method in a physically, geometrically, and structurally nonlinear formulation based on the stepwise direct integration method described in [6, 20]. The peculiarity of this method is that the tangent coefficients of the general stiffness matrix are constructed at each step of time integration for the deformed state of the system. In this case, the associated law of flow theory is used to determine the values of elastic and shear moduli. At the same time, to estimate the strength, the dynamic yield strength $\sigma_m^d$, determined by reference data as $\sigma_m^d = 1,1 \cdot \omega^{1/17} \cdot \sigma_m$, where $\omega$ is the frequency of the lowest tone of vibration, $\sigma_m$ is the yield strength obtained in static tensile tests, is introduced into the calculation. The calculation diagram of material performance was taken as a linear approximation of the actual steel deformation diagram obtained experimentally

## 3. RESULTS AND DISCUSSION

***3.1 Deformation measurement.*** The results of the experimental tests of rigid and hinged frames and the evaluation of their robustness are shown in Table 1. Figure 5 shows the resulting state of the experimental specimens..

*Table 1. Estimation of the resistance of frames to progressive collapse at the removal of the middle column*

| Rigid connection of elements, loading stage, result | | Hinge connection of elements loading stage, result | |
|---|---|---|---|
| I | The robustness is assured | I | The robustness is assured |
| II | The robustness is assured | II | Failure (tie rod and frame connection) |
| III | The robustness is assured | III | Failure (tie rod support assembly) |

Plots of strain histories for the frame with hinged beam-column joints according to the strain gauge arrangement (Figure 4, b) are shown in Figure 6, a-d. Similar plots for the frame with rigid joints are shown in Figure 6, e-h. To compare the deformation patterns of the frame correctly, only the first stage of loading was considered, at which the robustness is ensured for both frames.

*a*) *b*)

*Figure 5. Experimental specimens after testing: frame with hinge assemblies at loading stage II (a); frame with rigid assemblies at loading stage III (b)*

The displacement histiries for the first stage of loading is shown in Figure 7.

Analysis of the data presented in Table 1 and Figure 6 allows us to draw conclusions:

- The frame specimens with hinged joints failed at the loading level corresponding to 33.3 % of the planned one in the experiment, equal to 1170 kg, at which the frame with rigid joints has the property of robustness. This result is observed in the presence of safety suspender elements. Preliminary calculations have shown that without the presence of safety elements at hinge joints, both the experimental specimen and any other frame of the building at the initiation of the accident associated with the removal of the middle column does not have the property of robustness. This means that the local failure propagates to a complete collapse;

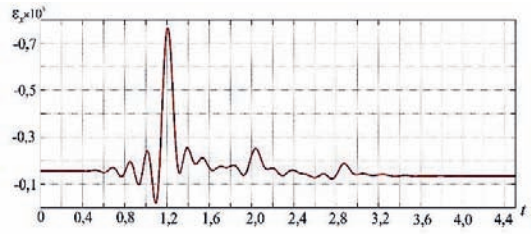

*a) readings of strain gauge SG 1*

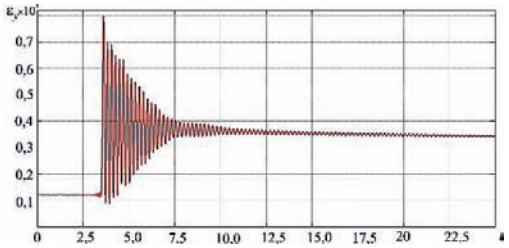

*e) readings of strain gauge SG 1*

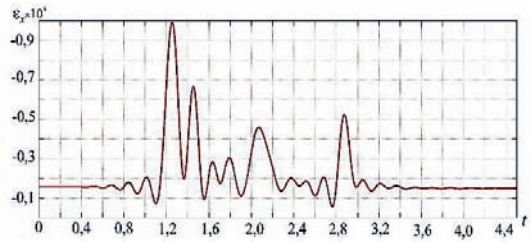

*b) readings of strain gauge SG 2*

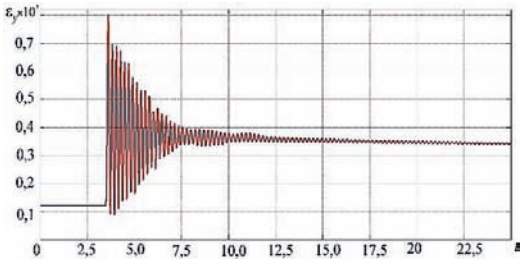

*f) readings of strain gauge SG 2*

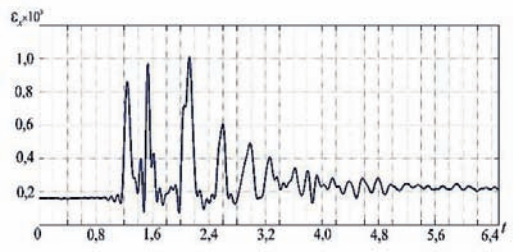

*c) readings of strain gauge SG 3*

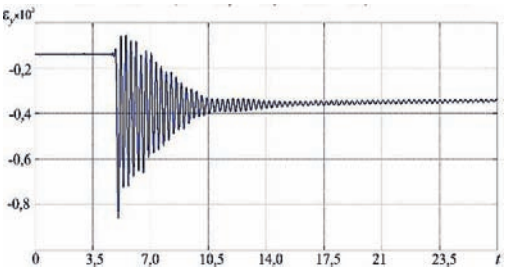

*g) readings of strain gauge SG 3*

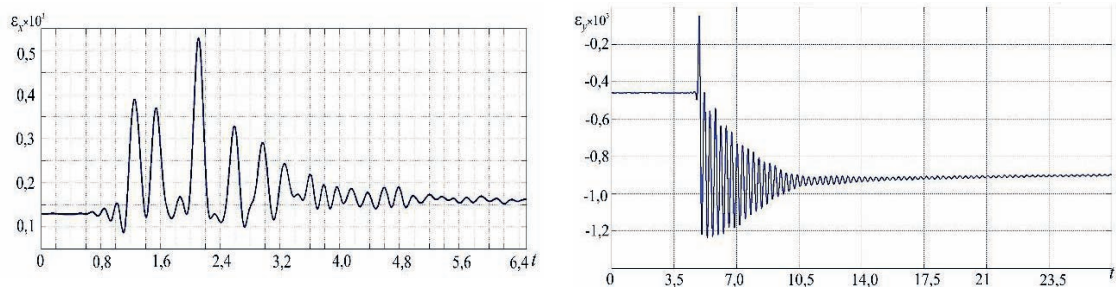


*d) readings of strain gauge SG 4* *h) readings of strain gauge SG 4*

*Figure 6. The strain histories for gauges mounted on the frame beam: a-d - with hinged nodes; e-h - with rigid nodes*

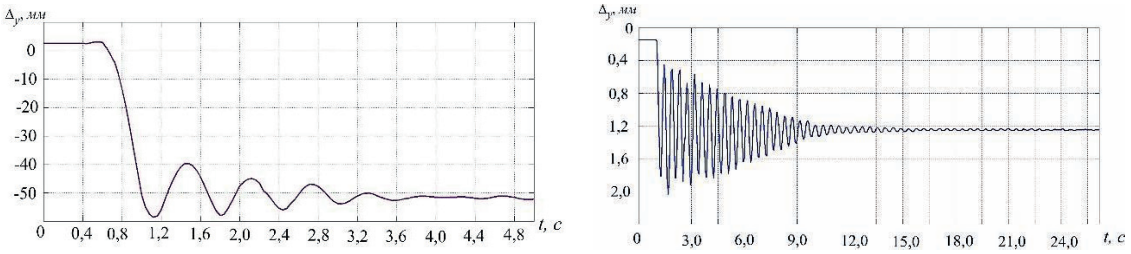


*a)* *b)*

*Figure 7. Displacement history of point D (Figure 4, b) of the frames: (a) with hinged joints; (b) with rigid joints*

- the type of frame assembly: rigid or hinged establishes a fundamentally different pattern of localization of structural failure. For hinge assemblies, it is a kinematic chain, the reliability of which is completely determined by the reliability of the hinge design. For rigid joints, the fracture pattern is a frame with a set of plastic joints, and the invariability of this system, according to the static theorem of A.A. Gvozdev, is determined by the limit conditions in one of the cross-sections;
- the pattern of deformation under dynamic loading of frames with safety elements (increasing the robustness property) has the following features. At hinged joints the system has a structural damping coefficient of 0.01, while for rigid joints this coefficient is 0.00074, i.e., it is 13.5 times higher. The coefficient was calculated based on the processing of experimental strain data using the peak method known in the literature;
- analysis of diagrams and measurements allowed to reveal that the frame with hinged joints has a lower frequency of the main vibration mode $f_1 \approx 1.42$ Hz , while the frame with rigid joints has a frequency of $f_2 \approx 4.3$ Hz , i.e. lower by 3 times;
- peak strain values for the frame with both hinged and rigid nodes are observed in the first half-period of vibrations, while in the compressed zone of elements these values may come in the second and even in the third period of vibrations, which can be explained by the redistribution of force flows between the main frame system and safety elements (ties);

The analysis of Figure 7 shows that the peak (maximum) deflections for frames with safety elements are observed in the first half of the vibration period, which agrees with the results given in the literature for a similar accidental situation for beam systems. It should also be noted that the transient dynamic process for the

frame with rigid joints has a value of 24 s on average, which is 4.8 times longer than the same value for the frame with hinged joints. This allows us to conclude that hinge joints are preferable for materials and design solutions sensitive to vibrations.

***3.2 Results of the calculation.*** To experimentally verify the calculation methodology for the accidental impact outlined in [6], a rod finite element model (Figure 8) was developed. The material properties were taken from the tests, and the kinematic constraints corresponded to the connections and supports made in the experimental setup.

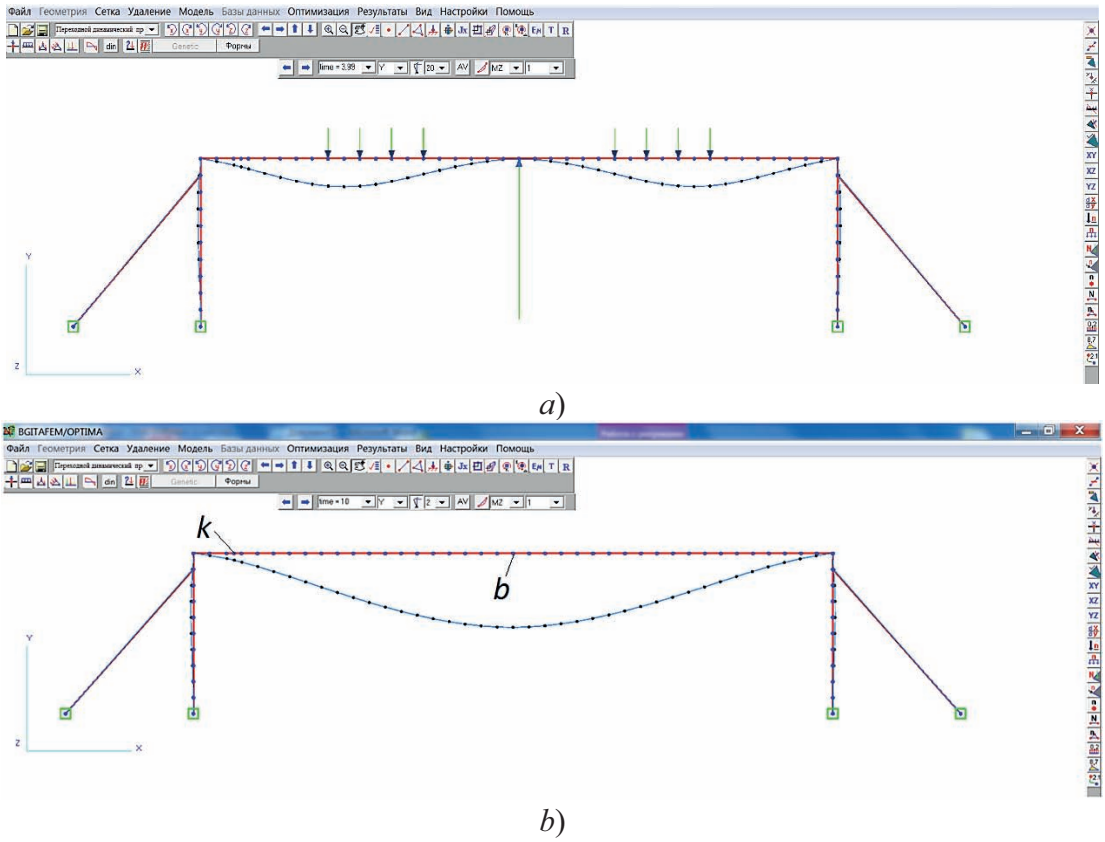


*Figure 8. Deformed schemes of the experimental setup model: state of the system after dynamic relaxation before removal of the middle column (a), after vibration damping without the middle column (b)*

According to the dynamic analysis procedure, initially the static equivalent of the support reaction was applied to the model. After that, the integration process continues and the system, passing the state of dynamic relaxation comes to the equivalent static state. The reaction is then quickly removed from the system, which begins to experience free vibrations under accidental loading. This process is shown in Figure 8 in the interface of the author's software package. The results of the comparison are presented in Table 2. It should be noted that the experimentally obtained displacements agree satisfactorily with the calculated ones (they differ on average by 15%). These differences are explained by the peculiarities of the nodes fixing the installation to the power floor. These nodes do not have absolute stiffness as in the design scheme, but a small ductility to tear-off, associated with the bolt fixing.

*Table 2. Comparison of frame displacement calculation results*

| Loading stage | Frame specimen | Maximum value, mm (dynamic) | | Static value, mm (after vibration damping) | | | |
|---|---|---|---|---|---|---|---|
| | | Experiment ( rope gauge) | According to [6] | Experiment | | Calculation [6] | |
| | | $y_к$ (fig. 8) | | $y_к$ | $y_b$ | $y_к$ | $y_b$ |
| 1 | PM-1 | 2,05 | 1,91 | 1,2 | 13 | 0,96 | 9,29 |
| 2 | PM-2 | 4,5 | 3,84 | 2,3 | 25 | 1,67 | 18,96 |
| 3 | PM-3 | 7,3 | 6,56 | 3,8 | 45 | 3,42 | 35,90 |

## 4. CONCLUSIONS

1. It has been established that safety elements such as tie rods absorb dynamic loads and redistribute forces. This increases the resistance to progressive collapse and, consequently, the mechanical safety of buildings and structures, especially those prefabricated elements with hinged joints.
2. The load-bearing capacity of frames with tie rods is 33.3% lower than for frames with rigid assemblies under an accidental impact associated with the support removal. However, the transient time during which the vibrations cease is 4.8 times shorter. This allows making reasonable decisions when designing structures with specified safety criteria, such as placement of equipment for which vibrations are dangerous or inadmissible.
3. The damping coefficients under accidental action have been determined experimentally. It is established that frames with hinged nodes have 13.5 times lower structural damping coefficient than frames with rigid nodes.
4. Comparison with experimental data established satisfactory accuracy of the approach to numerical modeling of the accidental situation.

## REFERENCES


1. **Tusnina O.A.** Vybor avariynykh situatsiy pri raschete na progressiruyushcheye obrusheniye promyshlennogo zdaniya [Selection of emergency situations when calculating the progressive collapse of an industrial building]. Promyshlennoe i grazhdanskoe stroitel'stvo. 2021. No. 9. Pp. 60–65. DOI:10.33622/0869-7019.2021.09.60-65. (In Russian).
2. **Zhong, W. hui; Zheng, Y. hui; Tan, Z.; Meng, B.; Zhang, Y.; Duan, S.C**. Controllable Design on Failure Mode for Steel Frames Considering Regional Collapse-Resistant Mechanism. 2023. Journal of Structural Steel Research 206, 107940, DOI:10.1016/J.JCSR.2023.107940.
3. **Tusnin A., Berger M.** Bearing capacity of steel trusses with local damage considering the exclusion time. 2023. Buildings Vol. 13, No. 4. P. 938. https://doi.org/10.3390/buildings 13040938.
4. **Liu, Y.; Zhu, Y.F.; Liang, W.; Zhang, H.; Yao, Y**. Progressive Collapse Resistance and Uncertainty Analysis of Post-Tensioned Steel Frames. 2023. Journal of Structural Steel Research 208, 108007. DOI:10.1016/J.JCSR.2023.108007.
5. **Wang, X.; Wang, P.; Ding, K.** The Collapse Evaluation Method of Steel Moment-Resisting Frames Based on Dynamic Increase Factor. 2023. Structures 58, 105515. DOI:10.1016/J.ISTRUC.2023.105515.
6. **Alekseytsev A.V.** Ensuring the safety of steel moment frames subjected to uncertain impacts. Buildings. 2023. Vol. 13, No. 8. P. 2038. https://doi.org/10.3390/buildings 13082038.
7. **He, Y.H.; Li, G.Q.; Zhang, J.Z.; Jiang, B.H.; Zhang, J.** Critical Collapse Deformation of 3-D Steel Frame with

Composite Floor System.2023. Journal of Structural Steel Research 208, 108034. DOI:10.1016/J.JCSR.2023.108034.
8. **Dong, S.; Yu, Y.; Ge, H.; Luo, Y.** Nonlinear Dynamic Collapse Analysis of Space Semi-Rigid Frames Using Finite Particle Method. 2024. Journal of Structural Steel Research 216, 108607. DOI:10.1016/J.JCSR.2024.108607.
9. **Zhang, J.Z.; He, Y.H.; Li, G.Q.; Hai, L.T.; Zhou, J.W**. A Novel Approach for Quantifying Dynamic Impacts on Steel Frames Induced by Instantaneous Interior Column Loss. 2024. Journal of Structural Steel Research 220, 108837. DOI:10.1016/J.JCSR.2024.108837.
10. **Ren, L.M.; Liew, J.Y.R.; Chen, K.; Yang, B.** Component Tests and Numerical Simulations of 3D Steel Frame Structures for Progressive Collapse. 2024. Engineering Structures 317, 118691. DOI:10.1016/J.ENGSTRUCT.2024.118691.
11. **Zong, L.; Fang, W.; Zhang, Y.; Cui, J**. Progressive Collapse Analysis on Modular Steel Construction Based on a Simplified Joint Model. 2024. Thin-Walled Structures 198, 111733, DOI:10.1016/J.TWS.2024.111733.
12. **Zheng, Y. hui; Zhong, W. hui; Zhang, Y.; Tan, Z.; Duan, S.C.; Meng, B.; Gao, Y.; Wang, H. chen** Failure Mechanism of Steel Frames with Angle Steel-Bolted Connections Exposed to Fire under Progressive Collapse Condition. 2024. Engineering Failures Analysis 155, 107744.DOI:10.1016/J.ENGFAILANAL.2023.107744.
13. **Possidente, L.; Freddi, F.; Tondini, N.** Dynamic Increase Factors for Progressive Collapse Analysis of Steel Structures Considering Column Buckling. 2024. Engineering Failures Analysis 160, 108209, DOI:10.1016/J.ENGFAILANAL.2024.108209.
14. **Wang, Y.; Li, J. ze; Bai, C.; Shen, H. xia; Tian, L. min** Novel Beam–Column Joint with the Folded Plates for Improving Progressive Collapse Resistance of Steel-Frame Structures.2024. Structures 61, 106047. DOI:10.1016/J.ISTRUC.2024.106047.
15. **Wang, X.; Wang, P.; Chen, W.** Test on Progressive Collapse of Steel Moment-Resisting Frame with Upper-and-Lower Flange Angle Steel Connection. 2024. Structures 68, 107171, DOI:10.1016/J.ISTRUC.2024.107171.
16. **Lan, X.; Li, Z.; Fu, F.; Qian, K.** Robustness of Steel Braced Frame to Resist Disproportionate Collapse Caused by Corner Column Removal. 2023. Journal of Building Engineering 69, 106226. DOI:10.1016/J.JOBE.2023.106226.
17. **Qu, Z.Y.; Zhong, W.H.; Tan, Z.; Chen, J.L.; Wang, H.C**. Research on the Anti-Collapse Performance of Steel Frame Structures with Infilled Walls in the Form of Reduced Beam Sections Connections. 2024. Journal of Building Engineering 91, 109600. DOI:10.1016/J.JOBE.2024.109600.
18. **Bregoli, G.; Vasdravellis, G.; Karavasilis, T.L.; Cotsovos, D.M.** Static and Dynamic Tests on Steel Joints Equipped with Novel Structural Details for Progressive Collapse Mitigation. 2021. Engineering Structures 232, 111829. DOI:10.1016/J.ENGSTRUCT.2020.111829.
19. **Wang, F.; Yang, J.; Wang, X. er; Azim, I.** Study on Progressive Collapse Behaviour of Steel-Framed Substructures with Sheathed CFS Stud Infill Walls. 2021. Journal of Building Engineering 42, 102720. DOI:10.1016/J.JOBE.2021.102720.

## СПИСОК ЛИТЕРАТУРЫ

1. **Туснина О.А.** Выбор аварийных ситуаций при расчете на прогрессирующее обрушение промышленного здания // Промышленное и гражданское строительство. 2021. № 9. С. 60–65. DOI:10.33622/0869-7019.2021.09.60-65.
2. **Zhong, W. hui; Zheng, Y. hui; Tan, Z.; Meng, B.; Zhang, Y.; Duan, S.C**. Controllable Design on Failure Mode for

Steel Frames Considering Regional Collapse-Resistant Mechanism. 2023. Journal of Structural Steel Research 206, 107940, DOI:10.1016/J.JCSR.2023.107940.

3. **Tusnin A., Berger M.** Bearing capacity of steel trusses with local damage considering the exclusion time. 2023. Buildings Vol. 13, No. 4. P. 938. https://doi.org/10.3390/buildings 13040938.
4. **Liu, Y.; Zhu, Y.F.; Liang, W.; Zhang, H.; Yao, Y**. Progressive Collapse Resistance and Uncertainty Analysis of Post-Tensioned Steel Frames. 2023. Journal of Structural Steel Research 208, 108007. DOI:10.1016/J.JCSR.2023.108007.
5. **Wang, X.; Wang, P.; Ding, K.** The Collapse Evaluation Method of Steel Moment-Resisting Frames Based on Dynamic Increase Factor. 2023. Structures 58, 105515, DOI:10.1016/J.ISTRUC.2023.105515.
6. **Alekseytsev A.V.** Ensuring the safety of steel moment frames subjected to uncertain impacts. Buildings. 2023. Vol. 13, No. 8. P. 2038. https://doi.org/10.3390/buildings 13082038.
7. **He, Y.H.; Li, G.Q.; Zhang, J.Z.; Jiang, B.H.; Zhang, J.** Critical Collapse Deformation of 3-D Steel Frame with Composite Floor System.2023. Journal of Structural Steel Research 208, 108034. DOI:10.1016/J.JCSR.2023.108034.
8. **Dong, S.; Yu, Y.; Ge, H.; Luo, Y.** Nonlinear Dynamic Collapse Analysis of Space Semi-Rigid Frames Using Finite Particle Method. 2024. Journal of Structural Steel Research 216, 108607. DOI:10.1016/J.JCSR.2024.108607.
9. **Zhang, J.Z.; He, Y.H.; Li, G.Q.; Hai, L.T.; Zhou, J.W**. A Novel Approach for Quantifying Dynamic Impacts on Steel Frames Induced by Instantaneous Interior Column Loss. 2024. Journal of Structural Steel Research 220, 108837. DOI:10.1016/J.JCSR.2024.108837.
10. **Ren, L.M.; Liew, J.Y.R.; Chen, K.; Yang, B.** Component Tests and Numerical Simulations of 3D Steel Frame Structures for Progressive Collapse. 2024. Engineering Structures 317, 118691. DOI:10.1016/J.ENGSTRUCT.2024.118691.
11. **Zong, L.; Fang, W.; Zhang, Y.; Cui, J**. Progressive Collapse Analysis on Modular Steel Construction Based on a Simplified Joint Model. 2024. Thin-Walled Structures 198, 111733, DOI:10.1016/J.TWS.2024.111733.
12. **Zheng, Y. hui; Zhong, W. hui; Zhang, Y.; Tan, Z.; Duan, S.C.; Meng, B.; Gao, Y.; Wang, H. chen** Failure Mechanism of Steel Frames with Angle Steel-Bolted Connections Exposed to Fire under Progressive Collapse Condition. 2024. Engineering Failures Analysis 155, 107744.DOI:10.1016/J.ENGFAILANAL.2023.107744.
13. **Possidente, L.; Freddi, F.; Tondini, N.** Dynamic Increase Factors for Progressive Collapse Analysis of Steel Structures Considering Column Buckling. 2024. Engineering Failures Analysis 160, 108209, DOI:10.1016/J.ENGFAILANAL.2024.108209.
14. **Wang, Y.; Li, J. ze; Bai, C.; Shen, H. xia; Tian, L. min** Novel Beam–Column Joint with the Folded Plates for Improving Progressive Collapse Resistance of Steel-Frame Structures.2024. Structures 61, 106047. DOI:10.1016/J.ISTRUC.2024.106047.
15. **Wang, X.; Wang, P.; Chen, W.** Test on Progressive Collapse of Steel Moment-Resisting Frame with Upper-and-Lower Flange Angle Steel Connection. 2024. Structures 68, 107171, DOI:10.1016/J.ISTRUC.2024.107171.
16. **Lan, X.; Li, Z.; Fu, F.; Qian, K.** Robustness of Steel Braced Frame to Resist Disproportionate Collapse Caused by Corner Column Removal. 2023. Journal of Building Engineering 69, 106226. DOI:10.1016/J.JOBE.2023.106226.
17. **Qu, Z.Y.; Zhong, W.H.; Tan, Z.; Chen, J.L.; Wang, H.C**. Research on the Anti-Collapse Performance of Steel Frame

Structures with Infilled Walls in the Form of Reduced Beam Sections Connections. 2024. Journal of Building Engineering 91, 109600. DOI:10.1016/J.JOBE.2024.109600.

18. **Bregoli, G.; Vasdravellis, G.; Karavasilis, T.L.; Cotsovos, D.M.** Static and Dynamic Tests on Steel Joints Equipped with Novel Structural Details for Progressive Collapse Mitigation. 2021. Engineering Structures 232, 111829. DOI:10.1016/J.ENGSTRUCT.2020.111829.
19. **Wang, F.; Yang, J.; Wang, X. er; Azim, I.** Study on Progressive Collapse Behaviour of Steel-Framed Substructures with Sheathed CFS Stud Infill Walls. 2021. Journal of Building Engineering 42, 102720. DOI:10.1016/J.JOBE.2021.102720.

---

*Anatoliy V. Alekseytsev,* docent, DSc, Professor of the Department «Industrial and civil engineering», Associated Professor of the Department "Reinforced concrete and stone structures"; National Research Moscow State University of Civil Engineering (NRU MGSU); Russia, 129337 Moscow, Yaroslavskoe sh., 26. e-mail: AlekseytsevAV@ mgsu.ru
Scopus ID: 57191530761; Researcher ID: I-3663-2017; ORCID: 0000-0002-4765-5819.

*Valentina M. Tusnina,* docent, candidate of technical sciences, associated professor of department "Architectural and construction design and physics of the environment"; National Research Moscow State University of Civil Engineering (National Research University); Russia, 129337 Moscow, Yaroslavskoe sh., 26. e-mail: valmalaz@mail.ru
Scopus ID: 56296961500; Researcher ID: AAD-8968-2022; ORCID: 0000-0003-0328-0848.

*Алексейцев Анатолий Викторович,* доцент, доктор технических наук, профессор кафедры «Промышленное и гражданское строительство», доцент кафедры «Железобетонные и каменные конструкции»; Национальный исследовательский московский государственный строительный университет (НИУ МГСУ); Россия, 129337 Москва, Ярославское шоссе, 26. e-mail: AlekseytsevAV@mgsu.ru
Scopus ID: 57191530761; Researcher ID: I-3663-2017; ORCID: 0000-0002-4765-5819.

*Туснина Валентина Матвеевна,* доцент, кандидат технических наук, доцент кафедры «Архитектурно-строительное проектирование и физика среды»; Национальный исследовательский московский государственный строительный университет (НИУ МГСУ); Россия, 129337 Москва, Ярославское шоссе, 26. e-mail: valmalaz@mail.ru
Scopus ID: 56296961500; Researcher ID: AAD-8968-2022; ORCID: 0000-0003-0328-0848.

DOI:10.22337/2587-9618-2025-21-3-135-147

# PARTICLE TRANSPORT WITH FINITE FILTRATION TIME

***Liudmila I. Kuzmina [1], Yuri V. Osipov [2]***
[1] HSE University, Moscow, RUSSIA
[2] Moscow State University of Civil Engineering, Moscow, RUSSIA

**Abstract:** Particle transport by a fluid flow occurs in many applied construction problems, including pumping mortar into porous soil, creating watertight diaphragm walls, and constructing dams and underwater structures. A model of deep bed filtration of suspensions and colloids in a homogeneous porous medium with a finite number of vacancies for retained particles is considered. A suspension of constant concentration is injected into the inlet of a porous medium containing clean water. If the sediment growth rate remains positive as the sediment concentration approaches the upper limiting value, the filtration process continues for a finite time. In this case, the filtration function that specifies the sediment growth rate in the mathematical model is not blocking. At each point of the porous medium, sedimentation begins from the moment the concentration front passes and ends after a finite period of time depending on the distance to the porous medium inlet. A global exact solution to the problem is constructed in the filtration domain, which consists of two zones. In the zone bordering the concentration front, the solution has a standard form, and in the zone adjacent to the upper limiting values of the concentrations of suspended and retained particles, it has the form of a traveling wave.

**Keywords:** deep bed filtration, porous medium, filtration function, retained particles concentration, exact solution

# ПЕРЕНОС ЧАСТИЦ С КОНЕЧНЫМ ВРЕМЕНЕМ ФИЛЬТРАЦИИ

***Л.И. Кузьмина [1], Ю.В. Осипов [2]***
[1] Национальный исследовательский университет «Высшая школа экономики», г. Москва, РОССИЯ
[2] Национальный исследовательский Московский государственный строительный университет, г. Москва, РОССИЯ

**Аннотация:** Перенос частиц потоком жидкости встречается во многих прикладных строительных задачах, в том числе при закачке раствора в пористый грунт, при создании водонепроницаемых стен в грунте и при конструировании плотин и подводных сооружений. Рассматривается модель глубинной фильтрации суспензий и коллоидов в однородной пористой среде, которая имеет конечное число вакантных мест для задержанных частиц. На вход пористой среды, содержащей чистую воду, впрыскивается суспензия постоянной концентрации. Если скорость роста осадка остается положительной при приближении концентрации осадка к предельной величине, то процесс фильтрации продолжается конечное время. В этом случае функция фильтрации, задающая скорость роста осадка в математической модели, не является блокирующей. В каждой точке пористой среды осаждение осадка начинается с момента прохождения фронта концентраций и заканчивается через конечный промежуток времени, зависящий от расстояний до входа пористой среды. Построено глобальное точное решение задачи в области фильтрации, которая состоит из двух зон. В зоне, граничащей с фронтом концентраций, решение имеет стандартный вид, а в зоне, примыкающей к предельным значениям концентраций взвешенных и осажденных частиц - вид бегущей волны.

**Ключевые слова:** глубинная фильтрация, пористая среда, функция фильтрации, концентрация осажденных частиц, точное решение

## 1. INTRODUCTION

Filtration of small particles in porous media occurs in natural phenomena and in technological processes and is one of the main problems of underground hydromechanics. The transport and sedimentation of particles in porous soil must be taken into account when designing foundations, tunnels and underground structures [1-6].

When filtering a suspension in a porous medium, sediment formation can be caused by various reasons. Electrical, gravitational and hydrodynamic forces act on particles in a fluid flow. If the sizes of pores and particles are close, then the size - exclusion capture mechanism plays an important role - particles freely pass through large pores and get stuck in small pores [7-10].

When the number of particles in the carrier liquid is small, the suspended particles do not interact with each other and the sediment growth rate is proportional to the suspended particles concentration. The proportionality coefficient between the sediment growth rate and the suspended concentration is called the filtration function. As a rule, the sediment growth rate decreases with increasing sediment concentration and becomes zero at a certain sediment limit. In this case, particle sedimentation ceases and suspended particles pass through the porous medium without hindrance, since all vacant places for retained particles are filled. The corresponding filtration functions are called blocking. For a monodisperse suspension, the filtration function is linear and is called the Langmuir coefficient. If the suspension contains different particles, the filtration function is nonlinear [11-14].

As a rule, mathematical models of such processes assume an infinite time to reach the maximum sediment. However, in some cases, the sediment growth rate remains significant throughout the filtration time and the maximum sediment is formed in a finite time. This model is considered in the article. The filtration function that ensures a finite filtration time can be blocking or non-blocking [15-18].

Mathematical difficulties in constructing a solution to a model with a non-blocking filtration function are associated with the ambiguity of the solution when the maximum sediment is reached. They were overcome using the condition of continuity of sediment concentration in a porous medium. In addition to the exact solution found, an example with an unlimited filtration function is considered.

## 2. MODEL OF PARTICLE TRANSPORT

The model of particle transport in a porous medium includes a mass balance equation and a sediment growth equation [19]. The initial and boundary conditions describe the injection of a constant concentration suspension into a porous medium that does not contain suspended or settled particles.

In the domain $\Omega = \{x \geq 0,\, t \geq 0\}$ consider the system

$$\frac{\partial C}{\partial t} + \frac{\partial C}{\partial x} + \frac{\partial S}{\partial t} = 0, \qquad (1)$$

$$\frac{\partial S}{\partial t} = \Lambda(S)C, \qquad (2)$$

where filtration function $\Lambda(S)$ is continuous and positive for $0 \leq S \leq S_m$, $S_m > 0$, and $\Lambda(S) = 0$ for $S > S_m$. At the point $S_m$ the function $\Lambda(S)$ is non-zero: $\Lambda(S_M) = \Lambda_M > 0$.

Unique solution of the system (1), (2) is determined by boundary-initial conditions

$$C\big|_{x=0} = 1, \qquad (3)$$

$$C\big|_{t=0} = 0, \quad S\big|_{t=0} = 0. \qquad (4)$$

Concentration front $t = x$ divides the domain $\Omega$ into two subdomains $\Omega_0 = \{x \geq 0,\, 0 \leq t < x\}$ and $\Omega_1 = \{x \geq 0,\, t > x\}$. In $\Omega_0$ the system (1)-(4) has zero solution: $C = 0,\, S = 0$. In $\Omega_1$ the solution is positive. Solution $C$ has a break on the concentration front; solution $S$ is continuous in $\Omega$ and

$$S\big|_{t=x} = 0. \qquad (5)$$

In the domain $\Omega_1$ the solution to the problem (1) - (4) coincides with the solution to problem (1) - (3), (5).

According to condition (3) at the porous medium inlet $x = 0$ Eq. (2) takes the form

$$\frac{\partial S}{\partial t} = \Lambda(S). \quad (6)$$

For $0 \le S < S_m$ filtration function $\Lambda(S)$ is continuous. Solution to Eq. (6) is given by implicit formula

$$\int_0^{S_0} \frac{dS}{\Lambda(S)} = t, \quad (7)$$

where

$$S_0(t) = S(x,t)\big|_{x=0}. \quad (8)$$

Denote

$$t_0 = \int_0^{S_m} \frac{dS}{\Lambda(S)}. \quad (9)$$

For $0 \le t \le t_0$ the solution (8) is given by the formula (7).
For $t > t_0$ Eq. (6) takes the form

$$\frac{\partial S}{\partial t} = 0. \quad (10)$$

Solution to Eq. (15) with initial condition $S_0(t_0) = S_m$ is constant:

$$S_0(\tau) = S_m. \quad (11)$$

At the inlet $x = 0$ the solution $S_0(t)$ increases from zero at $t = 0$ to $S_m$ at $t = t_0$ and is constant at $t > t_0$.
To obtain the solution at the concentration front substitute Eq. (2) into Eq. (1)

$$\frac{\partial C}{\partial t} + \frac{\partial C}{\partial x} + \Lambda(S)C = 0. \quad (12)$$

Solution to Eq. (12) with boundary condition (3) is

$$C^-(x) = e^{-\Lambda(0)x}. \quad (13)$$

The line $t = x + t_0$ divides the domain $\Omega_1$ into two zones

$$V_1 = \{x \ge 0,\ x \le t \le x + t_0\},$$
$$V_2 = \{x \ge 0,\ t > x + t_0\}.$$

$V_1$ is a standard filtration zone and $V_2$ is a traveling wave zone [20, 21].

## 3. EXACT SOLUTION

In zone $V_1$ the solution to system (1)-(3), (5) is obtained by the standard methods [22-24]. Express $C$ from Eq. (2):

$$C = \frac{\partial S / \partial t}{\Lambda(S)}, \quad (14)$$

and substitute into Eq. (12):

$$\frac{\partial}{\partial t}\left(\frac{\partial S / \partial t}{\Lambda(S)}\right) + \frac{\partial}{\partial x}\left(\frac{\partial S / \partial t}{\Lambda(S)}\right) + \frac{\partial S}{\partial t} = 0. \quad (15)$$

Using the formula

$$\frac{\partial}{\partial x}\left(\frac{\partial S / \partial t}{\Lambda(S)}\right) = \frac{\partial^2 S / \partial t \partial x}{\Lambda(S)} - \frac{\partial S}{\partial t}\frac{\partial S}{\partial x}\frac{\Lambda'(S)}{\Lambda^2(S)} = \frac{\partial}{\partial t}\left(\frac{\partial S / \partial x}{\Lambda(S)}\right),$$

change the order of differentiation in (15):

$$\frac{\partial}{\partial t}\left(\frac{\partial S / \partial t}{\Lambda(S)}\right) + \frac{\partial}{\partial t}\left(\frac{\partial S / \partial x}{\Lambda(S)}\right) + \frac{\partial S}{\partial t} = 0. \quad (16)$$

Integrate (16) in *t*:

$$\frac{\partial S / \partial t}{\Lambda(S)} + \frac{\partial S / \partial x}{\Lambda(S)} + S = K(x). \quad (17)$$

The integration constant $K(x)$ is determined from condition (5):

$$S\big|_{t=x} = 0 \;\Rightarrow\; \left(\frac{\partial S}{\partial x} + \frac{\partial S}{\partial t}\right)\Big|_{t=0} = 0 \;\Rightarrow\; K(x) = 0\,.$$

Eq. (17) takes the form

$$\frac{\partial S / \partial t}{\Lambda(S)} + \frac{\partial S / \partial x}{\Lambda(S)} + S = 0\,. \qquad (18)$$

Denote characteristic variables

$$\tau = t - x, \quad x = x\,.$$

In the characteristic variables Eq. 18) takes the form

$$\frac{\partial S / \partial x}{\Lambda(S)} + S = 0\,. \qquad (19)$$

Solution to Eq. (19) with boundary condition (8) has the form

$$\int_{S}^{S_0(\tau)} \frac{dS}{S\Lambda(S)} = x\,. \qquad (20)$$

In Cartesian variables the solution (20) takes the form

$$\int_{S(x,t)}^{S_0(t-x)} \frac{dS}{S\Lambda(S)} = x\,. \qquad (21)$$

Differentiate Eq. (21) in $t$:

$$\frac{\partial S_0 / \partial t}{S_0\Lambda(S_0)} - \frac{\partial S / \partial t}{S\Lambda(S)} = 0\,. \qquad (22)$$

Substitute Eqs. (2) and (6) in the formula (22):

$$\frac{1}{S_0} - \frac{C}{S} = 0\,. \qquad (23)$$

Express $C$ from Eq. (23):

$$C(x,t) = \frac{S(x,t)}{S_0(t-x)}\,. \qquad (24)$$

Formula (24) defines the Riemann invariant of the system (1)-(3), (5).
Denote the solution at the border $t = x + t_0$ of zone $V_1$:

$$S_1(x) = S(x,t)\big|_{t=x+t_0}\,, \qquad (25)$$

At the starting point of the border $x = 0,\ t = t_0$ and the solution is $S_0(t_0) = S_m$. Formula (21) takes the form

$$\int_{S_1(x)}^{S_m} \frac{dS}{S\Lambda(S)} = x\,. \qquad (26)$$

To obtain the solution in the travelling wave zone $V_2$ multiply Eq. (19) by $\Lambda(S)$:

$$\frac{\partial S}{\partial x} + S\Lambda(S) = 0\,. \qquad (27)$$

In zone $V_2$ the solution to Eq. (27) with condition

$$S(x,\tau)\big|_{x=0} = S_m\,, \qquad (28)$$

is not unique, because filtration function $\Lambda(S)$ has a break at the point $S = S_m$. For a fixed $\tau > t_0$ the solution is constant $S = S_m$ at $0 \le x \le x_m(\tau)$ and decrease at $x \ge x_m(\tau)$, where $x = x_m(\tau)$ is a continuous increasing function and

$$x_m(t_0) = 0\,. \qquad (29)$$

Denote the line $\Gamma$ separating subzones $U_1$ and $U_2$ of constant and non-constant solution

$$\Gamma = \{(x_m(\tau),\ \tau),\ \tau \ge t_0\}\,.$$

Solution in the domain $U_1$ is

$$S(x,\tau)=S_m,\quad C(x,\tau)=1. \qquad (30)$$

Note that Riemann invariant (24) holds in subzone $U_1$.

On line Γ

$$S(x,\tau)\big|_{x=x_m(\tau)}=S_m. \qquad (31)$$

The function $x=x_m(\tau)$ is determined from the continuity of the solution on Γ. Consider the tangent vector $l=\left(x_m'(\tau),-1\right)$ to the line Γ at the point $\left(x_m(\tau),\tau\right)$. From Eq. (31)

$$\left.\frac{\partial S}{\partial l}\right|_{(x_m(\tau),\tau)}=0. \qquad (32)$$

Calculate the derivative (32) using Eq. (2) and (27)

$$\left.\frac{\partial S}{\partial l}\right|_{(x_m(\tau),\tau)}=\frac{\partial S}{\partial x}x_m'(\tau)+\frac{\partial S}{\partial \tau}= \\ =-S\Lambda(S)x_m'(\tau)+\Lambda(S)C. \qquad (33)$$

Equate right parts of Eqs. (32) and (33) and reduce the multiplier $\Lambda(S)$:

$$-Sx_m'(\tau)+C=0 \qquad (34)$$

Substitution of solution (30) in Eq. (34) yields

$$x_m'(\tau)=\frac{1}{S_m}. \qquad (35)$$

Solution to Eq. (35) with initial condition (29) is

$$x_m(\tau)=\frac{\tau-t_0}{S_m}. \qquad (36)$$

In subzone $U_2$ the solution to Eq. (19) with condition (31) is

$$\int_S^{S_m}\frac{dS}{S\Lambda(S)}=x-x_m(\tau). \qquad (37)$$

It follows from Eq. (37) that the solution in subzone $U_2$ has the form of the traveling wave

$$S=\tilde{S}\left(x-x_m(\tau)\right). \qquad (38)$$

According to formula (29) at $\tau=\tau_0$ the formula (37) coincides with (26). Formula (38) takes the form

$$S=S_1\left(x-x_m(\tau)\right). \qquad (39)$$

Differentiate Eq. (37) in τ:

$$-\frac{\partial S/\partial\tau}{S\Lambda(S)}=-x_m'(\tau). \qquad (40)$$

Substitution of Eq. (2) and (39) into Eq. (40) yields Riemann invariant (24) in subzone $U_2$.

$$C=\tilde{C}\left(x-x_m(\tau)\right)=\frac{S_1\left(x-x_m(\tau)\right)}{S_m}. \qquad (41)$$

In Cartesian variables the formula (36) takes the form

$$x=\frac{t-x-t_0}{S_m}. \qquad (42)$$

Express *x* from (42):

$$x_\Gamma(t)=\frac{t-t_0}{S_m+1}. \qquad (43)$$

The boundary Γ between subzones $U_1$ and $U_2$ is a straight line (43) starting from *OX* axis at $t=t_0$.

The solution (39) takes the form

$$S=S_1\left(x-x_\Gamma(t)\right). \qquad (44)$$

In Cartesian variables, the formula (41) takes the form

$$C\left(x - x_{\Gamma}(t)\right) = \frac{S_1\left(x - x_{\Gamma}(t)\right)}{S_m}. \qquad (45)$$

The various zones into which the filtration domain is divided and the type of solutions in these zones are shown in Figure 1.

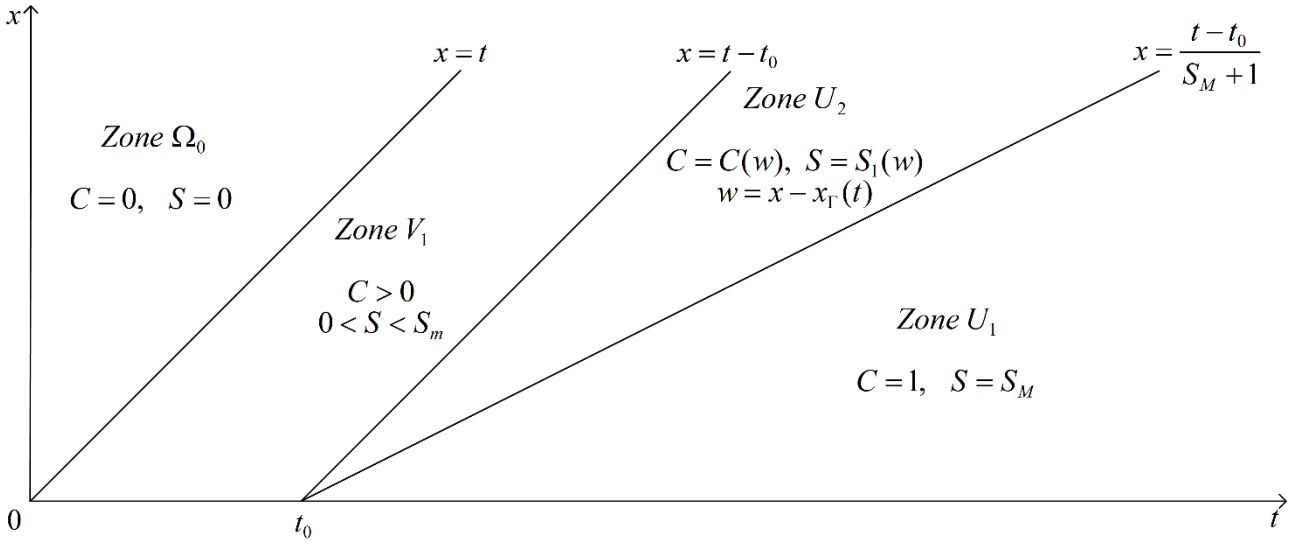


*Figure 1. Solution diagram of the model with finite filtration time*

## 4. EXAMPLE

As an example, consider an unlimited filtration function. Let

$$\Lambda(S) = \begin{cases} \dfrac{1}{\sqrt{1-S}}, & 0 \le S < 1; \\ 0, & S \ge 1. \end{cases}$$

Formula (7) takes the form

$$\int_0^{S_0} \sqrt{1-S}\, dS = t. \qquad (46)$$

Integration of (46) gives the solution in explicit form:

$$S_0 = 1 - \left(1 - \frac{3}{2}t\right)^{2/3}. \qquad (47)$$

From formula (47)

$$t_0 = \frac{2}{3}.$$

Finally, the solution at the inlet $x = 0$ is

$$S_0(t) = \begin{cases} 1 - \left(1 - \dfrac{3}{2}t\right)^{2/3}, & 0 \le t < \dfrac{2}{3}; \\ 1, & t \ge \dfrac{2}{3}. \end{cases} \qquad (48)$$

The deposit concentration increases from zero to 1 at finite time $t_0 = 2/3$ and becomes constant after reaching the upper limit $S_m = 1$. The graph of deposit concentration versus time at the inlet of the porous medium is shown in Fig. 2.

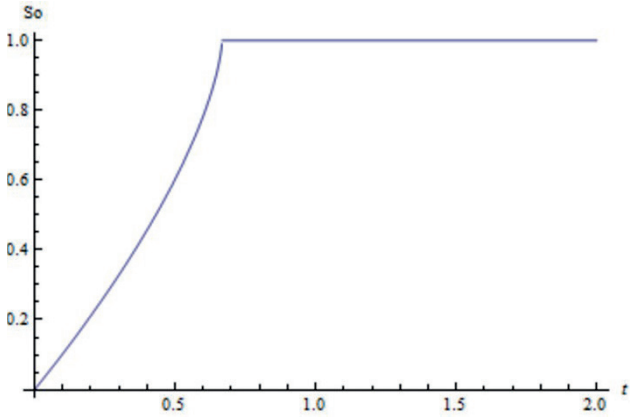


*Figure 2. Retained particles concentration at the inlet of the porous medium*

At the concentration front the suspended concentration is given by the formula

$$C^{-}(x) = e^{-x}.$$

Calculate the solution in zone $V_1 = \{x \geq 0,\ 0 \leq t - x \leq \frac{2}{3}\}$. The formula (26) takes the form

$$\int_{S(x,\tau)}^{S_0(\tau)} \frac{\sqrt{1-S}\,dS}{S} = x. \qquad (49)$$

Calculate the integral in Eq. (49):

$$2\left(\sqrt{1-S_0} - \sqrt{1-S}\right) - \\ -\ln\frac{\left(1+\sqrt{1-S_0}\right)}{\left(1-\sqrt{1-S_0}\right)}\frac{\left(1-\sqrt{1-S}\right)}{\left(1+\sqrt{1-S}\right)} = x. \qquad (50)$$

Substitute formula (47) into Eq. (50):

$$2\left(\sqrt[3]{1-1.5\tau} - \sqrt{1-S}\right) - \\ -\ln\frac{\left(1+\sqrt[3]{1-1.5\tau}\right)}{\left(1-\sqrt[3]{1-1.5\tau}\right)}\frac{\left(1-\sqrt{1-S}\right)}{\left(1+\sqrt{1-S}\right)} = x. \qquad (51)$$

In Cartesian variables the Eq. (51) takes the form

$$2\left(\sqrt[3]{1-1.5(t-x)} - \sqrt{1-S}\right) - \\ -\ln\frac{\left(1+\sqrt[3]{1-1.5(t-x)}\right)}{\left(1-\sqrt[3]{1-1.5(t-x)}\right)}\frac{\left(1-\sqrt{1-S}\right)}{\left(1+\sqrt{1-S}\right)} = x. \qquad (52)$$

Eq. (52) and the Riemann invariant (24) are the solution in zone $V_1$.

In the domain $V_2 = \{x \geq 0,\ t > x + \frac{2}{3}\}$ the boundary of zones $U_1$ and $U_2$ is

$$x_\Gamma(t) = \frac{t}{2} - \frac{1}{3}.$$

In subzone $U_2 = \left\{t \geq \frac{2}{3},\ 0 \leq x \leq \frac{t}{2} - \frac{1}{3}\right\}$ implicit formula (37) for the solution takes the form

$$\int_S^1 \frac{\sqrt{1-S}\,dS}{S} = x - \tau + \frac{2}{3}. \qquad (53)$$

Calculate the integral in the left side of Eq. (53) similarly to formula (49):

$$\int_S^1 \frac{\sqrt{1-S}\,dS}{S} = 2\left(z - \frac{1}{2}\ln\frac{1+z}{1-z}\right)\Bigg|_{\sqrt{1-S}}^{0} = \\ = -2\sqrt{1-S} - \ln\frac{\left(1-\sqrt{1-S}\right)}{\left(1+\sqrt{1-S}\right)}.$$

Eq. (53) takes the form

$$-2\sqrt{1-S} - \ln\frac{\left(1-\sqrt{1-S}\right)}{\left(1+\sqrt{1-S}\right)} = x - \tau + \frac{2}{3}. \qquad (54)$$

In Cartesian variables, the implicit solution (54) takes the form of the travelling wave

$$-2\sqrt{1-S} - \ln\frac{\left(1-\sqrt{1-S}\right)}{\left(1+\sqrt{1-S}\right)} = 2x - t + \frac{2}{3}. \qquad (55)$$

The travelling wave $S(w)$, $w = 2x - t + 2/3$ is shown in Figure 3.

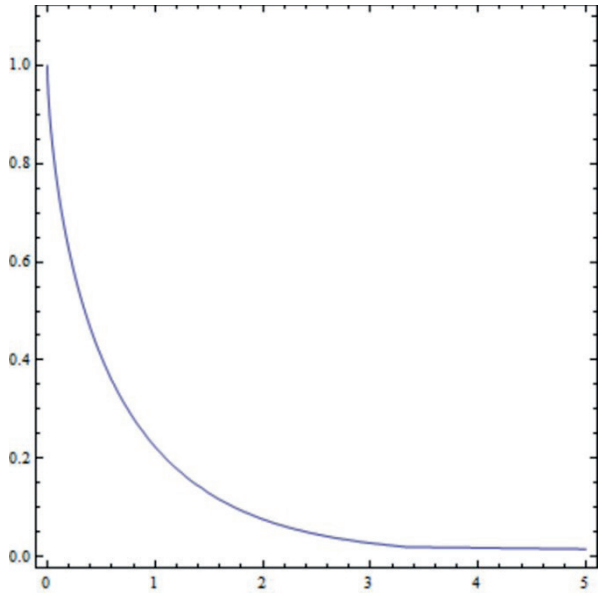


*Figure 3. Solution in travelling wave zone.*

In subzone $U_1 = \left\{ t \geq \frac{2}{3},\ \frac{t}{2} - \frac{1}{3} \leq x \leq t - \frac{2}{3} \right\}$ concentrations reach maximum values

$$S = 1, \quad C = 1. \tag{56}$$

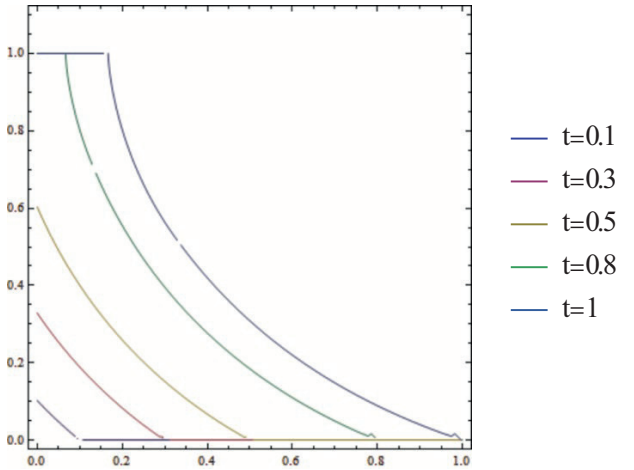


*Figure 4. Global retained concentration profiles*

A global exact solution to the model is obtained by combining local solutions (52), (55) and (56) in three zones. The filtration domain is the time interval during which the concentration of deposited particles decreases from 1 to zero. The global deposit concentration profiles - the dependence of retained particles concentrations on spatial coordinate $x$ at different times are shown in Figure 4 [25-28].

## 5. DISCUSSION

In particle transport problems, suspended and retained particle concentrations grow with time to limiting values. Filtration time determines the time dependence of suspended and retained particle concentrations. If time filtration is infinite, then the retained concentration is given by a single equation, the solution is smooth everywhere. At a finite filtration time, the domain of non-zero concentrations (behind the front) is divided into three zones: the standard filtration zone, the filtration zone with solutions in the form of traveling waves, and the zone of upper limiting values of suspended and retained particle concentrations. In the first two zones, the retained concentrations are given by different equations, their boundary is a straight line, which is not a characteristic of the original system. On this line, the derivatives of the solution are discontinuous.

One-dimensional models are rarely encountered in practical problems. However, the presence of exact solutions of one-dimensional models can significantly speed up numerical calculations of two-dimensional and three-dimensional problems. For this, the flow of a suspension in a porous medium must be represented as a bundle of one-dimensional jets - trajectories of particle transport in pores [29].

We studied the problem of particle transport in a homogeneous porous medium, in which at the initial moment there were no suspended and retained particles. The initial presence of particles in a porous medium complicates the problem, since the porous medium becomes inhomogeneous. Such a model will be considered separately.

Exact solutions to the direct filtration problem are used to solve the inverse problem - finding

the filtration function for known suspended concentrations at the inlet and outlet [30-32].

## 6. CONCLUSIONS

The study of the particle model transport with non - blocking filtration function leads to the following conclusions:

- The filtration time is finite, i.e. the retained particles concentration in the porous medium increases from zero to the limit value in a finite time.
- At each point in the porous medium, the filtration time depends linearly on the distance to the inlet.
- An exact solution to the model in explicit form is obtained. The solution has a different form in the standard filtration zone and in the traveling wave zone.
- The concentrations of suspended and retained particles are related by a simple algebraic relationship - the Riemann invariant.

## REFERENCES


1. **Zhou Z., Zang H., Wang S., Du X., Ma D., Zhang J.** Filtration Behavior of Cement-Based Grout in Porous Media // Transport in Porous Media, 2018, vol. 125, pp. 435–463.
2. **Xie B., Cheng H., Wang X., Yao Z., Rong C., Zhou R., Zhang L., Guo L., Yu H., Xiong, W., Xiang X.** Theoretical Research on Diffusion Radius of Cement-Based Materials Considering the Pore Characteristics of Porous Media // Materials, 2022, vol. 15, 7763.
3. **Zhu G., Zhang Q., Liu R., Bai J., Li W., Feng X.** Experimental and Numerical Study on the Permeation Grouting Diffusion Mechanism considering Filtration Effects // Geofluids, 2021, 6613990.
4. **Wang X., Cheng H., Yao Z., Rong C., Huang X., Liu X.** Theoretical Research on Sand Penetration Grouting Based on Cylindrical Diffusion Model of Tortuous Tubes // Water, 2022, vol. 14, 1028.
5. **Faramarzi L., Rasti A., Abtahi S.M.** An Experimental Study of the Effect of Cement and Chemical Grouting on the Improvement of the Mechanical and Hydraulic Properties of Alluvial Formations // Journal of Construction & Building Materials, 2016, vol. 126, pp. 32–43.
6. **Tsuji M., Kobayashi S., Mikake S., Sato T., Matsui H.** Post-Grouting Experiences for Reducing Groundwater Inflow at 500 m Depth of the Mizunami Underground Research Laboratory, Japan // Procedia Engineering, 2017, vol. 191, pp. 543–550.
7. **Rabinovich A., Bedrikovetsky P., Tartakovsky D.** Analytical model for gravity segregation of horizontal multiphase flow in porous media // Physics of Fluids, 2020, vol. 32 (4), pp. 1–15.
8. **Kuzmina L., Osipov Y.** Deep bed filtration with multiple pore-blocking mechanisms // MATEC Web of Conferences, 2018, vol. 196, 04003, pp. 1–6.
9. **Kuzmina L.I., Osipov Y.V., Sosedka M.G.** Modelling of filtration with two capture mechanisms // Lecture Notes in Civil Engineering, 2023, vol. 282, pp. 21–31.
10. **Santos A., Bedrikovetsky P.** Size exclusion during particle suspension transport in porous media: stochastic and averaged equations // Computational and Applied Mathematics, 2004, vol. 23(2-3), pp. 259–284.
11. **Altoe J.E., Bedrikovetsky P., Siqueira A.G., de Souza A.L.S., Shecaira F.S.** Correction of basic equations for deep bed filtration with dispersion // Journal of Petroleum Science and Engineering, 2006, vol. 51, pp. 68–84.
12. **Iritani, E., Katagiri, N.** Developments of Blocking Filtration Model in Membrane Filtration // KONA Powder and Particle Journal, 2016, vol. 33, pp. 179–202.
13. **Tien, C., Ramarao, B., Yasarla, R.** A blocking model of membrane filtration //

Chemical Engineering Science, 2014, vol. 111, pp. 421–431.
14. **Kuzmina L.I., Osipov Yu.V.** Determining the Lengmur coefficient of the filtration problem // International Journal for Computational Civil and Structural Engineering, 2020, vol. 16(4), pp. 48–54.
15. **Bedrikovetsky, P.** Upscaling of stochastic micro model for suspension transport in porous media // Transport in Porous Media, 2008, vol. 75, pp. 335–369.
16. **Kuzmina L.I., Osipov Yu.V., Vetoshkin N.V.** Calculation of long-term filtration in a porous medium. // International Journal for Computational Civil and Structural Engineering, 2018, vol. 14(1), pp. 92-101.
17. **Kuzmina L., Osipov Y.** Long-term filtration of particles in a porous medium // BIO Web of Conferences, 2024, vol. 107, 03003.
18. **Kuzmina L.I., Nazaikinskii V.E., Osipov Y.V.** On a Deep Bed Filtration Problem with Finite Blocking Time // Russian Journal of Mathematical Physics, 2019, vol. 26(1), pp. 130–134.
19. **Herzig J.P., Leclerc D.M., Le Goff P.** Flow of Suspensions Through Porous Media – Application to Deep Filtration // Journal of Industrial & Engineering Chemistry, 1970, vol. 62(8), pp. 8–35.
20. **Logan J.D.** Transport Modeling in Hydrogeochemical Systems, Interdisciplinary Applied Mathematics, vol 15, Springer, New York, 2001.
21. **Kuzmina L., Osipov Y.** Traveling Wave Solution to Filtration Model in Porous Medium // Advances in Transdisciplinary Engineering, 2023, vol. 43, pp. 450–455.
22. **Courant R., Hilbert D.** Partial differential equations, Reprint of the 1962 Original, Edited, Wiley-InterScience, New York, 1989.
23. **Polyanin A.D., Manzhirov A.V.** Handbook of mathematics for engineers and scientists, Chapman & Hall/CRC, Boca Raton, FL, 2006.
24. **Vyazmina E.A., Bedrikovetskii P.G., Polyanin A.D.** New classes of exact solutions to nonlinear sets of equations in the theory of filtration and convective mass transfer // Theoretical Foundations of Chemical Engineering, 2007, vol. 41(5), pp. 556–564.
25. **Wang D., Ge L., He J., Zhang W., Jaisi D.P., Zhou D.** Hyperexponential and nonmonotonic retention of polyvinylpyrrolidone-coated silver nanoparticles in an Ultisol // Journal of Contaminant Hydrology, 2014; vol. 164, pp. 35–48.
26. **Leisi R., Bieri J., Roth N.J., Ros C.** Determination of parvovirus retention profiles in virus filter membranes using laser scanning microscopy // Journal of Membrane Science, 2020, vol. 603, 118012.
27. **Yuan H., Shapiro A.A.** A mathematical model for non-monotonic deposition profiles in deep bed filtration systems // Chemical Engineering Journal, 2011, vol. 166, pp. 105–115.
28. **Malgaresi G., Collins B., Alvaro P., Bedrikovetsky P.** Explaining non-monotonic retention profiles during flow of size-distributed colloids // Chemical Engineering Journal, 2019, vol. 375, 121984.
29. **Bedrikovetsky, P.** Mathematical theory of oil and gas recovery: with applications to ex-USSR oil and gas fields, Springer Science & Business Media, Des Moines, 2013.
30. **Alvarez A.C., Bedrikovetsky P.G., Hime G., Marchesin A.O., Marchesin D., Rodrigues J.R.** A fast inverse solver for the filtration function for flow of water with particles in porous media // Inverse Problems, 2006, vol. 22, pp. 69–88.
31. **Alvarez A.C., Hime G., Marchesin D., Bedrikovetsky P.G.** The inverse problem of determining the filtration function and permeability reduction in flow of water with

particles in porous media // Transport in Porous Media, 2007, vol. 70(1), pp. 43–62.
32. **Kuzmina L., Osipov Y.** Inverse Filtration Problem of Multiparticle Suspension // Advances in Transdisciplinary Engineering, 2024, vol. 62, , pp. 2-11.
33. **Du X., Wong G.K.** Predicting filtration coefficient and formation damage coefficient for particle flow in porous media using machine learning // Results in Engineering, 2025, vol. 25, 104545.

## СПИСОК ЛИТЕРАТУРЫ

1. **Zhou Z., Zang H., Wang S., Du X., Ma D., Zhang J.** Filtration Behavior of Cement-Based Grout in Porous Media // Transport in Porous Media, 2018, vol. 125, pp. 435–463.
2. **Xie B., Cheng H., Wang X., Yao Z., Rong C., Zhou R., Zhang L., Guo L., Yu H., Xiong, W., Xiang X.** Theoretical Research on Diffusion Radius of Cement-Based Materials Considering the Pore Characteristics of Porous Media // Materials, 2022, vol. 15, 7763.
3. **Zhu G., Zhang Q., Liu R., Bai J., Li W., Feng X.** Experimental and Numerical Study on the Permeation Grouting Diffusion Mechanism considering Filtration Effects // Geofluids, 2021, 6613990.
4. **Wang X., Cheng H., Yao Z., Rong C., Huang X., Liu X.** Theoretical Research on Sand Penetration Grouting Based on Cylindrical Diffusion Model of Tortuous Tubes // Water, 2022, vol. 14, 1028.
5. **Faramarzi L., Rasti A., Abtahi S.M.** An Experimental Study of the Effect of Cement and Chemical Grouting on the Improvement of the Mechanical and Hydraulic Properties of Alluvial Formations // Journal of Construction & Building Materials, 2016, vol. 126, pp. 32–43.
6. **Tsuji M., Kobayashi S., Mikake S., Sato T., Matsui H.** Post-Grouting Experiences for Reducing Groundwater Inflow at 500 m Depth of the Mizunami Underground Research Laboratory, Japan // Procedia Engineering, 2017, vol. 191, pp. 543–550.
7. **Rabinovich A., Bedrikovetsky P., Tartakovsky D.** Analytical model for gravity segregation of horizontal multiphase flow in porous media // Physics of Fluids, 2020, vol. 32 (4), pp. 1–15.
8. **Kuzmina L., Osipov Y.** Deep bed filtration with multiple pore-blocking mechanisms // MATEC Web of Conferences, 2018, vol. 196, 04003, pp. 1–6.
9. **Kuzmina L.I., Osipov Y.V., Sosedka M.G.** Modelling of filtration with two capture mechanisms // Lecture Notes in Civil Engineering, 2023, vol. 282, pp. 21–31.
10. **Santos A., Bedrikovetsky P.** Size exclusion during particle suspension transport in porous media: stochastic and averaged equations // Computational and Applied Mathematics, 2004, vol. 23(2-3), pp. 259–284.
11. **Altoe J.E., Bedrikovetsky P., Siqueira A.G., de Souza A.L.S., Shecaira F.S.** Correction of basic equations for deep bed filtration with dispersion // Journal of Petroleum Science and Engineering, 2006, vol. 51, pp. 68–84.
12. **Iritani, E., Katagiri, N.** Developments of Blocking Filtration Model in Membrane Filtration // KONA Powder and Particle Journal, 2016, vol. 33, pp. 179–202.
13. **Tien, C., Ramarao, B., Yasarla, R.** A blocking model of membrane filtration // Chemical Engineering Science, 2014, vol. 111, pp. 421–431.
14. **Kuzmina L.I., Osipov Yu.V.** Determining the Lengmur coefficient of the filtration problem // International Journal for Computational Civil and Structural Engineering, 2020, vol. 16(4), pp. 48–54.
15. **Bedrikovetsky, P.** Upscaling of stochastic micro model for suspension transport in porous media // Transport in Porous Media, 2008, vol. 75, pp. 335–369.
16. **Kuzmina L.I., Osipov Yu.V., Vetoshkin N.V.** Calculation of long-term filtration in a porous medium. // International Journal for

Computational Civil and Structural Engineering, 2018, vol. 14(1), pp. 92-101.
17. **Kuzmina L., Osipov Y.** Long-term filtration of particles in a porous medium // BIO Web of Conferences, 2024, vol. 107, 03003.
18. **Kuzmina L.I., Nazaikinskii V.E., Osipov Y.V.** On a Deep Bed Filtration Problem with Finite Blocking Time // Russian Journal of Mathematical Physics, 2019, vol. 26(1), pp. 130–134.
19. **Herzig J.P., Leclerc D.M., Le Goff P.** Flow of Suspensions Through Porous Media – Application to Deep Filtration // Journal of Industrial & Engineering Chemistry, 1970, vol. 62(8), pp. 8–35.
20. **Logan J.D.** Transport Modeling in Hydrogeochemical Systems, Interdisciplinary Applied Mathematics, vol 15, Springer, New York, 2001.
21. **Kuzmina L., Osipov Y.** Traveling Wave Solution to Filtration Model in Porous Medium // Advances in Transdisciplinary Engineering, 2023, vol. 43, pp. 450–455.
22. **Courant R., Hilbert D.** Partial differential equations, Reprint of the 1962 Original, Edited, Wiley-InterScience, New York, 1989.
23. **Polyanin A.D., Manzhirov A.V.** Handbook of mathematics for engineers and scientists, Chapman & Hall/CRC, Boca Raton, FL, 2006.
24. **Vyazmina E.A., Bedrikovetskii P.G., Polyanin A.D.** New classes of exact solutions to nonlinear sets of equations in the theory of filtration and convective mass transfer // Theoretical Foundations of Chemical Engineering, 2007, vol. 41(5), pp. 556–564.
25. **Wang D., Ge L., He J., Zhang W., Jaisi D.P., Zhou D.** Hyperexponential and nonmonotonic retention of polyvinylpyrrolidone-coated silver nanoparticles in an Ultisol // Journal of Contaminant Hydrology, 2014; vol. 164, pp. 35–48.
26. **Leisi R., Bieri J., Roth N.J., Ros C.** Determination of parvovirus retention profiles in virus filter membranes using laser scanning microscopy // Journal of Membrane Science, 2020, vol. 603, 118012.
27. **Yuan H., Shapiro A.A.** A mathematical model for non-monotonic deposition profiles in deep bed filtration systems // Chemical Engineering Journal, 2011, vol. 166, pp. 105–115.
28. **Malgaresi G., Collins B., Alvaro P., Bedrikovetsky P.** Explaining non-monotonic retention profiles during flow of size-distributed colloids // Chemical Engineering Journal, 2019, vol. 375, 121984.
29. **Bedrikovetsky, P.** Mathematical theory of oil and gas recovery: with applications to ex-USSR oil and gas fields, Springer Science & Business Media, Des Moines, 2013.
30. **Alvarez A.C., Bedrikovetsky P.G., Hime G., Marchesin A.O., Marchesin D., Rodrigues J.R.** A fast inverse solver for the filtration function for flow of water with particles in porous media // Inverse Problems, 2006, vol. 22, pp. 69–88.
31. **Alvarez A.C., Hime G., Marchesin D., Bedrikovetsky P.G.** The inverse problem of determining the filtration function and permeability reduction in flow of water with particles in porous media // Transport in Porous Media, 2007, vol. 70(1), pp. 43–62.
32. **Kuzmina L., Osipov Y.** Inverse Filtration Problem of Multiparticle Suspension // Advances in Transdisciplinary Engineering, 2024, vol. 62, , pp. 2-11.
33. **Du X., Wong G.K.** Predicting filtration coefficient and formation damage coefficient for particle flow in porous media using machine learning // Results in Engineering, 2025, vol. 25, 104545.

*Liudmila I. Kuzmina*, Candidate of Physical and Mathematical Sciences, Associate Professor, Department of Applied Mathematics, National Research University Higher School of Economics, 101000, Russia, Moscow, Myasnitskaya st., 20, e-mail: lkuzmina@hse.ru.

*Yuri V. Osipov*, Candidate of Physical and Mathematical Sciences, Professor, Department of Computer Science and Applied Mathematics, Moscow State University of Civil Engineering, 129337, Russia, Moscow, Yaroslavskoe Shosse, 26, e-mail: yuri-osipov@mail.ru.

*Кузьмина Людмила Ивановна*, доцент, кандидат физико-математических наук, Департамент прикладной математики МИЭМ им. А.Н. Тихонова, Национальный исследовательский университет «Высшая школа экономики»; 101000, г. Москва, ул. Мясницкая, д. 20, e-mail: lkuzmina@hse.ru.

*Осипов Юрий Викторович,* профессор, кандидат физико-математических наук, кафедра информатики и прикладной математики Национального исследовательского Московского государственного строительного университета; 129337, Россия, г. Москва, Ярославское шоссе, д. 26; e-mail: yuri-osipov@mail.ru.

International Journal for Computational Civil and Structural Engineering, 21(3) 148–157 (2025)

DOI:10.22337/2587-9618-2025-21-3-148-157

# AXISIMMETRIC FLUID MOTION IN A POROUS MEDIUM IN THE PRESENCE OF A NON-STATIONARY EXTERNAL SOURCE OR ABSORPTION

***Yuri A. Chirkunov [1], Yuri L. Skolubovich [1], Mihail Yu. Chirkunov [1], Sergey V. Fedosov [2], Vladimir N. Sidorov [2], Evgeniy V. Alekseev [2]***

[1] Novosibirsk State University of Architecture and Civil Engineering (Sibstrin), Novosibirsk, RUSSIA
[2] National Research Moscow State University of Civil Engineering, Moscow, RUSSIA

**Abstract:** The generalized axisymmetric model of fluid motion in a porous medium in the presence of a non-stationary external source or absorption is studied by methods of group (symmetry) analysis of differential equations. All its invariant submodels of rank 1 are studied. They are specified by invariant solutions of rank 1 of the equation of the original model. These solutions are obtained either explicitly, or their search is reduced to solving systems of ordinary differential equations of the first order. For explicit solutions at specific values of the parameters included in their expressions, graphs of the pressure distribution in the porous medium are constructed. The remaining solutions are used to study physically meaningful boundary value problems for which, at the initial moment of time, the pressure and either the rate of its change along the axis of symmetry or the radial rate of its change are specified at a fixed point of the medium. These boundary value problems are solved numerically for some specific values of the parameters included in them. Graphs of the functions determining these solutions are obtained. The conducted research is relevant in many areas of applied science and technology: filtration, soil mechanics, rock mechanics, oil field engineering, construction engineering, petroleum geology, biology and biophysics, materials science.

**Keywords:** axisymmetric model of fluid motion, porous medium, non-stationary external source, non-stationary external absorption, symmetry analysis, invariant solutions, invariant submodels

# ОСЕСИММЕТРИЧНОЕ ДВИЖЕНИЕ ЖИДКОСТИ В ПОРИСТОЙ СРЕДЕ ПРИ НАЛИЧИИ НЕСТАЦИОНАРНОГО ВНЕШНЕГО ИСТОЧНИКА ИЛИ ПОГЛОЩЕНИЯ

***Ю.А. Чиркунов [1], Ю.Л. Сколубович [1], М.Ю. Чиркунов [1], С.В. Федосов [2], В.Н. Сидоров [2], Е.В. Алексеев [2]***

[1] Новосибирский государственный архитектурно-строительный университет (Сибстрин), г. Новосибирск, РОССИЯ
[2] Национальный исследовательский Московский государственный строительный университет, г. Москва, РОССИЯ

**Аннотация:** Методами группового (симметрийного) анализа дифференциальных уравнений изучается обобщенная осесимметричная модель движения жидкости в пористой среде при наличии нестационарного внешнего источника или поглощения. Изучаются все ее инвариантные подмодели ранга 1. Они задаются инвариантными решениями ранга 1 уравнения исходной модели. Эти решения либо получаются в явном виде, либо их поиск сводится к решению систем обыкновенных дифференциальных уравнений первого порядка. Для явных решений при конкретных значениях входящих в их выражения параметров строятся графики распределения давления в пористой среде. Оставшиеся решения используются для исследования физически содержательных краевых задач, для которых в начальный момент времени в фиксированной точке среды задаются давление и либо скорость его изменения вдоль оси симметрии, либо радиальная скорость его изменения. Эти краевые задачи решаются численно при некоторых конкретных значениях входящих в них параметров. Получены графики функций, определяющих эти решения. Проведенные исследования актуальны во многих областях прикладной науки и техники: фильтрация, механика грунтов, механика горных пород, нефтепромысловое дело, строительство, нефтяная геология, биология и биофизика, материаловедение.

**Ключевые слова:** осесимметричная модель движения жидкости, пористая среда, нестационарный внешний источник, нестационарное внешнее поглощение, симметрийный анализ, инвариантные решения, инвариантные подмодели

## INTRODUCTION

The classical model of fluid motion in a porous medium has been studied in many works (see, for example, [1 – 7] and the large bibliography provided there). However, the study of this fluid motion within the framework of the classical model does not always adequately describe real processes. First of all, this applies to processes with an external non-stationary source or absorption.

The study of rank 0 invariant submodels for a general three-dimensional model of fluid motion in a porous medium in the presence of an external non-stationary source or absorption was started in [8, 9].

In [10], rank 1 invariant submodels were studied for a general two-dimensional model of fluid motion in a porous medium in the presence of an external non-stationary source or absorption.

In our work we will study an axisymmetric model describing the motion of a fluid in a porous medium in the presence of an external non-stationary source or absorption. This model is obtained from the classical model by adding a term describing the presence of an external source or absorption. It is specified by the following partial differential equation

$$\partial_t q = \left(\partial_r^2 + \frac{1}{r}\partial_r + \partial_z^2\right)\left(q^\lambda\right) + g\left(t\right)q, \quad (1)$$

where $q = q\left(t,\boldsymbol{x}\right)$ is a pressure, $t$ is a time, $\boldsymbol{x} = \left(x,y,z\right) \in R^3$; $r = \sqrt{x^2 + y^2}$; $\lambda$ ($\lambda\left(\lambda - 1\right) \neq 0$) is arbitrary real number, characterizing the nonlinearity of the process, a function $g\left(t\right)$ defines a non-stationary external source or absorption. For each real process, this function is specified empirically. The case $g\left(t\right) > 0$ corresponds to the presence of an external source. The case $g\left(t\right) < 0$ corresponds to the presence of external absorption.

Let

$$g\left(t\right) = \frac{\left(\ln f'\left(t\right)\right)'}{\lambda - 1},$$

where $f\left(t\right) \neq k_1 \exp t + k_2$ ($k_1$, $k_2$ are arbitrary real numbers). The prime denotes, as everywhere below, the derivative of a function with respect to its argument.

Each solution of equation (1) defines a certain submodel of the general model. Our goal is to study all invariant submodels of rank 1.

## METHODS

The main method of studying equation (1) is group (symmetry) analysis of differential equations. Group analysis is one of the most effective ways of obtaining maximum information about the properties of solutions of differential equations. The basic concepts and algorithms of modern group analysis of differential equations can be found, for example, in [11–15] and the references provided there.

## RESULTS AND DISCUSSION

The following mathematical results were obtained by group (symmetry) analysis methods:

1. The main Lie group of transformations of differential equation (1) was found.
2. Using the obtained group of internal automorphisms, optimal systems of subgroups of the main group were constructed.

3. For each subgroup of these optimal systems, its universal invariant in the space $R^4(t,r,z,u)$ was found. This allows us to write down a representation of each invariant solution of equation (1).
For the convenience of the reader, we omit all the indicated calculations.
Using all the obtained representations of invariant solutions of rank 1, we investigate these solutions. These solutions define 4 sub-models of the main model.

**The first submodel**
This submodel is defined by a solution having the representation

$$p=\left(z^{2-\alpha}f'(t)\right)^{\frac{1}{\lambda-1}}U(\xi),\quad \xi=\frac{r}{z}, \qquad (2)$$

where $\alpha$ is arbitrary real number.
After substitution (2) into (1) we obtain the following equation for the function $U=U(\xi)$:

$$\left(\xi^2+1\right)\left(U^\lambda\right)''+\left(\frac{1}{\xi}+2\beta\xi\right)\left(U^\lambda\right)'+ \\ +\lambda\beta\left(\beta+1\right)U^\lambda=0,\quad \beta=\frac{\lambda(\alpha-2)}{\lambda-1}. \qquad (3)$$

**1.** At $\alpha=2$ the solution of this equation has a form

$$U=\left(c_1+c_2\left(\sqrt{\xi^2+1}+\ln\frac{\xi}{1+\sqrt{\xi^2+1}}\right)\right)^\lambda, \qquad (4)$$

where $c_1$, $c_2$ are arbitrary real numbers.
From (2) and (4) it follows that the pressure is determined by the formula

$$p=\left(f'(t)\right)^{\frac{1}{\lambda-1}}\left(c_1+c_2\left(\frac{\sqrt{r^2+z^2}}{z}+ \right.\right. \\ \left.\left.+\ln\frac{r}{z+\sqrt{r^2+z^2}}\right)\right)^\lambda. \qquad (5)$$

At each fixed moment in time, the pressure is the same at all points on each conical surface $r=cz$ $(c=const>0)$.
When $c_1=0$, $c_2=1$, $\lambda=2$, $f(t)=2t^2+2t+1$, $r=2$, $z>0$ the pressure distribution is shown in Fig. 1.

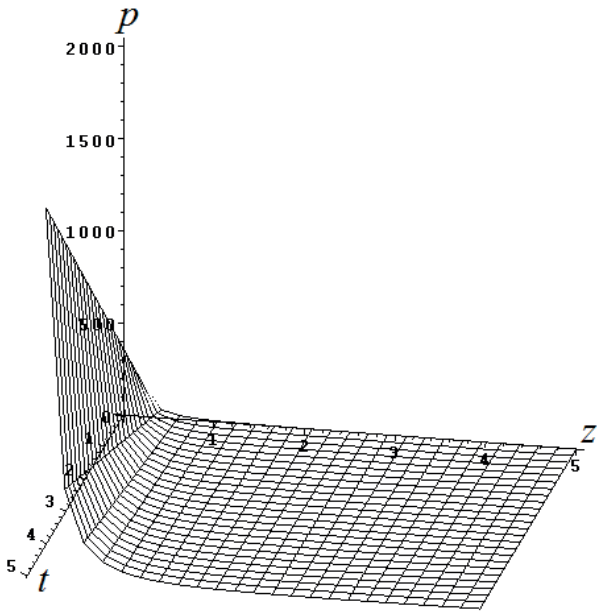


*Figure 1. Pressure distributions at $r=2$*

In this case, the pressure increases monotonically over time under the influence of an external source and tends to infinity at $t\to\infty$.
2. At $\alpha\neq 2$ the solution of equation (3) is equivalent to the following system

$$W'=\frac{1}{\xi^2+1}\left(V-\left(\frac{1}{\xi}+(2\beta-1)\xi\right)W\right), \\ V'=-\left(\beta^2+3\beta-2+\frac{1}{\xi}\right)W. \qquad (6)$$

Namely: 1) for any solution $\left(W\left(\xi\right),V\left(\xi\right)\right)$ of system (6) the function $U=W^{\frac{1}{\lambda}}$ satisfies to equation (3), 2) conversely, for any solution $U\left(\xi\right)$ of equation (3) pair of the functions

$$W\left(\xi\right)=U^{\lambda}\left(\xi\right),$$
$$V\left(\xi\right)=\lambda\left(\xi^2+1\right)U^{\lambda-1}\left(\xi\right)U'\left(\xi\right)+$$
$$+\left(\frac{1}{\xi}+2\left(\beta-1\right)\xi\right)U^{\lambda}\left(\xi\right)$$

satisfies to system (6).

Let us find the pressure distribution if at the initial moment of time $t=t_0\geq 0$ at a fixed point $\left(r_0,z_0\right)$ the pressure and its radial derivative are given

$$p\left(t_0,r_0,z_0\right)=p_0>0,\quad p_r\left(t_0,r_0,z_0\right)=p_1,$$
$$r_0>0,\quad z_0>0, \tag{7}$$

where $p_0>0,\quad p_1$ are arbitrary real numbers.

In this case the initial data for system (6) have the form

$$W\left(\xi_0\right)=\left(z_0^{2-\alpha}f'\left(t_0\right)\right)^{\mu}p_0^{\lambda},\quad \mu=\frac{\lambda}{1-\lambda},$$
$$V\left(\xi_0\right)=z_0^{\beta-1}\left(f'\left(t_0\right)\right)^{\mu}p_0^{\lambda-1}\cdot$$
$$\left(\lambda\left(r_0^2+z_0^2\right)p_1+\frac{1}{r_0}\left(2\left(\beta-1\right)r_0^2+z_0^2\right)p_0\right), \tag{8}$$
$$\xi_0=\frac{r_0}{z_0}.$$

Due to the smoothness of the right-hand sides of system (6), the solution to the Cauchy problem (6), (8) exists and is unique in the neighborhood of the point $\xi_0$.

According to the formula

$$p=\left(z^{2-\alpha}f'(t)\right)^{\frac{1}{1-\lambda}}W^{\frac{1}{\lambda}}\left(\xi\right),\quad \xi=\frac{r}{z}. \tag{9}$$

we obtain a unique solution of equation (1) satisfying to conditions (7), for which the value $\left(z^{\alpha-2}h(t)\right)^{\frac{1}{1-\lambda}}p\left(t,r,z\right)$ is constant along each conical surface $r=cz\quad\left(c=const>0\right)$.

For example, when $t_0=0,\quad \lambda=\frac{3}{2},\quad \alpha=1,$ $r_0=1,\quad z_0=1,\quad p_0=16,\quad p_1=-1,\quad z>0,$ $f\left(t\right)=t^2+t+1$ for the Cauchy problem (6), (8) the numerical solution by the Runge-Kutta-Felberg method [16] (with an order of accuracy of 4) is shown in Fig. 2.

From this graph, by virtue of formula (9), it follows that the pressure increases monotonically over time under the influence of an external source and tends to infinity at $t\to\infty$.

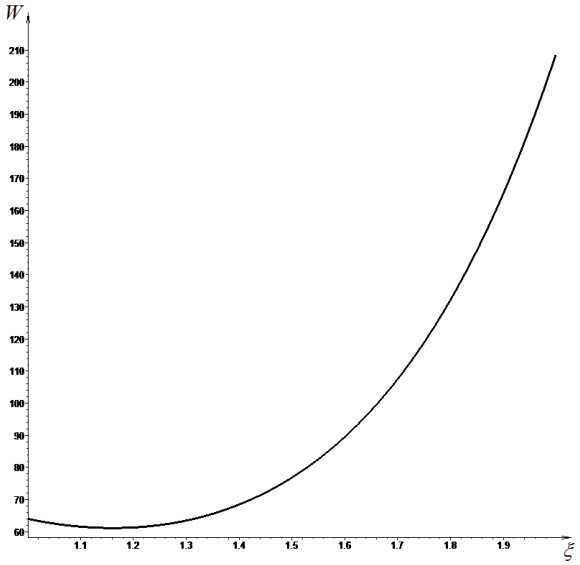


*Figure 2. Graph of the function* $W\left(\xi\right)$

From this graph, by virtue of formula (9), it follows that the pressure increases

monotonically over time under the influence of an external source and tends to infinity at $t \to \infty$.

**The second submodel**

This submodel is defined by a solution having the representation

$$p = \left(f'(t)\right)^{\frac{1}{\lambda-1}} \exp\left(\frac{z}{1-\lambda}\right) U\left(r\right). \qquad (10)$$

Substituting (10) into (1) yields the equation

$$\left(U^{\lambda}\right)'' + \frac{1}{r}\left(U^{\lambda}\right)' + \left(\frac{\lambda}{\lambda-1}\right)^2 U^{\lambda} = 0$$

whose general solution is

$$U = \left(c_3 J_0\left(\left|\frac{\lambda}{\lambda-1}\right| r\right) + c_4 Y_0\left(\left|\frac{\lambda}{\lambda-1}\right| r\right)\right)^{\frac{1}{\lambda}}$$

where $J_0(x)$ is the Bessel function of the first kind of the zero order, and $Y_0(x)$ is the Bessel function of the second kind of the zero order, $c_3$, $c_4$ are arbitrary real numbers.

The pressure is determined by the formula

$$p = \left(f'(t)\right)^{\frac{1}{\lambda-1}} \exp\left(\frac{z}{1-\lambda}\right) \cdot \left(c_3 J_0\left(\left|\frac{\lambda}{\lambda-1}\right| r\right) + c_4 Y_0\left(\left|\frac{\lambda}{\lambda-1}\right| r\right)\right)^{\frac{1}{\lambda}}. \qquad (11)$$

On each cylindrical surface $r = const > 0$ the pressure is distributed according to the formula

$$p = c\left(f'(t)\right)^{\frac{1}{\lambda-1}} \exp\left(\frac{z}{1-\lambda}\right).$$

For example, at $c_3 = 1$, $c_4 = 0$, $\lambda = \frac{1}{4}$, $r = 2$, $z > 0$, $f(t) = (t+1)^2$ the pressure distribution is shown in Fig. 3.

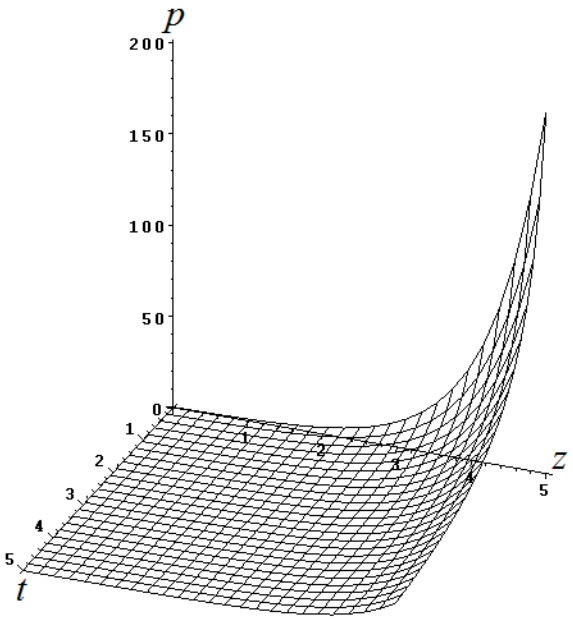


*Figure 3. Pressure distribution on a cylindrical surface $r = 2$*

In this case, the pressure on the cylindrical surface $r = 2$ decreases monotonically over time under the influence of external absorption and tends to zero at $t \to \infty$.

**The third submodel**

This submodel is defined by a solution having the representation

$$p = \left(rf'(t)\right)^{\frac{1}{\lambda-1}} U(\xi), \quad \xi = \frac{f(t)-z}{r}. \qquad (12)$$

Substituting (12) into (1) yields the equation

$$\left(\xi^2+1\right)\left(U^\lambda\right)''-\frac{\lambda+1}{\lambda-1}\xi\left(U^\lambda\right)'-U'+ \\ +\left(\frac{\lambda}{\lambda-1}\right)^2 U^\lambda=0. \tag{13}$$

Equation (13) is equivalent to the system

$$U'=U^{1-\lambda}W,$$

$$W'=\frac{1}{\xi^2+1}\left(\frac{1}{\lambda}U^{1-\lambda}W-\frac{\lambda}{\left(\lambda-1\right)^2}U^\lambda+\right. \tag{14}$$

$$\left.+\frac{\lambda+1}{\lambda-1}\xi W\right).$$

Let the pressure and its rate of change along the axis $Oz$ are given at the initial moment of time $t=t_0\geq 0$ at a fixed point with coordinates $r=r_0>0,\ \ z=z_0$:

$$p\left(t_0,r_0,z_0\right)=p_0>0,\ \ p_z\left(t_0,r_0,z_0\right)=p_1, \tag{15}$$

where $p_0>0,\ \ p_2$ are arbitrary real numbers. The initial data for system (14) have the form

$$U\left(\xi_0\right)=\left(r_0f'(t_0)\right)^{\frac{1}{1-\lambda}}p_0, \\ W\left(\xi_0\right)=r_0^{\frac{1}{1-\lambda}}\left(f'(t_0)\right)^{\frac{\lambda}{1-\lambda}}p_0^{\frac{1}{1-\lambda}}p_2, \tag{16}$$

$$\xi_0=\frac{f\left(t_0\right)-z_0}{r_0}.$$

Due to the smoothness of the right-hand sides of system (14), the solution of the Cauchy problem (14), (16) exists and is unique in the neighborhood of the point $\xi_0$.

Applying formula (12), we obtain a unique solution to equation (1) that satisfies to the conditions (15), for which the value $\left(rf'\left(t\right)\right)^{\frac{1}{1-\lambda}}p\left(t,r,z\right)$ is constant along each Trajectory $z=f\left(t\right)-cr\ \ \left(c=const\right)$.

For example, at $t_0=0,\ \beta=2,\ r_0=1,$ $z_0=1,\ \ p_0=4,\ \ p_2=1,\ \ z>0$ the Cauchy problem (14), (16) is solved numerically by the Runge-Kutta-Felberg method [16] (with an order of accuracy of 4). The graph of the function $U\left(\xi\right)$ is shown in Fig. 4.

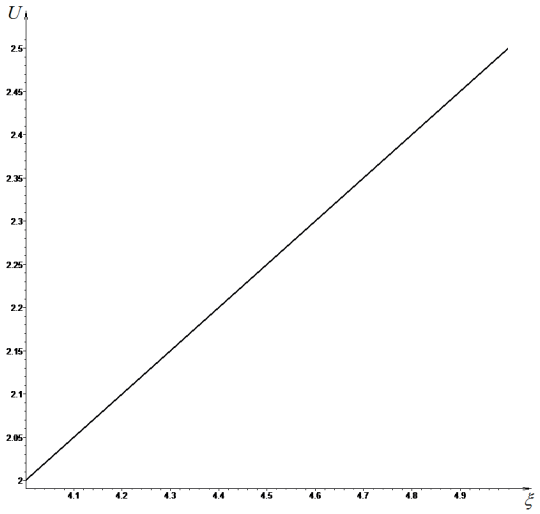


*Figure 4. Graph of the function* $U\left(\xi\right)$

From this graph, by virtue of formula (12), it follows that the pressure increases monotonically over time under the influence of an external source and tends to infinity at $t\to\infty$.

**The fourth submodel**

This submodel is defined by a solution having the representation

$$p=\left(\frac{f'(t)}{f\left(t\right)}z^2\right)^{\frac{1}{\lambda-1}}U\left(\xi\right),\ \ \xi=\frac{r}{z}. \tag{17}$$

After substitution (17) into (1) we obtain the following equation for the function $U = U(\xi)$:

$$\left(\xi^2+1\right)\left(U^\lambda\right)'' + \left(\frac{1}{\xi} - \frac{2(2\lambda-1)}{\lambda-1}\xi\right)\left(U^\lambda\right)' - \\ - \frac{\lambda^2\left(3\lambda-13\right)}{\lambda-1}U^\lambda - \frac{1}{(\lambda-1)}U = 0.$$

This equation is equivalent to the system

$$U' = U^{1-\lambda}W,$$
$$W' = \frac{1}{\xi^2+1}\left(\frac{1}{\lambda}U^{1-\lambda}W - \frac{\lambda}{(\lambda-1)^2}U^\lambda + \right. \quad (18)$$
$$\left. + \frac{\lambda+1}{\lambda-1}\xi W\right).$$

If at the initial moment of time $t = t_0 \geq 0$ at a fixed point with coordinates $r = r_0 > 0$, $z = z_0 > 0$ the pressure and its radial derivative are given by formulas (7), then the initial data for system (18) have the form

$$U\left(\xi_0\right) = \left(z_0^2\frac{f'(t_0)}{f(t_0)}\right)^{\frac{1}{1-\lambda}} p_0, \quad \xi_0 = \frac{r_0}{z_0}, \quad (19)$$
$$W\left(\xi_0\right) = z_0^{\frac{\lambda+1}{1-\lambda}}\left(\frac{f'(t_0)}{f(t_0)}\right)^{\frac{\lambda}{1-\lambda}} p_0^{\lambda-1}p_1.$$

Due to the smoothness of the right-hand sides of system (18), the solution of the Cauchy problem (18), (19) exists and is unique in the neighborhood of the point $\xi_0$.

Applying formula (17), we obtain a unique solution of equation (1) satisfying to conditions (7), for which the value

$$\left(\frac{f'(t)}{f(t)}z^2\right)^{\frac{1}{1-\lambda}} p\left(t,r,z\right)$$

is constant along each conical surface $r = cz$ $(c=const>0)$. For example, when $t_0 = 0$, $\alpha = 1.8$, $r_0 = 1$, $z > 0$ for the Cauchy problem (18), (19) the numerical solution by the Runge-Kutta-Felberg method [16] (with an order of accuracy of 4) is shown in Fig. 5.

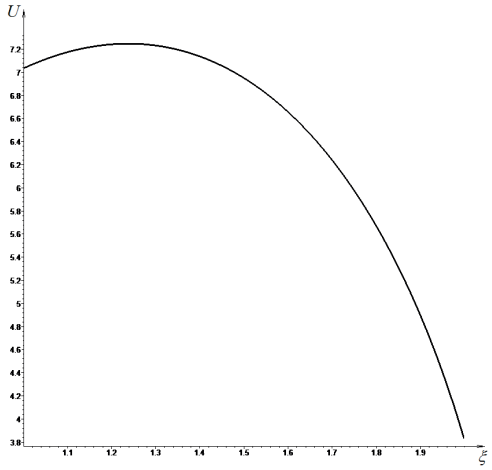


*Figure 5. Graph of the function* $U(\xi)$

From this graph, by virtue of formula (17), it follows that the pressure decreases monotonically over time under the influence of external absorption and tends to zero at $t \to \infty$.

## CONCLUSION

By the methods of group (symmetry) analysis of differential equations we used to study the generalized axisymmetric model of liquid or gas motion in a porous medium in the presence of a non-stationary external source or absorption, defined by equation (1).

All invariant submodels of rank 1 were obtained. They are defined by five invariant solutions of rank 1 of equation (1). These are solutions (5) and (11), found in explicit form, and solutions (9), (12) and (17), the search for which is reduced to systems of ordinary

differential equations of the first order (6), (14) and (18), respectively.

For solutions (5) and (11) for some specific values of the parameters included in them, pressure distribution graphs are constructed. These graphs are shown in Figures 1 and 2. The physical meaning of these solutions is indicated. Solutions (9), (12) and (17) were used to study physically meaningful problems for which at the initial moment of time at a fixed point of the medium the pressure and either the radial rate of its change or the rate of its change along the axis of symmetry are specified. These problems are solved numerically for some specific values of the parameters included in them. Graphs of the functions determining these solutions are obtained. These graphs are shown in Figures 3, 4 and 5.

The significance of the solutions found is as follows:

1. They describe specific physical processes.
2. These solutions can be used as tests in numerical calculations when studying the motion of liquid or gas in a porous medium in the presence of a non-stationary external source or absorption.
3. The solutions found in the work depend on 5 arbitrary numerical parameters and one arbitrary function, which are determined empirically depending on the physical process under study. This allows using the submodels determined by these solutions to study other physically meaningful problems different from those considered in this work.

## ACKNOWLEDGEMENTS

The research was carried out with the financial support of the Industry Consortium “Construction and Architecture”.

## REFERENCES

1. **L.S. Leibenzon.** Collection of works: V. 2. Underground Hydro and Gas Dynamics. Moscow: Publishing house of the Academy of Sciences of the USSR. (1953). (in Russian).
2. **L.S. Leibenzon.** Collection of works: V. 3. Oil field mechanics. Moscow: Publishing house of the Academy of Sciences of the USSR. (1955). (in Russian).
3. **G.I. Barenblatt.** On some unsteady motions of a liquid or a gas in a porous medium. Prikl. Mat. Mekh. 16, 1 (1952), 67–78. (in Russian).
4. **Otto F.** “The geometry of dissipative evolution equations: The porous medium equation,” Commun. Partial Differ. Equations. 26 (1-2). (2001). 101–174.
5. **J.L. V´azquez.** The Porous Medium Equation. Mathematical Theory, vol. Oxford Mathematical Monographs. Oxford University Press. Oxford. (2007).
6. **C. Kienzler, H. Koch, and J.L. V´azquez.** Flatness implies smoothness for solutions of the porous medium equation. preprint arXiv:1609.09048.vl
7. **P.S. Casas and R. Quintanilla.** Exponential decay in one-dimensional porous-thermo-elasticity,” Mech. Res. Commun. 32. (2005). 652–658.
8. **Yu.A. Chirkunov, Yu.L. Skolubovich.** Nonlinear three-dimensional diffusion models of porous medium in the presence of non-stationary source or absorption and some exact solutions. Int. J. Non-Linear Mech. 106. (2018). 29–37.
9. **Yu.A. Chirkunov.** Self-similar waves in a three-dimensional porous medium in the presence of non-stationary singular source or absorption. Int. J. Non-Linear Mech. 117. (2019). 103205.
10. **Yu.A. Chirkunov, M.Yu. Chirkunov.** Submodels of 2-d model of the motion of fluid or gas in a porous medium with an external non-stationary source or absorption. Int. J. Non-Linear Mech. V. 163 (2024). 104759.
11. **L.V. Ovsyannikov.** Group Analysis of Differential Equations. New York: Academic Press). (1982).

12. **P.J. Olver.** Application of Lie groups to differential equations. Springer-Verlag. New York. (1986).
13. **Yu.A. Chirkunov.** Group analysis of linear and quasilinear differential equations. Novosibirsk: NSUEM. (2007). (In Russian).
14. **Yu.A. Chirkunov, S.V. Khabirov.** The Elements of Symmetry Analysis of Differential Equations of Continuous Mechanics. Novosibirsk. NSTU. (2012). (In Russian).
15. **Yu.A. Chirkunov.** Generalized Equivalence Transformations and group classification of systems of differential equations. J. Appl. Mech. Techn. Phys. 53 (2). (2012). 147–155.
16. **Butcher John C.** Numerical Methods for Ordinary Differential Equations. 3rd Edition. John Wiley & Sons. New York.

## СПИСОК ЛИТЕРАТУРЫ

1. **L.S. Leibenzon.** Collection of works: V. 2. Underground Hydro and Gas Dynamics. Moscow: Publishing house of the Academy of Sciences of the USSR. (1953). (in Russian).
2. **L.S. Leibenzon.** Collection of works: V. 3. Oil field mechanics. Moscow: Publishing house of the Academy of Sciences of the USSR. (1955). (in Russian).
3. **G.I. Barenblatt.** On some unsteady motions of a liquid or a gas in a porous medium. Prikl. Mat. Mekh. 16, 1 (1952), 67–78. (in Russian).
4. **Otto F.** "The geometry of dissipative evolution equations: The porous medium equation," Commun. Partial Differ. Equations. 26 (1-2). (2001). 101–174.
5. **J.L. V´azquez.** The Porous Medium Equation. Mathematical Theory, vol. Oxford Mathematical Monographs. Oxford University Press. Oxford. (2007).
6. **C. Kienzler, H. Koch, and J.L. V´azquez.** Flatness implies smoothness for solutions of the porous medium equation. preprint arXiv:1609.09048.vl
7. **P.S. Casas and R. Quintanilla.** Exponential decay in one-dimensional porous-thermo-elasticity," Mech. Res. Commun. 32. (2005). 652–658.
8. **Yu.A. Chirkunov, Yu.L. Skolubovich.** Nonlinear three-dimensional diffusion models of porous medium in the presence of non-stationary source or absorption and some exact solutions. Int. J. Non-Linear Mech. 106. (2018). 29–37.
9. **Yu.A. Chirkunov.** Self-similar waves in a three-dimensional porous medium in the presence of non-stationary singular source or absorption. Int. J. Non-Linear Mech. 117. (2019). 103205.
10. **Yu.A. Chirkunov, M.Yu. Chirkunov.** Submodels of 2-d model of the motion of fluid or gas in a porous medium with an external non-stationary source or absorption. Int. J. Non-Linear Mech. V. 163 (2024). 104759.
11. **L.V. Ovsyannikov.** Group Analysis of Differential Equations. New York: Academic Press). (1982).
12. **P.J. Olver.** Application of Lie groups to differential equations. Springer-Verlag. New York. (1986).
13. **Yu.A. Chirkunov.** Group analysis of linear and quasilinear differential equations. Novosibirsk: NSUEM. (2007). (In Russian).
14. **Yu.A. Chirkunov, S.V. Khabirov.** The Elements of Symmetry Analysis of Differential Equations of Continuous Mechanics. Novosibirsk. NSTU. (2012). (In Russian).
15. **Yu.A. Chirkunov.** Generalized Equivalence Transformations and group classification of systems of differential equations. J. Appl. Mech. Techn. Phys. 53 (2). (2012). 147–155.
16. **Butcher John C.** Numerical Methods for Ordinary Differential Equations. 3rd Edition. John Wiley & Sons. New York.

*Chirkunov Yuri Aleksandrovich* – Doctor of Physical and Mathematical Sciences, Associate Professor, Head of the Department of Higher Mathematics of the Federal State Budgetary Educational Institution of Higher Education " Novosibirsk State University of Architecture and Civil Engineering (Sibstrin)" (FGBOU "NGASU (Sibstrin)", office 305, building 113, Leningradskaya Street, Novosibirsk, 630008, Russia; e-mail: chr101@mail.ru

*Skolubovich Yuri Leonidovich* – Doctor of Technical Sciences, Professor, Corresponding Member of the Russian Academy of Architecture and Civil Engineering, Rector of the Federal State Budgetary Educational Institution of Higher Education "Novosibirsk State University of Architecture and Civil Engineering (Sibstrin)" (FGBOU "NGASU (Sibstrin)", office 239, building 113, Leningradskaya Street, Novosibirsk, 630008, Russia; e-mail: rector@sibstrin.ru

*Chirkunov Mikhail Yuryevich* – postgraduate student of the Department of Higher Mathematics of the Federal State Budgetary Educational Institution of Higher Education "Novosibirsk State University of Architecture and Civil Engineering (Sibstrin)" (FGBOU "NGASU (Sibstrin)", office 308, building 113, Leningradskaya Street, Novosibirsk, 630008, Russia; e-mail: mihail0807@mail.ru

*Fedosov Sergey Viktorovich* - Doctor of Technical Sciences, Professor, Academician of the Russian Academy of Architecture and Civil Engineering Sciences, Professor of the Department of "Technologies and Organization of Construction Production" of the Federal State Budgetary Educational Institution of Higher Education "National Research Moscow State University of Civil Engineering" (NRU MGSU), office 414, building 26, Yaroslavskoe shosse, Moscow, 129337, Russia; e-mail: FedosovSV@mgsu.ru

*Sidorov Vladimir Nikolaevich* - Doctor of Technical Sciences, Professor, Academician of the Russian Academy of Architecture and Construction Sciences, Head of the Department of Informatics and Applied Mathematics of the Federal State Budgetary Educational Institution of Higher Education "National Research Moscow State University of Civil Engineering" (NRU MGSU), office 414 kmk, building 26, Yaroslavskoe shosse, Moscow, 129337, Russia; e-mail: SidorovVN@mgsu.ru

*Evgeny Valerievich Alekseev* - Doctor of Technical Sciences, Professor, Professor of the Department of Water Supply and Sanitation of the Federal State Budgetary Educational Institution of Higher Education "National Research Moscow State University of Civil Engineering" (NRU MGSU), office 314, building 26, Yaroslavskoe shosse, Moscow, 129337, Russia; e-mail: AlekseevE@mgsu.ru

*Чиркунов Юрий Александрович* – доктор физико-математических наук, доцент, заведующий кафедрой Высшей математики Федерального государственного бюджетного образовательного учреждения высшего образования «Новосибирский государственный архитектурно-строительный университет (Сибстрин)» (ФГБОУ «НГАСУ (Сибстрин)», офис 305, дом 113, улица Ленинградская, город Новосибирск, 630008, Россия; e-mail: chr101@mail.ru

*Сколубович Юрий Леонидович* – доктор технических наук, профессор, член-корреспондент РААСН, ректор Федерального государственного бюджетного образовательного учреждения высшего образования «Новосибирский государственный архитектурно-строительный университет (Сибстрин)» (ФГБОУ «НГАСУ (Сибстрин)»,офис 239, дом 113, улица Ленинградская, город Новосибирск, 630008, Россия; e-mail: rector@sibstrin.ru

*Чиркунов Михаил Юрьевич* – аспирант кафедры Высшей математики Федерального государственного бюджетного образовательного учреждения высшего образования «Новосибирский государственный архитектурно-строительный университет (Сибстрин)» (ФГБОУ «НГАСУ (Сибстрин)»,офис 308, дом 113, улица Ленинградская, город Новосибирск, 630008, Россия; e-mail: mihail0807@mail.ru

*Федосов Сергей Викторович* - - доктор технических наук, профессор, академик РААСН, профессор кафедры «Технологии и организация строительного производства» Федерального государственного бюджетного образовательного учреждения высшего образования «Национальный исследовательский Московский государственный строительный университет» (НИУ МГСУ), офис 414, дом 26, Ярославское шоссе, город Москва, 129337, Россия; e-mail: FedosovSV@mgsu.ru

*Сидоров Владимир Николаевич* - доктор технических наук, профессор, академик РААСН, заведующий кафедрой информатики и прикладной математики Федерального государственного бюджетного образовательного учреждения высшего образования «Национальный исследовательский Московский государственный строительный университет» (НИУ МГСУ), офис 414 кмк, дом 26, Ярославское шоссе, город Москва, 129337, Россия; e-mail: SidorovVN@mgsu.ru

*Алексеев Евгений Валерьевич* - доктор технических наук, профессор, профессор кафедры Водоснабжения и водоотведения Федерального государственного бюджетного образовательного учреждения высшего образования «Национальный исследовательский Московский государственный строительный университет» (НИУ МГСУ), офис 314, дом 26, Ярославское шоссе, город Москва, 129337, Россия; e-mail: AlekseevE@mgsu.ru

International Journal for Computational Civil and Structural Engineering, 21(3) 158–171 (2025)

DOI:10.22337/2587-9618-2025-21-3-158-171

# HYDRODYNAMIC LOADS ON THE WALLS OF A TURBINE BLOCK WITH A COUNTER VORTEX DAMPER

***Genrikh V. Orekhov, Andrey L. Zuykov, Mikhail K. Sklyadnev***

National Research Moscow State University of Civil Engineering, Moscow, RUSSIA

**Abstract:** The article discusses the use of a counter vortex water flow energy dissipater when using a medium-pressure hydroelectric power station's conduit as a spillway. A design of a counter vortex damper in the chamber of a hydraulic turbine impeller with damping of excess flow energy in the cone of the draft tube is proposed. Research was carried out on pressure pulsations on the walls of a hydraulic model of a turbine block, as a result of which spectra and standards of pressure pulsations on the walls of a draft tube cone were obtained during operation of the model with and without a damper. It has been shown that passing water through a turbine unit of a medium-pressure HPP with the working impeller removed is unacceptable and leads to the destruction of the structure. It was found that the installation of a counter vortex damper in the impeller chamber reduces the dynamic loads on the walls of the draft tube cone by 6–7 times compared to the mode without a damper. It is concluded that the flow of water through a turbine unit of a medium-pressure HPP with a counter vortex damper installed in the impeller chamber satisfies the safety standards of hydraulic structures. The need to supply atmospheric air to the counter vortex damper via a special air duct has been established.

**Keyword:** counter vortex spillway, flow energy dissipation, pressure pulsation spectra and standards, safety of hydraulic engineering structures

# ГИДРОДИНАМИЧЕСКИЕ НАГРУЗКИ НА СТЕНКИ ТУРБИННОГО БЛОКА С КОНТРВИХРЕВЫМ ГАСИТЕЛЕМ

***Г.В. Орехов, А.Л. Зуйков, М.К. Скляднев***

Национальный исследовательский Московский государственный строительный университет, г. Москва, РОССИЯ

**Аннотация:** В статье рассматривается применение контрвихревого гасителя энергии водного потока при использовании энергетического водовода гидроэлектростанции среднего напора в качестве водосброса. Предложена компоновка контрвихревого гасителя в камере рабочего колеса гидротурбины с гашением избыточной энергии потока в конусе отсасывающей трубы. Выполнены исследования пульсаций давления на стенках гидравлической модели турбинного блока, в результате которых получены спектры и стандарты пульсаций давления на стенках конуса отсасывающей трубы при работе модели без гасителя и с гасителем. Показано, что пропуск воды через турбинный блок ГЭС среднего напора с удаленным рабочим колосом является неприемлемым и ведет к разрушению сооружения. Получено, что установка контрвихревого гасителя в камере рабочего колеса снижает динамические нагрузки на стенки конуса отсасывающей трубы в 6 – 7 раз по сравнению с режимом без гасителя. Делается вывод, что пропуск расходов через турбинный блок ГЭС среднего напора с установленным в камере рабочего колеса контрвихревым гасителем удовлетворяет нормам безопасности гидротехнических сооружений. Установлена необходимость подвода атмосферного воздуха к контрвихревому гасителю по специальному воздуховоду.

**Ключевые слова:** контрвихревой водосброс, гашение энергии потока, спектры и стандарты пульсаций давления, безопасность гидротехнических сооружений

## 1. INTRODUCTION

The study focuses on improving the reliability and service life of hydroelectric power plants and multi-purpose hydroelectric complexes, many of which were built in the middle of the last century and require reconstruction of their hydraulic structures in line with modern requirements. It seems to be economically reasonable to use decommissioned energy waterways

as spillways when renovating these hydroelectric power plants.

The issue of bypassing idle flows through the energy flow path has been repeatedly raised in specialized literature regarding low-pressure hydroelectric power plants [1–8]. The most comprehensive review of this issue is provided in [9]. According to these works, the conclusion about the possibility of passing idle flows through the flow path of a turbine of an inactive hydroelectric unit and the resulting loads on the structure is based on an analysis of flow characteristics at relatively low speeds. It has been established that passing idle flows under these conditions is only possible with a remote impeller and a reliable supply of sufficient air under the hydro turbine cover. It should be noted that due to the high dynamic loads on the structure, turbine manufacturers do not recommend this procedure and are not responsible for the consequences. There is no experience in the world of bypassing idle flows through HPP turbine units at heads of more than 40 m.

Discharging idle water through the energy water pipes of non-operating hydroelectric power plants of medium-pressure HPPs without special measures is unacceptable due to the risk of destruction, both of the water pipes themselves, operating in uncalculated modes, and of the hydroelectric complex as a whole due to erosion in the lower reaches. Such a measure is the dissipation of flow energy within the pressure flow path in a special dissipation chamber, which allows the flow to be released into the suction pipe and the lower reach at low speeds close to the design turbine modes.

The idea of installing an energy dissipation chamber on a pressure water pipeline is not new. As an example, we can mention the operational deep spillway with a pressure chamber in the form of a sudden expansion of the flow at the Mica hydroelectric complex in Canada [10]. This spillway with a chamber diameter of 13.7 m has a flow rate of 850 $m^3/s$ at a head of 137 m. At the same time, pressure pulsations on the chamber walls due to high flow turbulence in the zone of intense energy dissipation reach 30% of the difference between the velocity heads of the flow at the chamber inlet and inside it. Such a pressure energy dissipator for the discharge flow is effective, but cannot be considered reliable due to the extremely high dynamic loads on the energy dissipation unit. It should be noted that such high hydrodynamic loads on the structure prevent the use of pressure dampers in spillways of medium- and high-pressure hydraulic structures. Thus, the problem of reducing the level of hydrodynamic loads on the walls of the structure becomes crucial.

In this regard, let us consider a pressure counter-vortex energy dissipator based on the interaction of coaxial layers of flows swirling in opposite directions [11–13]. In a counter-vortex energy dissipator, the zone of intense dissipation of the mechanical energy of the flow is located between the interacting concentric counter-rotating layers at a considerable distance from the walls of the dissipation chamber. This prevents the appearance of high hydrodynamic loads on the chamber walls, especially when air from the atmosphere is supplied to its central near-axis zone.

**Objective of the study** is to determine the hydrodynamic loads on the walls of the turbine block of a medium-pressure hydroelectric power plant with a counter-vortex energy dissipator for idle water flow.

## 2. DAMPER DESIGN

The design was developed for a hydroelectric power plant undergoing reconstruction with an operating head of $H_0$ = 50 m. One of the hydroelectric power plant's hydroelectric units, which has been decommissioned, is equipped with a spillway after the turbine has been dismantled, ensuring that water is discharged into the lower reach when the level in the upper reach rises when the hydroelectric power plant is shut down. The working range of levels in the upper reach of the spillway is from the operating level of 90.5 m to the forced level of 93.5 m, with levels in the lower reach of the power plant's

discharge channel ranging from a minimum of 39.5 m to a maximum of 42.0 m. The upper tail-race level of 93.0 m is taken as the initial level for shutting down the HPP units and activating the spillway. The design discharge capacity of the spillway is Q = 63.3 $m^3/s$. The design brief specifies that the damper must be simple to manufacture, require minimal changes to the flow path design, and be removable so that it can be dismantled for the installation of the hydroelectric unit's working wheel.

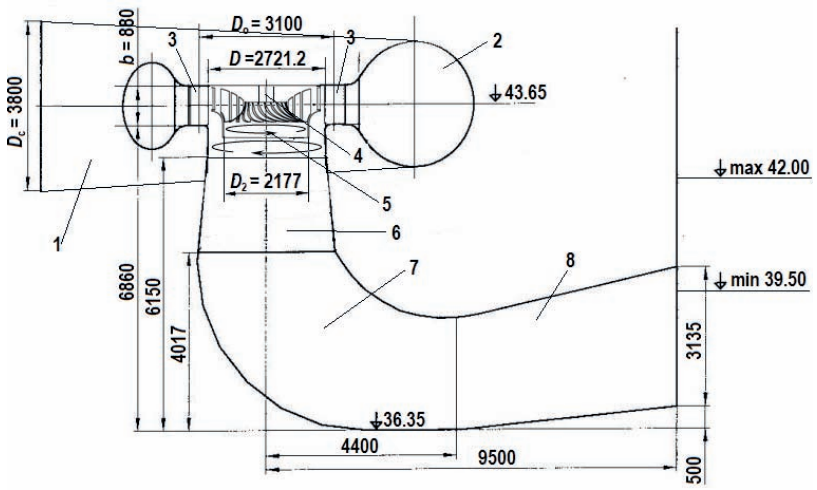


*Figure 1. Flowing part of the turbine unit: 1 – water supply pipe, 2 – spiral chamber, 3 – guide vanes of the hydro turbine, 4 – air duct, 5 – working wheel chamber with counter-vortex damper, 6 – suction pipe cone, 7 – suction pipe elbow, 8 – diffuser*

According to the task, the layout of the pressure counter-vortex damper is adopted in the chamber of the remote working wheel of the hydro turbine with energy damping in the cone of the suction pipe (Figure 1). The main dimensions of the flow part of the turbine chamber are as follows: Dc = 3800 mm is the diameter of the pressure water pipe at the inlet to the spiral chamber; D0 = 3100 mm is the diameter of the installation of the axes of rotation of the guide vane blades; b = 880 mm is the height of the guide vane blades of the hydro turbine; D = 2721.2 mm is the diameter of the inlet section of the suction pipe cone.

The anti-vortex damper includes the guide apparatus of the remote hydro turbine and a fairing with blades rigidly fixed to it. The guide apparatus of the hydro turbine with rotating blades performs the functions of a regulating valve and swirls part of the idle flow. The blades rigidly attached to the fairing swirl the other part of the idle flow in the opposite direction to the swirl of the guide apparatus blades. The fairing directs one part of the flow coaxially into the other, oppositely swirled part and leads them into a common damping chamber in the cone of the suction pipe.

In the cone of the suction pipe, coaxial concentric oppositely twisted parts of the flow mutually cancel each other's twist, thereby achieving the effect of damping the mechanical energy of the flow as a whole.

Figure 2 shows the design of the counter-vortex damper, carried out in accordance with proven methods for calculating pressure spillway hydraulic structures [9], regulatory documents [15-20], and recommendations contained in specialized literature [11-13].

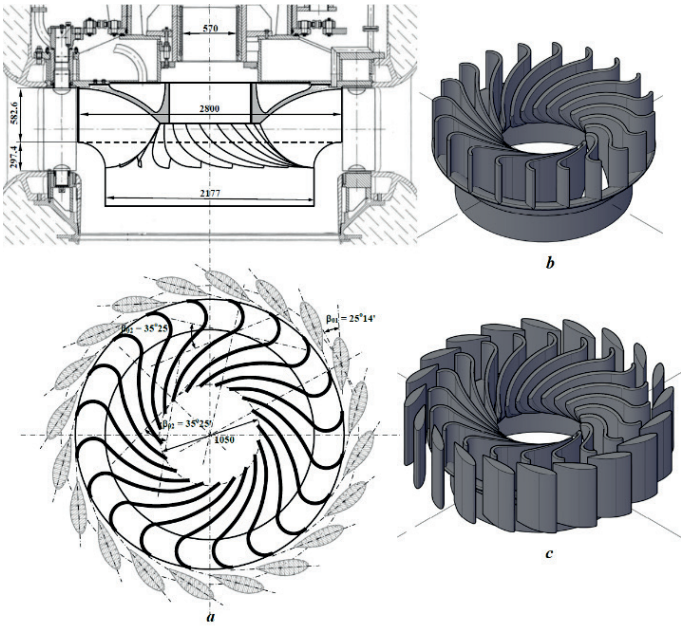


*Figure 2. Counter-vortex damper: a – preliminary design of the damper layout in the impeller chamber of a remote hydro turbine, b – fairing with blades for swirling the internal flow in isometric view, c – assembled unit with the hydro turbine guide apparatus*

A distinctive feature of the project was that the internal flow swirler blades, fixed on the fairing, have two sections. An inlet section reverses the flow in the opposite direction to the swirl of the peripheral flow formed by the blades
of the guide apparatus of the hydro turbine. And a main section, where the internal flow is given the required swirl parameters. In the main section, the blades have the shape of a logarithmic spiral [14].

## HYDRODYNAMIC INVESTIGATIONS

Hydrodynamic loads on the walls of the damping chamber located within the cone of the suction pipe presented in Figure 1 are of crucial importance when deciding on the use of a counter-vortex damper for discharging water into the lower reach through the power water conduit of the reconstructed hydroelectric power plant. To evaluate these loads, physical studies of a model of a turbine unit with a counter-vortex damper on a scale of 1:27.2 shown in Figure 3 were carried out in the hydraulic laboratory of the Moscow State University of Civil Engineering.

Using a laboratory model, pressure pulsations on the walls of the suction pipe cone were measured with silicon piezoresistive sensors XGZP6857A manufactured by CFSensor, China. The range of measurable pressures was from –40 to +40 kPa, the measurement error was ±8.0 Pa, and the range of measurable pressure pulsation frequencies was up to 1000 Hz.

Measurements were taken at two points at distances of 26 and 52 mm from the beginning of the suction pipe cone. Six pressure sampling points were evenly distributed around the perimeter of the cone at each location. At each of the 12 points, the pressure change $P(t) = Pi$ was recorded during an exposure time of approximately $T = 180$ seconds with a discretization step of $\Delta t = 0.001$ seconds.

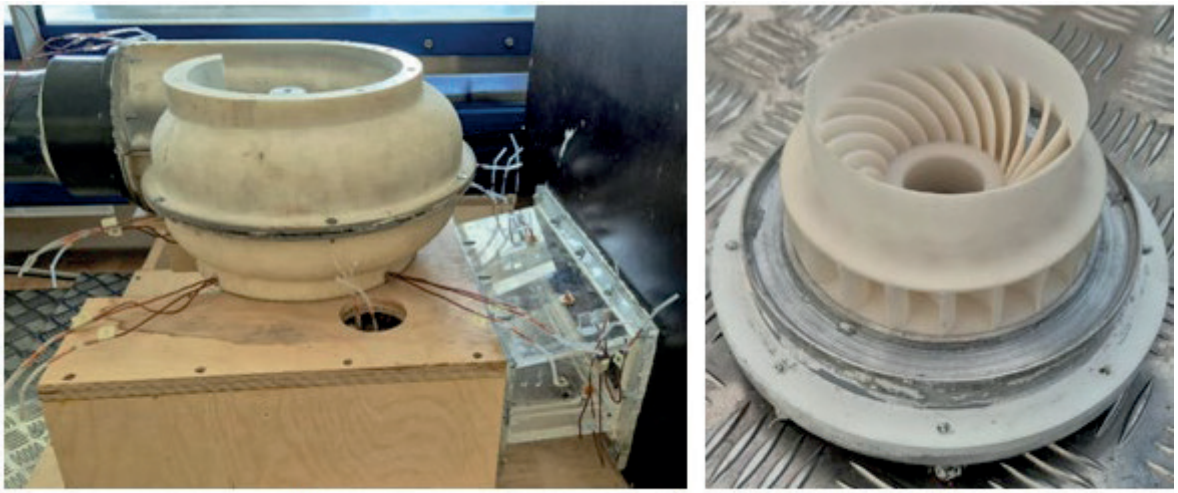

*a* *b*

*Figure 3. Turbine block model: a – general view, b – turbine cover with counter-vortex damper*

The experimental data sets were further subjected to statistical processing and spectral analysis. During statistical processing, the following were calculated:

– average pressure value at the point of sampling during the exposure period (mathematical mean value)

$$\overline{P} = \frac{1}{T}\sum_{i=1}^{N} P_i \Delta t \,,$$

where $N = T/\Delta t$ is the number of measurements;

– pressure pulsation standard (square root of dispersion)

$$\sigma_p = \sqrt{\sum_{i=1}^{N} \frac{\left(P_i - \overline{P}\right)^2}{N}} \,,$$

which was reduced to the pressure $H_0$ acting on the model

$$\sigma = \frac{\sigma_p}{\rho g H_0} \,. \qquad (1)$$

Spectral analysis was performed based on discrete Fourier transform. Assuming that the pressure change function over time P(t) is non-periodic (finite), i.e., a function completely defined on the interval [0, T]. The spectral analysis consisted of finding the coefficients $a_j$, $b_j$ of the Fourier series.

$$P(t) = \overline{P} + \sum_{j=1}^{\infty}\left[a_j \cos\left(2\pi\omega_j t\right) + b_j \sin\left(2\pi\omega_j t\right)\right] \,, \qquad (2)$$

where $\omega_j$ is the frequency of the $j^{th}$ mode.

In addition to series (2), the following series was used in the spectral analysis

$$P(t) = \overline{P} + \sum_{j=1}^{\infty} C_j \cos\left(2\pi\omega_j t + \varphi_j\right) \,,$$

where $C_j$ is the amplitude of the $j^{th}$ mode

$$C_j = \sqrt{a_j^2 + b_j^2} \,, \qquad (3)$$

$\varphi_j$ is the phase of the $j^{th}$ mode

$$\varphi_j = -\mathrm{arctg}\left(b_j / a_j\right) .$$

It is known that Fourier coefficients are determined by integrals

$$a_j = \frac{2}{T}\int_0^T P(t)\cos(2\pi\omega_j t)dt \quad (4)$$

,

$$b_j = \frac{2}{T}\int_0^T P(t)\sin(2\pi\omega_j t)dt \quad (5)$$

.

For finite functions, the components of the spectral density are also calculated.

$$S_{Cj} = \int_0^T P(t)\cos(2\pi\omega_j t)dt = \frac{a_j T}{2} \quad (6)$$

,

$$S_{Sj} = \int_0^T P(t)\sin(2\pi\omega_j t)dt = \frac{b_j T}{2} \quad (7)$$

,

spectral density module of the $j^{th}$ mode

$$S(\omega_j) = \sqrt{S_{Cj}^2 + S_{Sj}^2} = \sqrt{\left(\frac{a_j T}{2}\right)^2 + \left(\frac{b_j T}{2}\right)^2} = \frac{C_j T}{2} \quad (8)$$

,

and phase of spectral density of the $j^{th}$ mode

$$\varphi(\omega_j) = -\text{arctg}\left(S_{Sj}/S_{Cj}\right) = -\text{arctg}\left(b_j/a_j\right) = \varphi_j$$

.

Numerical spectral analysis, realized in the course of processing measurements of pressure pulsations on the walls of the cone of the suction pipe of the model, consisted in finding the coefficients $a_j$, $b_j$, $C_j$, $S_{Cj}$, $S_{Sj}$, $S(\omega_j)$ for finite functions defined on the interval [0, T] by discrete values P(t) = Pi with a time sampling step $\Delta t$ = 0.001 s. It was reduced to calculating integrals (4)-(7) using numerical integration formulas by the rectangle method.

$$a_j = \frac{2}{N}\sum_{i=0}^{N-1} P_i \cos(2\pi\omega_j i\Lambda t)$$

,

$$b_j = \frac{2}{N}\sum_{i=0}^{N-1} P_i \sin(2\pi\omega_j i\Delta t)$$

,

$$S_{Cj} = \Delta t\sum_{i=0}^{N-1} P_i \cos(2\pi\omega_j i\Lambda t) = \frac{a_j T}{2}$$

,

$$S_{Sj} = \Delta t\sum_{i=0}^{N-1} P_i \sin(2\pi\omega_j i\Delta t) = \frac{b_j T}{2}$$

.

Next, using formulas (3) and (8), the amplitude $C_j$ and the spectral density modulus $S(\omega_j)$ at the frequency of the $j^{th}$ mode $\omega_j$ were calculated. As a result, the doubled spectral density was normalized (reduced to a dimensionless form) according to the pressure $H_0$ and frequency $\omega_j$.

$$\frac{2S(\omega_j)\omega_j}{\rho g H_0} = \frac{C_j}{\rho g H_0}\cdot\frac{T}{T_j}$$

,

where $T_j = 1/\omega_j$ is the period of the $j^{th}$ mode.

The diagrams of the normalized spectral density of pressure pulsations on the stacks of the suction pipe cone of the model are shown in Figure 4. The caption below the figure indicates the operating mode of the model and the normalized pressure pulsation standards calculated using formula (1).

The spectral density curve obtained for the direct discharge of idle flow through the turbine flow path with the remote impeller of the hydraulic unit is shown in red in Figure 4. In this case, the guide vane of the hydro turbine was set to a blade rotation angle of $\beta_{01}$ = 25°14' (see Figure 2), no counter-vortex damper was installed in the impeller chamber, and no air was supplied under the chamber cover.

In this mode, the spectral density diagram of pressure pulsations on the walls of the suction pipe cone has a clear sharp peak with a leading frequency of 19.5 Hz. There is no doubt that this is the so-called cable frequency. It is obvious that a highly swirled flow descends from the blade system of the guide apparatus into the impeller chamber, in which, under the action of centrifugal forces in the near-axis zone, a vortex cord with a pressure significantly lower than atmospheric pressure is formed in the center of the swirled flow, even in the conditions of a low-pressure laboratory model.

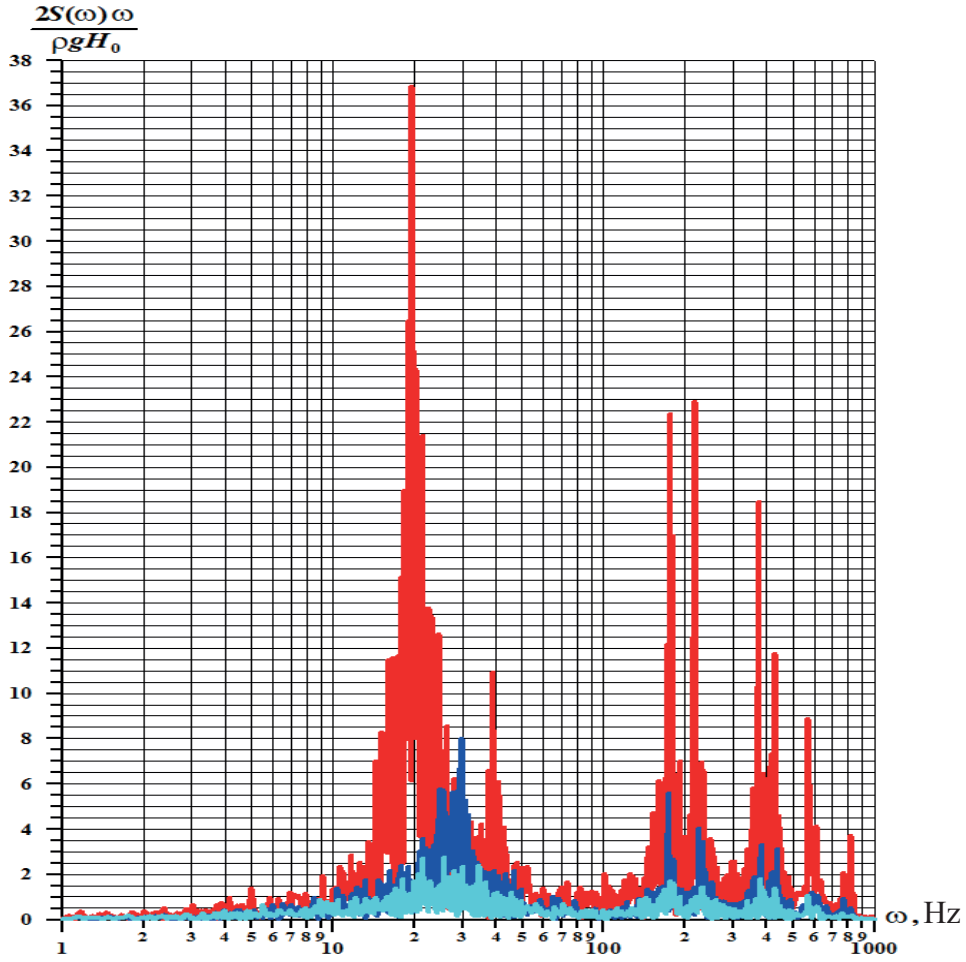


*Figure 2. Normalized spectral density of pressure pulsations on the walls of the suction pipe cone: mode 1 ($\sigma$ = 0.3834) is shown in red; mode 2 ($\sigma$ = 0.0915) is shown in blue; mode 3 ($\sigma$ = 0.0574) is shown in light blue*

Under natural conditions, the vortex bundle is a cylindrical cavity with a pressure equal to the pressure of saturated water vapor or atmospheric pressure (when the bundle is closed to the atmosphere). The vortex bundle is a source of high dynamics.

A large number of studies have been devoted to the investigation of vortex dynamics and the associated phenomenon of vortex decay. Examples include [3, 21], an excellent review covering 45 years [22], and related articles [23-27]. It is known that cable dynamics is characterized by low frequency and manifests itself in the precession of the core (cable) of a swirling flow, when the entire mass of the flow is drawn into the dynamic process, causing the flow to lose its stability as a whole. Due to the involvement of large water masses, cable dynamics pose an exceptional danger. For cable dynamics to occur, the pressure in the near-axis zone (core, cable) of the swirling flow must be lower than in the downstream sections. Then, under the influence of a negative pressure gradient, significant masses of water from the downstream sections are drawn into the core of the counter-rotating flow, interact with it, rotate, and are thrown back. The process of periodic splashes changes the structure of the swirling flow. The straight axis of the swirling flow becomes curved and begins to rotate around the geometric axis of the water pipe at a certain angular frequency, i.e., the flow loses its axial symmetry and stability. This phenomenon of loss of stability of the swirling flow is called vortex breakdown. These

conditions appear in the cone of the suction pipe in the absence of a working wheel and the formation of a swirling flow by the guide apparatus of the hydraulic turbine. The swirling flow formed in this way, which has a vacuum cavity in the axial zone, encounters a pressure drop determined by the level of the lower tailwater. As a result, the very negative pressure gradient arises, which activates the splash mechanism with subsequent cable dynamics.

If it is established that the dynamics of the cable are related to the loss of stability of the swirling flow as a whole, then it has the rotation frequency of the flow itself, or that part of the flow that is directly adjacent to the cable. Based on this position, let us consider what dynamics should be expected in the cone of the suction pipe under these conditions at the actual facility.

The geometric characteristic of the local swirler, calculated using Abramovich's formula [28, 29] and called the Abramovich number, for the guide apparatus of a hydroturbine is determined by the formula

$$A = \frac{R}{2b\left(1-\frac{nc}{\pi R_0}\right)\mathrm{tg}\beta_{01}} = \frac{1.3606}{2\cdot 0.88\left(1-\frac{20\cdot 0.0569}{3.14\cdot 1.55}\right)\mathrm{tg}(25^{\circ}14')} = 2.141,$$

where $R$ is the radius of the suction pipe cone, $R = D/2 = 2.7212/2 = 1.3606$ m; $R_0$ is the radius of installation of the guide vane rotation axes, $R_0 = D_0/2 = 3.1/2 = 1.55$ m; b is the height of the guide vanes of the hydro turbine, b = 0.88 m; $\beta_{01}$ is the angle of installation of the guide vanes, $\beta_{01} = 25^{\circ}14'$; n is the number of guide vanes, n = 20; c is the profile half-thickness of the guide vane on its axis of rotation, c = 56.9 mm.

Following the method of hydraulic calculation of local swirlers [11–13], the relative area of the critical annular cross-section of the swirling flow at A = 2.141 will be $\omega_0 = 0.4969$, and the flow rate passed through will be Q = 48.3 m$^3$/s.

On the other hand, the geometric characteristic of the swirling flow device is equal to the Higer-Barr swirl number [30–32], defined as the ratio of the azimuthal angular momentum (M) of the swirling flow to twice the product of its axial angular momentum (I) and the hydraulic radius ($R_h$) [12, 33]

$$A = \frac{M}{2R_h I},$$

where $M = \rho Q u_R R$; $I = \rho Q V$; $R_h = \omega_0 D/4$; $V$ is the average axial velocity across the flow cross-section at the inlet of the suction pipe cone, $V = Q/\omega_0 \pi R^2$; $u_R$ is the tangential flow velocity at the walls at the inlet of the suction pipe cone.

From the Higer-Bera swirling number, the following equality follows [11]

$$u_R = \frac{QA}{\pi R^2}.$$

Then the period of one flow cycle around the perimeter of the cone of the suction pipe is

$$T_R = \frac{2\pi R}{u_R} = \frac{2\pi^2 R^3}{QA},$$

and its rotation frequency will be equal to

$$\omega_R = \frac{1}{T_R} = \frac{QA}{2\pi^2 R^3}.$$

This period and frequency correspond to one revolution of the flow at the walls of the cone of the suction pipe. On the surface of the vortex bundle, the period and frequency will be different. Assuming a radial distribution of tangential velocities according to the law of potential rotation, where $u_{RR} = \mathrm{const}$, it can be shown that on the free surface of the vortex bundle they will be equal to

$$T_d = \frac{1-\omega_0}{\omega_R},$$

and

$$\omega_d = \frac{\omega_R}{1-\omega_0}.$$

Thus, the cable dynamics associated with the loss of flow stability as a whole will occupy the frequency band $\omega_R < \omega < \omega_d$, i.e.

$$\frac{QA}{2\pi^2 R^3} < \omega < \frac{1}{1-\omega_0} \cdot \frac{QA}{2\pi^2 R^3}.$$

By substituting numerical values, we obtain that the cable frequencies on the full-scale object will occupy the band $2.08 < \omega < 4.13$ Hz. Considering the scale of the model M 1:27.2, the range of cable frequencies in hydraulic modeling according to Euler's determining criterion should be between 10.8 and 21.5 Hz. In fact, this is the frequency range we observe in Figure 4.

The recorded normalized pressure standard of pulsations on the walls of the cone of the suction pipe on the model at this mode was $\sigma = 0.3834$. Assuming the maximum pressure pulsation amplitude equal to the Gaussian triple standard, at the actual operating pressure $H_0 = 50$ m, we obtain

$$P' = \pm 3\sigma\rho g H_0 = \\ = \pm 3 \cdot 0.3834 \cdot 1000 \cdot 9.81 \cdot 50 = \pm 564 \text{ кПа}$$

or $\Delta H = \pm 57.5$ m of water column.

It is obvious that under these conditions, half of the time spent discharging idle waste through the turbine flow path, the pressure at the faces of the suction pipe cone will drop to the vaporization pressure, meaning that they will be subject to intense cavitation.

In this regard, appropriate requirements must be imposed on the lining of the suction pipe. For example, the calculated alternating excess pressures on streamlined surfaces from –100 to +200 kPa require reliable interaction between the lining and the concrete structure. A disruption in their interaction, even in a small area, can lead to rapid destruction of the entire lining. As far as we know, there is no satisfactory technical solution to this problem for such a complex structure as a suction pipe.

In general, we consider the passage of idle flow through a hydro turbine unit with a remote working wheel to be unacceptable due to the high dynamic loads on the structure, leading to its destruction and a serious accident at the HPP.

Figure 4 shows in blue the diagram of the normalized spectral density of pressure pulsations on the walls of the cone of the suction pipe in the mode of passing cold flow through the turbine flow path when a counter-vortex damper is installed in the remote impeller chamber. Air was not supplied under the chamber cover.

It can be seen that the installation of a counter-vortex damper in the impeller chamber sharply, judging by the normalized pulsation standard equal to $\sigma = 0.0915$, reduced the dynamic loads on the structure by a factor of four compared to the previous mode without the damper installed.

The installation of the counter-vortex damper also changed the frequency distribution of the spectral density of pressure pulsations, shifting the band of cable dynamics toward higher frequencies with a maximum in the 30 Hz range and increasing the relative spectral density in the turbulent range at frequencies of 150–500 Hz. However, in the turbulent range, there is no shift in spectral density by frequency between the modes without and with the damper installed.

The calculation of the cable frequency band, performed according to the above method, with regard to the design and hydraulic characteristics of the developed counter-vortex damper, showed that under natural conditions this band will lie in the range of 2.17–5.35 Hz. On a 1:27.2 scale hydraulic model, it will occupy the range of 11.3–27.9 Hz, thus confirming the shift of the cable dynamics towards higher frequencies.

The diagram shown in Figure 4 in blue depicts the normalized spectral density of pressure pulsations on the walls of the suction pipe cone. It refers to the idle flow mode when a counter-vortex damper is installed and air is supplied from the atmosphere through the air duct under the impeller cover (see Figures 1 and 2).

It has been established that supplying air from the atmosphere through the impeller cover into the vacuum vortex core of the swirling flow formed by the blade system of the counter-vortex damper sharply reduces the hydrodynamic loads on the structure. Thus, the recorded normalized standard of pressure pulsations on the walls of the suction pipe cone, equal to s = 0.0574 in this mode, is 1.6 times lower than the standard of pressure pulsations in a similar mode, but without air supply. This indicates the need to supply atmospheric air to the counter-vortex damper at idle water outlets of medium-pressure hydraulic structures. It should be noted that the overall reduction in dynamic loads on the structure compared to the mode without the counter-vortex damper was 6.7 times.

As a result, with the installation of an anti-vortex damper and the supply of air from the atmosphere, the maximum amplitude of pressure pulsations on the walls of the suction pipe cone under field conditions will be

$$P' = \pm 3\sigma\rho g H_0 = \\ = \pm 3 \cdot 0.0574 \cdot 1000 \cdot 9.81 \cdot 50 = \pm 84.5 \text{ kPa}$$

or $\Delta H = \pm 8.61$ m of water column.

It can be stated that the considered option of passing the idle flow through the turbine unit with a counter-vortex damper installed in the working wheel chamber of the hydraulic turbine, while ensuring air supply, is quite satisfactory. A positive environmental effect is the significant aeration of the flow discharged into the lower reach.

The diagram of the normalized spectral density of pressure pulsations on the walls of the suction pipe cone shows that when air is supplied to the counter-vortex damper, the spectrum in the central part becomes flatter and wider, covering the range from 10 to 50 Hz, where there are no pronounced leading frequencies. This indicates suppression of the bundle dynamics. Instead, a spectrum corresponding to large vortex structures formed by the intense interaction of concentric counter-rotating flows is observed. In the turbulent frequency range from 150 to 500 Hz, suppression of pulsations is also observed, manifested in the flattening of the spectral density graph with a decrease in its modulus.

## 4. CONCLUSION

1. The article has examined the possibility of using a pressure counter-vortex energy dissipator for water flow in the power water pipeline of a medium-pressure hydroelectric power plant during its reconstruction into an operational spillway.
2. A configuration of a pressure counter-vortex damper in the chamber of a dismantled hydro turbine impeller with damping of idle flow energy in the suction pipe cone has been proposed
3. The study established the expediency of the design of the counter-vortex damper with its attachment to the cover of the remote hydraulic turbine.
4. A counter-vortex damper design has been developed. It includes a hydro turbine guide apparatus and a fairing with non-rotating blades rigidly fixed to it. In this design, the guide apparatus of the hydraulic turbine with rotating blades simultaneously performs the functions of a regulating valve and a swirl generator for part of the idle flow. The blades rigidly fixed to the fairing swirl the other part of the idle flow in the opposite direction to the swirl of the guide apparatus blades. The fairing directs one part of the flow coaxially into the other, oppositely swirled part and leads them into a common damping chamber in the cone of the suction pipe. In the cone of the suction pipe, the coaxial concentric oppositely twisted parts of the flow mutually dampen each other's twist, thereby achieving the effect of damping the energy of the flow as a whole.
5. Experimental studies of pressure pulsations on the walls of a hydraulic model of a turbine block with a counter-vortex damper were carried out. As a result of the studies, normalized spectra and standards of pressure pulsations on

the walls of the suction pipe cone were obtained for various operating modes of the model.

6. It has been established that in the direct discharge mode of idle flow through the turbine unit with the remote impeller of the hydraulic unit, the normalized pressure standard of pulsations on the walls of the suction pipe cone reaches $\sigma = 0.3834$. Thus, the walls of the suction pipe cone are subjected to high dynamic loads. The diagram of the spectral density of pressure pulsations has a sharp peak with a leading frequency of 19.5 Hz on the model (3.74 Hz in real conditions). This corresponds to the cable frequencies at the loss of flow stability in the process of the so-called vortex breakdown. It is shown that in this mode, in addition to dynamic loads, the walls of the suction pipe cone will be subjected to intense cavitation. It is concluded that passing idle flows through the hydro turbine unit of a medium-pressure HPP with a remote working shaft is unacceptable and leads to the destruction of the structure.

7. The method for calculating the range of cable frequencies associated with vortex decay has been experimentally confirmed

8. The installation of an anti-vortex damper in the remote impeller chamber significantly reduces the dynamic loads on the walls of the suction pipe cone, bringing the pulsation standard to a level of $\sigma = 0.0574$. This is 6.7 times lower than the standard in the idle flow discharge mode through the turbine unit without the damper installed.

9. Bypassing cold losses through the hydro turbine unit of a medium-pressure HPP with a counter-vortex damper installed in the remote impeller chamber meets the standards and requirements for the safety and reliability of hydraulic structures and hydroelectric power plants.

10. It has been established that atmospheric air must be supplied to the counter-vortex damper through a special air duct. This study was con-

## ACKNOWLEDGMENTS

The research was funded by the National Research Moscow State University of Civil Engineering (grant for fundamental scientific research, project No. 09-661/130).

## REFERENCES

1. **Sutherland R.A.** Free Discharge through a Turbine Distributer. Case and Draft Tube. Transactions of ASME. 1959. Vol. 81. ser. D.N. 4. pp. 488-492.
2. **Hagen, A.V.** On idle water flow through the flow section of a capsule unit. Leningrad: Proceedings of the Leningrad Polytechnic Institute. No. 289. 1968. pp. 131–134.
3. **Gorbachev S.I., Sarkisova M.F.** Water flow through the flow path of a hydro turbine in the absence of a pressure control valve. Hydraulic Engineering. 1970. No. 10.
4. Design and construction of large dams. Permanent and temporary spillway structures. International Congress on Large Dams. Compiled by M.B. Ginzburg, edited by A.A. Borovoy. Moscow. Energiya Publishing House. 1972. Issue 2. 160 pp.
5. **Rubinstein G.L., Rudakova M.D**. Construction costs incurred through unfinished concrete structures of hydraulic structures / Overview information: Hydroelectric Power Plants series / Moscow. Informenergo. 1980.
6. **Minshulov, A.Kh**. Study of water discharge through a model of a low-pressure hydroelectric power plant unit. Abstract of thesis... Candidate of Technical Sciences. Leningrad. 1982.
7. **Abelev, A.S., Solovyova, A.G.** Hydraulic conditions for flow through buildings of hydroelectric power stations under construction. Leningrad. Izvestiya VNIIG. 1983. Vol. 168. pp. 71–78.
8. Operating conditions of combined hydroelectric power plant units during construction and operation / I.I. Ivanov, G.A. Ivanova, V.M. Semenkov, T.V. Semenova // Proceedings of conferences and meetings on hydraulic engineering:

Methods of research and hydraulic calculations of spillway hydraulic structures / Leningrad. VNIIG. 1985. pp. 143-148.
9. Hydraulic calculations for spillway hydraulic structures: Reference manual. Moscow: Energoatomizdat. 1988. 624 p.
10. **Russel S.O., Ball I.W.** Suddenenlargement Energy Dissipation for Mica Dam. Journal of the Hydraulics Division. 1967. Vol. 94. No. 4. pp. 41-58.
11. **Volshanik V.V., Zuykov A.L., Mordasov A.P.** Swirling flows in hydraulic structures. Moscow. Energoatomizdat. 1990. 280 p.
12. **Akhmetov V.K., Volshanik V.V., Zuykov A.L., Orekhov G.V.** Modeling and calculation of counter-vortex flows. Moscow. MISi Publishing House – Moscow State University of Civil Engineering. 2012. 252 p.
13. **Akhmetov V.K., Volshanik V.V., Zuykov A.L., Orekhov G.V.** Physical modeling of counter-vortex structures and equipment (electronic resource). Moscow. MISI Publishing House – MGSU. 2018. 15 MB.
14. **Zuykov A.L.** Cylindrical flow swirler with elongated blade chord // Construction: Science and Education. 2023. Vol. 13. Issue 2. Art. 2.URL: http://nso-journal.ru. DOI: 10.22227/2305-5502.2023.2.2.
15. SP 58.13330.2012 Hydraulic structures. Basic provisions.
16. STO 17330282.27.140.002-2008 “Hydraulic structures of hydroelectric power plants and pumped storage power plants. Conditions for creation. Standards and requirements”.
17. STO 17330282.27.140.011-2008 “Hydroelectric power plants. Conditions for construction. Standards and requirements”.
18. STO 17330282.27.140.013-2008 “Mechanical equipment for hydroelectric power plant structures. Conditions for creation. Standards and requirements”.
19. STO 17330282.27.140.014-2008 “Technical systems of hydroelectric power plants. Conditions for creation. Standards and requirements.”
20. STO 17330282.27.140.022-2008 “Hydroelectric power plants and pumped storage power plants. Conditions for construction. Standards and requirements.”
21. **Benjamin T.B.** Theory of the Vortex Breakdown Phenomenon // Journal of Fluid Mechanics. 1962, Vol. 14, No 4, pp. 593-629.
22. **Lucca-Negro O., O’Doherty T.** Vortex Breakdown. A Review. Progress in Energy and Combustion Science. 2001. Vol. 27 (4). pp. 431-481.
23. **Akhmetov V.K.** Comparative analysis of mathematical models for studying the phenomenon of vortex decay // Scientific Review. 2015. No. 21. pp. 120–124.
24. **Akhmetov V.K.** Development of methods for mathematical modeling of the stability of swirling flows // Scientific Review. 2015. No. 21. pp. 125-129.
25. **Akhmetov V.K., Akhmetova V.V.** Mathematical modeling of hydrodynamics and stability of coaxially rotating flows // International Journal for Computational Civil and Structural Engineering. 2016. Vol. 12. No. 3. pp. 9–14.
26. **Akhmetov V.K.** Hydrodynamic stability of counter-vortex flows // Hydraulic Engineering. 2018. No. 2. pp. 13–18..
27. **Akhmetov V.K.** Hydrodynamic stability of coaxially rotating flows // Natural and Technical Sciences. 2025. No. 3. pp. 34-38.
28. **Abramovich, G.N.** Applied Gas Dynamics. Moscow. GITTL, 1953. 736 p..
29. **Abramovich, G.N.** Theory of Turbulent Jets. Moscow: Fizmatgiz, 1960. 715 p.
30. **Chigier N.A., Chervinsky A.** Experimental Investigation of Swirling Vortex Motion in Jets // Journal of Applied Mechanics. 1967. Vol. 34. Issue 2. pp. 443-451. DOI: 10.1115/1.3607703.
31. **Beér J.M., Chigier N.A.** Combustion Aerodynamics. New York. Halsted Press Division, Wiley, 1972. 264 p.
32. **Gupta A.K., Lilley D.G., Syred N.** Swirl Flows. England. Abacus Press, Tunbridge Wells, 1984. 475 p.

33. **Zuykov, A.L.** Hydrodynamics of Circulation Currents. Moscow. ASV Publishing House. 2010. 216 p.

## СПИСОК ЛИТЕРАТУРЫ

1. **Sutherland R.A.** Free Discharge through a Turbine Distributer. Case and Draft Tube. Transactions of ASME. 1959. Vol. 81. ser. D.N. 4. pp. 488-492.
2. **Hagen, A.V.** On idle water flow through the flow section of a capsule unit. Leningrad: Proceedings of the Leningrad Polytechnic Institute. No. 289. 1968. pp. 131–134.
3. **Gorbachev S.I., Sarkisova M.F.** Water flow through the flow path of a hydro turbine in the absence of a pressure control valve. Hydraulic Engineering. 1970. No. 10.
4. Design and construction of large dams. Permanent and temporary spillway structures. International Congress on Large Dams. Compiled by M.B. Ginzburg, edited by A.A. Borovoy. Moscow. Energiya Publishing House. 1972. Issue 2. 160 pp.
5. **Rubinstein G.L., Rudakova M.D**. Construction costs incurred through unfinished concrete structures of hydraulic structures / Overview information: Hydroelectric Power Plants series / Moscow. Informenergo. 1980.
6. **Minshulov, A.Kh**. Study of water discharge through a model of a low-pressure hydroelectric power plant unit. Abstract of thesis... Candidate of Technical Sciences. Leningrad. 1982.
7. **Abelev, A.S., Solovyova, A.G.** Hydraulic conditions for flow through buildings of hydroelectric power stations under construction. Leningrad. Izvestiya VNIIG. 1983. Vol. 168. pp. 71–78.
8. Operating conditions of combined hydroelectric power plant units during construction and operation / I.I. Ivanov, G.A. Ivanova, V.M. Semenkov, T.V. Semenova // Proceedings of conferences and meetings on hydraulic engineering: Methods of research and hydraulic calculations of spillway hydraulic structures / Leningrad. VNIIG. 1985. pp. 143-148.
9. Hydraulic calculations for spillway hydraulic structures: Reference manual. Moscow: Energoatomizdat. 1988. 624 p.
10. **Russel S.O., Ball I.W.** Suddenenlargement Energy Dissipation for Mica Dam. Journal of the Hydraulics Division. 1967. Vol. 94. No. 4. pp. 41-58.
11. **Volshanik V.V., Zuykov A.L., Mordasov A.P.** Swirling flows in hydraulic structures. Moscow. Energoatomizdat. 1990. 280 p.
12. **Akhmetov V.K., Volshanik V.V., Zuykov A.L., Orekhov G.V.** Modeling and calculation of counter-vortex flows. Moscow. MISi Publishing House – Moscow State University of Civil Engineering. 2012. 252 p.
13. **Akhmetov V.K., Volshanik V.V., Zuykov A.L., Orekhov G.V.** Physical modeling of counter-vortex structures and equipment (electronic resource). Moscow. MISI Publishing House – MGSU. 2018. 15 MB.
14. **Zuykov A.L.** Cylindrical flow swirler with elongated blade chord // Construction: Science and Education. 2023. Vol. 13. Issue 2. Art. 2.URL: http://nso-journal.ru. DOI: 10.22227/2305-5502.2023.2.2.
15. SP 58.13330.2012 Hydraulic structures. Basic provisions.
16. STO 17330282.27.140.002-2008 “Hydraulic structures of hydroelectric power plants and pumped storage power plants. Conditions for creation. Standards and requirements”.
17. STO 17330282.27.140.011-2008 “Hydroelectric power plants. Conditions for construction. Standards and requirements”.
18. STO 17330282.27.140.013-2008 “Mechanical equipment for hydroelectric power plant structures. Conditions for creation. Standards and requirements”.
19. STO 17330282.27.140.014-2008 “Technical systems of hydroelectric power plants. Conditions for creation. Standards and requirements.”
20. STO 17330282.27.140.022-2008 “Hydroelectric power plants and pumped

storage power plants. Conditions for construction. Standards and requirements."
21. **Benjamin T.B.** Theory of the Vortex Breakdown Phenomenon // Journal of Fluid Mechanics. 1962, Vol. 14, No 4, pp. 593-629.
22. **Lucca-Negro O., O'Doherty T.** Vortex Breakdown. A Review. Progress in Energy and Combustion Science. 2001. Vol. 27 (4). pp. 431-481.
23. **Akhmetov V.K.** Comparative analysis of mathematical models for studying the phenomenon of vortex decay // Scientific Review. 2015. No. 21. pp. 120–124.
24. **Akhmetov V.K.** Development of methods for mathematical modeling of the stability of swirling flows // Scientific Review. 2015. No. 21. pp. 125-129.
25. **Akhmetov V.K., Akhmetova V.V.** Mathematical modeling of hydrodynamics and stability of coaxially rotating flows // International Journal for Computational Civil and Structural Engineering. 2016. Vol. 12. No. 3. pp. 9–14.
26. **Akhmetov V.K.** Hydrodynamic stability of counter-vortex flows // Hydraulic Engineering. 2018. No. 2. pp. 13–18..
27. **Akhmetov V.K.** Hydrodynamic stability of coaxially rotating flows // Natural and Technical Sciences. 2025. No. 3. pp. 34-38.
28. **Abramovich, G.N.** Applied Gas Dynamics. Moscow. GITTL, 1953. 736 p..
29. **Abramovich, G.N.** Theory of Turbulent Jets. Moscow: Fizmatgiz, 1960. 715 p.
30. **Chigier N.A., Chervinsky A.** Experimental Investigation of Swirling Vortex Motion in Jets // Journal of Applied Mechanics. 1967. Vol. 34. Issue 2. pp. 443-451. DOI: 10.1115/1.3607703.
31. **Beér J.M., Chigier N.A.** Combustion Aerodynamics. New York. Halsted Press Division, Wiley, 1972. 264 p.
32. **Gupta A.K., Lilley D.G., Syred N.** Swirl Flows. England. Abacus Press, Tunbridge Wells, 1984. 475 p.
33. **Zuykov, A.L.** Hydrodynamics of Circulation Currents. Moscow. ASV Publishing House. 2010. 216 p.

---

*Genrih V. Orehov*, Doctor of Science, Professor, Department of Hydraulics and Hydrotechnical Engineering, National Research Moscow State University of Civil Engineering, 26, Yaroslavskoe Shosse, 129337, Moscow, RUSSIA, e-mail: OrehovGV@mgsu.ru

*Andrey L. Zuykov*, Doctor of Science, Professor, Department of Hydraulics and Hydrotechnical Engineering, National Research Moscow State University of Civil Engineering, 26, Yaroslavskoe Shosse, 129337, Moscow, RUSSIA, e-mail: ZuykovAL@mgsu.ru

*Mikhail K. Sklyadnev*, Department of Hydraulics and Hydrotechnical Engineering, National Research Moscow State University of Civil Engineering, 26, Yaroslavskoe Shosse, 129337, Moscow, RUSSIA, e-mail: SklyadnevMK@mgsu.ru

*Орехов Генрих Васильевич*, доктор технических наук, доцент, профессор кафедры гидравлики и гидротехнического строительства, Национальный исследовательский Московский государственный строительный университет, 129337, РОССИЯ, г. Москва, Ярославское шоссе, дом 26, e-mail: OrehovGV@mgsu.ru

*Зуйков Андрей Львович*, доктор технических наук, доцент, профессор кафедры гидравлики и гидротехнического строительства, Национальный исследовательский Московский государственный строительный университет, 129337, РОССИЯ, г. Москва, Ярославское шоссе, дом 26, e-mail: ZuykovAL@mgsu.ru

*Скляднев Михаил Константинович*, преподаватель кафедры гидравлики и гидротехнического строительства, Национальный исследовательский Московский государственный строительный университет, 129337, РОССИЯ, г. Москва, Ярославское шоссе, дом 26, e-mail: SklyadnevMK@mgsu.ru

DOI:10.22337/2587-9618-2025-21-3-172-187

# CHOOSING THE TYPE OF SHORE PROTECTION STRUCTURES IN RESERVOIRS (USING THE EXAMPLE OF THE NOVOSIBIRSK RESERVOIR)

***Tatiana V. Pilipenko [1], Dmitry V. Kozlov[2], Alexander Yu. Kudryashov [1], Vladimir V. Degtyarev [1], Anton S. Antonov[2], Alexander N. Yurchenko[2], Alexander S. Anshakov[2], Elena N. Guselnikova [1]***

[1] Novosibirsk State University of Architecture and Civil Engineering, Novosibirsk, RUSSIA
[2] National Research Moscow State University of Civil Engineering, Moscow, RUSSIA

**Abstract:** An increasingly urgent issue is the safety of the population, including the safety of living in the coastal zone of large bodies of water and in areas adjacent to hydraulic structures. The presence of such infrastructure facilities obligates the state to ensure their safe use for the population of the country: erecting and safely operating hydraulic structures, preventing the occurrence of emergency situations related to flooding and floodplain flooding, etc. However, adverse conditions and negative developments are increasingly occurring: dam collapses, accidents at waterworks, flooding and threats of urban areas flooding. All this directly relates to the condition of hydraulic structures (GS) and their service life; reconstruction is needed, as well as the construction of new ones. Protection of coastal areas of reservoirs is particularly important in today's world, as climate change and human impact have a negative effect on this area. One of the effective ways to protect is the use of coastal protective hydraulic structures (CPHS). The subject of study is an important part of the regional infrastructure - the Novosibirsk Reservoir, located in the Novosibirsk region and the Altai territory. The reservoir has multiple purposes (water supply, recreational and navigation). However, the coastline of the reservoir is constantly affected by various negative impacts, such as erosion, landslides, and flooding. Determining the optimal type of hydrological engineering structure for protecting the shoreline of the Novosibirsk reservoir based on analysis of existing CPHS types, their characteristics, and usage conditions is an urgent task for regions like the Novosibirsk area and Altai.

**Keywords:** hydraulic engineering structure, safe operation, emergency situation, shoreline, reservoir, shore-protecting hydraulic engineering structure

# ВЫБОР ТИПА БЕРЕГОУКРЕПИТЕЛЬНЫХ СООРУЖЕНИЙ НА ВОДОХРАНИЛИЩАХ (НА ПРИМЕРЕ НОВОСИБИРСКОГО ВОДОХРАНИЛИЩА)

***Т.В. Пилипенко[1], Д.В. Козлов[2], А.Ю. Кудряшов[1], В.В. Дегтярев[1], А.С. Антонов[2], А.Н. Юрченко[2], А.С. Аншаков[2], Е.Н. Гусельникова[1]***

[1]Новосибирский государственный архитектурно-строительный университет, г. Новосибирск, РОССИЯ
[2]Национальный исследовательский Московский государственный строительный университет, г. Москва, РОССИЯ

**Аннотация:** Все более актуальным вопросом является безопасность населения, в том числе безопасность проживания в прибрежной зоне крупных водных объектов и на территориях, примыкающих к гидротехническим сооружениям. Наличие таких объектов инфраструктуры обязывает государство обеспечивать население страны их безопасным использованием: возводить и безопасно эксплуатировать гидротехнические сооружения, не допускать возникновение чрезвычайных ситуаций (ЧС), связанных с подтоплением, затоплением пойменных территорий и пр. Однако, все чаще развиваются неблагоприятные условия и негативные события: происходят прорывы дамб, аварии на гидроузлах, наводнения и угрозы затопления урбанизированных территорий. Все это связано напрямую с состоянием гидротехнических сооружений (ГТС), сроком их службы, необходимостью реконструкции, потребностью в возведении новых ГТС. Защита береговой полосы водоемов приобретает особое значение в условиях современного мира, так как изменение климата и антропогенное воздействие

оказывают негативное влияние на эту территорию. Одним из эффективных способов защиты является использование берегозащитных гидротехнических сооружений (БГТС). Объектом исследования является важный элемент инфраструктуры региона - Новосибирское водохранилище, расположенное на территории Новосибирской области и Алтайского края. Водоем имеет многоцелевое назначение (водоснабжение, рекреация и судоходство). Однако, береговая полоса водохранилища постоянно подвергается различным негативным воздействиям, таким как эрозия, оползни и подтопление. Определение оптимального типа гидротехнического сооружения для защиты береговой полосы Новосибирского водохранилища на основе анализа существующих типов БГТС, их характеристик и условий применения, является актуальной задачей для таких регионов России как Новосибирская область и Алтайский край.

**Ключевые слова:** гидротехническое сооружение, безопасная эксплуатация, чрезвычайная ситуация, береговая линия, водохранилище, берегоукрепительное гидротехническое сооружение

## INTRODUCTION

Since the formation of the Novosibirsk Reservoir (more than 50 years ago), significant changes have taken place in the lives of the region, including those related to the development of coastal zones of this water body, a significant increase in population and infrastructure necessary for high-quality habitation on its shores. In addition, anthropogenic impact and climate change have undoubtedly had a significant impact on this area. It should be noted that Novosibirsk, created as a result of damming the Ob River to build the Novosibirsk Hydroelectric Power Station, was supposed to be located in a chain of reservoirs beginning with the Katun River in the Altai Republic, which merges with Biya in Biysk, Altai Krai, forming one of the world's largest lowland rivers, the Ob.. However, due to various compelling reasons, this project has not been implemented. Although in recent years, the question of its relevance has been raised again, it is reasonable to say, in connection with a number of the above-mentioned facts that the combination of these conditions significantly affected and continues to affect the state of the coastal zone of the Novosibirsk Reservoir. It is essential, first and foremost, to ensure the safety and stability of this area in the face of climate change and human impact.

## METHODS

Various methods are used to calculate coastal protection hydraulic structures (CPHS) at reservoirs, which take into account the natural conditions and features of the shoreline. The results of these calculations are refined based on field studies, laboratory tests, and experiments. The Novosibirsk valley reservoir regulates seasonal flow. According to its morphological features, it is divided into three sections: the upper section (130 km away from the dam), the middle section (60-130 km), and the lower section (up to 60 km). Nineteen small rivers flow into the reservoir, with the largest being the Berd River.

When designing a CPHS at a reservoir, the following factors must be considered:

*Natural conditions of the coastal zone.* In order to determine the dynamics of the collapse of the banks of the Novosibirsk reservoir, monitoring has been conducted since 2016.

Reference points were installed along shores of Novosibirsk Reservoir in 2017 to monitor dynamics of coastal collapse. 56 total rappers were installed: 31 on right bank and 25 on left bank. Coordinates of established reference points summarized in special table. Every year, specialists conduct on-site surveys in first decade of June and third decade of September. Surveys conducted by both road and water. Data on dynamics of coastal collapses generated in tabular format (Table 1)

In addition to monitoring the natural conditions of the coastal zone of the Novosibirsk reservoir, we used data from hydrometeorological surveys and the results of engineering and geological surveys ordered from third-party specialized organizations with necessary SRO permits to make constructive and design decisions for the

construction of CPHS. The data obtained was analyzed and applied to justify a particular type of construction that takes into account the type of soil, its properties and condition.

*The topography of the bottom and shore of the reservoir* was carried out by a team of specialists who were part of the group of authors for this work, independently using specialized calibrated instruments including an echo sounder, flow meter, and hydrometric turntable. Furthermore, in IndorCAD Rivier and IndorCad Drow programs we performed in-house processing of the results obtained. A sample map is shown in Figure 2.

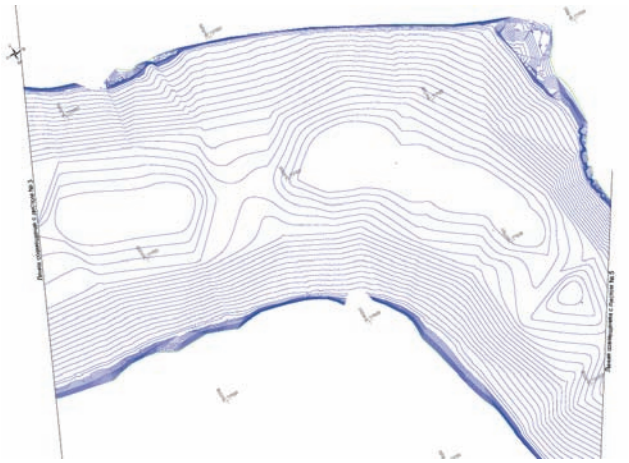

*Figure 2. An example of creating a hydrographic map*

An important aspect of the design of the CPHS is the analysis of *hydrological regimes*. Several hydraulic stations are in operation at the Novosibirsk reservoir, including the villages of Verkhny Beif and Spirino etc. Based on the available data, the amplitudes and the frequency of fluctuations in water levels are determined, which allow for making constructive decisions. The level regime of the reservoir is determined by periodic changes in volume due to water intake and use, as well as fluctuations caused by wind. Filling up in spring, the reservoir is triggered during the autumn-winter period, with an average operating amplitude of 4.76 m.

The basin of the reservoir is located in the territory of Novosibirsk Oblast and Altai Krai. The area of water surface is 1,070 square kilometers; the total volume is 8.8 cubic kilometers. The maximum width is 22 kilometers, the length is 185 kilometers, and the maximum depth is 29 meters. The average depth is 9 meters and 50 percent of the area is less than 5 meter deep. Sanatoria, boarding houses, recreation centers, children's health camps, and other facilities are located on the shore. Coastal erosion processes at the Novosibirsk Reservoir began during its filling and were intense. These processes continue today. The main cause of erosion is wind waves, which are associated with a lack of loose material in the coastal area. The consequences of coastal erosion lead to an aggravation of environmental problems, such as the reduction of fish resources, coastal destruction and bottom siltation. This leads to a deterioration in water quality. The total length of the coastal strip of the Novosibirsk reservoir is 550 kilometers, of which 332 kilometers are subject to treatment. When justifying a particular CPHS, we calculated current speeds, wave heights, ice conditions, and other parameters using existing calculation methods such as wave and ice loads described in the joint venture. The geological structure of the coast, consisting mainly of fine sands and loams, is the main factor in processing. During operation, the rate of coastal retreat has decreased somewhat, but only engineering protection can prevent further loss of land. Therefore, one of the most urgent problems is to protect the coast from the effects of wind and waves. Forecasts of dangerous engineering and geological processes (for example, landslides, earthquakes, etc.) are made based on the collected long-term data.

But the processes of coastal erosion lead not only to the loss of fertile land, but also to sedimentation of the river. During the operation period, the area of the reservoir at NPU = 113.5 m increased from 1070 km to 1082, and the volume increased from 8.8 to 8.02 km due to dead volumes. The useful capacity remained practically unchanged. According to observations, approximately 40,000 m3 of sediment settles annually in the bed of the reservoir, which causes the shallowing of the

water body and deterioration of its ecological condition as a whole. Because of the continuous impact of water on coastal areas, it is necessary to organize systematic and continuous monitoring of coastal areas, forecast related natural hazards, develop and implement effective methods to prevent or minimize their consequences.. The changes in the position of the coastline and the formation of islands in the area of predominantly fluvial morpholithogenesis of the Novosibirsk reservoir between 1960 and 2024 are shown in Figure 3. Based on the results of monitoring, if it is necessary to strengthen the coastline, specialists choose hydraulic structures based on feasibility studies.

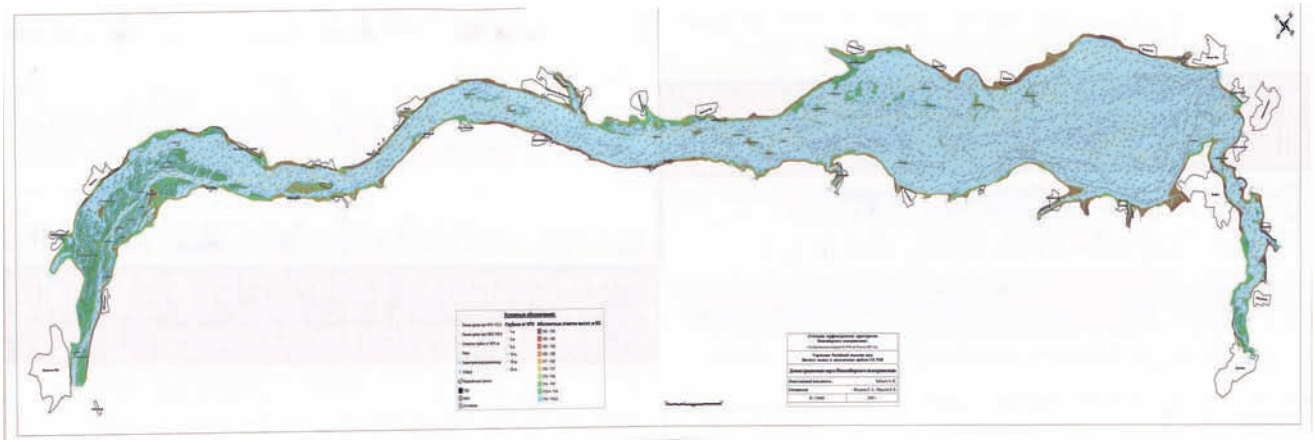

*Figure 1. A diagram of the Novosibirsk reservoir*

*Table 1. Table of the dynamics of changes in the distance from the reference point to the shore (in meters)*

| № Rp | location | 2016 | 06.2017 | 09.2017 | 06.2018 | 09.2018 | 06.2019 | 09.2019 | 06.2020 | 09.2020 | 06.2021 | 09.2021 | 06.2022 | 09.2022 | 06.2023 | 09.2023 | 06.2024 | 09.2024 | 06.2025 |
|---|---|---|---|---|---|---|---|---|---|---|---|---|---|---|---|---|---|---|---|
| 1 | Berdsk | 21,8 | 21,5 | 21,5 | 21,3 | 21,3 | 21,0 | 21,0 | 20,90 | 20,85 | 20,60 | 20,60 | 20,50 | 20,50 | 20,45 | 20,45 | 20,30 | 20,30 | 20.10 |
| 2 | Sosnovka | 59.9 | 47,1 | 43,3 | 43,0 | 42,8 | 42,5 | 42,4 | 42,2 | 42,1 | 42,0 | 39,5 | 39,3 | 39,2 | 38,9 | 38,7 | 38,5 | 38,3 | 37,9 |

Hydraulic structures designed to protect the shores and bottoms of reservoirs from the negative effects of water are classified as shore-protecting hydraulic structures, and provide engineering protection against the negative effects of the water.

The choice of the HS type depends on specific terrain conditions, such as topography, geological structure, hydrological regime, etc. It is important to consider not only the purpose of protecting the coastline when choosing a structure but also factors such as the type of reservoir, economics, environmental impact, durability, maintenance and safety. Only after a comprehensive analysis of these factors can specialists select the correct type of structure and design it.

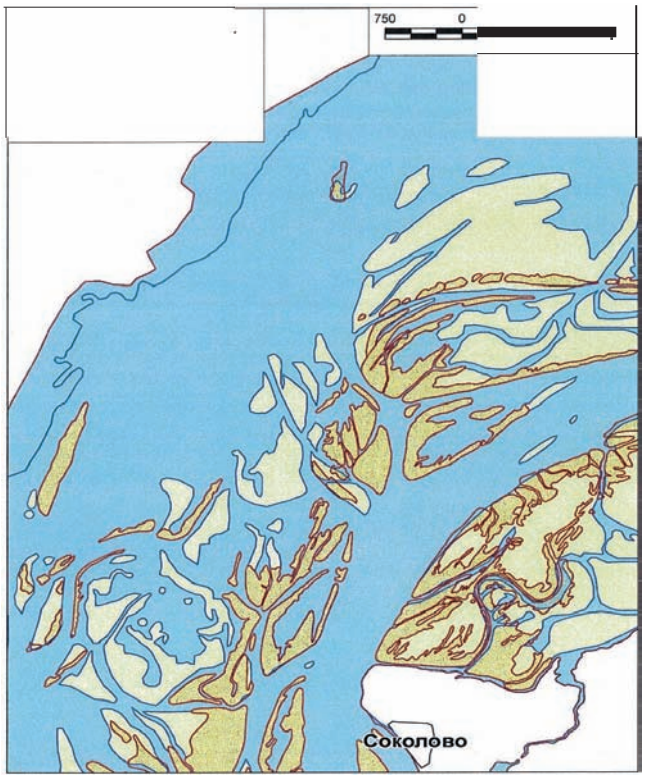


*Figure 3. Changes in the position of the coastline and the formation of islands in the area of predominantly fluvial morpholithogenesis of the Novosibirsk reservoir from 1960 to 2024*

In accordance with a number of regulatory and legal documents in force on the territory of the Russian Federation, coastal protection hydraulic structures belong to Class III. However, the class of coastal protection structure can be increased to Class II if destruction of coastal protection structures could lead to an emergency situation. To solve the problem of neutralizing negative effects of water on the Novosibirsk reservoir, we will consider the following options used in practice of coastal protection:

- rejuvenation of the coastal slope;
- biological protection applications;
- increasing the cross-section of the watercourse;
- filling with stone;
- applications of gabion structures;
- using geosoft;
- applications of monolithic (concrete, asphalt and other) coatings;
- applications of precast reinforced concrete structures;
- applications of sheet pile structures;
- applications of flexible concrete coverings.

All of these protection methods may be applicable to the specific case under consideration. However, some of them have been rejected due to their lack of compliance with the criteria for "safety" and "reliability". Other measures simply cannot be implemented because of the impossibility to do so, based on natural conditions in the area of the Novosibirsk Reservoir and its coastal zone. For example, when creating a "coastal slope rejuvenation", it is important to ensure that the angle of the slope is between 5.71 or 1 to 10 (the so-called "beach slope"). With this angle, the stability of adjacent concrete structures, as well as the stability of soil used as a base for those structures, is ensured. Thus, by flattening the coastline to a point less than 5.71 degrees, the coast is protected from destruction by breakwaters. Due to multi-storey buildings (e.g., Berdsk's right-bank section of the reservoir and the left-bank section fully developed by population), such methods as rejuvenating the banks cannot be used in our case to strengthen them.

The next method of coastal protection being considered is to increase the cross-section of a watercourse. However, the effectiveness of this method has not been confirmed by our calculations. With an increase in either depth or width in the water course, the flow rate slows down. It would not be constructive to increase the Novosibirsk reservoir's cross-section by increasing its width. Instead, an increase in depth would cause soil carried by currents to deposit in areas with slower currents. Over time, under natural processes, the cross-sectional area of the reservoir will return to its original size. This type of protection is only effective when combined with other types of defenses.

Protection of the coast by filling it with stones is one of the oldest methods to prevent erosion. Our hydraulic calculations show that the velocities of water flow in the Novosibirsk

Reservoir fully correspond to those calculated velocities at which there is no movement of stones from coastal protection structures along the shoreline. This movement begins at flow velocities between 0.8 and 1.3 meters per second. However, natural conditions in Siberia have their own limitations. In winter, stones of coastal defenses freeze into ice. When water levels rise in the river (during winter or spring floods), ice rises, tearing off layers of frozen stones from the surface. Currents can tear ice floes with frozen rocks away from the shore and carry them downstream. The filling of stones collapses. Also, as long-term experience shows, a stone deposit can be destroyed by a wind wave of over 1.7 meters high. According to hydraulic calculations carried out in the absence of winter floods on the Novosibirsk Reservoir, the ice thickness is at least 1 meter, so it is impractical to use stone filling due to significant destruction as an individual unit. However, in combination with other hydraulic structures, this type of shore protection is quite effective.

Gabion structures are another way to protect the coastal slope. They began to be widely used in hydraulic engineering construction in the late 1990s, i.e., more than 25 years ago. Practical experience with the use of gabions has revealed their unreliability, so the use of this type of structure entails high operational costs. As a result, gabion structures have lost their attractiveness, and their use is declining rapidly.

The gabion structures have been replaced by geogrids. Coastal protection structures using geogrid are very similar to gabion designs. At the same time, the strength of a "stone container" geogrid is far greater than that of a gabion grid. Unlike gabions, however, geogrid does not have a bottom, which can lead to accidents.

Monolithic coatings in relation to conditions of use, and importantly from the point of view of reliability of coastal protection structures, the manufacturing technology for this type of monolithic (concrete, asphalt, or other) coating on an open construction site often fails to meet the requirements for frost and water resistance, which leads to rapid destruction of the coating. In addition, constructing monolithic coatings requires precise alignment of the slope of the protected surface and subsequent compaction, which is difficult to achieve in practice. If the ground subsides during use, cracks will form on the coating, causing accidents and potentially leading to emergencies if not repaired promptly.

As for the experience of using precast reinforced concrete structures as shore protection structures in the conditions of water bodies, such as the Novosibirsk reservoir, they are inferior to other alternatives, even though they have a more complex construction process. This is because precast structures always have a lower support, on which the plates rest.

When it comes to protecting the shoreline of a reservoir, tongue-and-groove systems can be fragile and unreliable, based on years of experience. Based on 50 years of observation, the thickness of sheet piles is reduced from 10±1 mm to 2±1 mm, leading to complete destruction.

Let's consider the option of coastal protection in its relatively new form - using flexible concrete coverings. Flexible concrete slabs are placed on top of geotextiles, which act as an anti-diffusion barrier. In essence, the geotextile protects the object from negative effects of water. The main purpose of a flexible concrete slab is to prevent the destruction of the geotexiles. This type of coastal protection has been used recently. Facilities where pilot projects using flexible coverings have been implemented, including large reservoirs, are under our supervision. These projects were completed only five years ago and still meet requirements for operation and reliability.

## RESULTS AND DISCUSSION

Having considered all types of existing coastal protection structures and returned to the shoreline of the Novosibirsk reservoir, we can discuss the need to combine at least two types of hydraulic structures in design work. Only then will the purpose of this work be achieved. Engineering protection of reservoir shorelines

has gone through similar stages in its development to coastal protection history, but in a shorter time frame. Only 40 years ago, when selecting means to protect reservoir shores, priority was given to breakwater walls and various coastal coverings, such as stone-cast, reinforced concrete and asphalt concrete. It took less than ten years to realize all the disadvantages of passive structures and make significant adjustments to the strategy for coastal protection of artificial reservoirs. Coastal protection structures installed at the Novosibirsk Reservoir have truly prevented further erosion on the protected shorelines.. However, in the adjacent coastal areas, abrasive processes have noticeably intensified, on the contrary. Moreover, after several years, breakwater walls and coastal coverings have often begun to collapse quickly due to erosion of the bottom directly in front of them and violation of the integrity of their base.

Therefore, a different integrated approach to the design and construction of coastal protection structures is currently proposed. As an example, we should consider the section of the shoreline of Novosibirsk Reservoir near the village of Krasny Yar in Ordynsky District of Novosibirsk Region, which is undergoing active erosion (Fig. 4). A coastal protection structure with a length of 3,175 meters is required in this area. The construction of the facility was selected based on a comparison of similar projects located at the Novosibirsk reservoir and the estimated costs of implementing measures. After analyzing the initial data for the selected section of coastline, two integrated versions of coastal protection structures are proposed: a sheet pile wall made from composite material and a banquet made from rock mass, as well as an artificial division of coast into bays. The site was divided into segments for settlement. Wave effects were calculated for each site separately (see Fig. 5).

To prevent the abrasion of the coastal slope by wave load, it is planned to fill in the building profile of a sandy beach along the coast and install a beach-holding structure in the form of an intermittent breakwater.


*Figure 4. Estimated segments of the site being considered*

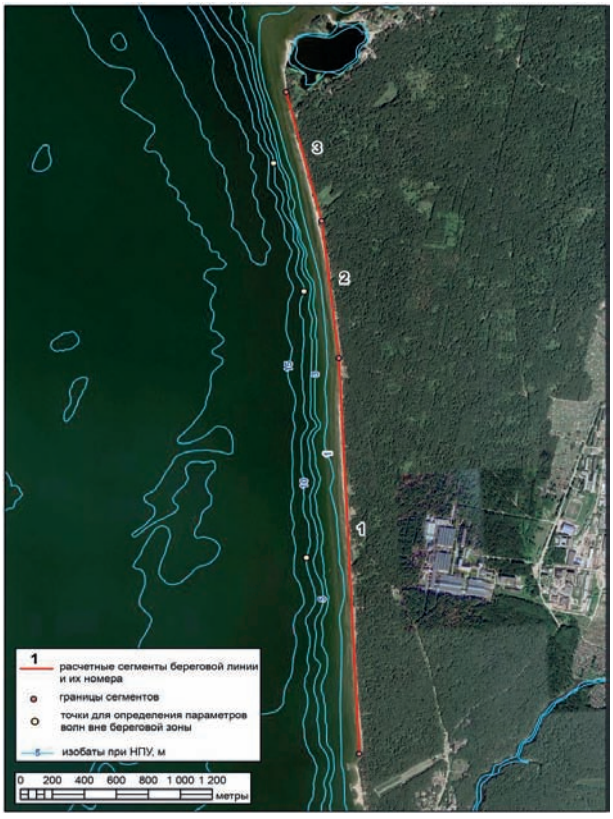


*Figure 5. Points for determining the parameters of waves in the coastal zone*

The first part of the complex structure is a rock banquet. After reshaping it by the excitement of water area of Novosibirsk reservoir, the banquet will take the form of natural stone beaches. Rock banquets have proven themselves as reliable structures that effectively perform their coastal protection function at Novosibirsk Reservoir. The disadvantage of rock banquets is the impossibility of using them for recreational purposes due to safety concerns. Calculations have been made for all segments and summarized in tables, based on which wave acceleration lines have been built in the most dangerous areas, an example of which is shown in Figure 6 for selected wave points along active wind directions.

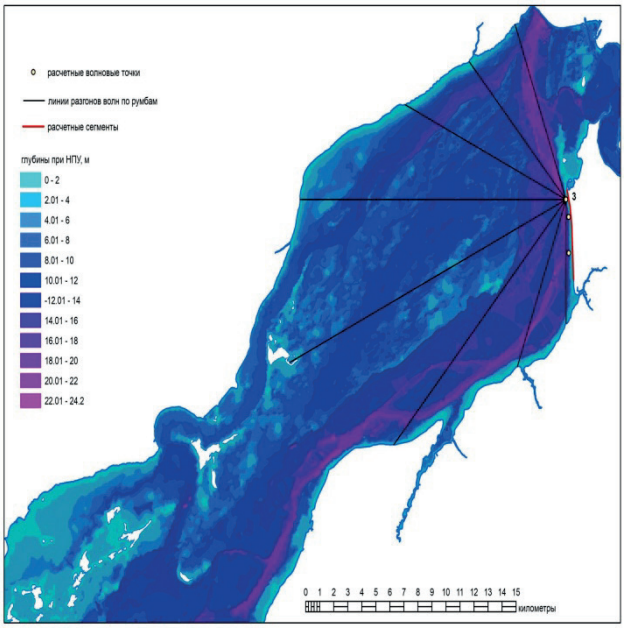


*Figure 6. lines of wave acceleration along active wind directions for point No. 3, segment No. 2 (Point No.3)*

The calculations of the wave elements were performed taking into account division into depth zones, which are clearly expressed in the approach to the projected section of the coast. The deep-sea area - has a depth $d > 0.5\bar{\lambda}_d$ (where the average $\bar{\lambda}_d$ wavelength is in the deep sea zone), and the bottom does not affect the main characteristics of waves.

Shallow - with a depth of $0.5\bar{\lambda}_d \geq d > d_{cr}$, where the bottom affects the development of waves and their main characteristics. (The critical depth of water is $d_{cr}$ at which the first wave collapses occurs).

Surf - with a depth of $d_{cr}$ to $d_{cu,r}$, within which wave destruction begins and ends.

Near-shore - with a depth of less than $d_{cu,r}$, within which the flow from destroyed waves periodically rolls onto the shore. The calculation of the deep-water zone is performed at the depth at the edge of the zone. The average height and average period of waves in the deep-sea zone are calculated according to formulas (P 31.3.07-01):

$$\frac{g\bar{h}}{V^2} = 0{,}16\left\{1-\left[1+6{,}0\cdot 10^{-3}\left(\frac{gL}{V^2}\right)^{1/2}\right]^{-2}\right\}\times \text{th}\left\{\frac{0{,}625\left(\frac{gd}{V^2}\right)^{0{,}8}}{1-\left[1+6{,}0\cdot 10^{-3}\left(\frac{gL}{V^2}\right)^{-2}\right]}\right\},$$

$$\frac{g\bar{T}}{V} = 19{,}47\left(\frac{g\bar{h}}{V^2}\right)^{0{,}625}$$

The average wavelength in the deep-sea zone is determined by the known value of the average period, according to the formula: $\bar{\lambda} = \frac{g\bar{T}^2}{2\pi}$.

The average wave height in shallow waters, $\bar{h}_s$, m, with bottom slopes less than 0.002, must be determined using the formula:

$$\bar{h}_s = \bar{h}_d \cdot \text{th}\left[\frac{0{,}1\left(\frac{gd}{V^2}\right)^{0{,}8}}{\frac{g\bar{h}_d}{V_w^2}}\right],$$

Where d is the depth of the water at the calculated point

The height of the waves in the i% zone must be determined by the formula, with decreasing depths and bottom slopes of i ≥ 0.02:

$$h_i = k_t \cdot k_r \cdot k_i \cdot \bar{h}_d,$$

where: $k_t$ – is the transformation coefficient;
$k_r$ – is the refractive index; $k_i$ – s the coefficient of transition to wave height; i % security; $\bar{h}_d$ – the initial average wave height in deep water.
The coefficients $k_t$, $k_r$ and $k_i$, cshould be determined according to regulatory documents.
The transformation coefficient $k_t$, must be calculated using the formula:

$$k_t = \left\{ \frac{C_N \left( 1 + \frac{4\pi}{C_n} \cdot \frac{d}{\bar{\lambda}_d} \right)}{\operatorname{sh}\left( \frac{4\pi}{C_N} \cdot \frac{d}{\bar{\lambda}_d} \right)} \right\}^{\frac{1}{2}}$$

Where

$$C_N = th^{0,5}\left( \frac{2\pi d}{\bar{\lambda}_d} \right)$$

d is the depth of water at the calculated point.
The refractive index for the bottom sections with rectilinear isobaths (with $0<a_d<60$, degrees) should be calculated using the formula

$$k_r = \left[ \frac{1 - C_N^2 \sin^2 \alpha_d}{\cos^2 \lambda_d} \right]$$

Where: $\alpha_d$ - The angle between the direction of the waves and the normal to the isobaths at a calculated point;
$C_N$ is a parameter defined by the formula.
The refractive index $k_r$ дfor bottom sections with curved isobaths can be determined in accordance with the recommendations.

The wavelength, $\bar{\lambda}$, m, moving from the deep-sea water area to the transformation zone, must be determined using the formula.

$$\bar{\lambda} = \bar{\lambda}_d th^{0,5}\left( \frac{2\pi d}{\bar{\lambda}_d} \right)$$

The depth of the first wave's collapse, $d_{cr}$, in the surf zone with a constant bottom slope, must be determined using the formula.

$$d_{cr} = a_i \left[ arcth\left( \frac{5,9 \cdot 2\pi (h_d)_{1\%}}{g\bar{T}^2} \right) \right] \cdot \frac{g\bar{T}^2}{2\pi}$$

where $\begin{cases} a_1 = 4,3 \\ a_2 = 5,4 \\ a_3 = 6,3 \end{cases}$ at $\begin{cases} 0,001 < i \le 0,033; \\ 0,033 < i < 0,049; \\ 0,05 \le i \le 0,2. \end{cases}$

The depth of the last wave, $d_{cr,u}$, m, from which the waves roll onto the shore is allowed to be calculated using a constant slope of the bottom, i: $d_{cr,u} = k_n^{n-1} d_{cr,}$
Where $d_{cr,u}$ – is the depth of the first wave collapse.
The wave height in the surf zone is 1% $h_{sur,1\%}$ at $d_{cr} \le d \le d_{cr,u}$ It must be determined using the formula.

$$h_{sur,1\%} = 0,18 \left[ th\left( a_i \frac{2\pi d}{g\bar{T}^2} \right) \right] \cdot \frac{g\bar{T}^2}{2\pi}$$

Where is the coefficient ai, it should be taken in accordance with the requirements of clause 2.17 these guidelines. where $\begin{cases} a_1 = 4,3 \\ a_2 = 5,4 \\ a_3 = 6,3 \end{cases}$ at $\begin{cases} 0,001 < i \le 0,033; \\ 0,033 < i < 0,049; \\ 0,05 \le i \le 0,2. \end{cases}$ The wavelength in the surf zone, $\bar{\lambda}_{sur}$, m, should be calculated using the formula.

$$\bar{\lambda}_{sur} = th^{0,5}\left( 9,2 \frac{2\pi d}{g\bar{T}^2} \right) \cdot \frac{g\bar{T}^2}{2\pi}$$

A wave surge is formed when waves collide and its

magnitude depends on the estimated height of the wave along the line of first collision ($h_{sur}$) and its average period. The calculation of the wave surge is performed according to the formula given in: $\Delta h = \frac{13,7}{g}\left(\frac{h_{sur}}{\overline{T}}\right)$. For Class III structures, in accordance with SP 38.13330.2012, p.5.9, the maximum calculated water level is assumed to be 5% secure. This is 113.70 mBS, in accordance with "Basic Provisions of the Rules for use of water resources in the Novosibirsk reservoir on the Ob river". The most dangerous wind directions are SSW, SW and WSW (highlighted in red).

To ensure the possibility of recreational use of the coast of the Novosibirsk reservoir, a beach 300 meters long is inserted into the considered variant. A system of enclosing boulders and breakwaters is envisioned to protect the sandy beach from significant losses of beach-forming sand. This will help reduce the loss of beach sand due to longshore sand transfer and the bay dissection of the beach inserts. The bay shape of this beach is most resistant to the effects of various storm directions due to its accumulating capacity for beach-holding structures. During the initial period of banquet formation, deepening and processing of the shoal will occur before the banquet. Processed products will be involved in long-range sediment flow. In order to accumulate the largest fraction from recycled soils of the shoals, we provide for installation of spurs that simultaneously act as technological platforms for machines and mechanisms. Beach-retaining structures will also play this role. The presence of accumulation zones reduces recycling of structures and extends their service life.

The outline of the banquet in the plan is close to the position of a cliff's brow. It should be noted that the jagged or broken position of the banquette in the plan has a greater resistance to the effects of excitement than a rectilinear position. This is because when exposed to wave fragments, waves change direction, leading to formation of oncoming currents. All this contributes to formation of sedimentation zones and accumulation zones, which ultimately leads to dissipation of excitation energy. The improvement of offshore areas and construction of anti-erosion structures allows the complex of coastal protection structures to be brought to parameters that ensure normal recreational use and enhance aesthetic appeal of coastal structures. Next, long-range sediment transport calculations were performed.. For sand deposits with a grain size range of $0.1 \leq d50 \leq 1$ mm, we used the widely used CERC formula. At the same time, it should be noted that the calculation formula uses the height of the significant wave ($H_s$) and the peak period of the wave spectrum (Tp), both of which are related to average wave parameters (H and T). An example of calculation results for a similar segment is shown in Figure 7.

The second part of the coastal protection structure is the artificial division of the coast into bays using various structures and elements made mostly of unsorted stone, such as bunks, breakwaters, blocking elements, and artificial capes. Bays can be filled (immediately or after formation by natural waves of a given size) with beach-forming material to form bay-shaped beaches, or they may not be filled with any imported soil in some cases.

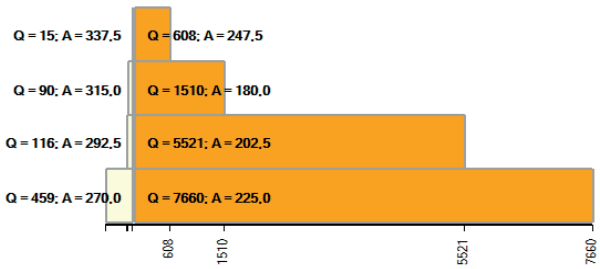


*Figure 7. The contribution of waves (wind) of various directions to the resulting sediment flow in the calculated segments: A is the direction of wind (waves) in degrees; Q is the total volume of sediment flow from waves in this direction (m³/year)*

Positive values of flow are shifted to the right, and negative values are shifted left. The direction and capacity of the resulting annual coastal sediment flow, caused by wind waves, for the area under onsideration are shown in Figure 8.

*Table 2. Calculation of wave elements in the deep-water zone for three segments*

| Naming of indicators | UOM | Designation | The value of the current points | | | | |
|---|---|---|---|---|---|---|---|
| Active points | - | - | S | SSW | SW | WSW | W |
| Wave acceleration length | m | L | 6198 | 9056 | 17363 | 21328 | 18954 |
| Wind speed 4% probability of Ob GMO | m/sec | V | 21 | 24 | 23 | 18 | 16 |
| Average wave parameters | | | | | | | |
| - height | m | $\overline{h_d}$ | 0,83 | 1,02 | 1,13 | 0,98 | 0,87 |
| - period | sec | $\overline{T}$ | 3,43 | 3,79 | 4,07 | 3,96 | 3,80 |
| - length | m | $\overline{\lambda_d}$ | 18,38 | 22,44 | 25,88 | 24,50 | 22,56 |
| Estimated wave height in storm mode with a 4% probability | | | | | | | |
| -1% P in the wave system | m | $h_{1\%}$ | 1,72 | 2,13 | 2,36 | 2,10 | 1,85 |
| -2% P in the wave system | m | $h_{2\%}$ | 1,57 | 1,94 | 2,19 | 1,91 | 1,70 |
| -5% P P in the wave system | m | $h_{5\%}$ | 1,44 | 1,79 | 1,99 | 1,75 | 1,55 |
| Depth at the boundary of the zone $0.5\bar{\lambda}_d$ | m | | 9,2 | 11,2 | 12,9 | 12,2 | 11,3 |

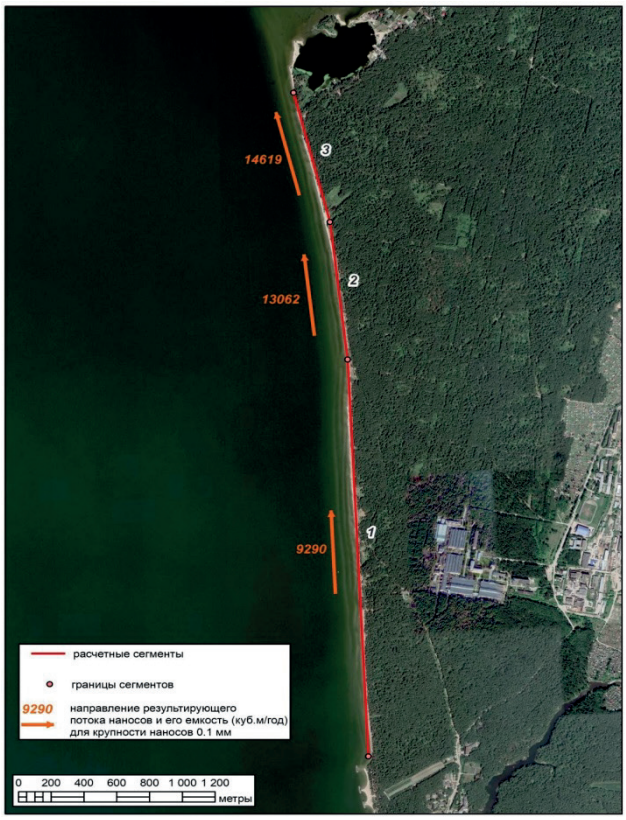


*Figure 8. The direction and capacity of the annual coastal sediment flow in the coastal zone of the site under consideration*

In the considered variant, beach-retaining structures are provided, which are intermittent breakwaters. In the shadow of these structures, the rudiments of overflows form, blocking the through movement of sediments along the coast and contributing to the dissection of the bay by an artificially created sand prism. With the division of the coast into bays, the beaches formed within them are the most stable. To ensure the formation of a wave shadow in the armhole of the breakwater, it is necessary that the length of this structure be 1.5 times greater than the distance between the shore and the breakwater. The calculated profile of the beach should also not extend beyond the line of breakwaters, while the beaches are most stable in bays with an approximately circular outline. At the same time, the length of a breakwater should be at least equal to the width of an underwater beach.. These conditions correspond to breakwaters, with an average

length of 90 m, and gaps between them averaging 90 meters, removed no more than 60 meters from the filled-out sand prism, which is the capital class of these shore protection structures. The construction of coastal protection structures as provided in the design documentation aims to prevent further damage to the coast from dangerous natural processes, such as coastal slope abrasion from waves during stormy periods.

The durability of the adopted design solution and its reliability during the service life (at least 50 years) is justified by several factors. The design solution is a proven system, and the applied polymer composite sheet pile profile SHK-150UM is produced using injection pultrusion with a polyurethane binder. This ensures high stability of properties and resistance to aggressive environmental influences, as confirmed by test reports. The resistance to temperature fluctuations and UV radiation, as well as low water absorption, are also confirmed. The anchor system's durability is further justified by its anti-corrosion protection, while the length of the tongue-and-groove wall measures 5260 meters. The calculation of the bearing capacity of the tongue-and-groove wall and anchor pile was performed using Midas GTS NX software in a two-dimensional formulation. Structural elements of the structure include: vertical element - sheet pile profile SHK-150UM, with a length of 5 meters and maximum depth of 3.8 meters; distribution belt of paired channels 12P GOST 8240-97 at levels 114.20 and 113.70; interconnected and attached to the sheetpile through a bolted connection M12; anchors made of A400 reinforcing bars with a diameter of 28 cm, GOST 5781-82, with a 4 meter length in increments of 0.4 meters, fastened to the tongue and groove wall through the distribution belt at 11.4. Anchors are mounted through steel plates GOST 19903 -74 measuring 0.2 x 0.02 m through bolted connections M18; anchor piles are channel 14 P GOST buried in ground with 3 meter lengths in 0.6 m steps, 4 meters apart from tongue-and groove walls.. The anchor rods are mounted to the anchor pile through a steel plate measuring 200 x 200 mm 15, through a bolted connection M18. Fastening metal parts with M12 and M18 bolts and nuts. The anchor system is protected with anti-corrosion coating that meets the requirements of SP 287.1325800.2016 and SP 2.13330.0201. The anchor must be painted with epoxy-based enamel to protect it. It is also recommended to fill attachment points and connections of anchor rods with bitumen-rubber paint / mastic to protect them. A drainage prism is used to relieve filtration pressure. This prism consists of small fractions of crushed stone separated by Geospan TS-110 geotextiles. The formed sinuses are filled with crushed stones. Filtration holes with a diameter of 20 mm are arranged in sinuses with a spacing of 11.37 mm at a step of 0.96 ft. An upper polyurethane composite belt PKSH-160 painted in bright color is installed on top of the walls for overall stability. Main angles of rotation are provided by angular polyurethane connectors USK-150.. Temperature-sedimentary seams with a pitch of no more than 25 meters are arranged in the upper belt and the distribution belt in the sheet pile joint. Backfilling is performed with soil (fine, homogenous, water-saturated, medium density sand) extracted using a hydro-mechanical method. The filling mark is 114.70, and the soil compaction coefficient is accepted according to SP 22.13330.2016 (clause 9.14), with $k_{com}$ =0.95. Fine and powdery sand is located at the base of the sheet-pile wall. To prevent erosion of the foundation, a stone berm has been arranged on the front side, with a width of 4800 m and a slope of 1: 1.5. The diameter of the stones used for fastening was estimated to be 0.45 m, and after reshaping the profile, stone fastening would provide a non-erosive foundation for the tongue-and-groove wall. Load-bearing capacity calculations for both the tongue and groove wall and anchor piles were performed. The mass of each element in the stone fastener was also calculated, as well as the parameters of stone fasteners.

## CONCLUSION

In conclusion, I would like to note that the authors of the work focus on the relevance of the problem of coastal protection of the Novosibirsk reservoir, primarily for the local population and the ecosystem as a whole. They demonstrate the need to develop and implement effective and efficient measures taking into account financing features and difficulties arising from natural changes. The CPHS construction considered in this paper is aimed at preventing further destruction of the coast by dangerous natural processes such as abrasion of the coastal slope by waves during storm periods. The durability of the adopted design solution and its reliability during the service life of the design (at least 50 years) is justified by the following factors:

- the constructive solution is a proven bolverk system (Abramov, D. S., Shielded bulwarks: A historical review, research, design competition and calculation methodology features. Hydraulic Engineering 1(30)/2013; Kostyukov, V.D., Reliability of marine berths and their reconstruction, Moscow: Transport, 1987). Many structures of this type built in the 1960s and 1970s are still operational and have exceeded their designed service lives (Reconstruction of bolverk berths by changing the structure from a spacer to a gravity-based one, Nikolaevsky, M.Yu., Gorgutsa, R.Yu. and Sokolov, A.V., HYDRAULICS AND HYDROTECHNICS OF THE XXI CENTURY, No.1 (17), 2014).
- the applied polymer composite sheet pile profile SHK-150UM is manufactured using injection pultrusion with a polyurethane binder, which ensures high stability of properties and high resistance to aggressive environmental influences. The resistance to temperature fluctuations, UV radiation, and low water absorption is confirmed by test reports.
- the durability of the anchor system is justified by the anti-corrosion protection applied that meets the requirements of SP 287.1325800.2016 and SP 28.13330.2012. To prevent the adverse effects of human activity on the coastal environment, a coastal protection zone has been established, where safe economic activity is regulated.

To prevent the adverse effects of man-made activities on the CPHS, a coastal protection zone is provided where safe economic activities are regulated.

## ACKNOWLEDGEMENTS

Having analyzed the proposed options for existing coastal protection structures, the authors of the article propose a way to assemble several types of coastal protection hydraulic structures. These structures can serve as a model for other regions facing similar problems. An experiment is currently being conducted on the basis of a laboratory. The aim of this experiment is to obtain confirmed data on the stability of these hydraulic structures to the effects of waves, currents, and ice.

## REFERENCES

1. **Pilipenko T., Enaki E.** Dynamics of processing of the Novosibirsk reservoir banks December 2021 IOP Conference Series Earth and Environmental Science 937(4):042097 DOI:10.1088/1755-315/937/4/042097
2. **Rubin O.; Kozlov D.; Antonov A.; Zhang J.** Strengthening of Rein-forced Concrete Hydraulic Structures with External Reinforcement System Made of Carbon Fiber-Based Composite Materials with Development of Cal-culation Recommendations. Buildings, 2024, №14, 3739, doi.org/10.3390/buildings14123739
3. **Oleg D. Rubin, Dmitry V. Kozlov, Anton S. Antonov, Amer Almasri, Zhang Junhao**. Design and experimental studies of strengthening of backwater type hydraulic structures with composite materials. *International Journal for Computational Civil and Structural*

*Engineering, 2024, Vol. 20 № 4., DOI: https://doi.org/10.22337/2587-9618-2024-20-4-119-140*

4. **Pilipenko T., Mihailova T., Suslikov E., Ahmatova N.** Assessment of the impact of the development of the floodplain of the Ob River on the safety of navigation. Springer Nature Link 2022, №2 (LNNS, том 403). https://doi.org/10.1007/978-3-030-96383-5_103
5. **Pilipenko T., Kalachnikov A., Botvinkov I.** Influence of the slot configuration on its stability (on the example of the Ob river); Springer Nature Link 2022, №2. In book: International Scientific Siberian Transport Forum TransSiberia - 2021, Volume 1 (pp.1133-1140) DOI:10.1007/978-3-030-96380-4_124
6. **A. Kudryashov, A. Sitnov**. Improving the strength characteristics of materials for hydraulic structures with reinforcing compositions. March 2022. In book: International Scientific Siberian Transport Forum TransSiberia - 2021, Volume 1 (pp.1141-1147). DOI:10.1007/978-3-030-96380-4_125
7. **Anshakov A.S.** Modeling of Hydrodynamic and Lithodynamic Coastal Processes in the Harbour Area. Fundamentaland Applied Hydrophysics. 2022, 15, 4, 101–108. doi:10.48612/fpg/xhaz-46hz-kk62 *(Scopus)*
8. **Ghinwa Hadla, Alexander Anshakov and Izmail Kantarzhi.** Composite Modelling in Port Engineering. FORM-2020, IOP Conf. Series: Materials Science and Engineering, 869 (2020), v.7, 1-9. (Scopus) doi: 10.1088/1757-899X/869/7/072044 (Scopus)
9. **Hadla, G., Anshakov, A.S. & Kantarzhi, I.G.** The Role of Currents and Waves in the Movement of Sediments in the Vicinity of Coastal Hydraulic Structures. Power Technol Eng 54, 841–847 (2021). DOI: 10.1007/s10749-021-01297-0 (Scopus)
10. **Rubin O. D., Britvin S. O., Baklykov I. V., Yurchenko A.N.** The Results of the Calculation Substantiation of the Stress-Strain State, Strength and Stability of the Construction of a Gravity Base. Industrial and Civil Construction, 2024, 436, pp 182-191 DOI: 10.1007/978-3-031-44432-6_24.

## СПИСОК ИСТОЧНИКОВ

1. **Pilipenko T., Enaki E.** Dynamics of processing of the Novosibirsk reservoir banks December 2021 IOP Conference Series Earth and Environmental Science 937(4):042097 DOI:10.1088/1755-315/937/4/042097
2. **Rubin O.; Kozlov D.; Antonov A.; Zhang J.** Strengthening of Rein-forced Concrete Hydraulic Structures with External Reinforcement System Made of Carbon Fiber-Based Composite Materials with Development of Cal-culation Recommendations. Buildings, 2024, №14, 3739, doi.org/10.3390/buildings14123739
3. **Oleg D. Rubin, Dmitry V. Kozlov, Anton S. Antonov, Amer Almasri, Zhang Junhao**. Design and experimental studies of strengthening of backwater type hydraulic structures with composite materials. *International Journal for Computational Civil and Structural Engineering, 2024, Vol. 20 № 4., DOI: https://doi.org/10.22337/2587-9618-2024-20-4-119-140*
4. **Pilipenko T., Mihailova T., Suslikov E., Ahmatova N.** Assessment of the impact of the development of the floodplain of the Ob River on the safety of navigation. Springer Nature Link 2022, №2 (LNNS, том 403). https://doi.org/10.1007/978-3-030-96383-5_103
5. **Pilipenko T., Kalachnikov A., Botvinkov I.** Influence of the slot configuration on its stability (on the example of the Ob river); Springer Nature Link 2022, №2. In book: International Scientific Siberian Transport Forum TransSiberia - 2021, Volume 1 (pp.1133-1140) DOI:10.1007/978-3-030-96380-4_124
6. **A. Kudryashov, A. Sitnov**. Improving the strength characteristics of materials for

hydraulic structures with reinforcing compositions. March 2022. In book: International Scientific Siberian Transport Forum TransSiberia - 2021, Volume 1 (pp.1141-1147). DOI:10.1007/978-3-030-96380-4_125

7. **Anshakov A.S.** Modeling of Hydrodynamic and Lithodynamic Coastal Processes in the Harbour Area. Fundamentaland Applied Hydrophysics. 2022, 15, 4, 101–108. doi:10.48612/fpg/xhaz-46hz-kk62 *(Scopus)*
8. **Ghinwa Hadla, Alexander Anshakov and Izmail Kantarzhi.** Composite Modelling in Port Engineering. FORM-2020, IOP Conf. Series: Materials Science and Engineering, 869 (2020), v.7, 1-9. (Scopus) doi: 10.1088/1757-899X/869/7/072044 (Scopus)
9. **Hadla, G., Anshakov, A.S. & Kantarzhi, I.G.** The Role of Currents and Waves in the Movement of Sediments in the Vicinity of Coastal Hydraulic Structures. Power Technol Eng 54, 841–847 (2021). DOI:10.1007/s10749-021-01297-0 (Scopus)
10. **Rubin O. D., Britvin S. O., Baklykov I. V., Yurchenko A.N.** The Results of the Calculation Substantiation of the Stress-Strain State, Strength and Stability of the Construction of a Gravity Base. Industrial and Civil Construction, 2024, 436, pp 182-191 DOI: 10.1007/978-3-031-44432-6_24.

---

*Tatiana Viktorovna Pilipenko* - PhD, Associate Professor at the Department of GTS BE of Federal State Budgetary Educational Institution of Higher Education Novosibirsk State University of Architecture and Civil Engineering (Sibstrin). Address: 113 Leningradskaya St., Novosibirsk, Russia. E-mail: taniavp_2005@rambler. ru

*Татьяна Викторовна Пилипенко* - к.т.н., доцент, доцент кафедры ГТС БЭ, Федеральное государственное бюджетное образовательное учреждение высшего образования «Новосибирский государственный архитектурно-строительный университет (Сибстрин)» (ФГБОУ ВО «НГАСУ (Сибстрин)»), дом 113, улица Ленинградская, город Новосибирск, 630008, Россия, эл. почта: taniavp_2005@rambler.ru

*Dmitry Vyacheslavovich Kozlov* - Doctor of Technical Sciences, Professor and Head of the Advanced School of Civil Engineering at National Research Moscow State University of Civil Engineering. Address: 26 Yaroslavskoe Shosse, Moscow, Russia. E-mail: kanz@mgsu. ru

*Дмитрий Вячеславович Козлов* - д.т.н., профессор, руководитель Передовой инженерно-строительной школы, заведующий кафедрой ГиГС, Национальный исследовательский Московский государственный строительный университет (НИУ МГСУ), член-корреспондент РААСН по Отделению строительных наук, дом 26, Ярославское шоссе, город Москва, 129337, Россия, эл. почта: kanz@mgsu.ru

*Alexander Yuryevich Kudryashov* - Corresponding Member of Russian Academy of Sciences. Candidate of Technical Sciences, Associate Professor, Associate Professor, Department of GTS BE, Federal State Budgetary Educational Institution of Higher Education Novosibirsk State University of Architecture and Civil Engineering (Sibstrin), 113 Leningradskaya Street, Novosibirsk, 630008, Russia. E-mail: as@sibstrin.ru

*Александр Юрьевич Кудряшов* - к.т.н., доцент, доцент кафедры ГТС БЭ, Федеральное государственное бюджетное образовательное учреждение высшего образования «Новосибирский государственный архитектурно-строительный университет (Сибстрин)» (ФГБОУ ВО «НГАСУ (Сибстрин)»), дом 113, улица Ленинградская, город Новосибирск, 630008, Россия, эл. почта: as@sibstrin.ru

*Vladimir Vladimirovich Degtyarev* - Doctor of Technical Sciences, Professor, Professor, Department of GTS BE, Federal State Budgetary Educational Institution of Higher Education Novosibirsk State University of Architecture and Civil Engineering (Sibstrin), 113 Leningradskaya Street, Novosibirsk, 630008, Russia. E-mail: as@sibstrin.ru

*Владимир Владимирович Дегтярев* - д.т.н., профессор, профессор кафедры ГТС БЭ, Федеральное государственное бюджетное образовательное учреждение высшего образования «Новосибирский государственный архитектурно-строительный университет (Сибстрин)» (ФГБОУ ВО «НГАСУ (Сибстрин)»), дом 113, улица Ленинградская, город Новосибирск, 630008, Россия, эл. почта: as@sibstrin.ru

*Anton Sergeevich Antonov* - Candidate of Technical Sciences, Associate Professor, Associate of the GiGS Department of National Research Moscow State University of Civil Engineering (NRU MGSU)- Address: 26 Yaroslavskoe Shosse, Moscow, Russia, kanz@mgsu.ru

*Alexander Nikolaevich Yurchenko*, Candidate of technical sciences, associate professor, and associate of the GiGS department at NRU MGSU, Address: 26 Yaroslavskoe Shosse, Moscow, Russia E-mail: kanz@mgs.ru

*Alexander Sergevich Anshakov*, Candidate of technical sciences, associate professor, and associate of the GiGS department at NRU MGSU, Address: 26 Yaroslavskoe Shosse, Moscow, Russia E-mail: anshakov@mgu.ru

*Elena Nikolaevna Guselnikova*, Candidate of Technical Sciences, Associate Professor, Head of the Department of GTS, BE, Federal State Budgetary Educational Institution of Higher Education, Novosibirsk State University of Architecture and Civil Engineering (Sibstrin), Address:113 Leningradskaya Street, Novosibirsk, 630008, Russia. e-mail address: as@sibstrin.ru

*Funding*. The research was funded by the National Research Moscow State University of Civil Engineering, registration number in the EGISU NIOKTR: 125070808055-3

*Антон Сергеевич Антонов* - к.т.н., доцент, доцент кафедры ГиГС, Национальный исследовательский Московский государственный строительный университет (НИУ МГСУ), дом 26, Ярославское шоссе, город Москва, 129337, Россия, эл. почта: kanz@mgsu.ru

*Александр Николаевич Юрченко* - к.т.н., доцент, доцент кафедры ГиГС, Национальный исследовательский Московский государственный строительный университет (НИУ МГСУ), дом 26, Ярославское шоссе, город Москва, 129337, Россия, эл. почта: kanz@mgsu.ru

*Александр Сергеевич Аншаков* - к.т.н., доцент, доцент кафедры ГиГС, Национальный исследовательский Московский государственный строительный университет (НИУ МГСУ), дом 26, Ярославское шоссе, город Москва, 129337, Россия, эл. почта: kanz@mgsu.ru

*Елена Николаевна Гусельникова* - к.т.н., доцент, заведующая кафедры ГТС БЭ, Федеральное государственное бюджетное образовательное учреждение высшего образования «Новосибирский государственный архитектурно-строительный университет (Сибстрин)» (ФГБОУ ВО «НГАСУ (Сибстрин)»), дом 113, улица Ленинградская, город Новосибирск, 630008, Россия, адрес электронной почты: as@sibstrin.ru

*Финансирование*. Работа выполнена при поддержке Федерального государственного бюджетного образовательного учреждения высшего образования «Национальный исследовательский Московский государственный строительный университет» (НИУ МГСУ) и имеет регистрационный номер карты в ЕГИСУ НИОКТР: 125070808055-3

DOI:10.22337/2587-9618-2025-21-3-188-200

# COMPARATIVE STUDY OF EARTHQUAKE-RESISTANT BUILDING DESIGN STANDARDS

***Dwi Yanto, Tavio***

Department of Civil Engineering, Institut Teknologi Sepuluh Nopember, East Java, INDONESIA

**Abstract:** Earthquakes are often disasters that cause significant damage to infrastructure, buildings, and even fatalities. As a result, many nations globally have established earthquake-resistant design standards to protect infrastructure, buildings, and human lives from the impacts of seismic events. The objective of this research is to assess how the implementation of earthquake-resistant construction standards influences the structural integrity and performance of buildings across Indonesia. The research was undertaken by comparing buildings designed based on SNI 1726:2019, Eurocode 8:2004, and IS 1893:2016. The method employed involves comparing both elastic and inelastic design results using pushover analysis for each standard to assess seismic performance using ETABS software as an analytical tool. Findings from the analysis reveal that structures designed following the SNI 1726:2019 required the smallest area of flexural reinforcement, followed by an increased requirement in Eurocode 8:2004, and the highest in IS 1893:2016. Furthermore, the nonlinear pushover analysis revealed that the performance point of SNI 1726:2019 was 8.38% higher than Eurocode 8:2004 and 24.03% higher than IS 1893:2016 in the X direction, and 12.15% higher than Eurocode 8:2004 and 27.76% higher than IS 1893:2016 in the Y direction.

**Keywords:** Design Standards, Disaster Risk Reduction, Earthquake-Resistant Buildings, Eurocode 8, IS 1893, SNI 1726, Structural Performance

# СРАВНИТЕЛЬНОЕ ИССЛЕДОВАНИЕ СТАНДАРТОВ ПРОЕКТИРОВАНИЯ СЕЙСМОСТОЙКИХ ЗДАНИЙ

***Дви Янто, Тавио***

Кафедра Гражданского Строительства, Институт Технологии Сепулух Нопембер, Восточная Ява, ИНДОНЕЗИЯ

**Аннотация:** Землетрясения часто являются катастрофами, вызывающими значительные повреждения инфраструктуры, зданий и даже человеческие жертвы. В связи с этим многие страны мира разработали стандарты сейсмостойкого проектирования, направленные на защиту инфраструктуры, зданий и человеческих жизней от последствий сейсмических событий. Цель данного исследования — оценить, как внедрение стандартов сейсмостойкого строительства влияет на структурную целостность и эксплуатационные характеристики зданий в Индонезии. Исследование проводилось путем сравнения зданий, спроектированных на основе стандартов SNI 1726:2019, Eurocode 8:2004 и IS 1893:2016. В качестве метода использовалось сравнение результатов упругого и неупругого расчета с применением метода пошагового анализа (pushover analysis) для каждого стандарта с целью оценки сейсмической устойчивости с использованием программного обеспечения ETABS в качестве аналитического инструмента. Результаты анализа показали, что конструкции, спроектированные в соответствии с SNI 1726:2019, требуют наименьшей площади гибкой арматуры, затем следует Eurocode 8:2004 с повышенными требованиями, и наибольшие требования предъявляет IS 1893:2016. Кроме того, нелинейный пошаговый анализ выявил, что точка эксплуатационной эффективности по SNI 1726:2019 была выше на 8,38 % по сравнению с Eurocode 8:2004 и на 24,03 % по сравнению с IS 1893:2016 в направлении X, а также на 12,15 % выше по сравнению с Eurocode 8:2004 и на 27,76 % выше по сравнению с IS 1893:2016 в направлении Y.

**Ключевые слова:** Стандарты проектирования, снижение рисков бедствий, сейсмостойкие здания, Еврокод 8, IS 1893, SNI 1726, эксплуатационные характеристики конструкций

## 1. INTRODUCTION

Seismic events, or earthquakes, occur as a consequence of energy release in the Earth's crust, leading to ground surface vibrations [1]. As earthquakes frequently inflict significant destruction on structures and critical infrastructure, they also pose serious risks to human safety and result in fatalities. Many countries around the world are at risk from seismic events. Indonesia, in particular, exhibits high vulnerability as a result of its location within the Pacific Ring of Fire, a zone distinguished by frequent and strong earthquakes. Given the frequency and intensity of earthquakes, safeguarding buildings to withstand seismic forces has become increasingly important. To mitigate the impacts of earthquakes, countries have developed seismic design standards to ensure that buildings can withstand seismic loads. As a result, the implementation of earthquake-resistant building design principles has become essential in the planning and development of infrastructure.

Sub-group B of the International Association for Bridge and Structural Engineering (IABSE) conducted a cross-country comparison of earthquake-resistant design regulations, identifying both the similarities and differences to uncover existing knowledge gaps [2]. In this context, comparative studies between seismic design standards are crucial. These studies aim to identify the strengths and weaknesses of each standard and to provide insights for the development of more effective building codes in Indonesia.

This research draws upon a number of prior studies that analyzed comparative standards for earthquake-resistant buildings in various countries. Building codes classify structures into varying levels of ductility categories and then determine and apply the relevant response modification factors, taking into account material properties, structural configuration, and detailing requirements. Despite variations in implementation, there is a significant convergence among modern national seismic codes regarding their overall design methodologies [3].

The infrastructure development in Gulf countries is widely regarded as exemplary, with many structural systems reportedly designed in accordance with European codes. Consequently, a critical evaluation of these codes is essential to support the adoption of best construction practices in emerging economies, including India [4]. Adhikari et al [5] compared four different seismic design codes using identical parameters, including site class, peak ground acceleration (PGA), building dimensions, and material specifications. Aksoylu et al [6] compared the Turkish seismic design standards with the American ASCE 7-16 code by evaluating several structural response parameters, namely seismic base shear force, roof displacement, time period, and inter-story drift.

Srikant et al [7] in their study conducted a comparative analysis of seismic responses using the Indian Standard through both static and dynamic methods. The results indicated that the static method produced more conservative outcomes, particularly at the top levels of the structure. The study conducted by Karthiga et al (2015) compared residential buildings designed in accordance with four seismic design codes: IS 1893 (Indian Standard), Eurocode 8, ASCE 7-10, and the British Standard using the SAP2000 structural analysis software. The study concluded that Eurocode 8 resulted in the most economical design, whereas IS 1893 produced the least economical outcome [8]. Mala et al [9] compared the seismic design standards NBC 105:1994 and NBC 105:2020 for reinforced concrete apartment buildings using pushover analysis in ETABS. The results demonstrated that NBC 105:2020 provides greater structural capacity compared to NBC 105:1994. Seismic analysis plays a crucial role in earthquake engineering, serving as an essential method to simplify the assessment of building responses under seismic loading. Historically, structural designs primarily focused on gravity loads, with seismic analysis

emerging as a more recent advancement in structural engineering practices [10].

Işık et al [11] compared in their study, which evaluates seismic risk and target displacement values by considering both measured and proposed peak ground acceleration (PGA) parameters for various earthquakes across different countries. Six nations with varying seismicity levels were selected for analysis, namely Bosnia and Herzegovina, Albania, Croatia, Iran, Türkiye, and Serbia, all of which fall within the scope of this research. Seismic design codes differ across regions and countries, each incorporating distinct control parameters aimed at improving the seismic performance of buildings. Extensive research has been conducted to evaluate the seismic behavior of existing structures [12]. By showing the limitations of pushover analysis when comparing structures built to older codes to new criteria, these findings advance the discipline [13].

Tapkire et al [14] noted that the design base shear specified in IS 1893 is lower than that in Eurocode 8, primarily due to the higher response reduction factor employed in IS 1893. A comparative analysis of various seismic design standards reveals a consensus on key characteristics essential for seismic-resistant structures, including simplicity, symmetry, uniformity, and redundancy. Suliman et al [15] compared the seismic performance of MRF-RC (Moment Resisting Frame – Reinforced Concrete) buildings by applying four distinct codes: the Ethiopian Building Code Standard (EBCS-8), the Egyptian Code for Design and Construction of Reinforced Concrete Structures (ECP-201), the Algerian Seismic Monitoring Code Regulations (RPA 99), and the Chinese Code for Seismic Design of Buildings (GB-50011). The comparative study involves modeling buildings of varying heights and configurations, followed by the simulation of realistic seismic events corresponding to different seismic zones. Through systematic analysis and performance evaluation, the study aims to identify optimal earthquake-resistant design strategies that achieve an effective balance between structural safety, cost-efficiency, and functional performance [16]. Kumar et al [17] compared four primary comparative parameters: maximum deflection, story shear, story drift, and maximum axial load. The analysis concludes that the inclusion of shear walls increases base shear capacity, enhances structural stability, and contributes to a reduction in axial forces.

This research focuses on comparing seismic design standards from several countries, namely the Indonesian National Standard (SNI) 1726:2019, Eurocode 8:2004, and Indian Standard IS 1893:2016, to analyze and understand their respective seismic parameters and the extent to which they affect the seismic loads imposed on building structures.

## 2. METHODS

The research methodology implemented in this study includes the following procedures:

1. Modeling the selected building using ETABS software.
2. Applying gravity loads to the structural model using ETABS software.
3. The fundamental period of the structure was obtained through modal analysis to assess the dynamic behavior of the structure.
4. Developing three separate models based on the specifications of different seismic codes: the Indonesian Standard (SNI 1726:2019), Eurocode 8, and Indian Standard IS 1893:2016
5. Applying lateral seismic forces, manually calculated according to the respective standards SNI 1726:2019, Eurocode 8, and IS 1893:2016, along with their respective load combinations.
6. Analyzing the models and presenting the resulting data in the form of graphs and tables.
7. A comparative evaluation of the analysis results was conducted, followed by drawing conclusions based on the findings of the study.

**Building Specification**

In this study, the building structural model is a reinforced concrete special moment-resisting frame system engineered to withstand both gravitational and seismic forces. A single structural model with identical geometry and gravity loading is used; however, variations are applied in the implementation of seismic loads. The building has a total length of 24 meters, a width of 13 meters, and a total height of 24 meters, consisting of 7 stories with a uniform story height of 4 meters. The structural elements include primary beams measuring 400 × 600 mm, columns of 600 × 600 mm, and floor slabs with a thickness of 120 mm. These elements are designed to support gravity loads comprising a dead load of 1.45 kN/m² and a live load of 2.4 kN/m². The applied seismic loads are based on three different seismic codes: SNI 1726:2019 (Indonesia), Eurocode 8:2004 (Europe), and IS 1893:2016 (India)

**Time Period**

The calculation of the equivalent static seismic load is carried out using a seismic coefficient that is determined by the natural vibration period of the structure. The seismic coefficient is essential for calculating the base shear force during the design of earthquake-resistant structures. The fundamental period of the structure is derived using modal analysis results simulated using ETABS software, and subsequently adjusted according to the requirements of each respective seismic design code to ensure compliance with the prescribed limitations [18].

**Earthquake Load**

Each seismic design standard has its own seismic parameters, procedures, and calculation provisions for seismic loading. As a result, the base shear force obtained from each standard will differ in magnitude. The resulting base shear is then distributed across each floor level of the building according to its height.

The seismic parameters based on SNI 1726:2016 used in this study include a Peak Ground Acceleration (PGA) of 0.3586g, a site classification of SE, a 1-second spectral acceleration ($S_1$) of 0.615, and a short-period spectral acceleration (Ss) of 0.65. The earthquake load is calculated using the following formula:

$$V = C_s W, \tag{1}$$

Subsequently, the equivalent static earthquake load is determined using Equation (2)

$$F = C_v V. \tag{2}$$

The equivalent seismic parameters based on the European standard include a Peak Ground Acceleration (PGA) of 0.3586, site class D, and a behavior factor of 5.85. The base shear force is calculated using the following formula:

$$Fb = Sd.(T1).m.\lambda \tag{3}$$

Subsequently, the equivalent static earthquake load is determined using Equation (4)

$$F_i = F_b . \frac{Z_i . m_i}{\sum Z_j . m_j} \tag{4}$$

The equivalent seismic parameters based on the Indian standard include a Peak Ground Acceleration (PGA) of 0.36, site class C, and an earthquake response modification factor (R) of 5. The base shear force due to seismic loading is calculated using the following formula:

$$Vb = Ah.W \tag{5}$$

Subsequently, the equivalent static earthquake load is determined using Equation (6)

$$Q_i = \left( \frac{W_i . h_i^2}{\sum_{j=1}^{n} W_j . h_j^2} \right) \tag{6}$$

The equivalent static load method is a simplified seismic analysis approach that estimates the structural response of buildings by representing

earthquake-induced forces as horizontal static loads applied at each story level [19] [20] [21]. The equivalent static seismic load is computed in accordance with various design codes, namely SNI 1726:2019, Eurocode 8:2004, and IS 1893:2016 along the x-axis; the results are summarized in Table 1.

*Table 1. The static earthquake load x direction*

| Floor level | SNI 1726:2019 (Ton) | Eurocode 8:2004 (Ton) | IS 1893:2016 (Ton) |
|---|---|---|---|
| Roof | 51,16 | 52,46 | 69,69 |
| 6 | 59,14 | 64,54 | 73,49 |
| 5 | 45,78 | 53,79 | 51,04 |
| 4 | 33,46 | 43,03 | 32,66 |
| 3 | 22,34 | 32,27 | 18,37 |
| 2 | 12,64 | 21,51 | 8,17 |
| 1 | 4,77 | 10,76 | 2,04 |

The equivalent static seismic load is computed in accordance with various design codes, namely SNI 1726:2019, Eurocode 8:2004, and IS 1893:2016, along the y-axis. The results are summarized in Table 2.

*Table 2. The static earthquake load y direction*

| Floor level | SNI 1726:2019 (Ton) | Eurocode 8:2004 (Ton) | IS 1893:2016 (Ton) |
|---|---|---|---|
| Roof | 51,58 | 52,44 | 69,69 |
| 6 | 59,69 | 64,51 | 73,49 |
| 5 | 46,27 | 53,76 | 51,04 |
| 4 | 33,88 | 43,01 | 32,66 |
| 3 | 22,67 | 32,26 | 18,37 |
| 2 | 12,86 | 21,50 | 8,17 |
| 1 | 4,88 | 10,75 | 2,04 |

Subsequently, the magnitude of the equivalent static earthquake load at each floor level was plotted in a graph illustrating the relationship between the seismic load and the height of each floor, resulting from seismic actions in the x direction and y direction, as shown in Figure 1 & 2.

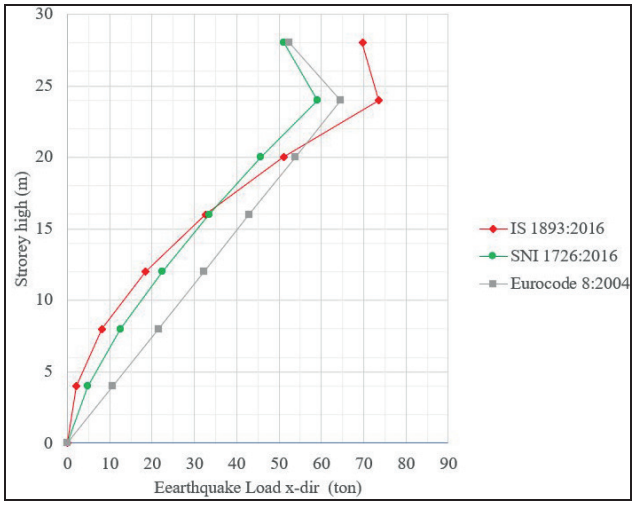


*Figure 1. Graph of equivalent static earthquake forces in x direction*

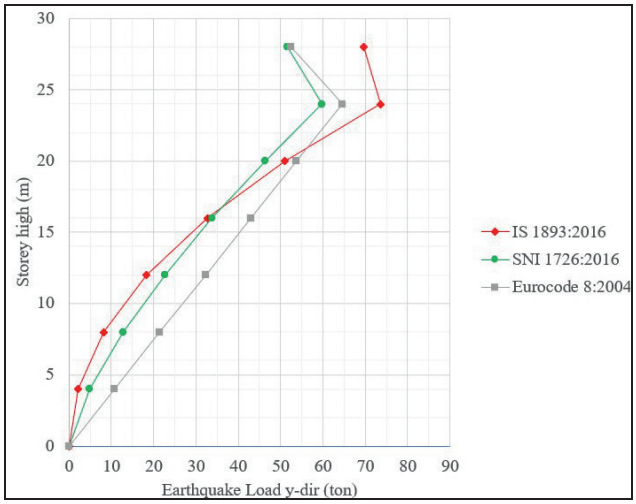


*Figure 2. Graph of equivalent static earthquake forces in y direction*

## Modeling

The three-dimensional structural modeling includes beam, column, floor slab elements, and boundary conditions. In addition to the geometry, material properties of concrete and reinforcement, as well as load applications and load combinations, are also defined within the software ETABS. The structural layout configuration and the 3D model are presented in Figure 3.

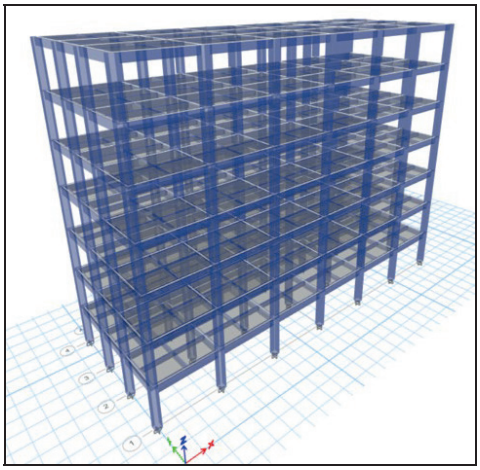

*Figure 3. 3D Representation of the building structure*

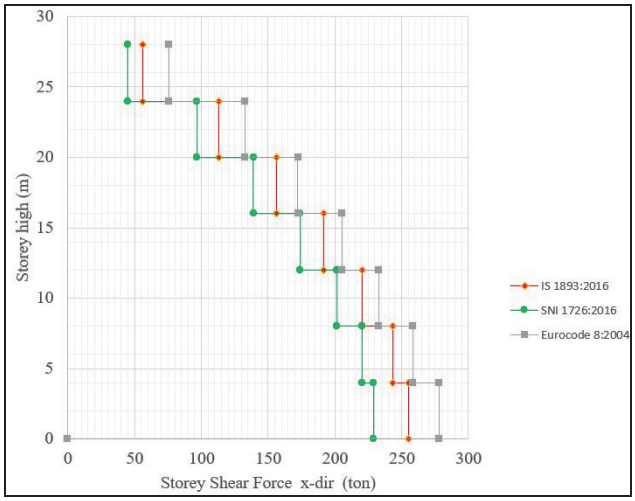


*Figure 4. Graph of story shear force in the x-direction*

## 3. RESULT AND DISCUSSION

The findings of this research include a comparative evaluation of seismic base shear forces, inter-story drift, flexural reinforcement requirements for beams and columns, and the structural performance of the building following nonlinear pushover analysis.

### Comparison of Base Shear Forces

According to the findings, the seismic base shear forces measured in the x-direction, ranked from highest to lowest, are as follows: Eurocode 8:2004 with 278.37 tons, followed by IS 1893:2016 with 255.46 tons, and SNI 1726:2019 with 229.29 tons. In the y-direction, the base shear values also follow a similar trend: Eurocode 8:2004 with 278.23 tons, IS 1893:2016 with 255.54 tons, and SNI 1726:2019 with 231.83 tons. This outcome is attributed to the differences in seismic coefficients, where Eurocode 8:2004 has the highest coefficient at 0.717, followed by IS 1893:2016 at 0.0659, and SNI 1726:2019 at 0.059.

A comparison of the third-story shear forces among the three standards is presented in a graph illustrating the relationship between story height and the magnitude of story shear force, as shown in Figures 4 and 5.

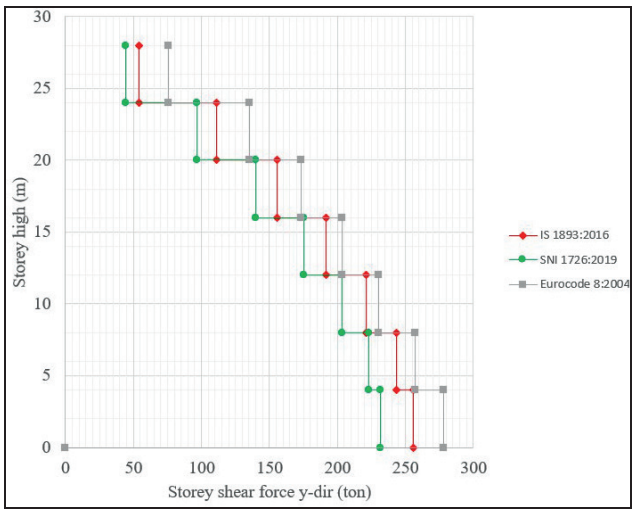


*Figure 5. Graph of story shear force in the y-direction*

### Comparison of Inter-story Drift

Seismic loading causes relative lateral displacement between stories, known as inter-story drift. To ensure structural safety under seismic loads, the inter-story drift values are limited according to the respective seismic design codes. However, the magnitude of inter-story drift does not always correlate directly with the seismic base shear values. This is because some codes, such as IS 1893:2016, do not include a drift amplification factor, resulting in the smallest drift values among the three codes when compared to SNI 1726:2019 and Eurocode

8:2004. Additionally, the allowable drift limit prescribed by IS 1893:2016 is also the most stringent, contributing further to the reduced drift values. A comparison of inter-story drifts is presented in Figures 6 & 7.

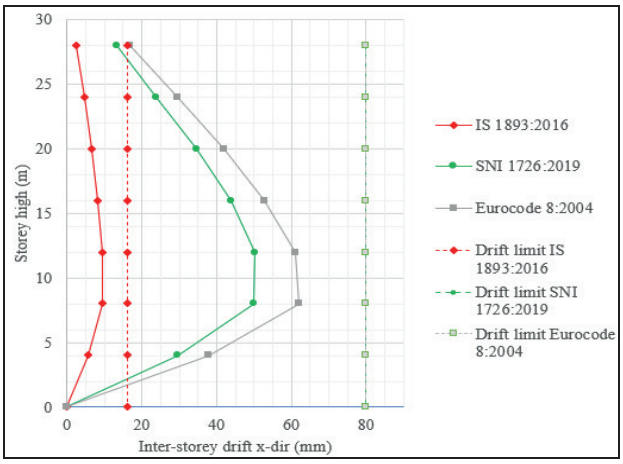


*Figure 6. Graph of of inter-story drift in the x-direction*

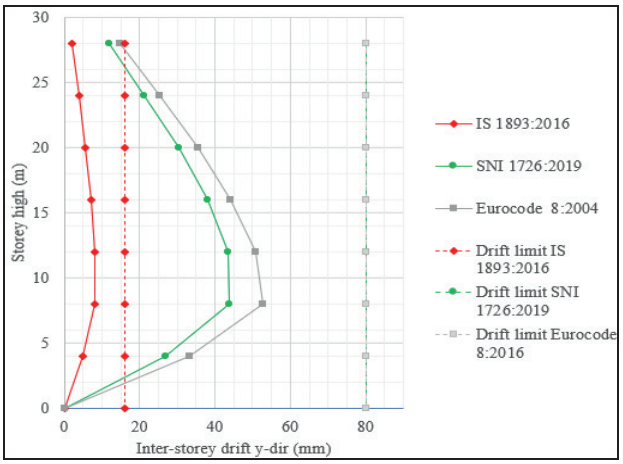


*Figure 7. Graph of of inter-story drift in the y-direction*

**Story Lateral Displacement**

he linear distribution of seismic forces on each floor in Eurocode 8:2004 results in the largest horizontal displacement among SNI 1726:2019 and IS 1893:2016, as shown in Figures 8 & 9.

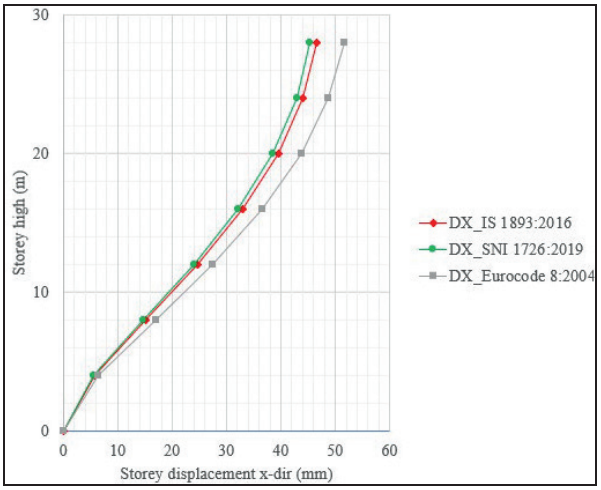


*Figure 8. Graph of lateral displacement in the x-direction*

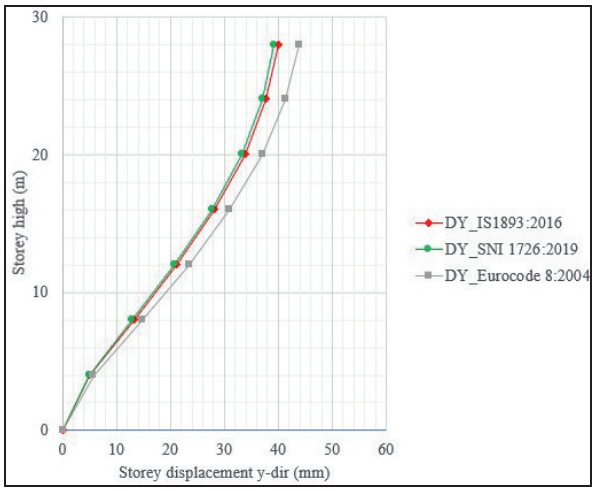


*Figure 9. Graph of lateral displacement in the x-direction*

**Comparison of Performance Points**

Nonlinear analysis methods are becoming increasingly important for evaluating the safety of structures under seismic loads. While traditional linear elastic analysis methods are sometimes inadequate to fully reflect the structural capacity limits, nonlinear static analyses, such as pushover analysis, provide more reliable results in determining the performance levels and collapse mechanisms of structures [22]. The maximum base shear that the structure can bear is outlined by push-over analysis. The building performance level combines the performance level of structures and non-structural components [23]. This

method aims to simulate the inelastic behavior of the structure by incrementally applying lateral loads until a collapse mechanism is formed. The analysis is based on the capacity-demand approach, and the parameters used in the evaluation of the pushover analysis results are the base shear that can be resisted by the building structure and the roof displacement, followed by the determination of the structural performance [24] [25].

Based on the pushover analysis in the X direction, it was found that the highest performance point, with a maximum base shear of V = 9,711.86 kN and a roof displacement of Δ = 0.261 m, was obtained using the Indonesian code. This was followed by the Eurocode, which resulted in a maximum base shear of V = 8,960.99 kN and a roof displacement of Δ = 0.189 m. The Indian code produced the lowest performance point, with a maximum base shear of V = 7,830.30 kN and a roof displacement of Δ = 0.116 m. The performance point resulting from the pushover analysis in x direction is presented in Table 3.

*Table 3. Performance Point x-direction*

| Code | Performance point | |
|---|---|---|
| | Shear V in kN | Displacement in m |
| Indonesian code | 9,711.9 | 0.26 |
| Euro code | 8,960.9 | 0.19 |
| Indian code | 7,830.3 | 0.12 |

Based on the pushover analysis in the Y direction, the highest performance point was also achieved using the Indonesian code, yielding a maximum base shear of V = 10,855.49 kN and a roof displacement of Δ = 0.248 m. Eurocode followed with a base shear of V = 9,679.50 kN and a roof displacement of Δ = 0.178 m. The Indian code again produced the lowest values, with a maximum base shear of V = 8,496.60 kN and a roof displacement of Δ = 0.109 m. The performance point resulting from the pushover analysis in y direction is presented in Table 4.

*Table 4. Performance Point y-direction*

| Code | Performance point | |
|---|---|---|
| | Shear V in kN | Displacement in m |
| Indonesian code | 10.855,5 | 0,25 |
| Euro code | 9.679,5 | 0,18 |
| Indian code | 8.496,6 | 0,11 |

The comparison of shear forces at the performance point is illustrated in the graph presented in Figures 10 and 11.

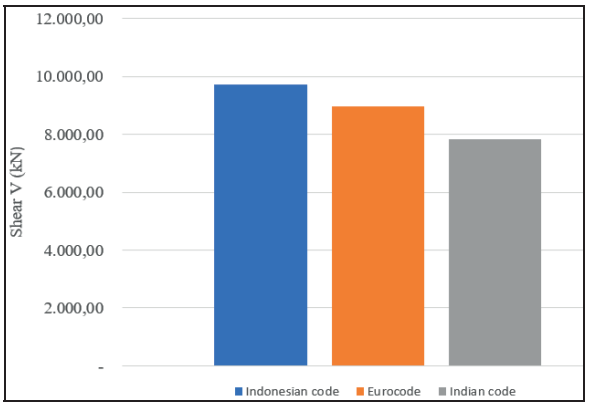


*Figure 10. Comparison graph of shear forces at the performance point in the x-direction*

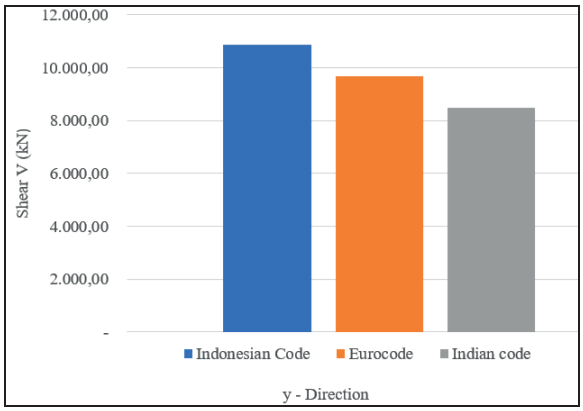


*Figure 11. Comparison graph of shear forces at the performance point in the y-direction*

**Comparison of capacity curves**

The pushover analysis results yield capacity curves representing the relationship between base shear and top displacement of the building structure, providing insights into the strength and ductility of the structure under increasing seismic loads. A comparison of the capacity

curves based on SNI 1726:2019, Eurocode 8:2004, and IS 1893:2016 is presented in Figures 12 and 13.

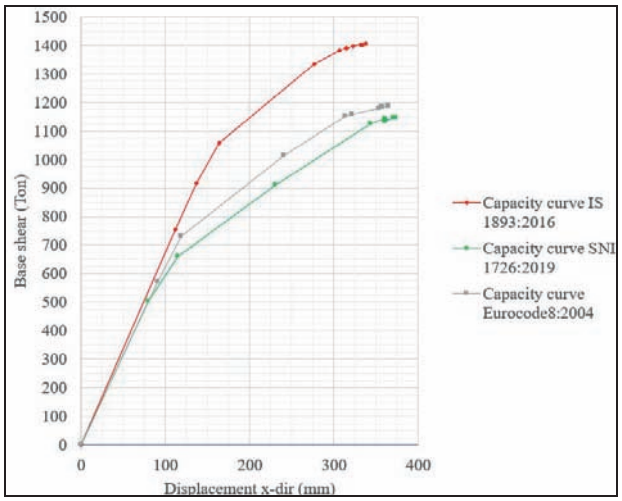


*Figure 12. Comparison of capacity curves in the x-direction*

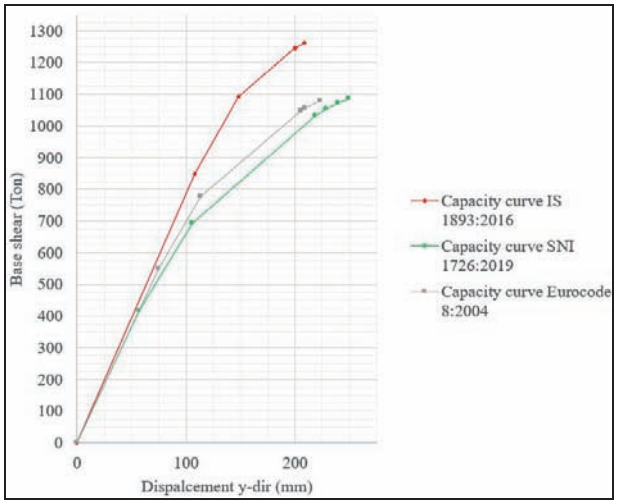


*Figure 13. Comparison of capacity curves in the y-direction*

The comparison of capacity curve graphs shows that the building designed based on SNI 1726:2019 undergoes the highest total deformation after the initial yielding (elastic stage), followed by inelastic deformation up to the failure point, compared to those designed using Eurocode 8:2004 and IS 1893:2016. This indicates that SNI 1726:2019 produces the most ductile structural performance among the three design codes.

## 4. CONCLUSION

From the analysis and discussions outlined in the preceding chapter, the following conclusions have been derived:

- Eurocode 8:2004 produced the highest seismic base shear, amounting to 278.23 tons, followed by the Indian Standard IS 1893:2016 with 255.54 tons, and the Indonesian Standard SNI 1726:2019 with 231.83 tons. This difference is attributed to the fact that Eurocode 8 uses the highest seismic force coefficient, followed by the Indian Standard and then the Indonesian Standard.
- The inter-story drift results indicated that IS 1893 yielded the lowest drift values, primarily because it does not incorporate a deflection amplification factor in the calculation.
- The performance point obtained from the pushover analysis indicated that structures designed in accordance with SNI 1726:2016 exhibited the highest values compared to those designed using Eurocode 8 and IS 1893:2016. This suggests that structures designed under SNI 1726:2019 demonstrate superior ductility performance.
- Building structures designed in accordance with SNI 1726:2019 demonstrated the highest levels of ductility, efficiency, and cost-effectiveness. In contrast, structures designed using IS 1893:2016 exhibited the lowest ductility and were found to be the least economical.

## ACKNOWLEDGEMENTS

The authors gratefully acknowledge financial support from the Institut Teknologi Sepuluh Nopember for this work, under the project scheme of the Publication Writing and IPR Incentive Program (PPHKI) 2025.

## REFERENCES

1. **Dhanvijay, V., Telang, D., & Nair, V.** (2015). Comparative study of different

codes in seismic assessment. *International Research Journal of Engineering and Technology (IRJET), 2*(4), 1371. https://www.irjet.net/archives/V2/i4/IRJET-V2I4062.

2. **Santos S.H., Giarlelis C., Jara J., Lampropoulos A., Lo Presti D., Montens S., Sutcu F., Takeuchi T., Traikova M., Varum H., White J., Zmigrodzki S., Pinto J. & Arai A.** (2020, May 20–22). Comparative study of international major codes for the seismic design of buildings. In Synergy of Culture and Civil Engineering – History and Challenges (IABSE Symposium).
3. **Eirgash, M.A.** (2019). A comparative study of seismic performance of the building designed using four major codes. *International Journal of Engineering Research & Technology (IJERT), 8*(8), Article 80180. http://www.ijert.org/ijertv8is080180
4. **Kour, J., & Chand, J.** (2021). Comparative study of seismic analysis of vertically irregular R.C. frame using Indian and Euro code. In IOP Conference Series: Earth and Environmental Science (Vol. 889, Article 012042). IOP Publishing. https://doi.org/10.1088/1755-1315/889/1/012042
5. **Adhikari, D., Adhikari, S., & Thapa, D.** (2022). A comparative study on seismic analysis of national building code of Nepal, India, Bangladesh and China. Open Access Library Journal, 9, e8933. https://doi.org/10.4236/oalib.1108933
6. **Aksoylu, C., Mobark, A., Arslan, M.H., & Erkan, İ.H.** (2020). A comparative study on ASCE 7-16, TBEC-2018 and TEC-2007 for reinforced concrete buildings. *Research on Design and Construction*, 19(2), 282–[halaman akhir jika diketahui]. https://doi.org/10.7764/RDLC.19.2.282
7. **Srikanth, B., & Ramesh, V. (2013).** Comparative study of seismic response for seismic coefficient and response spectrum methods. *International Journal of Engineering Research and Applications, 3*(5), 1919–1924. http://www.ijera.com
8. **Karthiga, S., Titus, H.E., Hazarika, R. R., & Harrish, M.** (2015). Design and comparison of a residential building (G+10) for seismic forces using the codes: IS1893, Euro code 8, ASCE 7-10 and British code. *International Journal of Research in Engineering and Technology (IJRET), 4*(6), 205. http://www.ijret.org
9. **Karthiga, S., Titus, H.E., Hazarika, R. R., & Harrish, M.** (2015). Design and comparison of a residential building (G+10) for seismic forces using the codes: IS1893, Euro code 8, ASCE 7-10 and British code. *International Journal of Research in Engineering and Technology (IJRET), 4*(6), 205. http://www.ijret.org
10. **Malla, S., Alagirisamy, M., Dangol, P., & Giri, O.P.** (2024). Comparative analysis of an apartment building using seismic codes NBC 105:1994 and NBC 105:2020 (A case study). *[Nama Jurnal jika ada]*. https://doi.org/10.48084/.7858
11. **Isık, E., Hadzima-Nyarko, M., Bilgin, H., Ademović, N., Büyüksaraç, A., Harirchian, E., Bulajić, B., Özmen, H.B., & Aghakouchaki Hosseini, S.E.** (2022). A comparative study of the effects of earthquakes in different countries on target displacement in mid-rise regular RC structures. *Applied Sciences, 12*(23), 12495. https://doi.org/10.3390/app122312495
12. **Rajeev, A., Meena, N.K., & Pallav, K.** (2019). Comparative study of seismic design and performance of OMRF building using Indian, British, and European codes. *Infrastructures, 4*(4), 71. https://doi.org/10.3390/infrastructures4040071
13. **Salim, J.T., & Sidi, I.D.** (2024). Comparative seismic evaluation of building codes: A case study on structural performance and safety. *Journal of Engineering and Technological Sciences, 56*(6), 793–807. https://doi.org/10.5614/j.eng.technol.sci.2024.56.6.10

14. **Tapkire, P.P., & Birajdar, S.J.** (2015). Comparative study of high rise building using Indian standards and Euro standards under seismic forces. *International Journal of Science and Research (IJSR), 4*(7). http://www.ijsr.net
15. **Suliman, M., & Lu, L.** (2024). A comparative study of seismic performance evaluation of reinforced concrete frame structures using Chinese and African seismic codes. *Advances in Civil Engineering, 2024*, Article ID 5588833, 18 pages. https://doi.org/10.1155/2024/5588833
16. **Ramteke, S., Gaikwad, S.A., Khatkale, A.A., Pawar, R.M., & Temak, R.S.** (2024). Comparative study of earthquake resistant buildings using STAAD-Pro software. *International Journal of Innovative Research in Technology (IJIRT), 10*(12). https://www.ijirt.org/paper_details.php?id=164773
17. **Pragnya, C., Kumar, M.S., Raju, K.H. V., Raju, K.L., Krishna, K., & Bharathi, K.P.** (2021). Comparative study of earthquake resistant design techniques on multistorey building. *International Journal for Advanced Research in Science & Technology, 11*(8). http://www.ijarst.in
18. **Computers and Structures, Inc.** (2022). *ETABS (Version 20) [Computer software]*. CSI Inc. https://www.csiamerica.com/products/etabs
19. **Badan Standardisasi Nasional.** (2019). *Procedures for seismic resistance design for building and non-building structures (SNI 1726:2019)*. Badan Standardisasi Nasional.
20. **European Committee for Standardization.** (2004). *Eurocode 8: Design of structures for earthquake resistance – Part 1: General rules, seismic actions and rules for buildings (EN 1998-1:2004)*. European Committee for Standardization.
21. **Bureau of Indian Standards.** (2016). *IS 1893 Part 1: Indian standard criteria for earthquake resistant design of structures*. Bureau of Indian Standards.
22. **Akman, B.G., & Seçer, M.** (2025). Pushover analysis of a reinforced concrete frame and calculation of $CO_2$ emissions. *International Journal of Advanced Natural Science and Engineering Research, 9*(2), 319–326.
23. **Soetjipto, J.W., Nurmalia, I.E., & Krisnamurti.** (2024). Integrating push-over analysis and FEMA guidelines for building vulnerability assessment. *Research on Engineering Structures and Materials, 10*(2), 691–709. https://doi.org/10.17515/resm2023.56st1024rs
24. **Kurniati, D., & Loko, P.B.** (2020). Pushover study analysis of PGRI Faculty of Engineering building. *International Journal of Engineering, Technology and Natural Sciences, 2*(1).
25. **Doodala, S., Jaswanth, P., Nagendra, T., Khan, P.N., & Kumar, A.A.** (2024). Pushover analysis of G+14 story building by using ETABS software. *International Journal of Research in Engineering, IT and Social Sciences, 14*(6), 434–446.

СПИСОК ИСТОЧНИКОВ

1. **Dhanvijay, V., Telang, D., & Nair, V.** (2015). Comparative study of different codes in seismic assessment. *International Research Journal of Engineering and Technology (IRJET), 2*(4), 1371. https://www.irjet.net/archives/V2/i4/IRJET-V2I4062.
2. **Santos S.H., Giarlelis C., Jara J., Lampropoulos A., Lo Presti D., Montens S., Sutcu F., Takeuchi T., Traikova M., Varum H., White J., Zmigrodzki S., Pinto J. & Arai A.** (2020, May 20–22). Comparative study of international major codes for the seismic design of buildings. In Synergy of Culture and Civil Engineering – History and Challenges (IABSE Symposium).
3. **Eirgash, M.A.** (2019). A comparative study of seismic performance of the

building designed using four major codes. *International Journal of Engineering Research & Technology (IJERT), 8*(8), Article 80180. http://www.ijert.org/ijertv8is080180

4. **Kour, J., & Chand, J.** (2021). Comparative study of seismic analysis of vertically irregular R.C. frame using Indian and Euro code. In IOP Conference Series: Earth and Environmental Science (Vol. 889, Article 012042). IOP Publishing. https://doi.org/10.1088/1755-1315/889/1/012042
5. **Adhikari, D., Adhikari, S., & Thapa, D.** (2022). A comparative study on seismic analysis of national building code of Nepal, India, Bangladesh and China. Open Access Library Journal, 9, e8933. https://doi.org/10.4236/oalib.1108933
6. **Aksoylu, C., Mobark, A., Arslan, M.H., & Erkan, İ.H.** (2020). A comparative study on ASCE 7-16, TBEC-2018 and TEC-2007 for reinforced concrete buildings. *Research on Design and Construction*, 19(2), 282–[halaman akhir jika diketahui]. https://doi.org/10.7764/RDLC.19.2.282
7. **Srikanth, B., & Ramesh, V. (2013).** Comparative study of seismic response for seismic coefficient and response spectrum methods. *International Journal of Engineering Research and Applications, 3*(5), 1919–1924. http://www.ijera.com
8. **Karthiga, S., Titus, H.E., Hazarika, R. R., & Harrish, M.** (2015). Design and comparison of a residential building (G+10) for seismic forces using the codes: IS1893, Euro code 8, ASCE 7-10 and British code. *International Journal of Research in Engineering and Technology (IJRET), 4*(6), 205. http://www.ijret.org
9. **Karthiga, S., Titus, H.E., Hazarika, R. R., & Harrish, M.** (2015). Design and comparison of a residential building (G+10) for seismic forces using the codes: IS1893, Euro code 8, ASCE 7-10 and British code. *International Journal of Research in Engineering and Technology (IJRET), 4*(6), 205. http://www.ijret.org
10. **Malla, S., Alagirisamy, M., Dangol, P., & Giri, O.P.** (2024). Comparative analysis of an apartment building using seismic codes NBC 105:1994 and NBC 105:2020 (A case study). *[Nama Jurnal jika ada]*. https://doi.org/10.48084/.7858
11. **İsık, E., Hadzima-Nyarko, M., Bilgin, H., Adamović, N., Büyüksaraç, A., Harirchian, E., Bulajić, B., Özmen, H.B., & Aghakouchaki Hosseini, S.E.** (2022). A comparative study of the effects of earthquakes in different countries on target displacement in mid-rise regular RC structures. *Applied Sciences, 12*(23), 12495. https://doi.org/10.3390/app122312495
12. **Rajeev, A., Meena, N.K., & Pallav, K.** (2019). Comparative study of seismic design and performance of OMRF building using Indian, British, and European codes. *Infrastructures, 4*(4), 71. https://doi.org/10.3390/infrastructures4040071
13. **Salim, J.T., & Sidi, I.D.** (2024). Comparative seismic evaluation of building codes: A case study on structural performance and safety. *Journal of Engineering and Technological Sciences, 56*(6), 793–807. https://doi.org/10.5614/j.eng.technol.sci.2024.56.6.10
14. **Tapkire, P.P., & Birajdar, S.J.** (2015). Comparative study of high rise building using Indian standards and Euro standards under seismic forces. *International Journal of Science and Research (IJSR), 4*(7). http://www.ijsr.net
15. **Suliman, M., & Lu, L.** (2024). A comparative study of seismic performance evaluation of reinforced concrete frame structures using Chinese and African seismic codes. *Advances in Civil Engineering, 2024*, Article ID 5588833, 18 pages. https://doi.org/10.1155/2024/5588833
16. **Ramteke, S., Gaikwad, S.A., Khatkale, A.A., Pawar, R.M., & Temak, R.S.** (2024). Comparative study of earthquake resistant buildings using STAAD-Pro software.

*International Journal of Innovative Research in Technology (IJIRT), 10*(12). https://www.ijirt.org/paper_details.php?id=164773

17. **Pragnya, C., Kumar, M.S., Raju, K.H. V., Raju, K.L., Krishna, K., & Bharathi, K.P.** (2021). Comparative study of earthquake resistant design techniques on multistorey building. *International Journal for Advanced Research in Science & Technology, 11*(8). http://www.ijarst.in
18. **Computers and Structures, Inc.** (2022). *ETABS (Version 20) [Computer software]*. CSI Inc. https://www.csiamerica.com/products/etabs
19. **Badan Standardisasi Nasional.** (2019). *Procedures for seismic resistance design for building and non-building structures (SNI 1726:2019)*. Badan Standardisasi Nasional.
20. **European Committee for Standardization.** (2004). *Eurocode 8: Design of structures for earthquake resistance – Part 1: General rules, seismic actions and rules for buildings (EN 1998-1:2004)*. European Committee for Standardization.
21. **Bureau of Indian Standards.** (2016). *IS 1893 Part 1: Indian standard criteria for earthquake resistant design of structures*. Bureau of Indian Standards.
22. **Akman, B.G., & Seçer, M.** (2025). Pushover analysis of a reinforced concrete frame and calculation of $CO_2$ emissions. *International Journal of Advanced Natural Science and Engineering Research, 9*(2), 319–326.
23. **Soetjipto, J.W., Nurmalia, I.E., & Krisnamurti.** (2024). Integrating push-over analysis and FEMA guidelines for building vulnerability assessment. *Research on Engineering Structures and Materials, 10*(2), 691–709. https://doi.org/10.17515/resm2023.56st1024rs
24. **Kurniati, D., & Loko, P.B.** (2020). Pushover study analysis of PGRI Faculty of Engineering building. *International Journal of Engineering, Technology and Natural Sciences, 2*(1).
25. **Doodala, S., Jaswanth, P., Nagendra, T., Khan, P.N., & Kumar, A.A.** (2024). Pushover analysis of G+14 story building by using ETABS software. *International Journal of Research in Engineering, IT and Social Sciences, 14*(6), 434–446.

---

*Dwi Yanto* - master student, Department of Civil Engineering, Institut Teknologi Sepuluh Nopember, ITS Campus, Sukolilo, Surabaya 60111, East Java, Indonesia

*Tavio* - Professor, Department of Civil Engineering, Institut Teknologi Sepuluh Nopember, ITS Campus, Sukolilo, Surabaya 60111, East Java, Indonesia

*Дви Янто* — магистрант, кафедра гражданского строительства, Технологический институт Сепулух Нопембер (Institut Teknologi Sepuluh Nopember), кампус ITS, Суколио, Сурабая 60111, Восточная Ява, Индонезия.

*Тавио* — профессор, кафедра гражданского строительства, Технологический институт Сепулух Нопембер (Institut Teknologi Sepuluh Nopember), кампус ITS, Суколио, Сурабая 60111, Восточная Ява, Индонезия.

International Journal for Computational Civil and Structural Engineering, 21(3) 201–208 (2025)
DOI:10.22337/2587-9618-2025-21-3-201-208

# THE MODIFIED METHOD OF SEQUENTIAL LOADS FOR THE ANALYSIS OF SLENDER SHALLOW SHELLS

***Vladilen V. Petrov, Olga A. Gorbacheva***
Yuri Gagarin State Technical University of Saratov, Saratov, RUSSIA

**Abstract:** This study discusses specific features of analyzing shallow shells using a modified sequential load method and a collocation method. This combination shows a rapid rate of convergence when the golden section principle is used to select the collocation node system.

**Keywords:** geometric nonlinearity, zero approximation selection, collocation method, collocation node selection, golden ratio, solution residual, critical load

# ОСОБЕННОСТИ ПРИМЕНЕНИЯ МОДИФИЦИРОВАННОГО МЕТОДА ПОСЛЕДОВАТЕЛЬНЫХ НАГРУЖЕНИЙ ПРИ РАСЧЕТЕ ГИБКИХ ПОЛОГИХ ОБОЛОЧЕК

***В.В. Петров, О.А. Горбачева***
СГТУ имени Гагарина Ю.А., г. Саратов, РОССИЯ

**Аннотация:** В статье рассматриваются особенности расчета пологих оболочек модифицированным методом последовательных нагружений с применением метода коллокаций. Показано, что наблюдается быстрая сходимость модифицированного метода последовательных нагружений с применением метода коллокаций, если использовать принцип «золотого сечения» для выбора системы узлов коллокаций.

**Ключевые слова:** геометрическая нелинейность, выбор нулевого приближения, метод коллокаций, выбор узлов коллокаций, золотое сечение, невязка решения, критическая нагрузка

Slender shells can be described by nonlinear differential equations. There is extensive literature on methods for solving geometrically nonlinear problems in structural mechanics. An overview of some of these methods can be found in references [1-4]. Often, there is a practical need to analyze the stress-strain state of slender structures over the entire range of load variations. However, analyzing the relationship between variable lateral load parameters and the corresponding stress-strain state of the structure, while considering the loading history, is labor-intensive. Many iterative methods are sensitive to the initial zero approximation, especially near upper and lower critical loads or bifurcation points. In these regions, the convergence region of the solution tends to a single point.

The modified method of sequential loads (MMSL), which combines the capabilities of the method of sequential loads (MSL) — convenient for studying similar and other nonlinear problems — and the Newton-Kantorovich method (NKM), which converges well when solving nonlinear problems, is sensitive to the choice of zero approximation, especially near limit and bifurcation points. Combining them expands the possibilities for implementing various calculation schemes.

The essence of the MMSL method is that, initially, a force-displacement curve should be constructed for the entire load range using the method of sequential loads with the leading parameter of load increment. This curve will then serve as a carrier of zero approximations while refining the MMSL solution at each selected loading stage. The refined results are connected by a smooth line that characterizes the structure's behavior throughout the entire range of load changes. To reduce the labor intensity of solving the problem, strategies for coordinating the alternation of MSL and MNK can be employed.

Slender shells have areas of multi-valued solutions limited by upper and lower critical loads. If a zero approximation is in an area with a

small radius of convergence, it will be difficult to find a solution due to solution instability, even with a large number of iterations. Changing the load parameter helps overcome this. The displacement increment at the center of the shell is taken as the leading parameter, and the load increment becomes the desired parameter alongside the other deflection parameter increments. This change in parameters was proposed in [7]. Many authors have employed it in solving similar problems, and it has proven effective.

Some specific features of applying the modified sequential load method to the analysis of geometrically nonlinear shallow shells are discussed below. For example, consider the flexural problem of a slender, shallow shell that is hinged along its contour and loaded with a uniformly distributed load of intensity $q_0$, as shown in Figure 1. A rectangular system of dimensionless coordinates $\xi = x/a, \quad \eta = y/b$ has been chosen, where a and b represent the shell's dimensions in plan view. The system of equations for the flexure of slender, shallow shells in the dimensionless, incremental form of the sequential load method [1] is as follows:

$$\left.\begin{aligned} &\nabla^4 \Delta\psi_n + \nabla_k^2 \Delta u_n + L\left(u_{n-1}, \Delta u_n\right) = 0 \\ &\nabla^4 \Delta u_n - 12(1-\mu^2)\left[ L\left(\psi_{n-1}, \Delta u_n\right) + \nabla_k^2 \Delta\psi_n + L\left(u_{n-1}, \Delta\psi_n\right) + \Delta p_n(\xi,\eta) \right] = 0 \end{aligned}\right\} \quad (1)$$

$$\left(n = 1, 2, 3, \ldots\right)$$

and the system of incremental equations of the Newton-Kantorovich method in dimensionless form has the form [1]

$$\left.\begin{aligned} &\nabla^4 \Delta\psi_r + \nabla_k^2 \Delta u_r + L\left(u_{r-1}, \Delta u_r\right) = -\nabla^4 \psi_{r-1} - \nabla_k^2 u_{r-1} - \frac{1}{2} L\left(u_{r-1}, u_{r-1}\right) \\ &\nabla^4 \Delta u_r - 12(1-\mu^2)\left[ L\left(\psi_{r-1}, \Delta u_r\right) + L\left(u_{r-1}, \Delta\psi_r\right) + \nabla_k^2 \Delta\psi_r \right] = \\ &= -\nabla^4 u_{r-1} + 12(1-\mu^2)\left[ L\left(\psi_{r-1}, u_{r-1}\right) + \nabla_k^2 \psi_{r-1} + p(\xi,\eta) \right] \end{aligned}\right\} \quad (2)$$

$$\left(r = 1, 2, 3, \ldots\right)$$

where $n$ is the number of sequential loading stages when using MSL, $r$ is the iteration number when refining the MNK solution, $\Delta u_n\left(\xi,\eta\right) = \Delta W_n(x,y)/h$ is the increment of dimensionless deflection when using MSL at the $n^{th}$ loading stage, $u_{n-1}\left(\xi,\eta\right) = W(x,y)/h$ is the total dimensionless deflection determined at previous loading stages, $\Delta\psi_n\left(\xi,\eta\right) = \Delta\varphi(x,y)/Eh^3$ is the increment of the dimensionless MSL force function, $\psi_{n-1}(\xi,\eta) = \varphi(x,y)/Eh^3$ is the dimensionless total force function determined at previous loading stages, $u_{r-1}, \psi_{r-1}$ are the dimensionless deflection and force function obtained at previous iterations, $\Delta u_r, \Delta\psi_r$ are the increments of dimensionless deflection and force function at the $n^{th}$ loading stage, $\Delta p_n\left(\xi,\eta\right) = \Delta q\left(x,y\right) a^2 b^2/Eh^4$ is the increment of dimensionless lateral load $p\left(\xi,\eta\right)$, $\nabla_k^2 = K_2 \dfrac{\partial^2}{\partial\xi^2} + K_1 \dfrac{\partial^2}{\partial\eta^2}$ is the Laplace operator depending on dimensionless curvatures $K_1 = k_1 a^2/h, \quad K_2 = k_2 b^2/h$, where $k_1, k_2$ are the principal dimensional curvatures of the shell, $L$ is the differential operator:

$$L = \frac{\partial^2}{\partial\xi^2}\frac{\partial^2}{\partial\eta^2} + \frac{\partial^2}{\partial\eta^2}\frac{\partial^2}{\partial\xi^2} - 2\frac{\partial^2}{\partial\xi\partial\eta}\frac{\partial^2}{\partial\xi\partial\eta} \quad (3)$$

The left sides of equations (1) and (2) are the same. The calculation begins by solving system (1) using the sequential load method (MSL). The lateral load is divided into thin layers in our minds and applied sequentially to the shell, and the calculation results are summed up. After several loading stages, the solution is refined

using the Newton-Kantorovich method. In this method, the total solution obtained by MSL is assumed to be the zero approximation. By sequentially solving system (2), one can analyze the convergence of the method and make appropriate corrections.

Various approximate methods for solving linear differential equations can be used to solve the linearized systems of equations (1) and (2). Two problems need to be solved beforehand for this purpose: constructing systems of coordinate functions and setting the coordinates of collocation nodes optimally.

The coordinate functions are represented as the product of the main parts of the solution $\omega(\xi,\eta)$ and $\varphi(\xi,\eta)$, satisfying the given boundary conditions, on a system of correction functions of variables $\xi$ and $\eta$, containing unknown parameters (generalized coordinates). In the case of shell deflection symmetrical about the coordinate axes $\xi$ and $\eta$, we will choose the coordinate functions and their increments in the form of an incomplete polynomial with even degrees. As a result, we obtain:

$$\begin{aligned}
u^*_{n-1}(\xi,\eta) &= \omega(\xi,\eta)\sum_N K_N\xi^{2N}\eta^{2N}, & \Delta u^*_n(\xi,\eta) &= \omega(\xi,\eta)\sum_N \Delta K_N\xi^{2N}\eta^{2N},\\
\psi^*_{n-1}(\xi,\eta) &= \varphi(\xi,\eta)\sum_N T_N\xi^{2N}\eta^{2N}, & \Delta \psi^*_n(\xi,\eta) &= \varphi(\xi,\eta)\sum_N \Delta T_N\xi^{2N}\eta^{2N},\\
u^*_{r-1}(\xi,\eta) &= \omega(\xi,\eta)\sum_N M_N\xi^{2N}\eta^{2N}, & \Delta u^*_r(\xi,\eta) &= \omega(\xi,\eta)\sum_N \Delta M_N\xi^{2N}\eta^{2N},\\
\psi^*_{r-1}(\xi,\eta) &= \varphi(\xi,\eta)\sum_N P_N\xi^{2N}\eta^{2N}, & \Delta \psi^*_r(\xi,\eta) &= \varphi(\xi,\eta)\sum_N \Delta P_N\xi^{2N}\eta^{2N},
\end{aligned} \qquad (4)$$

$$(N = 1,2,3,....)$$

where $K_N$, $\Delta K_N$, $T_N$, $\Delta T_N$, $M_N$, $\Delta M_N$, $P_N$, $\Delta P_N$ are the generalized coordinates and their increments, $N$ is the number of collocation nodes, and the approximate solution is marked with an asterisk (*). The number of members in the correction functions must be equal to the number of collocation nodes and determines the approximation number.

The main parts of the solution $\omega(\xi,\eta)$ and $\varphi(\xi,\eta)$, satisfying the given boundary conditions, are constructed in various ways. One of them is the first approximation obtained from solving a similar problem using some approximate method. For the hinged support of the shell along the contour, the main parts of the solution of the function $\omega(\xi,\eta)$ and $\varphi(\xi,\eta)$ are selected in the form [4]

$$\begin{aligned}
\omega(\xi,\eta) &= \cos\pi\xi\cdot\cos\pi\eta\\
\varphi(\xi,\eta) &= \cos\pi\xi\cdot\cos\pi\eta
\end{aligned}. \qquad (5)$$

Substituting the constructed functions (4) into the systems of equations MMSL (1) and (2), one obtains expressions for the discrepancies in solutions of the incremental equations of systems (1) and (2)

$$\left.\begin{aligned}
&F_1(\xi,\eta,\Delta K_N,\Delta T_N) = \nabla^4\Delta\psi^*_n + \nabla^2_k\Delta u^*_n + L\left(u_{n-1},\Delta u^*_n\right)\\
&F_2(\xi,\eta,\Delta K_N,\Delta T_N) = \nabla^4\Delta u^*_n - 12(1-\mu^2)\Big[L\left(\psi_{n-1},\Delta u^*_n\right) +\\
&+\nabla^2_k\Delta\psi^*_n + L\left(u_{n-1},\Delta\psi^*_n\right) + \Delta p(\xi,\eta)\Big]
\end{aligned}\right\}$$

$$\left.\begin{aligned}
&F_3(\xi,\eta,\Delta M_N,\Delta P_N) = \nabla^4\Delta\psi^*_r + \nabla^2_k\Delta u^*_r + L\left(u_{r-1},\Delta u^*_r\right) +\\
&+\nabla^4\psi_{r-1} + \nabla^2_k u_{r-1} + \frac{1}{2}L\left(u_{r-1},u_{r-1}\right)\\
&F_4(\xi,\eta,\Delta M_N,\Delta P_N) = \nabla^4\Delta u^*_r - 12(1-\mu^2)\Big[L\left(\psi_{r-1},\Delta u^*_r\right) +\\
&+L\left(u_{r-1},\Delta\psi^*_r\right) + \nabla^2_k\psi_{r-1} + p(\xi,\eta) + L\left(\psi_{r-1},u_{r-1}\right)\Big] + \nabla^4 u_{r-1}
\end{aligned}\right\} \qquad (6)$$

According to the collocation method, set the solution discrepancies equal to zero at each collocation node. To obtain a solution with the required accuracy, one should specify a certain number of collocation nodes and their coordinates. Next, set the solution discrepancy at these nodes equate to zero, resulting in a system of linear equations with respect to the increments

of the parameters of the generalized coordinate correction functions.

The selection of coordinates for the arrangement of collocation nodes faces a certain challenge. To reduce the number of collocation nodes without significant loss of accuracy, a method for selecting a system of collocation nodes has been proposed by the authors based on the use of the "golden ratio." This method has been studied in numerous calculations of linear and physically nonlinear problems [8,9] and has demonstrated rapid convergence of the solution. One variant of this method is shown in Figure 1, using the example of calculating a slender shallow shell under axisymmetric loading and boundary conditions. It is sufficient to consider one quarter of the shell plan, which in dimensionless form has dimensions 1 x 1. To determine the coordinates of the first collocation node $A_1$, the distance from the center to the edge of the shell is divided in the "golden ratio" proportion, and the length of the short segment (near the center) determines the coordinate $\eta$ of the collocation node $A_1(0.191;0.191)$. Next, the second (long segment) is similarly divided in the "golden ratio" proportion, and we determine the coordinate of the collocation node $A_2(0.309;0.309)$. In the same way, we find the coordinates of the collocation nodes $A_3(0.382;0.382)$ and $A_4(0.427;0.427)$. If necessary, this process can be continued.

By equating the discrepancies of solution (6) to zero in the constructed collocation nodes (Figure 1), we obtain systems of linear algebraic equations by MSL

$$\left\{\begin{matrix} F_1(\xi_s,\eta_s,\Delta K_N,\Delta T_N)=0 \\ F_2(\xi_s,\eta_s,\Delta K_N,\Delta T_N)=0 \end{matrix}\right\}\Bigg|_{s=A_N}, \quad N=1,2,3,4 \tag{7}$$

and systems of linear algebraic equations for calculating by MNK

$$\left\{\begin{matrix} F_3(\xi_s,\eta_s,\Delta M_N,\Delta P_N)=0 \\ F_4(\xi_s,\eta_s,\Delta M_N,\Delta P_N)=0 \end{matrix}\right\}\Bigg|_{s=A_N}, \quad N=1,2,3,4 \tag{8}$$

where $\xi_s,\eta_s$ are the coordinates of specific collocation nodes: node $A_1$ - in the first approximation; nodes $A_1$, $A_2$ - in the second approximation; nodes $A_1$, $A_2$, $A_3$ - in the third approximation; nodes $A_1$, $A_2$, $A_3$, $A_4$ - in the fourth approximation by MK. Solving the system of algebraic equations (7), one finds the coefficients $\Delta K_N,\Delta T_N,\Delta M_N,\Delta P_N$ and, substituting them into (4), obtains the desired values of the deflection increment function and the force function of the slender shallow shell. Next, one determines the necessary characteristics of the shell's internal forces.

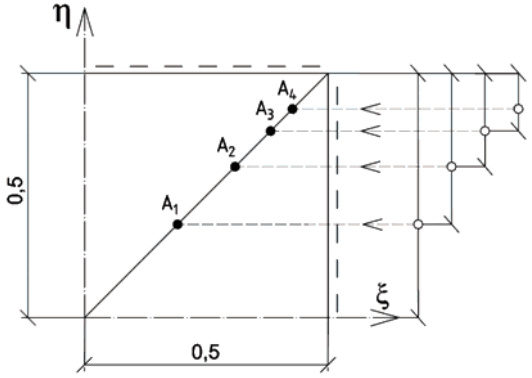


*Figure 1.* Scheme for selecting collocation points on a quarter of the shell plan

Figure 2 shows the load-displacement dependencies at the center of a shallow shell with dimensionless curvatures $K_1$=$K_2$=18, obtained by MMSL using the MK. The curve number corresponds to the number of the approximate solution. Curve 5 was obtained by the MBG in the fourth approximation [7].

Alternating convergence of the collocation method has been observed. The difference in the upper critical loads between the first, second, and fourth approximations of the MK and the fourth approximation of the MBG is less than 10%. The values of the second and fourth approximations of the MK are close to the lower critical load obtained by the MBG. The difference is less than 8%. The curve obtained in the second approximation of MK almost merges with the dependence obtained by MBG in the fourth approximation. This allows us to conclude that the second approximation of MK is sufficient to determine the upper critical load for the shell under consideration.

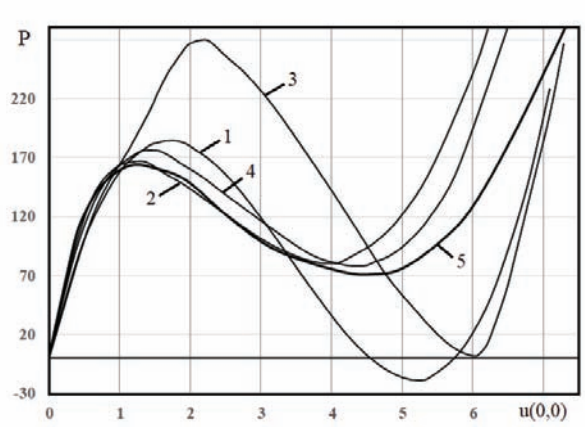


*Figure 2*. Load-displacement relationships at the center of a shallow shell in different MK approximations

Note that such rapid convergence of the solution is directly dependent on the rational selection of collocation nodes using the "golden ratio" proportion.

The "golden ratio" is a rule of proportion: "the smaller part relates to the larger part as the larger part relates to the whole." It is also called "divine harmony." This concept was first used by Pythagoras and has accompanied human civilization throughout its development. It is a marker of beauty and harmony. Works of art have been created according to the canons of this proportion. This proportion is present everywhere: in art, in nature, in spiral galaxies, and in humans themselves. The golden ratio is a universal numerical constant, perfect for the development of all objects, systems, and processes, that is, with minimum potential energy. According to Euclid of Alexandria, at the points of the "golden ratio," there is a balance between the whole and its parts, as well as between the parts themselves, and the increase in potential energy is zero. The "golden ratio" ensures the development of living beings and all processes in the most energy-efficient way. It is believed that in nature it is the basis for development. Extensive literature is devoted to the study of these issues. We recommend that those interested in these issues refer, for example, to monograph [10], which contains an extensive bibliography.

Figure 3 (to the left of the axis line) shows the graphs of the solution discrepancies in the section $\eta = 0$, obtained by the MMSL at a load of $P$=120 and in the upper critical load region (to the right of the axis line). The curve numbers coincide with the approximation numbers obtained by the MK.

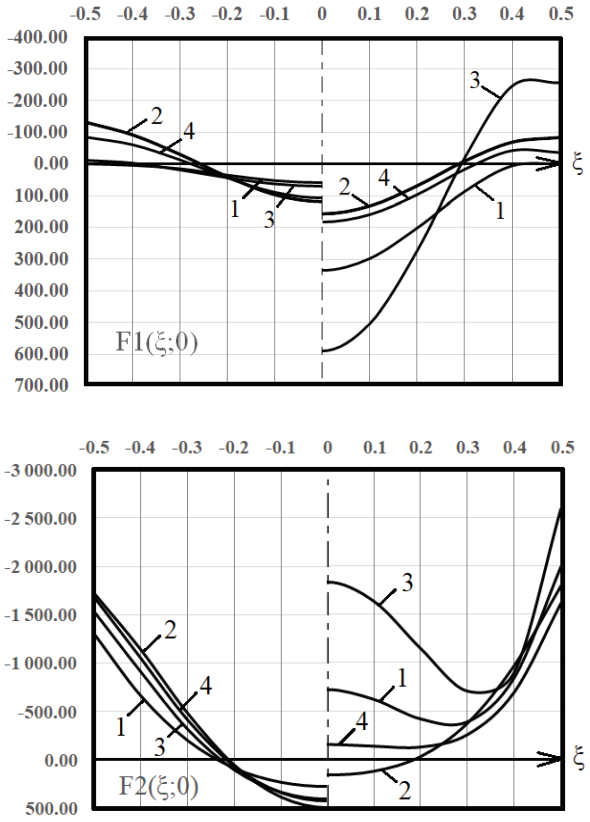


*Figure 3.* Changes in the discrepancies of solutions $F_1$ and $F_2$ with increasing load

Analysis of the results shown in Figure 3 demonstrates the convergence of solution discrepancies at the center of the shell is alternating in nature. The solution discrepancies obtained in the vicinity of the upper critical load are significantly smaller than the solution discrepancies at a load of $P$=120.

Figures 4-7 show the change in the surfaces of the solution discrepancies of the continuity equation $F_1$ and the equilibrium equation $F_2$ at maximum load in the first and fourth approximations of the collocation method.

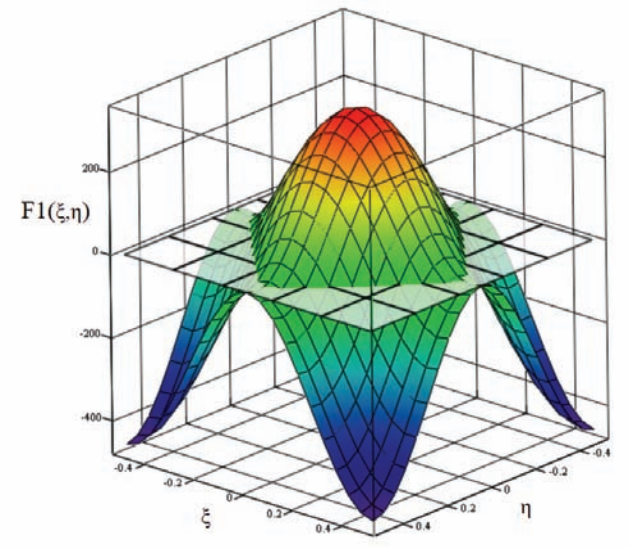


*Figure 4.* Surface of the solution $F_1$ discrepancy (1st approximation by MK)

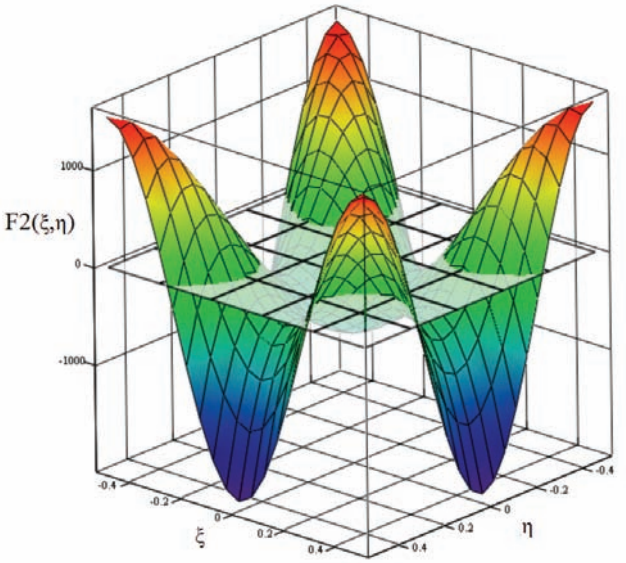


*Figure 5.* Surface of the solution $F_2$ discrepancy (1st approximation by MK)

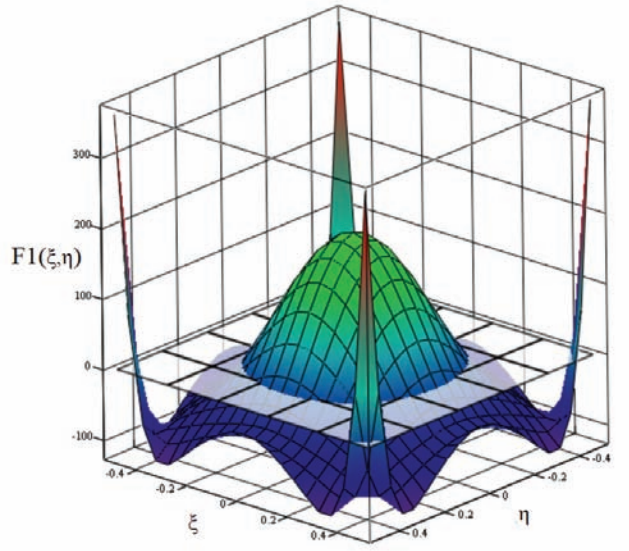


*Figure 6.* Surface of the solution $F_1$ discrepancy (4th approximation by MK)

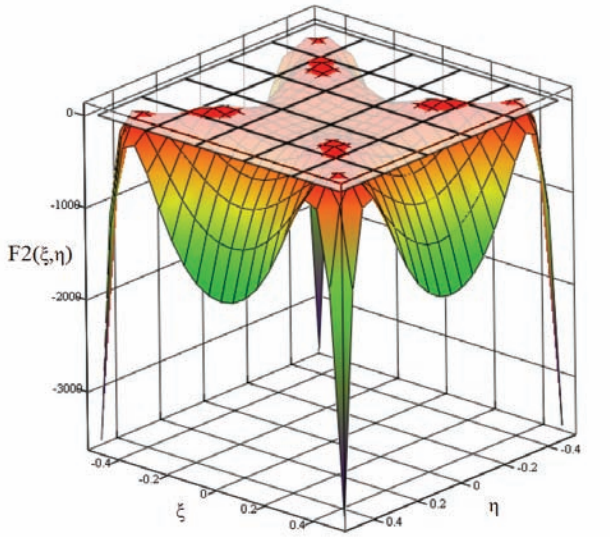


*Figure 7.* Surface of the solution $F_2$ discrepancy (4th approximation by MK)

These figures show that maximum changes in solution discrepancy values occur near the corner points of the contour and in the central region of the shell. Increasing the number of collocation nodes significantly decreases the values of solution discrepancies in these regions. The corner points of the shell are "special points" where a volumetric stress state arises that is not described by the equations of the shallow shell model adopted in the analysis. Therefore, these areas should be excluded from the analysis.

The following conclusion can be drawn: The modified method of sequential loads combined with the collocation method can obtain an engineering-sufficient solution for geometrically nonlinear shallow shells in the second approximation if the collocation node selection scheme is based on the "golden ratio." This allows the final solution to be presented in a form that facilitates calculations.

## REFERENCES

1. **Petrov, V.V.** Nonlinear Structural Mechanics, second edition, expanded: textbook / V.V. Petrov. – Moscow: ASV Publishing House, 2024. – 504 p.
2. **Zenkevich, O.** The Finite Element Method in Engineering. Moscow: Mir Publishing House, 1975. 541 pp.
3**. Ilyin, V.P., Karpov, V.V., Maslennikov, A.M.** Numerical Methods for Solving Problems in Structural Mechanics. Moscow: ASV Publishing House, 2005. 425 p.
4. **Volmir, A.S.** Slender Plates and Shells / A.S. Volmir. Moscow: Gostekhizdat, 1956. 419 p.
5. **Petrov V.V.** Nonlinear Structural Analysis Based on the Modified Sequential Load Method / V. V. Petrov // International Journal for Computational Civil and Structural Engineering. – 2021. – Vol. 17, No. 4. – P. 146-152.
6. **Petrov, V. V.** Modified method of sequential loads in nonlinear structural mechanics / V. V. Petrov, R. V. Mishchenko, O. A. Gorbacheva // Fundamental, exploratory, and applied research by the RAASN on scientific support for the development of architecture, urban planning, and the construction industry in the Russian Federation in 2021: Collection of scientific works by the RAASN / Russian Academy of Architecture and Construction Sciences. Volume 2. – Moscow: ASV Publishing House, 2022. – Pp. 339-349.
7. **Petrov V.V.** The method of sequential loads in nonlinear plate and shell theory / Saratov: Saratov University Press, 1975. – 119 p.
8. **Gorbacheva O.A.** On the calculation of plates using the collocation method / O.A. Gorbacheva // Expert: Theory and Practice. – 2023. – No. 1(20). – P. 69-72.
9**. Petrov V.V., Gorbacheva O.A.** Calculation of a plate made of nonlinearly elastic material using the collocation method // Bulletin of the Volga Regional Branch of the Russian Academy of Architecture and Construction Sciences: Collection of scientific papers. – Nizhny Novgorod: Nizhny Novgorod State University of Architecture and Civil Engineering, 2023. – Pp. 124-128.
10. **Korobko V.I. , Korobko G.N.** The Golden Ratio and Man, second edition, supplemented and revised. – Moscow: ASV Publishing House, 2002. – 394 p.

## СПИСОК ЛИТЕРАТУРЫ

1. **Петров, В.В.** Нелинейная строительная механика, *издание второе, дополненное*: учебник / В.В. Петров. – М.: Изд-во АСВ, 2024. - 504 с.
2. **Зенкевич О.** Метод конечных элементов в технике. – М.: Изд-во «Мир», 1975. – 541 с.
3**. Ильин В.П., Карпов В.В.** Масленников А.М. Численные методы решения задач строительной механики. – М.: Издательство АСВ, 2005. – 425 с.
4. Вольмир, А.С. Гибкие пластинки и оболочки / А.С. Вольмир. – Москва: Гостехиздат, 1956. – 419 с.
5. **Petrov V.V.** Nonlinear Structural Analysis Based on the Modified Sequential Load Method / V. V. Petrov // International Journal for Computational Civil and Structural Engineering. – 2021. – Vol. 17, No. 4. – P. 146-152.
6. Петров, В. В. Модифицированный метод последовательных нагружений в нелинейной строительной механике / В. В. Петров, Р. В. Мищенко, О. А. Горбачева // Фундаментальные, поисковые и прикладные исследования РААСН по научному обеспечению развития архитектуры, градостроительства и строительной отрасли Российской Федерации в 2021 году : Сборник научных трудов РААСН / Российская академия архитектуры и строительных наук. Том 2. – Москва: Издательство АСВ, 2022. – С. 339-349.
7**. Петров В.В.** Метод последовательных нагружений в нелинейной теории пластинок и оболочек / Саратов: Изд-во Сарат. ун-та, 1975. - 119 с.
8. **Горбачева О.А.** К расчету пластин методом коллокаций / О.А. Горбачева // Эксперт: теория и практика. – 2023. – № 1(20). – С. 69-72.
9. **Петров В.В., Горбачева О.А.** Расчет пластины из нелинейно-упругого материала ме-

тодом коллокаций // Вестник Приволжского территориального отделения Российской академии архитектуры и строительных наук: Сборник научных трудов. – Нижний Новгород: Нижегородский государственный архитектурно-строительный университет, 2023. – С. 124-128.

10. **В.И. Коробко, Г.Н. Коробко** / Золотая пропорция и человек, *издание второе*, *дополненное и исправленное*. – М.: Издательство АСВ, 2002. – 394 с.

---

*Vladilen Vasilievich Petrov* — full member of the Russian Academy of Architecture and Construction Sciences (RAACS), Doctor of Technical Sciences, Professor of the Department of Building Materials, Structures, and Technologies, Saratov State Technical University named after Y.A. Gagarin; 410054, Russia, Saratov, Polytechnicheskaya St., 77; e-mail: vvp@sstu.ru, vladilen307@gmail.com

*Olga Alexandrovna Gorbacheva* — Assistant Professor, Department of Building Materials, Structures and Technologies, Saratov State Technical University named after Y.A. Gagarin; 410054, Russia, Saratov, Polytechnicheskaya St., 77; e-mail: olga12zakirova@inbox.ru

*Петров Владилен Васильевич* — академик Российской академии архитектуры и строительных наук (РААСН), доктор технических наук, профессор кафедры «Строительные материалы, конструкции и технологии» Саратовского государственного технического университета имени Гагарина Ю.А.; 410054, Россия, г. Саратов, ул. Политехническая, 77; e-mail: vvp@sstu.ru, vladilen307@gmail.com

*Горбачева Ольга Александровна* — ассистент кафедры «Строительные материалы, конструкции и технологии» Саратовского государственного технического университета имени Гагарина Ю.А.; 410054, Россия, г. Саратов, ул. Политехническая, 77; e-mail: olga12zakirova@inbox.ru